



The University of
Nottingham

The Stress-Strain and Strength Characteristics of Portaway Sand

by

Jun Wang, B.Eng.

Thesis submitted to The University of Nottingham

for the degree of Doctor of Philosophy

January 2005

Abstract

Despite the large number of modifications proposed to the standard Cam-clay models over the last three decades, the critical state concept has been much less successful for modelling sand behaviour. This thesis is concerned with understanding the stress-strain and strength characteristics of Portaway sand, a quartz sand, and the validity of several recently developed critical state models formulated in terms of the state parameter concept.

The laboratory investigation consisted of the evaluation and modification of two triaxial systems and 83 triaxial tests performed under monotonic and cyclic loading conditions. Emphasis has been placed on assessing the applicability of critical state theory and state parameter concept to sands. Portaway sand was chosen in this research work because it is a typical granular material for which the deformation behaviour can be obtained and used to verify the newly developed constitutive models.

The critical state model concerned is known as CASM developed by Yu (1995, 1998). CASM is a relatively simple model because it only requires seven model constants, five of which are the same as those used in the modified Cam-clay model. Three extensions of CASM referred to as CASM-b, CASM-d and CASM-c were developed recently based on the combined hardening concept and the bounding surface plasticity theory. These enable the smooth transition of stiffness, phase transformation and cyclic behaviour to be simulated. For the first time, a simple procedure for determining all the model parameters from triaxial results has been established.

The validities of the theoretical assumptions introduced in the new models are critically assessed in light of results obtained from both element testing and numerical modelling. In general, the overall stress-strain behaviour of Portaway sand observed in triaxial tests under various stress paths is well captured by the models.

Keywords: Critical state model, triaxial tests, plasticity, sand, state parameter, experimental evaluation

Acknowledgements

The work described in this thesis was carried out at the Nottingham Centre for Geomechanics during the period of October 2001 to January 2005.

My sincere thanks are due to my supervisor Professor Hai-Sui Yu, who first interested me in this topic, for his supervision, guidance and financial support throughout this research. Without his support, this thesis would not have been possible.

Dr. Guoping Zhang, co-supervisor, provided crucial guidance and assistance while I was involved in experimental work on two triaxial testing systems. I would also like to thank Professor Stephen Brown for his help during the early stages of the research.

I would like to thank all the technicians in the School of Civil Engineering for their help and advice with the experimentation, in particular Michael Langford, Ian Richardson and Barry Brodrick. I would like to thank Graham Hanley for his help in the development and modification of the electronic equipment.

Dr. Cuong Doan Khong provided valuable assistance in the use of his finite element program described in Chapter 6. I would also like to thank my fellow students and co-workers for their friendship and support. My thanks are extended to Vikas Gupta, Dr. Cuong Doan Khong and Sia Min Tan for their valuable time spent proof reading this thesis.

Last, but by no means least, I am grateful to my parents and brothers for their constant support and encouragement during my research.

This work is dedicated to my parents

Contents

LIST OF TABLES	VII
LIST OF FIGURES	IX
NOMENCLATURE	XVIII
ACRONYM	XXI

Chapter 1 INTRODUCTION

1.1 BACKGROUND	1-1
1.2 RESEARCH OBJECTIVES	1-4
1.3 STRUCTURE OF THE THESIS	1-5

Chapter 2 LITERATURE REVIEW

2.1 INTRODUCTION	2-1
2.2 STRESS-STRAIN AND STRENGTH CHARACTERISTICS OF SANDS	2-2
2.2.1 Background	2-2
2.2.2 Intrinsic Properties and Structures	2-3
2.2.3 Shear Strength, Dilatancy and Critical State	2-8
2.2.4 State Parameter Concept	2-16
2.2.5 Behaviour Subjected to Monotonic Loading	2-17
2.2.6 Behaviour Subjected to Cyclic Loading	2-23
2.3 PREVIOUS TRIAXIAL TESTING AT THE UNIVERSITY OF NOTTINGHAM	2-29
2.3.1 Experimental Techniques	2-29

2.3.2	Stress Path Subjected to Traffic Loading	2-35
2.3.3	Modelling of Resilient Behaviour.....	2-37
2.3.4	Modelling of Permanent Behaviour.....	2-38
2.4	NUMERICAL MODELLING OF SANDS	2-39
2.4.1	Elasticity and Plasticity Theory.....	2-39
2.4.2	Critical State Models	2-42
2.4.3	Other Constitutive Models	2-45
2.5	CASM-A SIMPLE UNIFIED CRITICAL STATE MODEL	2-45
2.5.1	Experimental Evidence	2-46
2.5.2	Description of the Model	2-49
2.6	SUMMARY.....	2-53

Chapter 3 DESCRIPTION OF EXPERIMENTAL TECHNIQUES

3.1	INTRODUCTION.....	3-1
3.2	EQUIPMENT EVALUATIONS AND MODIFICATIONS.....	3-2
3.2.1	Introduction	3-2
3.2.2	Nottingham Dynamic Triaxial Testing System.....	3-3
3.2.3	Advanced Stress Path Triaxial Testing System	3-17
3.3	MATERIAL TESTED.....	3-24
3.3.1	Descriptions of Portaway Sand	3-24
3.3.2	Index Properties.....	3-25
3.3.3	Minerals and Structures of Portaway Sand	3-27
3.4	DATA CORRECTIONS	3-31
3.4.1	Introduction	3-31
3.4.2	Determination of Initial Void Ratio	3-32
3.4.3	Area and Membrane Correction.....	3-35
3.5	SUMMARY.....	3-37

Chapter 4 MONOTONIC LOADING TRIAXIAL TESTS

4.1	INTRODUCTION.....	4-1
4.2	PRELIMINARY TESTS ON DRY SANDS.....	4-2
4.2.1	Testing Program	4-2
4.2.2	Results and Discussion.....	4-4
4.3	EXAMINATION OF CRITICAL STATE CONCEPT	4-9
4.3.1	Introduction	4-9
4.3.2	Series A: Drained Compression Tests (CIDC-1~5)	4-11
4.3.3	Series B: Drained Extension Tests (CIDE-1~2)	4-17
4.3.4	Series C: Undrained Compression Tests (CIUC-1~12).....	4-20
4.3.5	Series D: Undrained Extension Tests (CIUE-1~4)	4-27
4.3.6	Series E: Drained Tests with Variable Confining Pressures	4-30
4.3.7	Series F: Pre-sheared Undrained Tests (CIPU-1~2).....	4-33
4.4	INTERPRETATION AND DISCUSSION.....	4-36
4.4.1	Identification of the Critical State Line.....	4-36
4.4.2	Determination of CASM Constants	4-45
4.4.3	Undrained Instability	4-51
4.4.4	Experimental State Boundary Surface.....	4-57
4.5	SMALL STRAIN BEHAVIOUR.....	4-59
4.5.1	Series G: Tests Measured with Hall Effect Transducers (S-1~S-6)..	4-59
4.5.2	Results and Discussion.....	4-60
4.6	SUMMARY.....	4-66

Chapter 5 CYCLIC LOADING TRIAXIAL TESTS

5.1	INTRODUCTION.....	5-1
5.2	OVERVIEW OF THE TESTING METHOD	5-2
5.3	ONE-WAY CYCLIC LOADING.....	5-4

5.3.1	Drained Tests (OWDC-1~4)	5-5
5.3.2	Undrained Tests (OWUC-5 and OWUE-6)	5-8
5.4	TWO-WAY CYCLIC LOADING	5-11
5.4.1	Drained Tests (TWD-1~4)	5-13
5.4.2	Undrained Tests (TWU-5 and TWU-6)	5-19
5.4.3	Drained Tests with Small Cyclic Loops (TWDS-7 and TWDS-8) ..	5-20
5.5	MOVING WHEEL LOADING	5-21
5.6	INTERPRETATION AND DISCUSSION.....	5-24
5.6.1	Stress Ratio – State Parameter Relation	5-25
5.6.2	Shear Strength – State Parameter Relation.....	5-28
5.6.3	Volumetric Strain – State Parameter Relation.....	5-31
5.6.4	Excess Pore Pressure – State Parameter Relation.....	5-33
5.7	SUMMARY.....	5-35

Chapter 6 EVALUATION AND VERIFICATION OF CASM AND ITS EXTENSIONS

6.1	INTRODUCTION.....	6-1
6.2	FINITE ELEMENT METHOD	6-2
6.2.1	Finite Element Programme – CRISP	6-2
6.2.2	Implementation and Analysis.....	6-3
6.3	THEORETICAL BACKGROUND OF EXTENDED PLASTICITY MODELS FOR CASM	6-4
6.3.1	CASM-d: A Combined Hardening Model	6-4
6.3.2	CASM-b: A Monotonic Bounding Surface Model.....	6-7
6.3.3	CASM-c: A Cyclic Bounding Surface Model	6-10
6.4	PARAMETRIC STUDY	6-13
6.4.1	The Effect of Initial State Parameter ξ_0	6-13
6.4.2	The Effect of Spacing Ratio r	6-15

The stress-strain and strength characteristics of Portaway sand

6.4.3	The Effect of Stress-State Coefficient n	6-17
6.4.4	The Effect of Elastic Constant μ	6-18
6.4.5	The Effect of Elastic Constant κ	6-18
6.4.6	The Effect of Parameter α	6-19
6.5	MODEL PERFORMANCE – CASM	6-21
6.5.1	Drained Tests (CIDC-1, 3, 4 and 5).....	6-22
6.5.2	Undrained Tests (CIUC-1 and CIUC-3).....	6-22
6.5.3	Undrained Test in Extension (CIUE-1).....	6-25
6.6	MODEL PERFORMANCE – CASM-D.....	6-27
6.6.1	Undrained Tests (CIUC-7, 9 and 12).....	6-27
6.6.2	Drained Tests (CIDC-1, 3, 4 and 5).....	6-32
6.7	MODEL PERFORMANCE – CASM-B.....	6-33
6.7.1	Drained Tests (CIDC-2 and CIDC-3).....	6-33
6.7.2	Undrained Tests (CIUC-4 and CIUC-6).....	6-35
6.8	MODEL PERFORMANCE – CASM-C.....	6-36
6.8.1	One-Way Drained Cyclic Loading Tests (OWDC-1).....	6-37
6.8.2	One-Way Undrained Cyclic Loading Tests (OWUC-5 and OWUE-6) 6-37	
6.8.3	Two-Way Drained Cyclic Loading Tests (TWD-3).....	6-41
6.9	SUMMARY.....	6-43

Chapter 7 CONCLUDING REMARKS

7.1	SUMMARY AND CONCLUSIONS.....	7-1
7.1.2	Experimental Techniques	7-2
7.1.3	Main Experimental Results	7-3
7.1.4	Experimental Evaluation of CASM and Its Extensions	7-6
7.2	ORIGINAL CONTRIBUTIONS	7-7
7.3	RECOMMENDATIONS FOR FUTURE RESEARCH.....	7-8

7.3.1	Experimental Testing	7-8
7.3.2	Theoretical Modelling	7-9

REFERENCES	R-1
APPENDIX A - UPDATED NOTTINGHAM DYNAMIC TRIAXIAL TESTING SYSTEM	A-1
APPENDIX B - ADVANCED STRESS PATH TRIAXIAL TESTING SYSTEM	B-1
APPENDIX C - RESULTS FROM MONOTONIC LOADING TESTS	C-1
APPENDIX D - RESULTS FROM CYCLIC LOADING TESTS	D-1
APPENDIX E - NUMERICAL MODELLING	E-1

List of Tables

Table 2-1. Summary of small strain measuring devices developed at the University of Nottingham.	2-33
Table 3-1. The LVDTs used in the NDTTS.....	3-9
Table 3-2. Comparison of soil properties between six sands (Yu, 2000) and Portaway sand.	3-25
Table 3-3. Index properties of Portaway sand and Leighton Buzzard sand.	3-26
Table 4-1. Summary of tests on dry sands (series A).....	4-3
Table 4-2. Summary of tests on dry sands (series B).....	4-4
Table 4-3. Summary of Series A: CIDC tests.....	4-12
Table 4-4. Comparison of characteristic states and critical states.....	4-15
Table 4-5. Summary of Series B: CIDE tests.	4-17
Table 4-6. Summary of Series C: CIUC tests.....	4-20
Table 4-7. Comparison of the phase transformation states and steady states.	4-24
Table 4-8. Summary of Series D: CIUE tests.....	4-27
Table 4-9. Summary of Series E: drained tests with variable confining pressures.	4-30
Table 4-10. Summary of Series F: CIPU tests.	4-33
Table 4-11. Material constants of sands used in equation (4-7).	4-45
Table 4-12. CASM constants and their physical meanings (Yu, 1998).....	4-46
Table 4-13. Initial and peak parameters for loose specimens.	4-55
Table 4-14. Summary of Series G: tests with small strain measurement.	4-60
Table 4-15. Elastic limit axial strain (Lo Presti, 1995).....	4-64
Table 5-1. Summary of one-way cyclic loading program.	5-5

Table 5-2. Summary of two-way cyclic loading program.....	5-11
Table 5-3. Summary of moving wheel loading program.	5-22
Table 6-1. CASM constants for Portaway sand.	6-21
Table 6-2. The triaxial tests used for CASM predictions.....	6-21
Table 6-3. CASM-d constants for Portaway sand.....	6-27
Table 6-4. The triaxial tests used for CASM-d predictions.	6-27
Table 6-5. CASM-b constants for Portaway sand.....	6-33
Table 6-6. The triaxial tests used for CASM-b predictions.	6-33
Table 6-7. CASM-c constants for Portaway sand.	6-36
Table 6-8. The triaxial tests used for CASM-c predictions.....	6-36
Table 7-1. Critical state and elastic constants for Portaway sand.	7-4

List of Figures

Figure 2-1. Range of particle sizes in soils.....	2-4
Figure 2-2. Effect of fines content on position of the <i>SSL</i> (Been and Jefferies, 1985)....	2-5
Figure 2-3. Characterisation of particle shapes of sands and flake shapes of clays.....	2-6
Figure 2-4. Isotropic compression of the calcarenite: (a) stronger-bounded samples, (b) weaker-bounded samples (Cuccovillo and Coop, 1999).....	2-7
Figure 2-5. Influence of specimen preparation method on stress-strain-strength behaviour for sands: (a) drained tests (Oda, 1972), (b) undrained tests (Mitchell, 1993).	2-8
Figure 2-6. Contributions to the shear strength of granular soils (Mitchell 1993).....	2-11
Figure 2-7. The definition of various states of sand subject to undrained loading (Ishihara, 1996).	2-13
Figure 2-8. A unique critical state line for Erksak 330/0.7 sand (Been et al., 1991)....	2-15
Figure 2-9. Definition of the state parameter ξ	2-17
Figure 2-10. Effective stress paths for triaxial compression tests.....	2-19
Figure 2-11. Stress path test used to identify yield envelope in triaxial apparatus (modified from Tatsuoka and Ishihara, 1974a).....	2-20
Figure 2-12. Definition of permanent strain, resilient strain and calculation of resilient modulus.	2-24
Figure 2-13. Drained one-way cyclic triaxial test (Wood, 1982, data obtained from Tatsuoka, 1972).	2-25
Figure 2-14. Drained two-way cyclic triaxial test (Tatsuoka and Ishihara, 1974b).....	2-25
Figure 2-15. Comparison of stress-strain response of Fairbank's sand undergoing two type of stress paths: (a) resilient modulus stress path CD, (b) moving wheel	

stress path ABCD, (c) stress paths in the $q - p'$ space (Mcvey and Taesiri, 1985).....	2-28
Figure 2-16. Schematic of Nottingham triaxial facilities: (a) testing of clay and silt (Raybould, 1992), (b) testing of unbound granular materials (Brown, 1996).	2-31
Figure 2-17. Source of errors in external axial deformation measurements.....	2-32
Figure 2-18. 'Location stud' technique for small strain measurement (Brown et al., 1989).	2-34
Figure 2-19. 'Key-in' technique for small strain measurement (Cheung, 1994).....	2-34
Figure 2-20. Principal stress rotation under a moving load (Lekarp et al., 2000).	2-36
Figure 2-21. Shear strain contours for undrained loading in normalised stress spaces (modified from Sladen and Oswell, 1989).....	2-46
Figure 2-22. Yield surfaces: (a) original Cam-clay model, (b) modified Cam-clay model.	2-47
Figure 2-23. State boundary surface of a Dog Bay sand: (a) drained tests, (b) undrained tests (Modified from Coop, 1990).....	2-48
Figure 2-24. State boundary surface of a silica sand (McDowell et al., 2002).....	2-49
Figure 2-25. General stress-state relations assumed in CASM.	2-50
Figure 2-26. The yield surfaces of CASM normalised by preconsolidation stresses.....	2-51
Figure 2-27. (a) shapes of different plastic potential surfaces, (b) plastic strain increments for CASM (Khong, 2004).	2-52
Figure 3-1. The Nottingham dynamic triaxial testing system.....	3-4
Figure 3-2. Diagram of the pressure sources at the NCG research laboratory.	3-5
Figure 3-3. The effect of frequency on load and displacement control methods.	3-6
Figure 3-4. Triaxial cell built at the NCG.	3-7
Figure 3-5. Triaxial cell used in preliminary tests.	3-8

Figure 3-6. Data acquisition and control system.....	3-12
Figure 3-7. Connector of the transducers.....	3-12
Figure 3-8. Data acquisition and control signal flow chart.	3-13
Figure 3-9. The ‘on-specimen’ measuring device used by Coop (Private communication, Appendix A).....	3-14
Figure 3-10. ‘On-specimen’ measuring device developed at the NCG.....	3-15
Figure 3-11. The arrangement of the ADVTTTS at the NCG research laboratory.....	3-18
Figure 3-12. Details of the classical Bishop and Wesley stress path triaxial cell.....	3-20
Figure 3-13. Set up of specimen in the ADVTTTS with Hall effect transducers.....	3-21
Figure 3-14. Testing setup for the ADVTTTS.....	3-24
Figure 3-15. Particle size distribution of Portaway sand.....	3-27
Figure 3-16. EDS analysis for Portaway sand showing: (a) a sand particle, (b) fines content.	3-28
Figure 3-17. SEM micrograph of Portaway sand showing carbonate minerals.	3-29
Figure 3-18. SEM micrographs of Portaway sand: (a) sand particles, (b) clays exists on the particle surface.....	3-30
Figure 3-19. Sources of problems during triaxial testing (modified from Germaine and Ladd, 1988).....	3-31
Figure 3-20. Axial displacement measured after back pressure saturation.....	3-33
Figure 3-21. Membrane penetration effects for Portaway sand.....	3-34
Figure 4-1. Typical stress-strain curves on dry Portaway sand.....	4-5
Figure 4-2. Recalibration of equation (2-13) proposed by Bolton (1986) on dry Portaway sand.	4-6
Figure 4-3. Recalibration of equation (2-13) proposed by Bolton (1986) on dry Leighton Buzzard sand.....	4-6

Figure 4-4. Volumetric strains obtained from ‘on-specimen’ measuring device.	4-7
Figure 4-5. Stress-dilatancy relation of dry Portaway sand.	4-8
Figure 4-6. Stress paths of dry Portaway sand (up to 8-15% shear strains).....	4-8
Figure 4-7. Definition of total stress paths used in triaxial tests.....	4-11
Figure 4-8. Stress-strain relationships (Series A: CIDC).	4-13
Figure 4-9. Comparison of experimental and various stress-dilatancy relations (Series A: CIDC).	4-16
Figure 4-10. Evolution of dilatancy rate for dense and loose Portaway sand (CIDC-1 and CIDC-5).	4-17
Figure 4-11. Stress-strain relationships (Series B: CIDE).....	4-18
Figure 4-12. Typical specimen shape after the occurrence of necking (Series B: CIDE-1).	4-19
Figure 4-13. Stress-strain relationships and stress paths (A) (Series C: CIUC).....	4-22
Figure 4-14. Stress-strain relationships, stress paths and excess pore pressure changes (B) (Series C: CIUC).	4-25
Figure 4-15. Stress-strain relationships, stress paths and excess pore pressure changes (C) (Series C: CIUC).	4-26
Figure 4-16. Instability of load-controlled test (Series D:CIUE-1).....	4-28
Figure 4-17. Stress-strain relationships, stress paths and excess pore pressure changes (Series D: CIUE).	4-29
Figure 4-18. Stress-strain relationships and stress paths (A) (Series E: CID tests with variable confining pressures).	4-31
Figure 4-19. Stress-strain relationships and stress paths (B) (Series E: CID tests with variable confining pressures).	4-32
Figure 4-20. Stress-strain relationships and stress paths (A) (Series F: CIPU).	4-34
Figure 4-21. Stress paths and excess pore pressure changes (B) (Series F: CIPU).....	4-35

Figure 4-22. Overall stress paths (Series A~F).....	4-37
Figure 4-23. <i>CSL</i> in the $\ln p' - \nu$ space.	4-38
Figure 4-24. <i>CSL</i> in the $q - p'$ stress space.	4-38
Figure 4-25. Specimens sheared at the same void ratio ($e_0 = 0.705 \pm 0.006$) but from different consolidation pressure levels.	4-39
Figure 4-26. Specimens sheared at the same effective confining pressure (300 kPa) but with different initial densities.....	4-40
Figure 4-27. Specimens sheared at the same effective confining pressure (50 kPa) but with different initial densities.....	4-41
Figure 4-28. <i>CSLs</i> : (a) Dog's Bay sand (Klotz and Coop, 2002), (b) Toyoura sand (data from Verdugo and Ishihara, 1996).	4-42
Figure 4-29. Comparison of the <i>CSLs</i> between Portaway sand and Erkask 330/0.7 sand.	4-43
Figure 4-30. <i>CSLs</i> of Portaway sand and Erkask 330/0.7 sand in arithmetic plot.	4-44
Figure 4-31. Predicted <i>CSLs</i> of Portaway sand and Erkask 330/0.7 sand.	4-44
Figure 4-32. State parameter, reference state parameter and critical state constants (Yu, 1998).....	4-46
Figure 4-33. Determination of Poisson's ratio μ by drained triaxial tests.	4-48
Figure 4-34. Determination of slope of swelling line κ by isotropic compression tests.	4-49
Figure 4-35. Determination of stress-state coefficient n from drained and undrained tests.	4-51
Figure 4-36. Effective stress paths of three normally consolidated specimens in the $p' - \nu -$ q space.....	4-52
Figure 4-37. Definition of flow liquefaction line.	4-53
Figure 4-38. State-dependent flow liquefaction line.	4-53
Figure 4-39. Effective stress paths normalised by equivalent critical state pressure.....	4-54

Figure 4-40. The relationship between peak stress ratio and initial state parameter in compression tests: (a) Leighton buzzard sand, (b) Toyoura sand (Yang, 2002).....	4-56
Figure 4-41. The relationships between peak stress ratio and the current state parameter on Portaway sand: (a) compression tests (CIUC), (b) extension tests (CIUE).....	4-56
Figure 4-42. Stress paths and state boundary surface normalised with respect to the preconsolidation pressure.	4-57
Figure 4-43. Stress paths and state boundary surface normalised by equivalent critical state pressure.....	4-59
Figure 4-44. Comparison of internal and external measurements (S-2).	4-61
Figure 4-45. Typical stress-strain curves measured from two Hall effect transducers (S-1).	4-62
Figure 4-46. Comparisons of external and internal measurements: (a) undrained (S-7), (b) drained (S-8).....	4-62
Figure 4-47. Degradation in the stiffness of Portaway sand.	4-63
Figure 4-48. Effects of effective confining pressure and density on small strain shear modulus: dense sand (S-1~S-3), (b) loose sand (S-4~S-6).	4-65
Figure 5-1. One-way drained cyclic loading in compression ($\xi_0 = 0.026$, OWDC-1).....	5-6
Figure 5-2. One-way drained cyclic loading in compression (OWDC-2~4).	5-7
Figure 5-3. One-way undrained cyclic loading (A) ($\xi_0 = 0.06$, OWUC-5; $\xi_0 = 0.06$, OWUE-6).....	5-9
Figure 5-4. One-way undrained cyclic loading (B) ($\xi_0 = 0.06$, OWUC-5; $\xi_0 = 0.06$, OWUE-6).....	5-10
Figure 5-5. The deviatoric-plane view of the applied stress paths for tests TWD-1~4.	5-12
Figure 5-6. Applied stress paths in the $p^l - q$ stress space (TWD-1~4).....	5-13

Figure 5-7. Two-way drained cyclic loading ($\xi_0=-0.112$, constant $p^l=300$ kPa, TWD-1).	5-15
Figure 5-8. Two-way drained cyclic loading ($\xi_0=0.060$, constant $p^l=300$ kPa , TWD-3).	5-16
Figure 5-9. Two-way drained cyclic loading ($\xi_0 =-0.109$, constant $p^l=100$ kPa , TWD-4).	5-17
Figure 5-10. Comparison of strength characteristics ($\xi_0 = -0.112$, TWD-1; $\xi_0 = -0.119$, CIDCP-1).	5-18
Figure 5-11. Stress-dilatancy relations of two-way cyclic loading (TWD-1 and TWD-2).	5-18
Figure 5-12. Two-way undrained cyclic loading (A) ($\xi_0 = 0.06$, TWU-5; $\xi_0 = 0.06$, TWU-6).	5-19
Figure 5-13. Two-way undrained cyclic loading (B) ($\xi_0 = 0.06$, TWU-5; $\xi_0 = 0.06$, TWU-6).	5-20
Figure 5-14. Comparison of external and internal measurements (TWDS-7).	5-21
Figure 5-15. Cyclic deviatoric stress, effective confining stress and moving wheel loading stress path (MV-2).....	5-23
Figure 5-16. Stress-strain curve of moving wheel loading path ABCD (MW-2).....	5-23
Figure 5-17. Stress-strain curve of moving wheel loading path BCD (MW-1).....	5-24
Figure 5-18. Stress-strain curve of moving wheel loading path CD (OWDC-4).	5-24
Figure 5-19. Stress ratio-state parameter relations (TWD-1 and TWD-3).....	5-26
Figure 5-20. Stress ratio-state parameter relations (OWUC-5 and CIUC-1).....	5-26
Figure 5-21. Stress ratio-state parameter relations (OWUE-6 and CIUE-1).....	5-27
Figure 5-22. Stress ratio-state parameter relations (TWU-5, CIUC-1 and CIUE-1) ..	5-27
Figure 5-23. Stress ratio-state parameter relations (TWU-6, CIUC-1 and CIUE-1) ..	5-28
Figure 5-24. Predicted and measured peak friction angles on dense sands.	5-29

Figure 5-25. Comparison of cyclic shear resistance of Portaway sand under different loading paths ($\xi_0 = 0.060$, OWUC-5, OWUE-6 and TWU-6).....	5-30
Figure 5-26. Volumetric strain-state parameter relations (CIDC-1~5, TWD-1)	5-32
Figure 5-27. Dilatancy-state relations with $\xi_r = 0.06$	5-33
Figure 5-28. Excess pore pressure-state parameter relations (CIUC-1, OWUC-5 and CIUE-1).	5-34
Figure 5-29. Excess pore pressure-state parameter relations (CIUC-1, OWUE-6 and CIUE-1).	5-34
Figure 5-30. Excess pore pressure-state parameter relations (CIUC-1, TWU-6 and CIUE-1).	5-35
Figure 6-1. Finite element mesh used in the numerical analysis (Khong, 2004).....	6-3
Figure 6-2. Undrained test on medium loose Portaway sand predicted by CASM and CASM-d.....	6-6
Figure 6-3. The mapping rule adopted in CASM-b (Khong, 2004).....	6-8
Figure 6-4. Drained test on loose Portaway sand (CIDC-3) predicted by CASM and CASM-b.....	6-9
Figure 6-5. Calculation of the hardening modulus H in CASM-c and shakedown behaviour (TWD-3).	6-12
Figure 6-6. Effect of initial condition on drained behaviour of Portaway sand.	6-14
Figure 6-7. Effect of initial condition on undrained behaviour of Portaway sand.	6-15
Figure 6-8. Effect of spacing ratio r on dense Portaway sand (CIDC-5).	6-16
Figure 6-9. Effect of spacing ratio r on very loose Portaway sand (CIDC-1).	6-16
Figure 6-10. Effect of stress-state coefficient n on dense Portaway sand (CIDC-5).	6-17
Figure 6-11. Effect of stress-state coefficient n on loose Portaway sand (CIDC-1).	6-17
Figure 6-12. Effect of μ on dense Portaway sand (CIDC-5).....	6-18
Figure 6-13. Effect of κ on dense Portaway sand (CIDC-5).....	6-19

Figure 6-14. Effect of the parameter α on very loose Portaway sand (CIUC-7).....	6-20
Figure 6-15. Comparison of CASM with measured behaviour for CIDC tests on dense and loose Portaway sand (CIDC-1, 3, 4 and 5).....	6-23
Figure 6-16. Comparison of CASM with measured behaviour for CIUC tests on very loose Portaway sand (CIUC-1 and 3).....	6-24
Figure 6-17. Comparison of CASM with measured behaviour for CIUE tests on very loose Portaway sand (CIUE-1).	6-26
Figure 6-18. Comparison of CASM-d with measured behaviour for CIUC tests (CIUC-7, 9 and 12).....	6-28
Figure 6-19. Comparison of CASM-d with measured behaviour for CIUC tests on excess pore pressure changes (CIUC-7, 9 and 12).....	6-29
Figure 6-20. Effect of the initial state parameter on the occurrence of liquefaction and phase transformation.	6-31
Figure 6-21. Enlarged view of the stress paths shown in Figure 6-20 (b).....	6-31
Figure 6-22. Effect of new parameter α on the drained tests (CIDC-1, 3, 4 and 5)....	6-32
Figure 6-23. Comparison of CASM-b with measured behaviour for CIDC tests (CIDC-2 and 3).....	6-34
Figure 6-24. Comparison of CASM-b with measured behaviour for CIUC tests (CIUC-4 and 6).....	6-35
Figure 6-25. Comparison of CASM-c with measured behaviour for test OWDC-1.....	6-37
Figure 6-26. Comparison of CASM-c with measured behaviour for test OWUC-5.....	6-39
Figure 6-27. Comparison of CASM-c with measured behaviour for test OWUE-6.....	6-40
Figure 6-28. Comparison of CASM-c with measured behaviour for test TWD-3.....	6-42

Nomenclature

d	= Dilatancy rate
D_r	= Relative density
e	= Void ratio
e_c	= Void ratio at critical state
e_{\max}	= Maximum void ratio
e_{\min}	= Minimum void ratio
E	= Young's modulus
f	= Yield function
g	= Plastic potential function
G	= Shear modulus
G_0	= Initial shear modulus at small strain
h	= Model parameter introduced in CASM-b
H	= Hardening modulus at the current stress point
H_j	= Hardening modulus at image stress point
H_R	= Model parameter introduced in CASM-c
H_U	= Model parameter introduced in CASM-c
I_R	= Relative dilatancy index
k	= Model parameter introduced in CASM-c
K	= Bulk modulus
l	= Current height of specimen
m	= Model parameter introduced in CASM-b
M	= Slope of the <i>CSL</i> in the $q-p'$ space
M_c	= Value of M in triaxial compression
M_e	= Value of M in triaxial extension
M_r	= Resilient modulus
n	= Stress-state coefficient

N	= Specific volume of isotropically normal consolidated soil when $p'=1$ kPa
p'	= Mean effective stress
p'_c	= Mean effective stress at critical state
p'_e	= Equivalent consolidation stress (see Figure 4-32)
p'_o	= Preconsolidation stress
p'_u	= Equivalent critical state stress (see Figure 4-32)
p'_x	= Mean effective stress at critical state which has the same preconsolidation pressure as the current stress (see Figure 4-32)
q	= Deviatoric stress
q_c	= Deviatoric stress at critical state
q_{cyc}	= Amplitude of cyclic deviatoric stress
Q	= Material constant in Bolton's relative dilatancy relation
r	= Spacing ratio
R	= Material constant in Bolton's relative dilatancy relation
α	= Model parameter introduced in CASM-d
β	= Controlling parameter in plastic potential
γ	= Ratio between the current stress and image stress
Γ	= Intersection of the <i>CSL</i> with $p' = 1$ kPa line in the v - $\ln p'$ space
$\delta\epsilon_1$	= Major principal strain increment
$\delta\epsilon_3$	= Minor principal strain increment
$\delta\epsilon_p^p$	= Plastic volumetric strain increment
$\delta\epsilon_q^p$	= Plastic shear strain increment
Δu	= Excess pore pressure
ϵ_1	= Major principal strain
ϵ_3	= Minor principal strain
ϵ_a	= Axial strain
ϵ_p	= Volumetric strain
ϵ_p^e	= Elastic volumetric strain
ϵ_p^p	= Plastic volumetric strain
ϵ_q	= Shear strain

ε_q^e	= Elastic shear strain
ε_q^p	= Plastic shear strain
η	= Stress ratio
η_{cyc}	= Cyclic stress ratio
η_{peak}	= Peak stress ratio
θ	= Lode angle
κ	= Slope of the swelling line in the ν - $\ln p'$ space
λ	= Slope of the critical state line in the ν - $\ln p'$ space
Λ	= Plastic volumetric strain ratio
μ	= Poisson's ratio
ν	= Specific volume
ξ	= State parameter
ξ_{peak}	= State parameter at the peak point in undrained monotonic loading
ξ_R	= Reference state parameter
σ'_1	= Effective major principal stress
σ'_3	= Effective minor principal stress
σ_f	= Normal stress on the failure plane
τ_f	= Shear stress at failure
ϕ_c	= Critical state friction angle
ϕ_m	= Mobilised friction angle
ϕ_p	= Peak friction angle
ψ_m	= Mobilised dilatancy angle

Conventions

(1) Compressive stresses and strains are taken as positive. Other symbols are defined and used in restricted conditions as required.

(2) Stresses listed are total stresses. Effective stresses are denoted by the use of primes.

Acronym

AC	= Alternating current
ADVDPCC	= Advanced digital pressure controller
ADVTTS	= Advanced stress path triaxial testing system
A/D	= Analogue to digital converter
ATS	= Automated testing system
BRD	= Bellofram rolling diaphragm
BS	= British standard
CASM	= A unified clay and sand model
CASM-b	= CASM's extension: a new bounding surface model
CASM-c	= CASM's extension: a new cyclic bounding surface model
CASM-d	= CASM's extension: a new combined volumetric-deviatoric hardening model
CCP	= Constant confining pressure
CSL	= Critical state line
CSR	= Cyclic stress ratio
EDS	= Energy dispersive spectrum
GDS	= Geotechnical digital systems instruments Ltd
HCA	= Hollow cylinder apparatus
LVDT	= Linear variable differential transformer
MT	= Moist tamping method
NCG	= Nottingham Centre for Geomechanics
NCL	= Normal consolidation line
NDTTS	= Nottingham dynamic triaxial testing system
OCR	= Overconsolidation ratio
PV	= Pluviation method
RCL	= Reference consolidation line
RDP	= RDP electronics Ltd

SAGE	= SAGE engineering Ltd
SEM	= Scanning electron microscopy
SSA	= Simple shear apparatus
SSL	= Steady state line
STDDPC	= Standard digital pressure controller
TTA	= True triaxial apparatus
VCP	= Variable confining pressure

Chapter 1

Introduction

1.1 BACKGROUND

A reliable assessment of the mechanical behaviour of soils by means of experiments is an essential part of any rational geotechnical design and analysis. Fundamental properties such as strength, deformation modulus and stress-strain characteristics are generally obtained by laboratory or in-situ tests. Both methods have their inherent merits and disadvantages, which have been comprehensively discussed by Jamiokowski et al. (1985) and Yu (2004) in their state-of-the-art review on the developments in laboratory and in-field testing of soils.

Among various methods, triaxial testing is the most widely used procedure for determining the stress-strain and strength characteristics of soils. The outstanding advantages of this method are the control of drainage conditions, well-defined boundary conditions and control over stress paths.

Demand for better measurements, better recording and better processing data has developed with growing appreciation of the inadequacy of standard triaxial testing.

Consequently, in the last four decades, a large number of research activities have been carried out to develop advanced triaxial equipments, testing techniques and interpretation methods (notably Tatsuoka, 1988; Baldi et al., 1988). In addition, emphasis has recently been placed on obtaining a wide variety of stress paths in order to establish the validity of the constitutive models implemented in the numerical analysis, such as developments of True Triaxial Apparatus (TTA) and Hollow Cylinder Apparatus (HCA). However, they are complicated in configuration and have limited productivity (Brown, 1996). The triaxial apparatus allows the field stress regime to be expressed in terms of octahedral shear and normal stresses, but only a jump rotation of 90° in the principal stress directions can be achieved. In spite of this limitation, it is still a useful means to investigate stress path effects and anisotropic behaviours of soils subjected to a variety of loading conditions.

With the advent of increasingly powerful computers over the last three decades, it has become feasible to perform stress analysis of geotechnical structures involving complex geometries and material behaviour. The numerical modelling plays an important role in such analysis. Based on different approaches, the modelling of soils may be classified as (a) non-linear models based on empirical correlations and (b) rational elastic-plastic models.

The first class of models allows practical problems to be addressed, and accounts for a large proportion of the work carried out on pavement engineering at the University of Nottingham. However, the models provide limited insight into the fundamental mechanisms of soil deformations. As pointed out by Brown (1996), the current practice of pavement engineering has lagged some way behind the knowledge accumulated through research.

In contrast, elastic-plastic models have a rigorous theoretical basis and are frequently used by other branches of soil mechanics, such as earthquake engineering and offshore foundation engineering. However, most of the models are

complicated in their mathematical expressions and have a large number of model constants that have no apparent physical meanings.

Yu (1995, 1998) developed a unified constitutive model for both clay and sand. This simple model is referred to as CASM (standing for Clay And Sand Model), which was formulated in terms of the state parameter. The advantages of CASM over many existing models were presented in great detail by Yu (1998). To summarise these, the novel and main attractive features of CASM include:

- The CASM model is of a unified nature: only a single set of yield and plastic potential functions is needed to model the behaviour of both clay and sand under both drained and undrained loading conditions. Many existing models are applicable for either clay or sand, but not for both materials. This is not convenient from the application point of view.
- The CASM model is relatively simple and therefore can be easily applied in practice. While a few other unified clay and sand models have appeared in the literature (such as MIT-S1 proposed by Pestana and Whittle, 1999), they tend to be much more complex and require many more model parameters, which would be very difficult to measure in reality.
- A further innovative feature is that the CASM model is based on the newly established but well-accepted state parameter concept introduced by Been and Jefferies (1985). The state parameter, which accounts for the effect of both void ratio and pressure, has been proven to be of fundamental importance in modelling the behaviour of sands and overconsolidated clays. The model CASM represents one of the first attempts to reformulate the standard Cam-clay models in terms of the state parameter.

However, the initial development of CASM is mainly focused on its simplified nature. Inevitably, some important aspects of the stress-strain and strength characteristics of clay and sand could not be modelled realistically by this elastic-

plastic strain hardening (or softening) model. Based on the combined hardening concept and the bounding surface plasticity theory, Yu et al. (2004) and Khong (2004) extended CASM to produce three new plasticity models:

- CASM-d, a combined volumetric-deviatoric hardening model, in order to provide better prediction of the behaviour of undrained loose sand;
- CASM-b, a bounding surface model, in order to provide a more realistic prediction of sand behaviour inside the state boundary surface;
- CASM-c, a cyclic bounding surface model, in order to provide a good prediction of sand behaviour under cyclic loading conditions.

1.2 RESEARCH OBJECTIVES

The ultimate objective of this research work is to gain a better understanding of the stress-strain and strength characteristics of Portaway sand and to assess several critical state models for sand. This has involved the laboratory testing and numerical modelling of Portaway sand behaviour under monotonic and cyclic loading conditions. In particular, the research aims:

- (a) To evaluate and extend the capabilities of the triaxial systems at the University of Nottingham to include the testing of sands;
- (b) To gain a better understanding of the stress-strain and strength characteristics of Portaway sand;
- (c) To present a simple procedure for determining all the model parameters from the triaxial test results;
- (d) To evaluate and verify the unified critical state model CASM and its extensions through comparison of experimental and numerical studies.

1.3 STRUCTURE OF THE THESIS

The material presented in this thesis is contained within seven chapters. The organisation of these is as follows.

Chapter 1 gives an introduction to this research work. In **Chapter 2**, the literature review is divided into four parts: stress-strain and strength characteristics of sands, previous triaxial testing at the University of Nottingham, numerical modelling of sands and the critical state model CASM.

Chapter 3 describes the experimental techniques employed in the testing program. Initially, the evaluation and modification of two triaxial systems are presented. The material tested is then introduced. Finally, detailed testing procedures and data correction methods are described.

Chapter 4 consists of the results and the interpretations of extensive monotonic triaxial tests on Portaway sand. Six series of triaxial tests are designed to examine the validity of the critical state concept on Portaway sand. A simple procedure for determining CASM constants is demonstrated. The experimental state boundary surface, undrained instability and some aspects of small strain behaviour of Portaway sand are discussed.

Chapter 5 describes the results and the interpretations of several one-way and two-way cyclic triaxial tests on Portaway sand. The correlations of the results obtained from monotonic loading condition to the cyclic loading condition are presented in terms of the state parameter concept.

In Chapter 6, the numerical techniques used in this thesis are described, followed by the introduction of three extensions of CASM. The abilities of these plasticity models together with CASM in modelling the behaviour of Portaway sand are demonstrated by the parametric studies. The evaluation and verification of CASM

and its extensions are then carried out by comparison of the numerical results and the experimental data obtained from Chapter 4 and Chapter 5.

Chapter 7 summarises the main findings of the research and gives some suggestions for future work.

The specification and the calibration curves associated with the different components of the NDTTS are presented in Appendix A. Appendix B contains a description of the specimen preparation methods developed in the current research work and a summary of accuracy and range of measurement. The complete experimental results described in Chapter 4 and Chapter 5 with associated numerical inputs used in Chapter 6 are summarised in Appendix C and Appendix D, respectively. Appendix E shows the graphical relationships between CASM and its extensions.

Chapter 2

Literature Review

2.1 INTRODUCTION

It is widely recognised that the behaviour of sands is anisotropic, effective stress level and stress path dependent. A fundamental assessment of their influences on the mechanical behaviour of sands is made possible by performing controlled element tests in the laboratory. Based on accumulated experimental data, a large number of elastic-plastic models have been developed over the last three decades. Initially, these models were all developed for the case of a triaxial test. During such a test, the two effective principal stresses are equal and the directions of principal stresses are fixed with respect to the material element. Therefore, acquiring a set of good quality triaxial data is an important step towards establishing a robust constitutive model.

This literature review is comprised of four parts: (1) stress-strain and strength characteristics of sands, (2) previous triaxial testing at the University of Nottingham, (3) numerical modelling of sands and (4) CASM - a simple unified critical state model. The first part presents a brief review on intrinsic properties

and structures of sands followed by the concepts of shear strength, dilatancy and critical state. This review is considered necessary as many of the following discussions and interpretations are based on those concepts. After introducing the state parameter concept, some of the typical behaviours of sands subjected to monotonic and cyclic loading are described. The second part reviews the triaxial testing techniques developed at the University of Nottingham. Modelling techniques of resilient and permanent deformations on unbound granular materials are also briefly reviewed. In the third part, an overview of numerical modelling of sand behaviour is given. Finally, some selected experimental evidences are presented in order to support the general relationship between stress ratio and state parameter (from here on referred to as stress ratio-state parameter relation) assumed in CASM. Subsequently, a complete description of this elastic-plastic model is given.

2.2 STRESS–STRAIN AND STRENGTH CHARACTERISTICS OF SANDS

2.2.1 Background

It is always a good practice to carry out both laboratory tests and analyses in order to obtain as broad a view as possible of the design properties being considered. Consequently, a large number of sophisticated testing systems have been developed to measure the stress-strain and strength properties of soils over the last two decades and a large number of plasticity models have been proposed. Models based on the critical state concept (known as Cam-clay models) are able to reproduce with accuracy the behaviour of clays (e.g. Roscoe and Schofield, 1963). The essence of this concept is that the behaviour of soils depends not only on their density but also on the stress level. The true state of soils cannot be quantified simply by

relative density, but by the location of its current stress and volume state relative to the critical state line (*CSL*, a concept explained later in this Chapter). However, most critical state models are less successful to model the behaviour of sands among other granular materials. The main problems, as noted by Yu (1998) are:

- Existing Cam-clay models fail to predict observed softening and dilatancy of dense sands and undrained response of very loose sands.
- The lack of success in developing a critical state model for sands is also due to the experimental difficulties in obtaining the *CSL* and normal consolidation line (*NCL*).

This review has been restricted to the literature of those that are relevant to this thesis. In particular, a number of important behaviours exhibited by sands have been highlighted. The behaviour of unsaturated sands is beyond the scope of this research, which centres only on the behaviour of fully saturated sands.

2.2.2 Intrinsic Properties and Structures

To date the laboratory testing of sands has been focused almost exclusively on the reconstituted sands. Much less emphasis was placed on the testing of natural sands due to the difficulty in sampling and its complicated nature. It has been well established that the mechanical behaviour of reconstituted sands is governed by a few material properties. Examples are mineralogy, grain size distribution, grain shape, specific gravity and true friction angle. Been et al. (1991) grouped those as intrinsic material properties because they can be uniquely defined and are independent of the state of the sands. The term ‘structure’ was first introduced for clays by Mitchell (1976), and has been used to account for differences between the properties of clays in its natural state and destructed (or remoulded) state. More recently, research work on sands (e.g. Cuccovillo and Coop, 1997) has revealed that the ‘structure’ plays an important role and should also be considered as an element in addition to the intrinsic properties.

2.2.2.1 Intrinsic properties

The physical characteristics of sands are normally determined by the particle size, shape, surface texture and size distribution. The mineral composition determines the hardness, cleavage, and resistance to physical and chemical breakdown. In this section, their definitions and effects on the mechanical behaviour of sands within the context of triaxial testing are briefly described.

Particle size and distribution

The range of particle sizes in engineering soils is very large. Commonly used particle ranges are shown in Figure 2-1. As can be seen from the figure, the particle size for clean sand ranges from 0.06–2 mm. Generally speaking, individual sand-sized particles are visible to the naked eye. However, silts and clays can be seen only with optical or electron microscopes. The distribution of particle of sands is conveniently shown as a grading curve on a particle size distribution chart. If the grading curve is flat and the sand specimen contains a wide variety of particle sizes, it is said to be well graded. If the curve is steep and one size predominates, the specimen is said to be poorly graded.

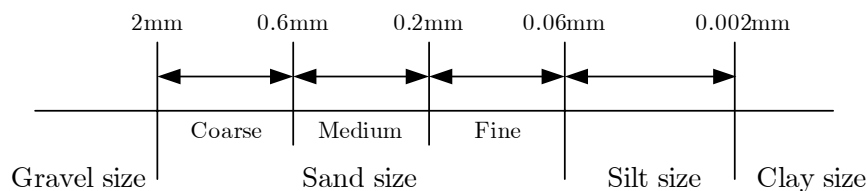


Figure 2-1. Range of particle sizes in soils.

In triaxial testing, the specimen should be large enough to represent adequately the material whose properties are to be determined. Typically, the specimen should be of a diameter at least 5 times that of the largest particle.

In recent years, many studies have highlighted the essential role of fines contents (≤ 0.074 mm) on the mechanical behaviour of sands. Researchers working on the steady state of saturated sands (e.g. Sladen et al., 1985; Been and Jefferies, 1985)

found that the position of the steady state line (*SSL*) could change when the specimens comprised different fines contents. Steady-state conditions in the $e - \ln p'$ space for Kogyuk 350 sand are shown in Figure 2-2. This figure shows the sensitivity of the location of the *SSL* to the fines contents. It can be seen that the density required for a given steady-state shear strength is much lower for a clean sand than for a silty sand.

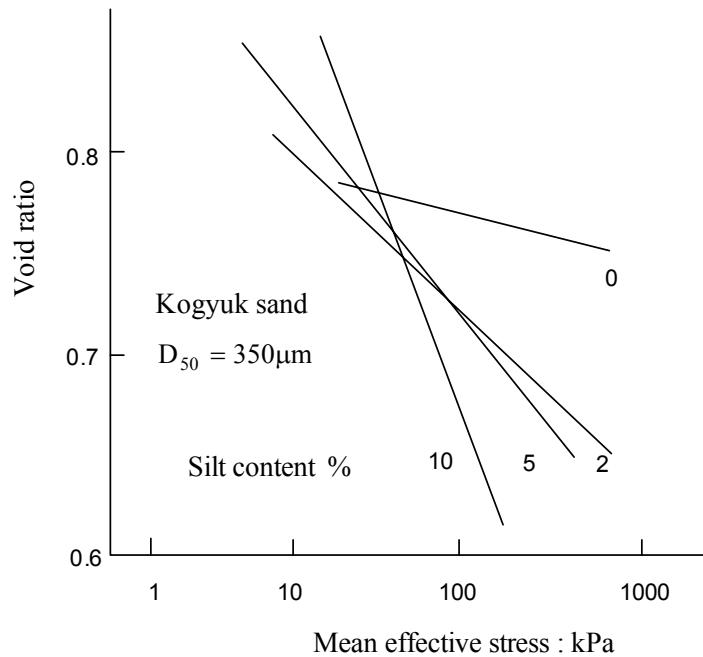


Figure 2-2. Effect of fines content on position of the *SSL* (Been and Jefferies, 1985).

Particle shape

The particle shape is normally described in terms of angularity and roundness. Elongated and platy particles can develop preferred orientations, which may be responsible for anisotropic properties of the specimen. The stress-strain and strength properties are also influenced by the surface texture of the particles of sands. Figure 2-3 illustrates the different particle shapes found in sand together with clay platelets.

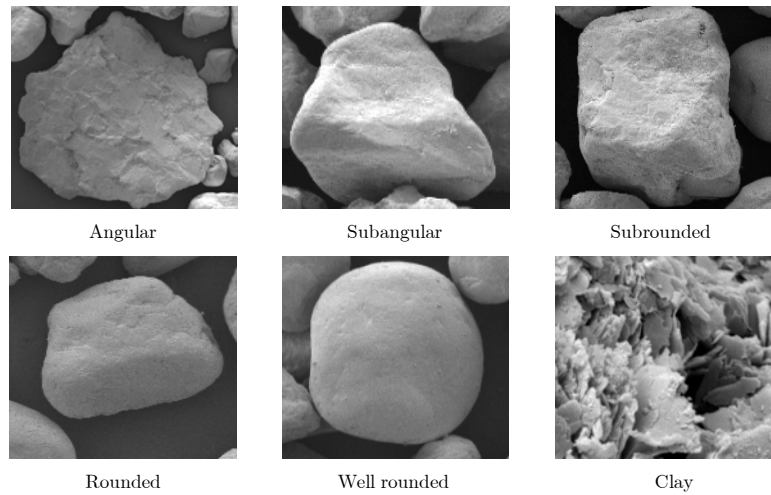


Figure 2-3. Characterisation of particle shapes of sands and flake shapes of clays
(Microphotograph of Portaway sand).

Mineralogy

Sands are predominantly rock fragments or mineral grains of common rock-forming minerals. The most abundant mineral is quartz. Calcareous (or carbonate) sediments are widely distributed in oceans and in the tropical and temperate regions of the world. They can occur as bulky particles, shells, precipitates or in solution. Feldspars are silicate minerals and are easily broken down. It has been observed by some researchers (Koerner, 1970; Lee, 1966) that the critical state friction angles are higher for felspathic sand than that for quartz sand. Bolton (1986) also found that the critical state friction angles and crushing are linked to the presence of substantial proportions of mica, calcite, limestone, chalk and other materials.

2.2.2.2 Structure

It is well known that the matrix structure is an important controlling factor for the mechanical behaviour of sands. In view of the literature, there is no unique definition for the structure of sands. The term 'structure' was first introduced for clays (Mitchell, 1976) and has since been described by Been et al. (1991) as being the arrangement of sand grains on a particulate scale. This includes a description of

particle contacts, their orientations and distribution, and cementation at the contacts. Been et al. referred to these descriptions as ‘fabric’ and used the term ‘anisotropy’ to refer to fabric anisotropy in which there exist unequal particle contacts and forces between particles in different directions. However, Verdugo (1992) excluded cementation at contact from the term ‘fabric’ given by Been et al. He defined it as the microstructure of a soil mass that involves only the orientation of individual particles and the distribution of normal contacts between particles. The structure of a soil mass defined by him includes the particle size, distribution of particle size, voids throughout the soil mass, interparticle forces and bonding between grains. Researchers working on natural sands (e.g. Cuccovillo and Coop, 1997, 1999) have used ‘structure’ to represent both bonding-dominated and fabric-dominated sands. They suggested that structure should be considered as an element of sands in addition to the intrinsic properties. An example to demonstrate the effect of bonding is shown in Figure 2-4. Cuccovillo and Coop (1999) found that when they compressed intact calcarenite isotropically, it reached a state which cannot be reached with reconstituted sands (see Figure 2-4 (a)). However, when the bonding became weaker, the yield points of the specimens were closer to the intrinsic *NCL* determined from reconstituted sands (see Figure 2-4 (b)).

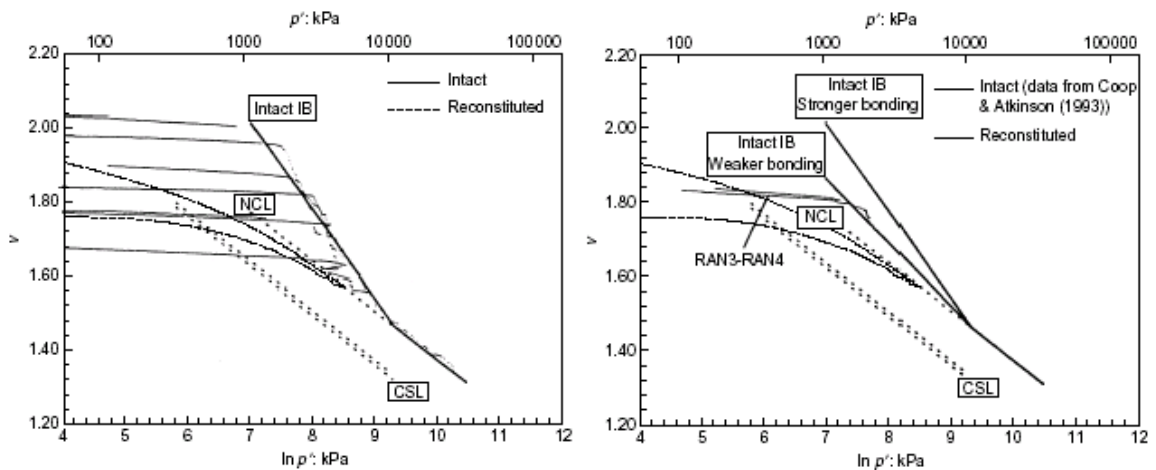


Figure 2-4. Isotropic compression of the calcarenite: (a) stronger-bounded samples, (b) weaker-bounded samples (Cuccovillo and Coop, 1999).

There is sufficient experimental evidence to suggest that by adopting different specimen preparation methods, the stress-strain curves may show marked differences (e.g. Oda, 1972; Mitchell, 1993). Figure 2-5 shows both drained and undrained triaxial tests on the same initial conditions (confining pressures and void ratios), but with different specimen preparation techniques. The observed differences may be attributed to the initial fabric of the sands. However, the absence of a practical method to quantify the packing arrangement of particles has led to a large number of conflicting conclusions from the different experimental techniques used for testing of sands (Been et al. 1992).

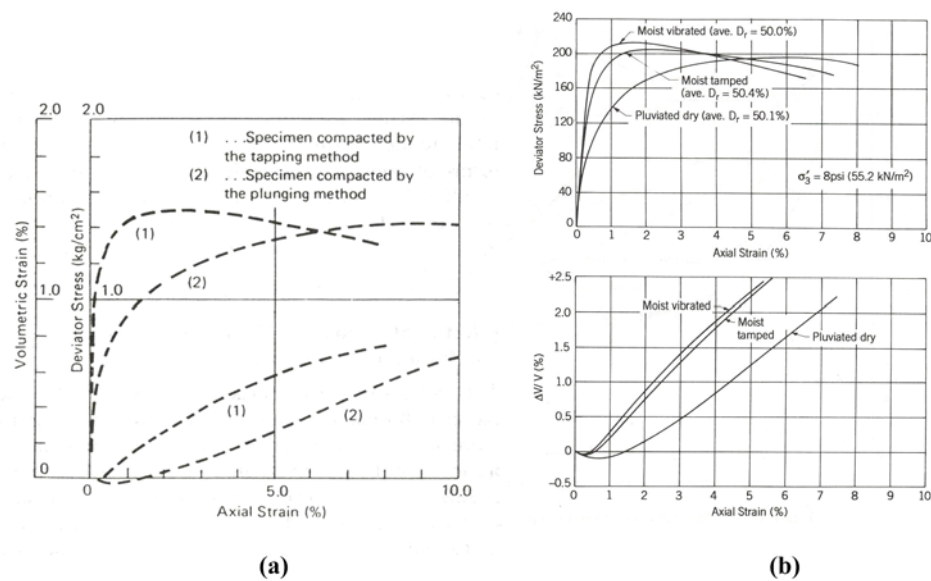


Figure 2-5. Influence of specimen preparation method on stress-strain-strength behaviour for sands: (a) drained tests (Oda, 1972), (b) undrained tests (Mitchell, 1993).

2.2.3 Shear Strength, Dilatancy and Critical State

Shear strength

The strength of sand is usually characterised by the peak friction angle ϕ_p , dilatancy angle ψ_m and critical state friction angle ϕ_c . In the absence of any bonds between the grains, the shear strength of sand can be defined by the Mohr-Coulomb failure criterion with zero cohesive intercept:

The stress-strain and strength characteristics of Portaway sand

$$\tau_f = \sigma_f \tan \phi_m \quad (2-1)$$

where τ_f is the shear stress at failure on the failure plane, σ_f is the normal stress on the failure plane and ϕ_m is the mobilised friction angle.

In triaxial testing condition, it is practical to write ϕ_m and ψ_m in terms of the effective principal stresses and strains:

$$\sin \phi_m = \frac{\frac{\sigma'_1}{\sigma'_3} - 1}{\frac{\sigma'_1}{\sigma'_3} + 1} \quad (2-2)$$

$$\sin \psi_m = \frac{\delta\varepsilon_1 + 2\delta\varepsilon_3}{\delta\varepsilon_1 - 2\delta\varepsilon_3} \quad (2-3)$$

where σ'_1 and σ'_3 denote the effective principal major and minor stresses respectively. $\delta\varepsilon_1$ and $\delta\varepsilon_3$ are the principal major and minor strain increments respectively. Assuming compressive stresses and strains as positive, the two stress variables, the so-called mean normal effective stress and deviatoric stress that are normally used in the critical state soil mechanics are defined as follows, with the triaxial condition in which $\sigma'_2 = \sigma'_3$:

$$p' = \frac{\sigma'_1 + \sigma'_2 + \sigma'_3}{3} = \frac{\sigma'_1 + 2\sigma'_3}{3} \quad (2-4)$$

$$q = \sqrt{\left[(\sigma'_1 - \sigma'_2)^2 + (\sigma'_2 - \sigma'_3)^2 + (\sigma'_3 - \sigma'_1)^2 \right] / 2} = \sigma'_1 - \sigma'_3 \quad (2-5)$$

Where σ'_2 denotes the effective principal intermediate stress. Corresponding to the stress parameters p' and q are the strain parameters ε_p (volumetric strain) and ε_q (deviatoric strain):

$$\varepsilon_p = \varepsilon_1 + \varepsilon_2 + \varepsilon_3 = \varepsilon_1 + 2\varepsilon_3 \quad (2-6)$$

$$\varepsilon_q = \frac{2}{3}(\varepsilon_1 - \varepsilon_3) \quad (2-7)$$

where ε_1 and ε_3 denote the principal major and minor strains respectively. The deviatoric strain ε_q is defined in this way so that the work ΔW done by a small increment of straining can be expressed as:

$$\sigma'_1 \delta\varepsilon_1 + 2\sigma'_3 \delta\varepsilon_3 = q\delta\varepsilon_q + p'\delta\varepsilon_p \quad (2-8)$$

Dilatancy

A great deal of attention has been focused on the relationship between ϕ_m and ψ_m (e.g. Rowe, 1962; Bolton, 1986; Wood, 1990; Been et al., 1991). Rowe (1962) developed the well-known stress-dilatancy theory, which defined the relationship between stress ratio η and dilatancy rate d and is expressed as:

$$d = \frac{\delta\varepsilon_p^p}{\delta\varepsilon_q^p} = \frac{9(M - \eta)}{9 + 3M - 2M\eta} \quad (2-9)$$

where $\eta = q/p'$ and M is the slope of the *CSL* in the p' - q space which can be related to the critical state friction angle ϕ_c by:

$$M_c = \frac{6 \sin \phi_c}{3 - \sin \phi_c} \quad (2-10)$$

$$M_e = \frac{6 \sin \phi_c}{3 + \sin \phi_c} \quad (2-11)$$

where M_c and M_e are the slopes in compression and extension respectively.

From the equations above, it would be appropriate to expect $M_c > M_e$ if the critical state friction angle is constant in both compression and extension spaces. Rowe (1962) also proposed that for dense sands, the mobilised friction angle ϕ_m could be interpreted as the sum of the sliding resistance at contact (true friction angle ϕ_u), particle rearrangement and dilation as shown in Figure 2-6.

Bolton (1986) examined the strength and dilatancy of 17 sands from biaxial (plane-strain) and triaxial tests and proposed a very simple correlation between the

mobilised friction angle ϕ_m , critical state friction angle ϕ_c and mobilised dilatancy angle ψ_m , which he found to be operationally equivalent to:

$$\phi_m = \phi_c + 0.8\psi_m \quad (2-12)$$

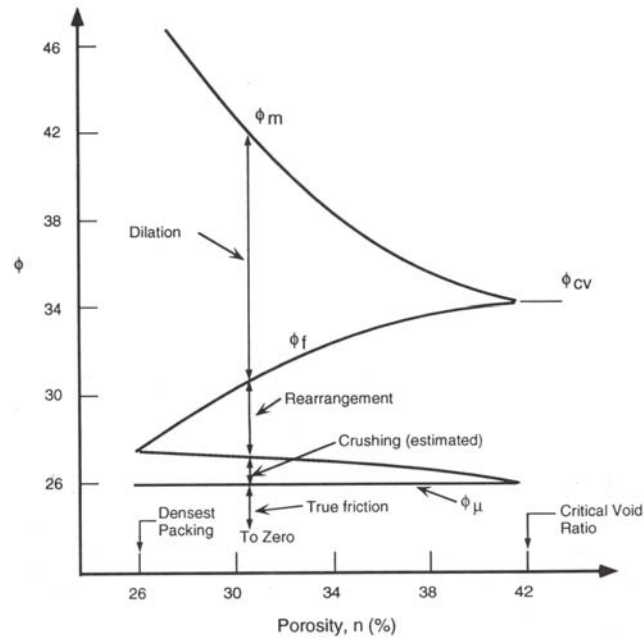


Figure 2-6. Contributions to the shear strength of granular soils (Mitchell 1993).

Bolton also introduced a parameter so-called relative dilatancy index I_R , which relates the density and applied stress level:

$$I_R = D_r(Q - \ln p') - R \quad (2-13)$$

He found that $Q = 10$ and $R = 1$ give the best fit for various sands and I_R can be used to correlate peak frictional angle ϕ_p and maximum rate of dilatancy $(\delta\varepsilon_p/\delta\varepsilon_1)_{\max}$ by:

$$\phi_p = \phi_c + 3I_R \quad (2-14)$$

$$I_R = -\frac{10}{3} \left(\frac{\delta\varepsilon_p}{\delta\varepsilon_1} \right)_{\max} \quad (2-15)$$

Critical state

Clearly, the critical state theory has increasingly become one of the most widely used fundamental concepts in interpreting the behaviour of soils since the pioneering work of Roscoe et al. (1958).

The critical state is an ultimate condition where all soils during shear will eventually attain a unique stress ratio M or critical state friction angle ϕ_c and reach a critical void ratio e_c . This condition can be formulated as:

$$\frac{\delta p'}{\delta \varepsilon_q} = \frac{\delta q}{\delta \varepsilon_q} = \frac{\delta \nu}{\delta \varepsilon_q} = 0 \quad (2-16)$$

The progress of a soil specimen during a drained tests can be represented by a series of points describing a path in a three dimensional space with axes p' , q and ν . When the critical state is reached, the critical states for a given soil form a unique line in the p' - q - ν space referred to as the *CSL*, which has the following equations:

$$q = Mp' \quad (2-17)$$

$$\nu = \Gamma - \lambda \ln p' \quad (2-18)$$

where M , Γ and λ are soil constants.

Normal consolidation line

For isotropic stress conditions (e.g. $q = 0$), the plastic compression of a normally consolidated soil can be represented by a unique line called the isotropic normal compression line (*NCL*), which takes the following form:

$$\nu = N - \lambda \ln p' \quad (2-19)$$

where N is the specific volume of isotropically normally consolidated soil at $p' = 1$ kN.

Unlike clays, the measurement of the *NCL* for sands is difficult and can only be achieved by compressing sands to high pressures. Coop and Lee (1993) investigated three diverse granular materials over a wide range of stresses (50 kPa–58 MPa). They concluded that the *NCL* resulted from crushing of the sand particles. The stress level at which this breakage starts and the *NCL* is encountered depends on both the strength of sand particles and the density of sands.

Steady, quasi-steady and phase transformation states

Poulos (1981) defined the steady state as a state at which soil mass is continually deforming at constant volume, constant normal effective stress, constant shear stress and constant velocity.

The definition of the steady state, quasi-steady state and phase transformation state is shown in Figure 2-7. It can be seen that the steady state corresponds to a state of residual undrained strength at ‘C’ following a peak at ‘B’. The state of transient minimum strength at ‘A’ corresponds to the phase transformation state (Ishihara et al. 1975).

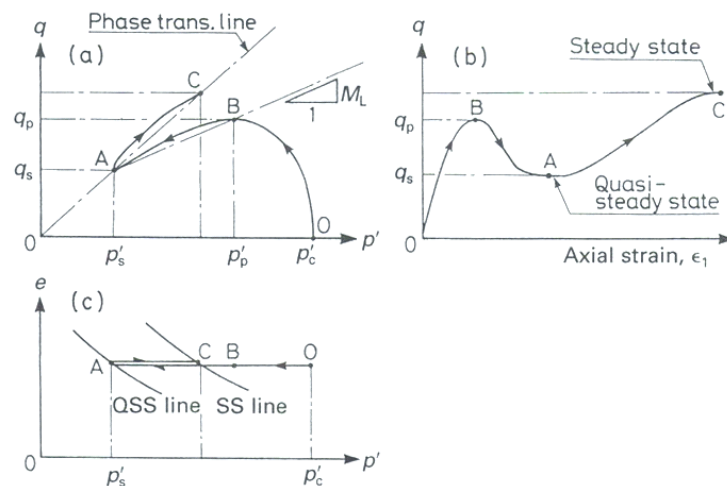


Figure 2-7. The definition of various states of sand subject to undrained loading (Ishihara, 1996).

Experimental evidence suggests that a single line in the p' – q plot (Figure 2-7) would exist for steady state and phase transformation state, named as the *SSL* and

phase transformation line respectively. This implies that the friction angle at steady state and phase transformation state has a unique value. However, in the $e - p'$ or $\nu - p'$ space, the state 'A' (Figure 2-7 (c)) cannot be regarded as a steady state and therefore is termed as the 'quasi steady state'.

In recent years, researchers have increasingly focused on identifying the critical and steady state lines for various sands. It is surprising that many divergent conclusions have appeared in the geotechnical literature accumulated from various sands.

Early experimental researches on clays (Roscoe et al., 1958) and sands (Stroud, 1971) supported the concept that, for a given soil, the stresses existing at the critical state were solely a function of the soil's density. It has been seen that a growing number of researchers re-examined such fundamental properties of sands by using more advanced testing facilities and interpretation methods. A partial list of those presenting important data on the subject includes (alphabetically) Been et al. (1991), Castro (1975), Chu (1995), Hird and Hassona (1990), Ishihara (1993, 1996), Klotz and Coop (2002), Kolymbas and Wu (1990), Poulos (1981), Riemer and Seed (1997), Sladen et al. (1985), Tatsuoka et al. (1986), Vaid et al. (1990) and Vasquez and Dobry (1988).

In a classical paper by Been and his co-workers (1991), the critical state of sands has been examined by carrying out extensive triaxial tests on Erksak sands. Figure 2-8 shows a unique *CSL* does exist for Erksak 330/0.7 sand regardless of the specimen preparation method, drainage, initial condition and stress path effects. However, the conflicting experimental results obtained by Poulos (1981), Vaid et al. (1990), Hird and Hassona (1990) among others suggested that the *CSL* and *SSL* were not unique but stress path dependent. The results from Vasquez and Dobry (1988) and Verdugo et al. (1989) indicated that the effects of specimen preparation method and aging might affect the location of the *CSL* or *SSL*. The effects of consolidation stress (Konrad, 1990), drainage conditions (Alarcon-Guzman et al., 1988) and loading modes (Riemer and Seed, 1997) have been identified as additional factors that may significantly affect the position of the *CSL* or *SSL*.

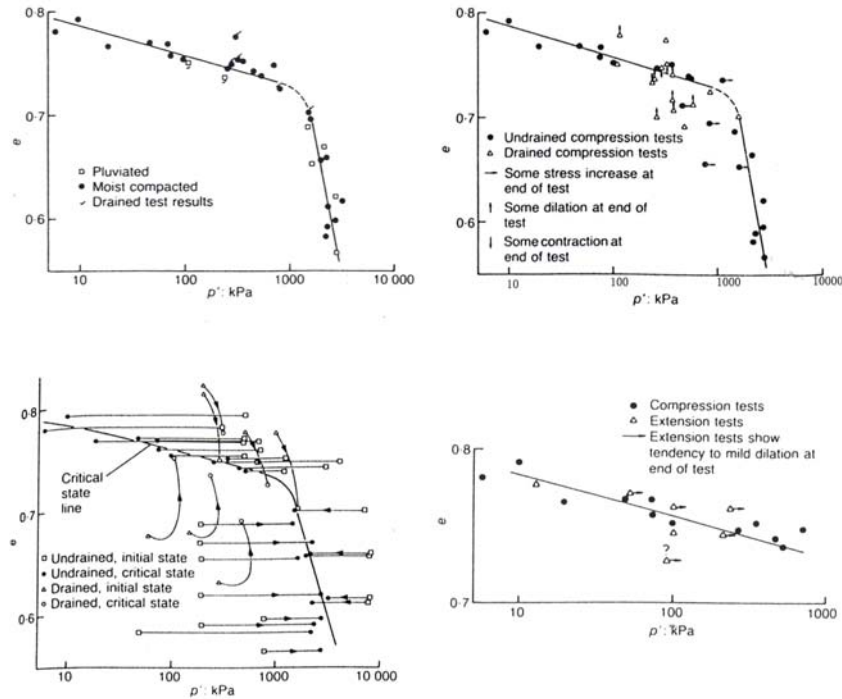


Figure 2-8. A unique critical state line for Erksak 330/0.7 sand (Been et al., 1991).

The propositions that the critical state friction angle ϕ_c is a function of density by Been et al. (1991) and stress level dependent by Chu (1995) have been questioned by other researchers. Experimental results obtained from Verdugo and Ishihara (1991) and Tatsuoka et al. (1986) suggested that a unique ϕ_c existed and was not affected by void ratios and stress levels.

Chu (1995) questioned whether the critical state parameters of dense sands could be measured by conventional drained and undrained triaxial testing. He suggested that significant non-homogeneous deformation might develop within the specimens prior to the achievement of the critical state so that the observed strain softening was not a material behaviour. Klotz and Coop (2002) used both global and local measurements on dense sands and revealed that identifying critical state could be handicapped by strain localisation and barrelling of specimens.

A strain path testing technique has been developed by Chu et al. (1992) in order to measure the critical state of dense sands in the homogeneous deformation region. However, their testing techniques seem too complicated to be used in the majority

of geotechnical laboratories. Been et al. (1992) argued that such non-homogeneous deformation might be a fundamental aspect of the sands, which has been theoretically predicated by the plasticity theory (Drucker's stability postulate) under work softening condition.

As reviewed above, it is difficult to assess the different influencing factors on the critical (or steady) state by comparing different testing programs and different types of sands. In light of these unresolved issues, the present research was motivated to carry out a systematic testing program and to evaluate the validity of the critical state theory on Portaway sand.

2.2.4 State Parameter Concept

Roscoe and Poorooshasb (1963) first proposed the fundamental principle of similarity of soils during shear. They suggested that any two specimens of soil would behave in a similar manner provided the difference between the initial void ratio e and the void ratio at critical state e_c at the same mean effective stress are the same for each specimen. Later, Wroth and Bassett (1965) used this concept in the development of a stress-strain relationship for sands. After 20 years, Been and Jefferies (1985) defined the state parameter ξ based on their extensive triaxial testing results on sands. They demonstrated that the state parameter was a very useful normalising parameter for characterising sand behaviour.

The state parameter concept has also been successfully used to develop constitutive models for sands (e.g. Jefferies, 1993; Yu, 1998) and to interpret the data from in-situ tests (Yu, 1994, 1996). This parameter combines the influences of density and confining pressure on sands in a unique way as shown in Figure 2-9, which can be formulated as:

$$\xi = \nu + \lambda \ln p' - \Gamma \quad (2-20)$$

where $\nu = 1 + e$ is known as the specific volume and e is the void ratio. The state parameter is a measure of how far the soil state is from the critical state in terms of density. It is noted that ξ is zero at the critical state, positive on the loose state and negative on the dense state.

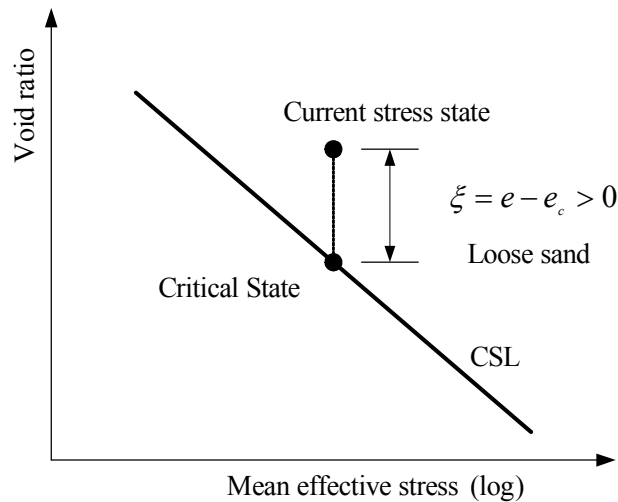


Figure 2-9. Definition of the state parameter ξ .

Yu (1998) compared the roles of over consolidation ratio (OCR) and state parameter ξ for developing a unified clay and sand model. As noted by him, the role of the OCR in sands is less clear, mainly because the preconsolidation pressure can only be determined accurately at high pressures. Since the state parameter ξ may be determined easily for both clay and sand, it is regarded as a better quantity than OCR for describing soil response under various loading conditions.

2.2.5 Behaviour Subjected to Monotonic Loading

In this section, constitutive behaviour of sands subjected to monotonic loading is briefly described. Unlike many other materials, the behaviour of sands is in general dependent on the effective stress history, stress path and fabric. The stress and/or strain path loading are normally used to characterise the stress-strain and strength characteristics of soils using triaxial apparatus. Therefore, it is necessary to review and compare some recently developed experimental techniques. A rather extensive

review of recent developments in triaxial testing systems for cohesionless soils can be found in the paper by Tatsuoka (1988).

2.2.5.1 Stress and strain paths

Stress path and/or strain path controlled methods are commonly used in the laboratory testing. It allows the probing stress or strain increments to be applied in any direction and to investigate the stress history and stress path dependent response. The conventional drained triaxial compression corresponds to a controlled stress path test with a linear path when $\delta\sigma'_3 = 0$. For conventional undrained compression test, the loading mechanism is rather a strain path-controlled type, which corresponds to the linear path with $\delta\varepsilon_p = 0$. Axial symmetric stress paths have just two degrees of freedom: an major principal stress σ'_1 and a minor principal stress σ'_3 . It has been convenient to display triaxial stress paths in terms of the mean effective stress p' and deviatoric stress q to emphasise the distinction between volumetric and distortional components of stress.

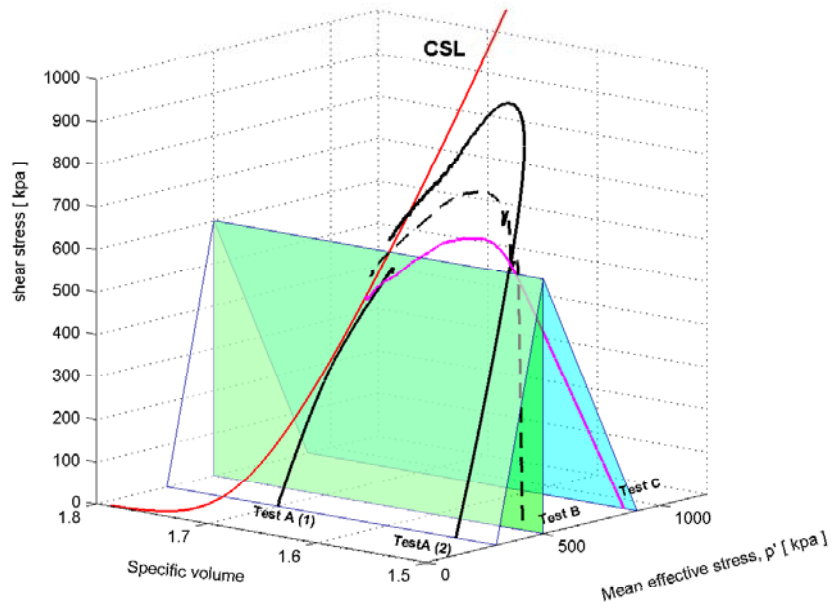
Stress path method

The stress path method originally described by Lambe (1967) was used to predict the settlement of foundations. Since then, this method has become a powerful tool for both practising engineers and researchers. Figure 2-10 (a) shows the typical drained stress paths in the $p'-q-\nu$ space. Test A is the most commonly performed triaxial test, in which the cell pressure σ_3 is held constant and the axial load is increased. This type of test is termed as the 'conventional triaxial test'.

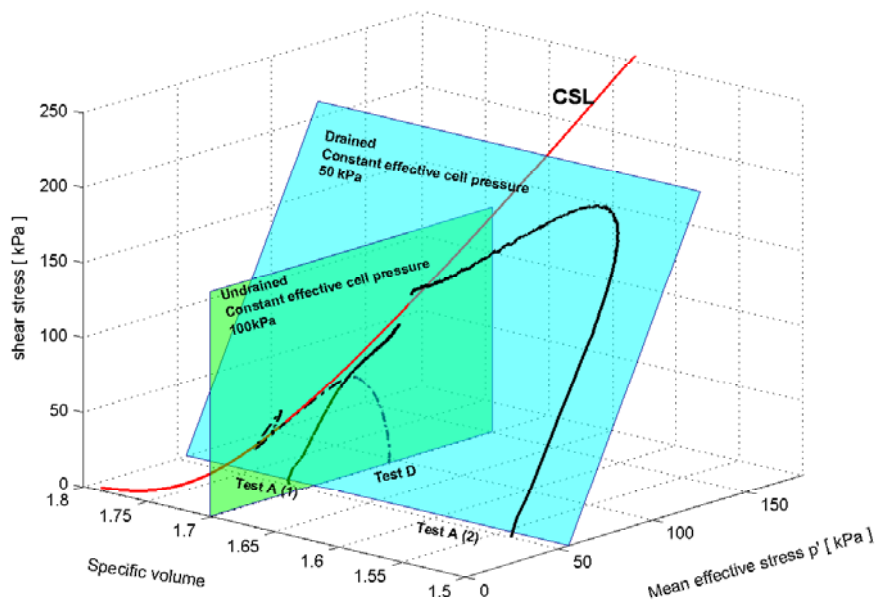
Strain path method

Test D shown in Figure 2-10 (b) is a typical undrained test on loose sand, in which the effective stress path experienced by the soil element cannot be positively controlled. Chu and Leong (2001) and Vaid et al. (2001) regarded such a test as a

special case of strain-path testing. A strain-path is defined as the strain increment ratio $\delta\varepsilon_p/\delta\varepsilon_1$. An undrained condition corresponds to $\delta\varepsilon_p/\delta\varepsilon_1 = 0$.



(a)



(b)

Figure 2-10. Effective stress paths for triaxial compression tests.

2.2.5.2 Drained monotonic loading

Yielding of sands

The determination of a yield surface for sands in their in-situ condition is not feasible due to disturbances of the particle structure. Most experimental works on identifying yield surfaces of sands are focused on reconstituted sands. A series of stress paths used by Tatsuoka and Ishihara (1974a) for this purpose are illustrated in Figure 2-11.

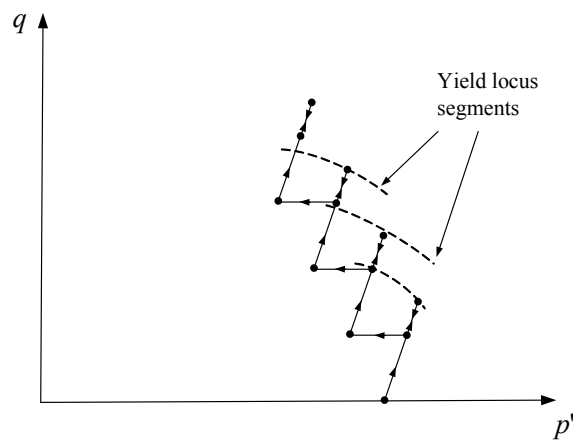


Figure 2-11. Stress path test used to identify yield envelope in triaxial apparatus (modified from Tatsuoka and Ishihara, 1974a).

It has been observed by Tatsuoka and Ishihara (1974a) among other researchers (e.g. Sladen et al., 1985; Coop, 1990) that for many sands, the critical state point occurs to the left of the peak yield locus in the $q - p'$ space. Chandler (1985) theoretically predicted this feature using an energy-based plasticity theory that allowed for volume changes due to particle deformation and particle rearrangement.

Compression of sands

The unique *NCL* has been generally accepted as an intrinsic property for clays while the validity of this concept for sands is still in debate. Generally speaking, there are two concepts on the *NCL* which were examined by Jefferies and Been (2000):

- A *NCL* exists and can only be reached when particle breakage becomes prevalent at high pressure.
- A number of *NCLs* exists that is unrelated to particle breakage.

Most critical state soil models are based on the first assumption and assume that the *CSL* is parallel to the *NCL*. Wroth and Houlsby (1985) referred to a term called ‘spacing ratio’ to define the distance between the *CSL* and the *NCL*. With the availability of high pressure triaxial apparatus, Coop (1990) and Coop and Lee (1993) verified this assumption.

Jefferies and Been (2000) questioned the unique *NCL* concept and revealed that there might be a number of *NCLs* regardless of the stress level on Erksak sand. Therefore, they pointed out that the use of the state parameter ξ as a variable had much advantage over *OCR* for sands.

Stress-strain and strength characteristics

The drained strength characteristics of sands were investigated by Lee and Seed (1967) by carrying out a series of conventional triaxial tests on Sacramento River sand. They confirmed Rowe’s theory that the drained shearing resistance of sands might be controlled by three components: sliding friction, dilatancy and particle crushing (see Figure 2-6). Lee and Seed (1967) also concluded that the stress-strain relation of sands was governed by both the densities and confining pressure applied. However, due to the limitations of their apparatus, the stress-strain and strength characteristics could only be studied in limited stress paths. Many studies have highlighted the essential role of the stress path history to the strength, dilatancy and stress-strain relation on sands. Particularly, Tatsuoka and Ishihara (1973) studied the relation between stress path and dilatancy performance. Lade and Duncan (1976) investigated the stress path dependent behaviour. Vaid and Sasitharan (1992) evaluated the correlation between peak friction angle and dilatancy along various loading directions.

2.2.5.3 Undrained monotonic loading

The undrained behaviour of sands has received much attention recently, in particular on instability of very loose sands. The continuous generation of excess pore pressure and occurrence of a large reduction of strength are normally observed in this type of tests. The term ‘static liquefaction’ is used widely to describe this particular behaviour (Castro, 1969; Poulos, 1981; Sladen et al., 1985; Ishihara, 1993; Yamamuro and Lade, 1997).

The mechanism that triggers the instability can be explained in many different ways. Among these, two approaches are commonly used to interpret the location of the occurrence of static liquefaction in the $q - p'$ space:

- *Collapse line* (Sladen et al., 1985): the locus of points triggering liquefactions is a straight line that passes through the *steady-state* point with the same void ratio at different confining pressures.
- *Instability line* (Lade et al., 1988) or *flow liquefaction line* (Vaid et al., 1990): the locus of points triggering liquefactions is a straight line that passes through the *origin* point and is regardless of stress path, initial void ratio and confining pressure.

Based on some published data on various sands, Yang (2002) found that the concept of uniqueness of the flow liquefaction line was not valid. Instead, he proposed a new interpreting method, in which the flow liquefaction lines varied with the state of the sands. This correlated the initial state parameter ξ_0 and stress ratio η_{peak} at the point of triggering liquefaction. However, the validity of this approach needs further examination by using more high quality experimental data, which is discussed in more detail in Chapter 4.

2.2.6 Behaviour Subjected to Cyclic Loading

The cyclic behaviour of soils has been investigated extensively during the last four decades. Among the various approaches, research work can generally be divided into two groups. The first is focused on studying the overall behaviour of soils subjected to cyclic loading. The resilient and permanent deformations of soils are studied by conducting several thousands of cycles, while less attention is paid to the stress-strain and strength characteristics of each single cycle. Work in this area, such as the research undertaken at the University of Nottingham on the characterisation of unbound granular material is reviewed in section 2.3.

The second group of work examines the mechanism of soil deformations by investigating the stress-strain and strength characteristics during each cycle. The constitutive models are formulated based on rigorous elastic-plastic theory. The literature survey conducted herein is mainly based on the latter.

2.2.6.1 Terminology used in cyclic loading tests

To avoid confusion in the use of terminology, a brief review on some key definitions and terms commonly used in cyclic loading testing is considered necessary and is given in following.

Definition of cyclic loading

In view of the literature, no unique definition for ‘cyclic loading’ exists. The triaxial tests for studying non-monotonic behaviour are commonly referred to as ‘repeated load’ or ‘cyclic load’ triaxial tests. Sweere (1990) stated that in classical soil mechanics, the term ‘repeated load’ was used to denote triaxial tests with only a few stress repetitions and the term ‘cyclic loading’ was generally used with tests up to one million load applications. O’Reilly and Brown (1991) extended the scope of the term ‘cyclic loading’ to cover all repetitious loading experienced by soils such as

foundation resonance, earthquake transient loading and even vibration, which is high-frequency dynamic loading.

The cyclic triaxial tests with slow loading rate and a few loading numbers are generally used to develop and verify elastic-plastic models (Wood, 1982). The main reason is that one can be certain of the reliability of the measured pore water pressure and the experimental data is more likely to provide useful information for the development of constitutive models. Hence, in this thesis, the cyclic triaxial tests carried out and associated interpretations specifically refer to this type of loading condition.

Elastic and plastic deformations vs. resilient and permanent deformations

In monotonic loading condition, the behaviour of soils is conveniently characterised by elastic and plastic strains. Equivalently, during cyclic loading as shown in Figure 2-12, the recoverable strain for one loading and unloading loop is termed as ‘resilient deformation’. The accumulated non-recoverable strain after a few cycles is denoted as ‘permanent strain’.

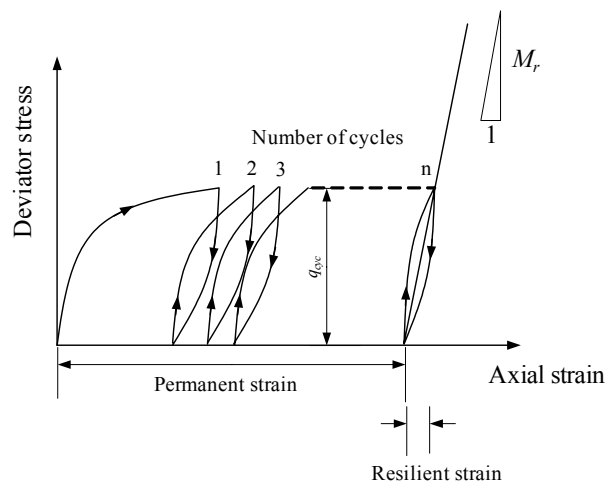


Figure 2-12. Definition of permanent strain, resilient strain and calculation of resilient modulus.

The resilient modulus M_r is defined as the instant stiffness of a specimen during each cycle and is commonly used as an input parameter for structural analysis. In pavement engineering, M_r is typically obtained after a large numbers of load

applications on pavement base materials. However, the resilient modulus was also used by many other researchers (e.g. Mcvay and Taesiri, 1985) on sands for limited numbers of load applications.

2.2.6.2 Drained cyclic loading

Experimental results for Fuji River sand subjected to one-way and two-way loading may be taken as typical cyclic behaviour of loose sands as shown in Figure 2-13 and Figure 2-14. It is not the intention here to describe every aspect of those tests. Rather, the common features observed in drained cyclic loading tests are mentioned.

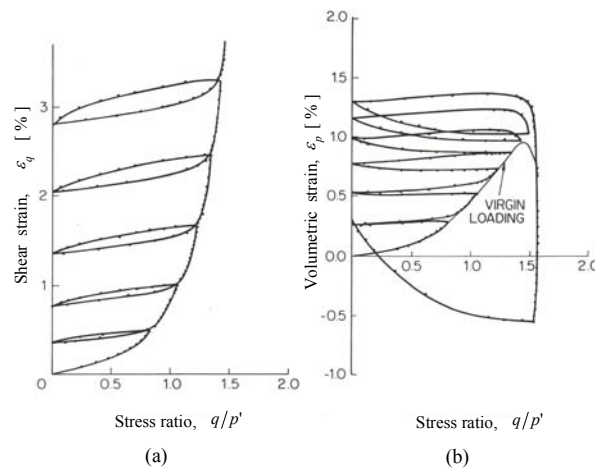


Figure 2-13. Drained one-way cyclic triaxial test (Wood, 1982, data obtained from Tatsuoka, 1972).

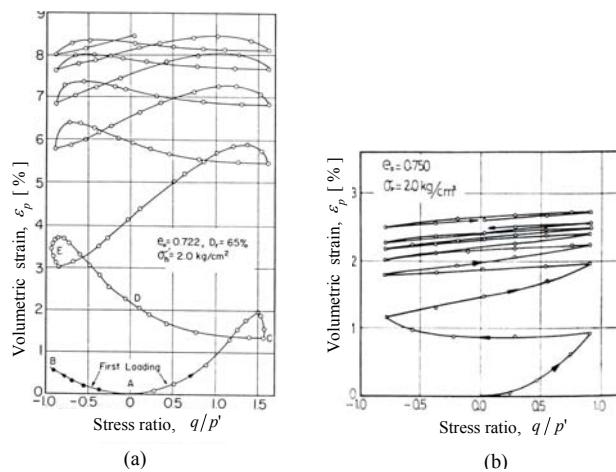


Figure 2-14. Drained two-way cyclic triaxial test (Tatsuoka and Ishihara, 1974b).

Hysteretic stress-strain curve

It can be seen from Figure 2-13 and Figure 2-14, the response of strains always lags behind the applied stresses, which is termed 'hysteretic loop'. The energy is dissipated through the hysteretic loop of each cycle. When shear strain is approximately within the range 10^{-3} – 10^{-10} % (small strain), the stress-strain relation of sands can be modelled with the damping ratio and shear modulus, such as the models used in earthquake engineering (Ishihara, 1996).

Incremental collapse and shakedown

The accumulated irrecoverable deformation is another main feature of the behaviour of a given sand. However, a distinct difference can be found in Figure 2-14 when two specimens were tested in approximately the same conditions except the cyclic amplitudes. The response of the specimen in Figure 2-14 (a) shows an incremental collapse with a relatively large cyclic stress. However, the ultimate response is nearly elastic for the other specimen (see Figure 2-14 (b)) after a number of cycles and this is known as 'shakedown'.

Wroth and Houlsby (1985) stated that:

'In drained tests, cycling to stress ratios higher than the characteristic state resulted in dilation of sand, a loss of strength and stiffness, and increasing strains, i.e. to incremental collapse. Low stress ratio cycling results in compaction of the sand, a gain of strength and stiffness, and shakedown to elastic conditions'.

The deformation characteristics of sands subjected to reversal of triaxial to extension or vice versa were also investigated by Arthur (1971) and Thurairajah (1973). The findings in their experimental works indicated that there might be a 'threshold' cyclic stress amplitude. Whether the stress path (or history) affects the deformation characteristics of sands or not depends on the imposed cyclic stress amplitude.

Effect of stress path

Figure 2-15 illustrates the influence of stress path on the behaviour of sands ($D_r = 95\%$, dry sand) subjected to cyclic moving wheel loads (Mcvay and Taesiri, 1985). The first stress path (CD), commonly used in characterising the resilient modulus of pavement base materials, involves only the positive deviatoric stress $+q$. The second stress path (ABCD), referred to as the moving wheel stress path, has a 90° jump rotation in the principal planes (from compression to extension). The stress-strain curves of these two stress paths are shown in Figure 2-15 (a) and (b), respectively. It can be seen that greater cyclic permanent strain and lower resilient modulus were produced in path ABCD than in path CD. Based on a series of cyclic triaxial tests, Mcvay and Taesiri (1985) concluded that the influence of past stress history on the cyclic response diminishes as the initial confining pressure applied to the specimen increases.

2.2.6.3 Undrained cyclic loading

Recent research on undrained cyclic loading has revolved around the resistance of sands to liquefaction, whereby very loose sands experience a large reduction in their undrained strength. This topic has been treated comprehensively by Ishihara (1993, 1996).

As with the drained condition, the behaviour of sands in the undrained condition is far too complex to be represented solely by the confining pressure and density. For example, the different consolidation history may have a profound effect on sands during shear although their pre-shearing conditions are nearly identical. Other factors, such as the pre-shearing history, specimen preparation method and stress path would have various degrees of influence on the behaviour of sands.

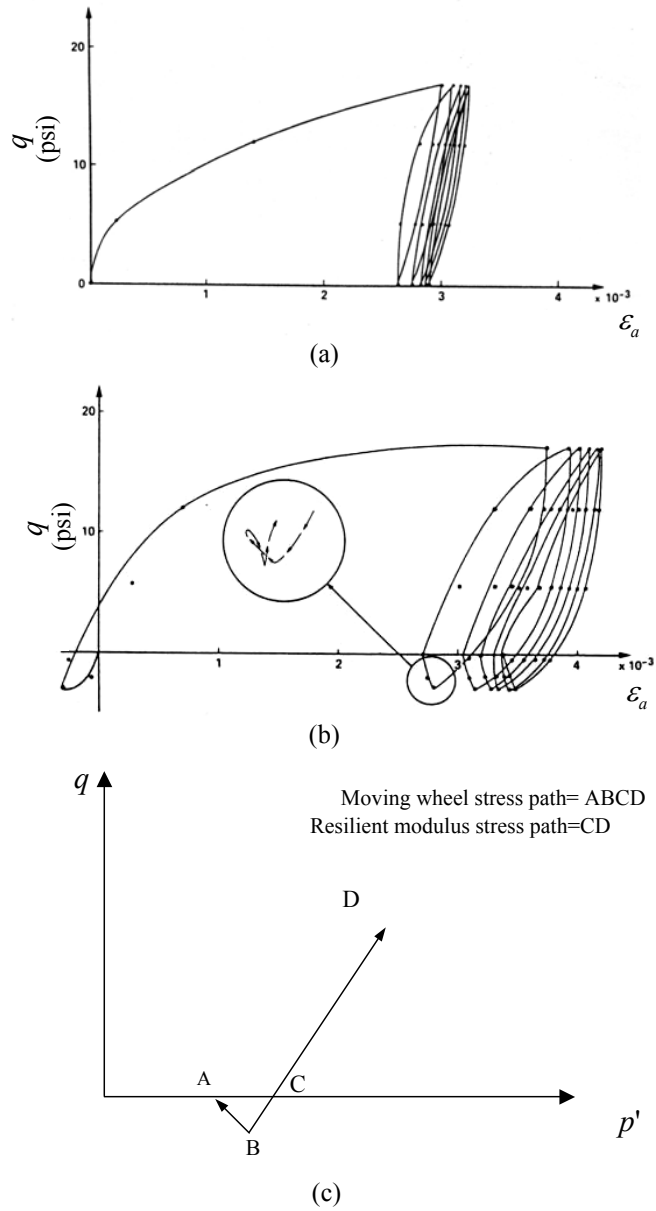


Figure 2-15. Comparison of stress-strain response of Fairbank's sand undergoing two type of stress paths: (a) resilient modulus stress path CD, (b) moving wheel stress path ABCD, (c) stress paths in the $q - p'$ space (McVay and Taesiri, 1985).

2.3 PREVIOUS TRIAXIAL TESTING AT THE UNIVERSITY OF NOTTINGHAM

The purpose of this section is to examine the various testing and interpreting techniques available at the University of Nottingham for analysing the behaviour of granular materials under monotonic and cyclic loading. Although previous research works have focused on cyclic loading behaviours of clays (Brown, 1967), silt-clays (Raybould, 1992) and pavement base materials (Shaw, 1980), some of the facilities and methods have been modified for the current research work on Portaway sand.

In order to reproduce the field situation, the Simple Shear Apparatus (SSA) (Shaw and Brown, 1986), Hollow Cylinder Apparatus (HCA) (Chan and Brown, 1994; Richardson, 1999) and Nottingham Dynamic Triaxial Testing System (NDTTS) (Brown et al., 1980; Raybould, 1992) have been developed at the University of Nottingham. Detailed descriptions of these were given by Brown (1996) in the 36th Rankine Lecture on the soil mechanics in pavement engineering.

After an initial appraisal, a few modifications to apparatus and specimen preparation methods were made and will be described in Chapter 3. The preliminary tests on dry Leighton Buzzard sand and Portaway sand were carried out on updated NDTTS and will be described in Chapter 4.

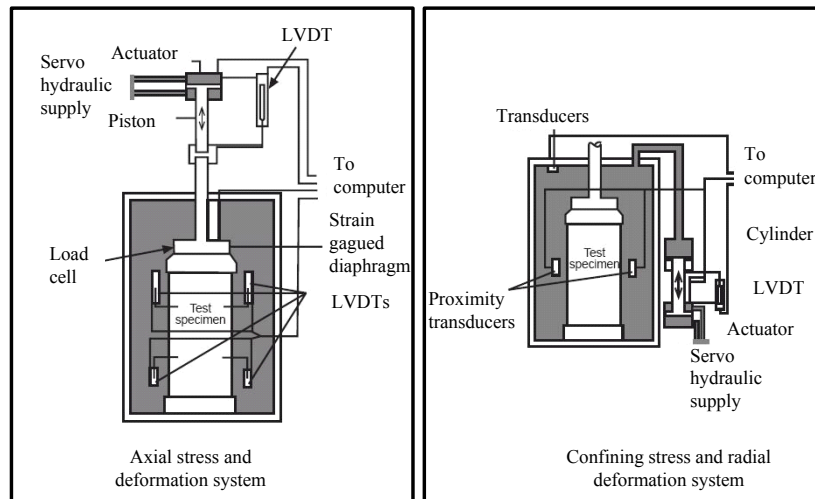
2.3.1 Experimental Techniques

The development of cyclic loading triaxial apparatus for soil testing at Nottingham University has a long history since the 1960s. Two types of testing systems are currently available: one for testing unbound granular materials (150 mm in diameter) with particle sizes up to 30 mm, another is for testing silts and clays (50 mm in diameter). With emphasis on the testing of granular materials, the apparatus, the specimen preparation methods and the stress-strain-strength measurement techniques are briefly reviewed in this section.

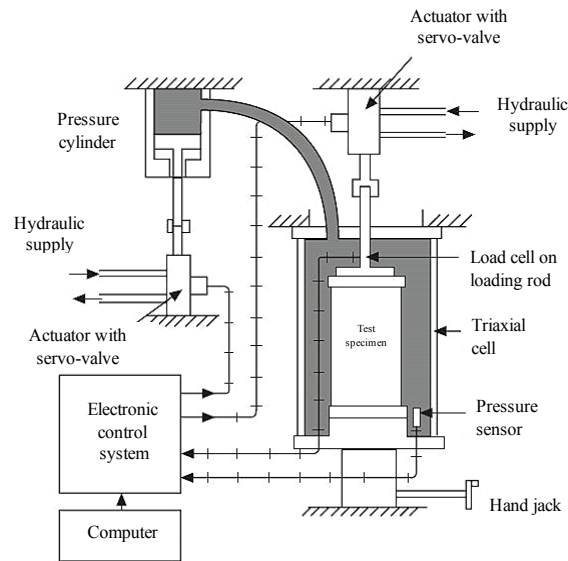
2.3.1.1 Apparatus

The schematics of two triaxial systems are shown in Figure 2-16. Both of them are driven by servo-hydraulic equipments, which send a ‘command’ signal to drive an actuator, the movement of which is monitored by a ‘feedback’ transducer (Load cell or external LVDT). The command output and feedback input are compared and the differences is amplified, and then, transmitted to an electro-mechanical control device. This device is a servo-valve, which uses the electrical error signal to move a shuttle valve, which in turn directs high-pressure oil to a piston within a cylinder. The piston moves to reduce the error so that the command signal in the form of a dynamic or monotonic load is maintained. The triaxial cell used for the testing silts and clays (Figure 2-16 (a)) is comprised of three parts:

- An aluminium cell top;
- A perspex cell wall;
- An epoxy resin base.



(a)



(b)

Figure 2-16. Schematic of Nottingham triaxial facilities: (a) testing of clay and silt (Raybould, 1992), (b) testing of unbound granular materials (Brown, 1996).

Figure 2-16 (b) shows the triaxial cell for testing unbound granular materials. To accommodate the 150 mm diameter specimens, the triaxial cell was constructed primarily from aluminium alloy and sealed outlets were incorporated in the base for 49 electrical terminals and 4 pressure or vacuum lines.

For conventional drained and undrained tests (constant cell pressure), both cells can withstand a pressure of 1000 kPa by compression of air. To apply versatile stress paths, the confining pressures are varied by compression of silicone oil. The control systems and transducers of both triaxial systems have been updated following the advancement of electronic technologies during the last 30 years.

2.3.1.2 Measurement instrumentations

For the accurate measurement of the stress-strain behaviour of soils, instrumentation capable of measuring strains to a resolution of 10^{-4} % is required. This degree of accuracy can be achieved only if the strains are measured internally within the triaxial cell. In addition, the strains should be measured locally ('on-

specimen' measurement), away from the top cap and base pedestal and typically within the central one-third of the specimen. The axial displacement errors obtained from an external measuring device are illustrated in Figure 2-17 and are summarised as follows:

- Alignment errors result from equipment, specimen non-uniformity and from the end faces of the specimen being non-perpendicular to the vertical axis of symmetry.
- Seating errors are due to the closing of the gaps between ram, internal load cell and top cap, and between top cap or base pedestal and porous stones.
- Bedding errors are caused by lack of fit or surface irregularities or voids at the ends of the specimen.
- Tie bars, internal load cell, filter paper, porous stones, the loading system in the hydraulic triaxial apparatus, and lubricated ends can all cause errors.

In order to eliminate the errors outlined above, several 'on-specimen' measuring devices for both axial and radial measurements have been developed at the University of Nottingham. Table 2-1 gives a summary of the various devices developed for small strain measurements.

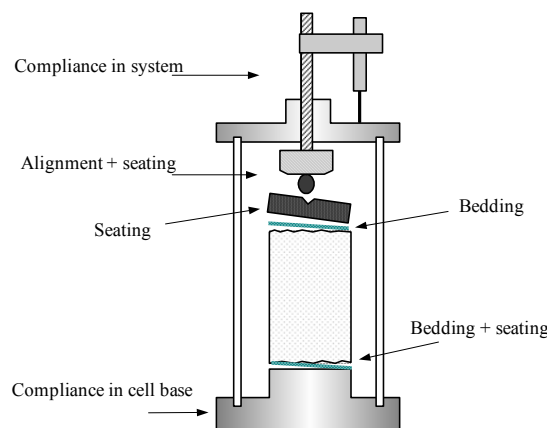


Figure 2-17. Source of errors in external axial deformation measurements.

Mounting method	Transducers	Description of the devices	Material tested	References
Circular split-sprung collars	LVDTs	The collars are circumferentially mounted against targets embedded in the specimen. The axial displacement of the targets is recorded by two diametrically opposite LVDTs. The purpose of the spring mechanism is to hold the collars in contact with the targets, while permitting radial deformation and maintaining alignment of the LVDT body and the core.	Clays	Brown and Snaith (1974)
Location stud	LVDTs Strain-gauged rings	By using a location stud, the LVDTs and strain-gauged rings are attached to the specimens to measure the axial strain and radial strain respectively (see Figure 2-18).	Granular materials	Boyce and Brown (1976); Brown et al. (1989)
'Glue on' block	LVDTs	The LVDTs are attached to the specimens by using adhesives.	Granular materials	Cheung (1994)
Holding frame	LVDTs	Four LVDTs are mounted on a frame secured to the base of the triaxial cell to measure the axial displacement.	Clays	Brown et al. (1980)
'Key in' stud	Strain gauges	The schematic of the device is shown in Figure 2-19, the active element being a strain gauged phosphor bronze strip on an assembly weighing just 26g. Measurements are made at diametrically opposite locations for axial displacement.	Clays	Cheung (1994)
Holding frame	Proximity transducers	The radial strain is measured by a non-contacting technique using proximity transducers.	Clays	Brown et al. (1980)

Table 2-1. Summary of small strain measuring devices developed at the University of Nottingham.

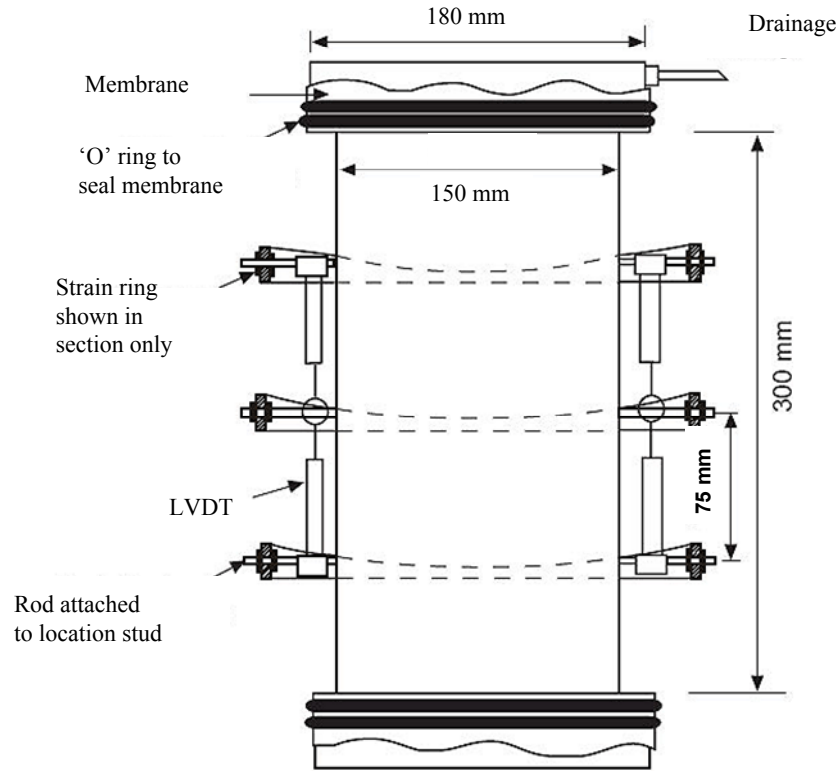


Figure 2-18. 'Location stud' technique for small strain measurement (Brown et al., 1989).

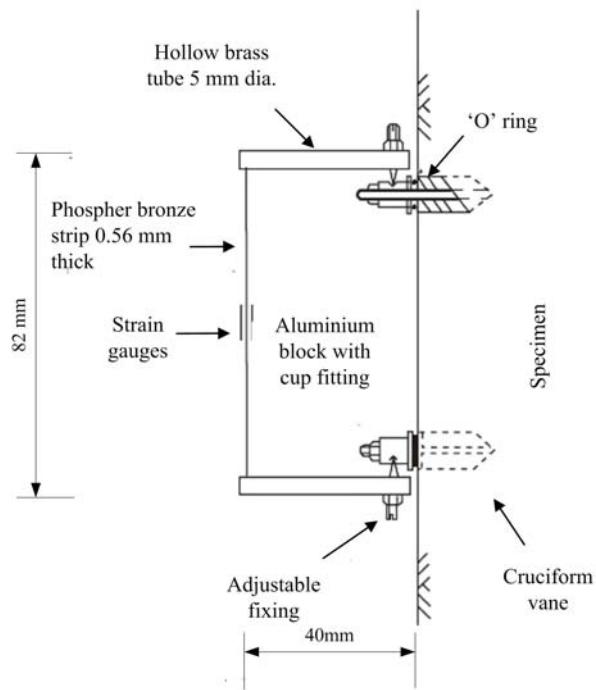


Figure 2-19. 'Key-in' technique for small strain measurement (Cheung, 1994).

2.3.1.3 Specimen preparations

Considerable research has been carried out on granular materials in relation to pavement engineering. The compaction technique was commonly used previously by researchers (e.g. dry limestone: Pappin, 1979; various types of aggregate: Cheung, 1994) in order to produce specimens representing in-situ conditions.

Although the procedures need to be modified for each specific material, there are some common features:

- Various types of compaction mould were used.
- The inner and outer membranes were employed.
- The materials were placed into the mould in six to eight layers.
- The desired densities were achieved using a vibrating table or hammer.
- A vacuum was applied after the removal of the mould.

The specimen preparation methods developed at the University of Nottingham, however, are suitable for characterisation of pavement base materials with large grain sizes. For the investigation of the fundamental behaviour of saturated or dry sands, those techniques need to be further modified and are discussed in Chapter 3.

2.3.2 Stress Path Subjected to Traffic Loading

Previous research has shown that the stress path plays a very important role in characterising the resilient and permanent behaviour of granular materials. Brown (1996) demonstrated that a soil element beneath a pavement might experience very complicated stress paths or histories during construction and in-service periods. For a moving wheel load condition, the stress pattern induced in traffic loading is illustrated in Figure 2-20.

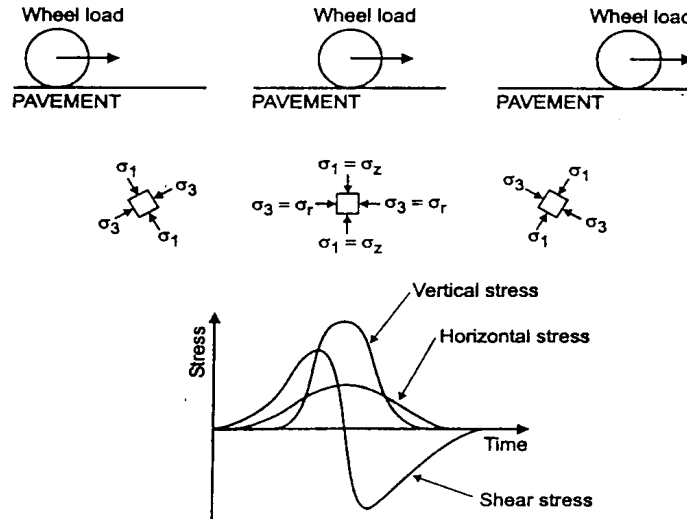


Figure 2-20. Principal stress rotation under a moving load (Lekarp et al., 2000).

In the early days of testing, most triaxial tests employed a constant cell pressure and only the deviatoric stress could be cycled. Therefore, the conventional stress paths ($\delta q/\delta p' = 3$) were commonly applied. Based on this type of tests, Hicks and Monismith (1971) concluded that the Poisson's ratio was constant and the resilient behaviour could be modelled by the well-known $K - \theta$ model. Later, following the advancement of testing techniques, Brown and Hyde (1975) cycled both confining pressure and deviatoric stress simultaneously. They verified performance of the $K - \theta$ model in various stress paths but found that the Poisson's ratio was not a constant value.

The rotation of principal stress on the behaviour of granular materials has received much attention in both ground engineering and pavement engineering. In the past two decades, a few investigations (O'Reilly, 1985; Chan, 1990; Richardson, 1999) investigated the resilient and permanent characteristics of pavement base materials using HCA. In those investigations, the stress path was closely matched by controlling both the normal and shear stresses as shown in Figure 2-20. Unfortunately, as pointed out by Brown (1996), HCA was essentially a research tools and had limited productivity.

2.3.3 Modelling of Resilient Behaviour

The resilient modulus (Seed, 1962) was the most widely used parameter to characterise the resilient behaviour of unbound granular materials. The definition of M_r has been graphically shown in Figure 2-12. The well-known $K - \theta$ model is commonly used to interpret the stiffness-stress relationship of unbound granular materials by:

$$M_r = k_1 \theta^{k_2} \quad (2-21)$$

where k_1 and k_2 are the material parameters and θ is the sum of the maximum effective principal stresses. Hicks and Monismith (1971) proposed this empirical relationship based on constant cell pressure (CCP) tests on aggregates.

This model has several drawbacks, however, that were summarised by Lekarp et al. (2000) in their state-of-the-art review on resilient response of unbound aggregates. One of the drawbacks is that constant Poisson's ratio assumed in the models has been found to be incorrect by many researchers (e.g. Brown and Hyde, 1975; Boyce, 1980). Another one is that in the $K - \theta$ model, the effect of stress on resilient modulus is solely dependent on the sum of the stresses, without consideration of other factors, such as deviatoric stress.

Karasahin (1993) carried out a series of variable confining pressure (VCP) tests and suggested that anisotropy should be taken into account when calculating the Poisson' ratio. Brown and Hyde (1975) considered that a better interpretation of the resilient behaviour is obtained by using the bulk modulus K and shear modulus G . The advantage of this approach is that the stresses and strains are separated as shear and volumetric components. Following this concept, Boyce (1980) proposed the $G - K$ model based on the theorem of reciprocity.

The resilient volumetric strain ε_p^r and the resilient shear strain ε_q^r are expressed as:

$$\varepsilon_p^r = \frac{1}{K_1} p^n \left(1 - \beta \frac{q^2}{p'^2} \right) \quad (2-22)$$

$$\varepsilon_q^r = \frac{1}{3G_1} p^n \frac{q}{p'} \quad (2-23)$$

where $\beta = (1 - n)K_1/6G_1$, K_1 , G_1 and n are model parameters.

This model has proved to be useful to predict both CCP and VCP tests by many researchers. (e.g. Dawson et al., 1996).

Pappin (1979) plotted contours of volumetric and shear strains in the p' – q stress space. This approach implies that the volumetric strain is solely a function of maximum values of stresses, whereas the shear strain depends on both the maximum stresses and the length of the stress path.

2.3.4 Modelling of Permanent Behaviour

Less attention has been paid in the past to the characterisation of permanent behaviour. Several researchers (e.g. Barksdale, 1972; Sweere, 1990) have proposed various empirical relationships between plastic axial strains and the number of cycles based on a large number of load applications. Pappin (1979) demonstrated an alternative modelling technique, in which the plastic shear strain ε_q^p was expressed as a function of the number of load applications, the length of the stress path in the p' – q space and the imposed stress ratio:

$$\varepsilon_q^p = f(N) l_r \hat{\eta}^t \quad (2-24)$$

where $f(N)$ depends on the number of load applications, l_r is the stress path length, $\hat{\eta}$ is the peak stress ratio q_{\max}/p'_{\max} and t is the material constant.

Based on a large amount of cyclic triaxial testing data, Brown (1996) pointed out that the threshold stress concept discussed for clays might be applicable for

granular materials. By comparing results from static loading and cyclic loading tests, insignificant plastic strains develop when the peak cyclic stress ratio is within 70% of the static failure.

Chan (1990) investigated the effect of principle stress rotation on plastic strain development using HCA. The experimental results indicated that large plastic strain occurs due to shear stress reversal. This conclusion is consistent with the findings by Mcvay and Taesiri (1985) on Fairbank's sand (see Figure 2-15). Chan further demonstrated that the large permanent deformation could occur in bi-directional shear reversal (moving the load in both forward and backward direction) compared with unidirectional shear reversal (moving the load in one direction only).

2.4 NUMERICAL MODELLING OF SANDS

Many problems in civil engineering involve predicting the response of soils due to external forces. The general solutions to these problems often involve defining a constitutive model and then carrying out numerical analysis. This section first reviews some basic elasticity and plasticity theory before giving descriptions of the Cam-clay, modified Cam-clay models and more advanced critical state models. Other approaches in modelling behaviour of sands are also summarised.

2.4.1 Elasticity and Plasticity Theory

2.4.1.1 Elasticity

Elastic deformations are characterised by complete recovery to the undeformed shape upon removal of the applied loads. In addition, elastic deformation depends solely upon the stress magnitude and not upon the straining or loading history. In classical linear elastic theory, the model for an isotropic homogeneous soil specimen

is formulated in axisymmetric conditions (e.g. triaxial testing in compression) as follows:

$$\delta\varepsilon_1 = \frac{1}{E}(\delta\sigma'_1 - 2\mu\delta\sigma'_3) \quad (2-25)$$

$$\delta\varepsilon_3 = \frac{1}{E}\{-\mu\delta\sigma'_1 + (1 - \mu)\delta\sigma'_3\} \quad (2-26)$$

where $\delta\varepsilon_1$ is the axial strain increment, $\delta\varepsilon_3$ is the radial strain increment, μ is Poisson's ratio, and $\delta\sigma'_1$ and $\delta\sigma'_3$ are the effective axial stress increment and the effective radial stress increment respectively.

To uncouple the effect of changing size and changing shape, two parameters have been introduced into soil mechanics, which are the shear modulus G and bulk modulus K . Assuming isotropy, the above equations can be re-formulated in terms of the triaxial invariants, deviatoric stress q and mean effective stress p' as:

$$\begin{bmatrix} \delta\varepsilon_p^e \\ \delta\varepsilon_q^e \end{bmatrix} = \begin{bmatrix} \frac{1}{K} & 0 \\ 0 & \frac{1}{3G} \end{bmatrix} \begin{bmatrix} \delta p' \\ \delta q \end{bmatrix} \quad (2-27)$$

$$K = \frac{E}{3(1 - 2\mu)} \quad (2-28)$$

$$G = \frac{E}{2(1 + \mu)} \quad (2-29)$$

where the superscript e denotes the elastic component.

2.4.1.2 Plasticity

Soils are more often seen to deform plastically than elastically. Their onset is characterised by the existence of a yield stress beyond which permanent strains

appear. In the constitutive modelling for soil plasticity, four basic requirements have been defined:

- Elastic properties;
- Yield surface;
- Plastic potential;
- Hardening rule.

Lo Presti (1995) among others suggested that the yielding strain for uncemented sands was about 0.00015 (i.e. 0.015%). Within this strain range, the behaviour of sands is purely elastic.

The relative magnitudes of various components of plastic deformation are expressed in terms of the plastic potential.

In the triaxial space, the yield surface and plastic potential can be expressed as:

$$f(p', q, \varsigma) = 0 \quad (2-30)$$

$$g(p', q, \beta) = 0 \quad (2-31)$$

Where ς is a hardening or softening parameter and β is a parameter controlling the size of the plastic potential. If $f = g$, then the soil obeys the principle of associated flow rule which implies that plastic strain increment vector is normal to the yield surface, otherwise, the flow rule is said to be non-associated.

Rowe's stress-dilatancy relation (Rowe, 1962) provides satisfactory results for most practical problems and has been widely used in the geotechnical community. However, continuing effort has been devoted in the past (e.g. Li et al., 1999) to develop a better stress-dilatancy relation. Inevitably, increasing model parameters are needed in these models.

The relationship between the magnitude of the plastic strain increment and the magnitude of an increment of stress is manifested by the hardening rule. The use of both volumetric and deviatoric plastic strain hardening (e.g. Nova, 1977) may be able to capture the strong dilation behaviour in dense sands, but more material constants are needed. For the sake of simplicity, some researchers (Bardet, 1986; Crouch et al., 1994; Yu, 1998) have successfully modelled the behaviour of sands using volumetric plastic strain hardening models in a wide stress region.

2.4.2 Critical State Models

Roscoe and co-workers in Cambridge University proposed the critical state theory for soils in the 1960's. Since then, many elastic-plastic models based on the critical state concept have been developed and implemented into finite element code. The original Cam-clay was presented by Roscoe and Schofield (1963). Later, Roscoe and Burland (1968) modified the model and formulated it into three dimensions. Detailed descriptions of the mathematical formulations can be found in references, notably Roscoe and Burland (1968) and Wood (1990). The key assumptions of the models are:

- The soil is isotropic.
- The soil behaviour is elastic-plastic.
- The soil deforms as a continuum.
- The soil behaviour is not affected by creep.

2.4.2.1 The original and modified Cam-clay models

The original Cam-clay model assumes that recoverable changes in volume accompany any changes in mean effective stresses p' according to the expression:

$$\delta\varepsilon_p^e = \kappa \frac{\delta p'}{\nu p'} \quad (2-32)$$

The critical state is fully defined by equation (2-16) as described previously.

It is assumed that the plastic flow obeys the principle of normality or has an associated flow rule: that is, the plastic potential and the yield surface coincide ($g = f$). The yield surface of the original Cam-clay model is expressed as:

$$\frac{\eta}{M} = \ln \frac{p_o'}{p'} \quad (2-33)$$

The volumetric hardening rule can be adopted in original Cam-clay model to give:

$$\delta\varepsilon_p^p = \frac{(\lambda - \kappa)}{\nu} \frac{\delta p_o'}{p_o'} \quad (2-34)$$

where the superscript p denotes plastic component.

The original Cam-clay model implies the following stress-dilatancy relation:

$$d = \frac{\delta\varepsilon_p^p}{\delta\varepsilon_q^p} = M - \eta \quad (2-35)$$

The physical meanings of the parameters: λ , M , κ and p_o' can be found in section 2.2.4.

The basic assumption of the modified Cam-clay model is the same as the original one, except a different yield surface is adopted:

$$\frac{M^2}{M^2 + \eta^2} = \frac{p'}{p_o'} \quad (2-36)$$

The modified Cam-clay model implies the following stress-dilatancy relation:

$$d = \frac{\delta\varepsilon_p^p}{\delta\varepsilon_q^p} = \frac{M^2 - \eta^2}{2\eta} \quad (2-37)$$

2.4.2.2 Modelling behaviour of sands within the critical state framework

There is a general understanding that that the original and modified Cam-clay models were unsuccessful in predicting the behaviour of sands. Although a large number of modifications have been proposed during the last two decades, most of them have not properly take the effects of densities and confining pressures into consideration. In addition, there is an undesirable trend to increase the model parameters without clear physical meanings.

Wroth and Bassett (1965) first introduced the state parameter concept in the development of stress-strain relationship for sands. Later, Been and Jefferies (1985) generalised this parameter and demonstrated that the state parameter could be used to interpret many engineering properties. Since then, the explicit incorporation of the state parameter concept into critical state models has been used by many researchers.

The bounding surface concept (further described in section 6.3.2) has been used in some models so that plastic deformation can occur for stress states within the yield surface, such providing a very flexible variation in the plastic modulus during a loading path. McVay and Taesiri (1985) have successfully used this type of model to predict the stress path dependent behaviour of sands under moving wheel loading conditions.

In modelling the cyclic loading behaviour, the approach based on the kinematic hardening concept offers an attractive way to model some of the essential features of sands under cyclic loading conditions. This concept was originally applied to metal plasticity and subsequently to soils by Prévost (1978). Ghaboussi and Momen (1982) among others have proposed several models using the kinematic hardening concept. More recently, Hau (2003) adopted this approach in predicting the response of lightly trafficked pavements to repeated loading.

2.4.3 Other Constitutive Models

The standard and more advanced critical state models described above are built based on the prevailing plasticity theory, which consists of the elastic properties, the yield surface, the plastic potential and the hardening rule. As an alternative to these, the use of the hypoplastic and hyperplastic constitutive models to predict the behaviour of granular materials has achieved certain success.

The theory of hypoplasticity originally proposed by Kolymbas (1977) differs substantially from the conventional plasticity theory in that the basic concepts introduced by elastoplasticity (such as yield surface, flow rule etc.) are abandoned. This approach treats strain rate as a whole rather than separating it into elastic and plastic parts. Consequently, the inelastic deformation predicted by hypoplastic models may occur from the very beginning of the loading process. Recent investigations show that this approach is capable of predicting many characteristics of granular materials. Examples of these developments include research on the following topics: (a) the bound and instability surfaces in granular materials (Wu and Niemunis, 1997); (b) inherent anisotropy of sand (Wu, 1998); (c) shear band formation in sand (Wu, 2000).

It is important to clarify that Collin and Houlsby (1997) proposed another approach to plasticity based on thermodynamics, which is called the hyperplasticity theory. The constitutive models in this approach are normally specified by two potential functions: an energy function and a dissipation function.

2.5 CASM-A SIMPLE UNIFIED CRITICAL STATE MODEL

CASM was developed by Yu (1995, 1998) based on the state parameter concept. The main feature of the original model CASM is that a single set of yield and plastic potential functions is used. CASM requires only seven material constants

(two more than the classical Cam-clay models), all of which have clear physical meanings and can be easily identified in routine triaxial tests.

In this section, a brief introduction of CASM is given. A detailed mathematical formulation and finite element implementation are given by Khong (2004).

2.5.1 Experimental Evidence

2.5.1.1 Similarity principle and state parameter concept

Roscoe and Poorooshasb (1963) first proposed the similarity principle for clays and sands. It states that any two specimens of a soil will behave in a similar manner regardless of their stress-strain history provided the difference between the initial void ratio and the void ratio at the critical (steady) state at the same mean effective stress is the same.

Sladen and Oswell (1989) compared four different sands in very loose states and confirmed the similarity principle. Figure 2-21 shows stress paths normalised by the mean effective stress at the critical state at the same void ratio.

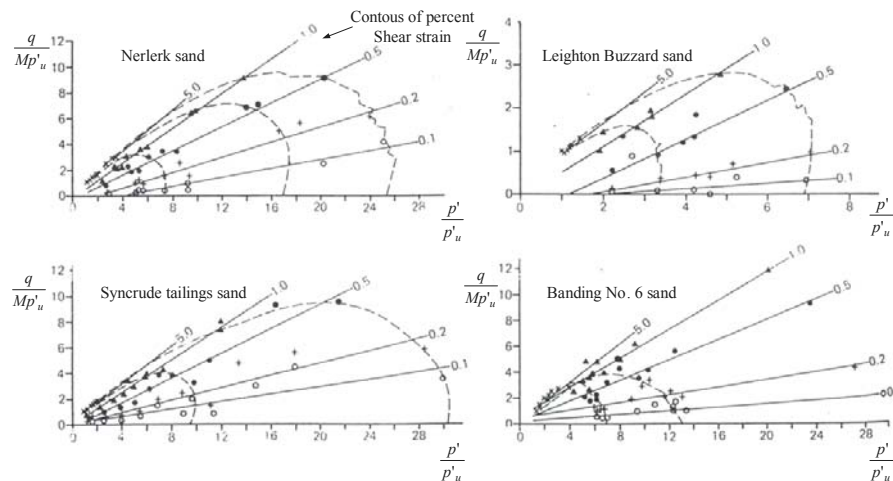


Figure 2-21. Shear strain contours for undrained loading in normalised stress spaces (modified from Sladen and Oswell, 1989).

Been and Jefferies (1985) extended the similarity principle and used the state parameter ξ to describe the sand behaviours over a wide ranges of stresses and densities. The reasons for choosing state parameter in the development of CASM were presented in great detail by Yu (1998). The main reason is that the state parameter does not eliminate the influence of either density or confining pressure on the behaviour of sands. Instead, it properly places emphasis on the fact that it is a combination of these parameters that is relevant to the description of granular material behaviour.

2.5.1.2 State boundary surface for sands

The boundary (or yield) surfaces adopted in the original Cam-clay and modified Cam-clay models are shown in Figure 2-22. It can be seen that the intersection points between the *CSL* and the yield surface for both original and modified Cam-clay models occur at the maximum deviatoric stress. However, experimental evidence (e.g. Tatsuoka and Ishihara, 1974a; Coop, 1990; McDowell et al., 2002) has indicated that this might not be true for sands.

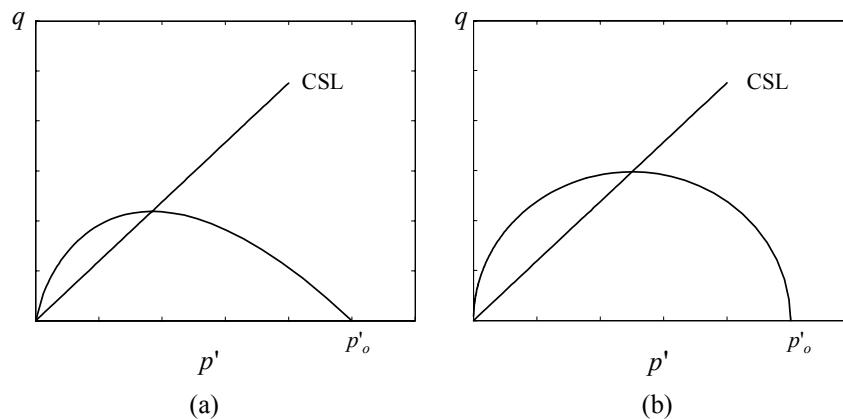


Figure 2-22. Yield surfaces: (a) original Cam-clay model, (b) modified Cam-clay model.

For example, Coop (1990) identified the state boundary surface of a carbonate sand (called Dog Bay sand) as shown in Figure 2-23 (a) and (b) for drained and undrained tests, respectively. Coop (1990) normalised his triaxial data in terms of the current preconsolidation stress p'_o and found that the shapes of state

boundary surfaces were similar regardless of the types of tests. However, the Roscoe surface appeared to a peak before reaching the critical state, which cannot be predicted by the standard Cam-clay models. In addition, he concluded that the shape of the stress paths below the state boundary surface was dependent on the types of tests.

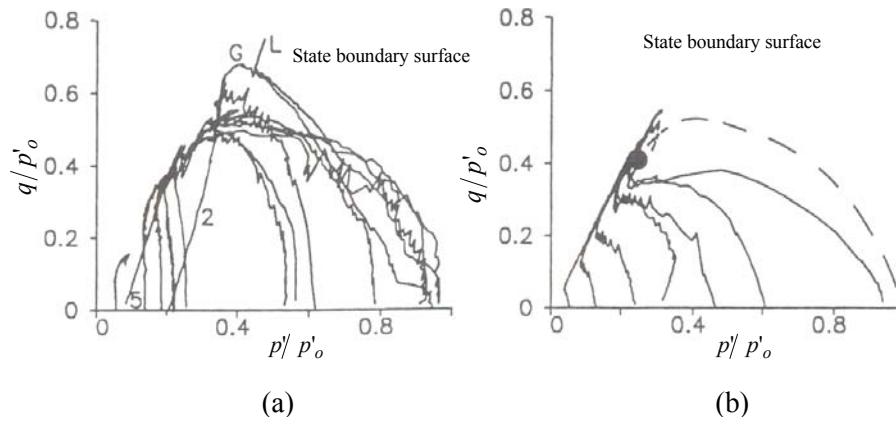


Figure 2-23. State boundary surface of a Dog Bay sand: (a) drained tests, (b) undrained tests (Modified from Coop, 1990).

McDowell et al. (2002) established a very similar shape of the state boundary surface for a silica sand subjected to a range of high pressure stress path testing using triaxial apparatus. The experimental state boundary surface obtained is shown in Figure 2-24 and can be expressed as:

$$\eta = N \left[(a + 1) \ln \left(p_o' / p' \right) \right]^{1/(a+1)} \quad (2-38)$$

where N and a are material constants. In Figure 2-24, parameters N and a are taken as 0.8 and 1, respectively. It will be demonstrated in the following sections that the theoretical state boundary surface produced in CASM has a very similar shape as these experimental state boundary surfaces described above by choosing certain values of model constants.

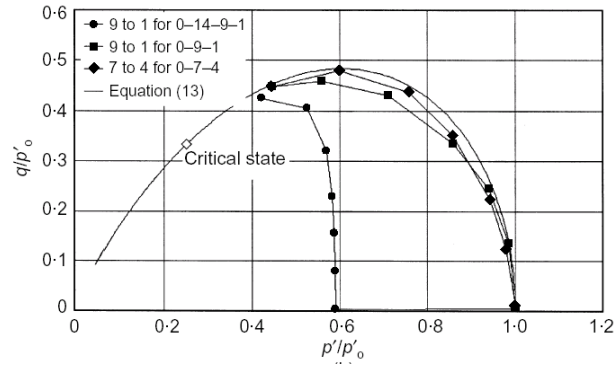


Figure 2-24. State boundary surface of a silica sand (McDowell et al., 2002).

2.5.2 Description of the Model

2.5.2.1 Elastic properties

Following the standard Cam-clay models, the soils have been modelled by adopting a state dependent bulk modulus K :

$$K = \frac{\nu p'}{\kappa} \quad (2-39)$$

The shear modulus G is derived from equations (2-28) and (2-29) as follows:

$$G = \frac{3(1 - 2\mu) K}{2(1 + \mu)} \quad (2-40)$$

2.5.2.2 Yield surface (or state boundary surface)

Yu (1995, 1998) proposed a general stress-state relation for both clays and sands based on published triaxial data on various sands, which can be expressed as:

$$\left(\frac{\eta}{M}\right)^n = 1 - \frac{\xi}{\xi_R} = -\frac{\ln(p'/p'_o)}{\ln r} \quad (2-41)$$

where n is a material constant, r is another material constant which is related to the reference state parameter $\xi_R = (\lambda - \kappa) \ln r$.

Figure 2-25 shows the stress-state relations for different values of n , in which the original and modified Cam-clay models are two special cases by choosing certain n and r values. The yield surface function for CASM can be expressed in terms of the triaxial parameters p' and q as follows:

$$f(p', q, p'_o) = \left(\frac{q}{Mp'} \right)^n + \frac{\ln(p'/p'_o)}{\ln r} = 0 \quad (2-42)$$

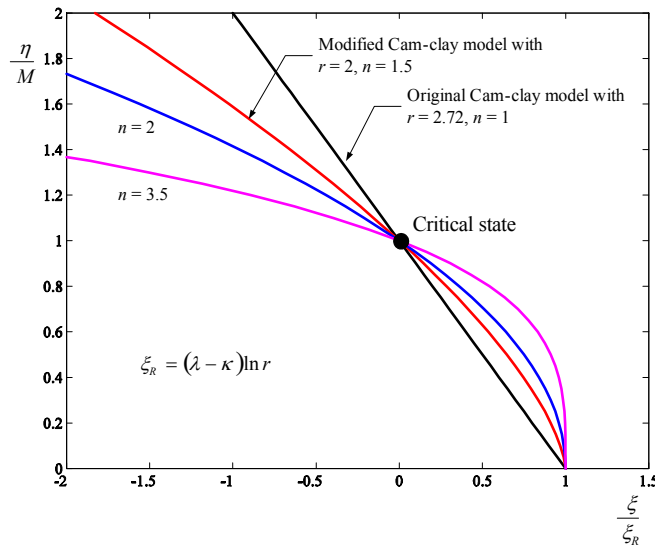


Figure 2-25. General stress-state relations assumed in CASM.

Figure 2-26 shows the shapes of CASM yield surface along the elastic wall (normalised by preconsolidation pressure) with $r = 2.72$ and different values of n . It should be noted that the original Cam-clay model can be obtained exactly from CASM by choosing $r = 2.72$ and $n = 1$. In addition, by choosing $r = 2$ and a suitable n value (ranging from 1.5–2), the ‘wet’ side of the modified Cam-clay model can be matched accurately. It is evident that the intersection point between the *CSL* and the yield surface in CASM does not necessarily occur at the peak, which agrees well with experimental observations as shown in Figure 2-23 and Figure 2-24.

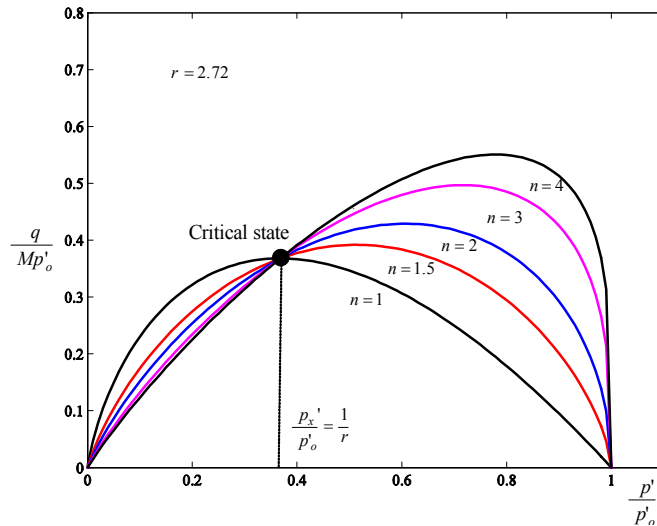


Figure 2-26. The yield surfaces of CASM normalised by preconsolidation stresses.

2.5.2.3 Stress-dilatancy relation and plastic potential

Rowe's stress-dilatancy relation defined in equation (2-9) has been used in CASM.

The plastic potential can be obtained by integration as:

$$g = 3M(\ln p' - \ln \beta) + (3 + 2M) \ln \left(\frac{2q + 3p'}{p'} \right) - (3 - M) \ln \left(\frac{3p' - q}{p'} \right) = 0 \quad (2-43)$$

The size parameter β can be determined easily for any given stress state (p', q) by solving the above equation. Figure 2-27 compares the shapes of the plastic potentials of the three models and directions of the plastic strain increments. It demonstrates that the plastic flow rule adopted in CASM is non-associated, as the plastic potential is not identical to the yield surface and the plastic strain increments are not perpendicular to the yield surface at the point of yielding.

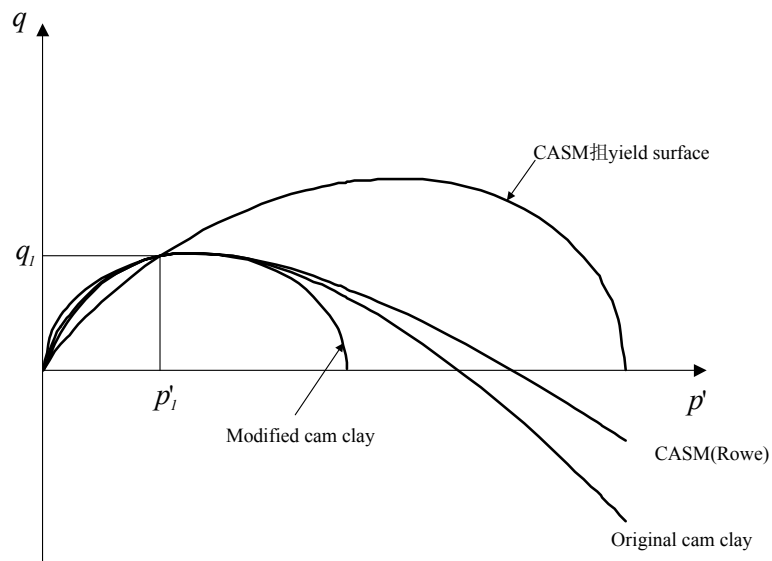
2.5.2.4 Hardening rule

Similar to the Cam-clay models, in CASM the change in size of the yield surface is assumed to be related to the incremental plastic volumetric strain by:

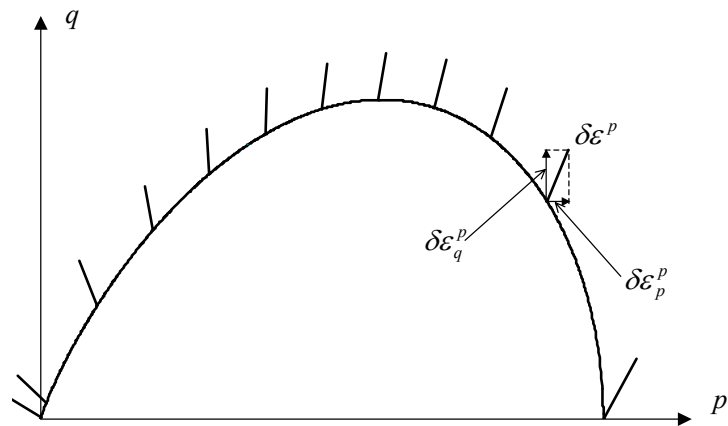
$$\delta p'_o = \frac{\nu p'_o}{(\lambda - \kappa)} \delta \varepsilon_p^p \quad (2-44)$$

This implies that CASM is a volumetric plastic hardening model. The plastic hardening modulus H can be derived as follows:

$$H = \frac{3\nu}{(\lambda - \kappa) \ln r} \left(\frac{3 + 2M}{2q + 3p'} - \frac{3 - M}{3p' - q} \right) \quad (2-45)$$



(a)



(b)

Figure 2-27. (a) shapes of different plastic potential surfaces, (b) plastic strain increments for CASM (Khong, 2004).

2.6 SUMMARY

In this chapter, some aspects of the stress-strain and strength characteristics, triaxial testing techniques and numerical modelling on sands have been reviewed. It has been shown that the behaviour of sands depends mainly on the combined effects of density, effective confining pressure, structure and stress history. The state parameter concept provides a unified way to describe much of the behaviour of sands over a wide range of stresses and densities. However, numerous laboratory studies on sands reported in the literature have shown conflicting results, in particular regarding the uniqueness of the critical or steady state line. The need to clarify this issue forms one of the major points in the testing programs described in Chapter 4 and Chapter 5. It is also noted that the stress path plays a very important role in the stress-strain and strength characteristics of sands. Without taking into account such effect, the data obtained from triaxial testing can be wrongly interpreted. Therefore, the triaxial testing technique was briefly reviewed with emphasis on the work carried out at the University of Nottingham.

Most models developed at the University of Nottingham on granular materials are based on the empirical relations for specific materials under certain conditions. Without sound theoretical basis, it is difficult to apply these models to various materials under various loading conditions. A large number of models based on the critical state concept have been proposed over the last 30 years. However, as pointed out by Yu (1998), there is an undesirable trend in recent years in the area of constitutive modelling of sands, where models require a large number of model constants, many of which offer no clear physical meanings.

For practical purposes, these models cannot be applied in most geotechnical problems. For this reason, CASM and its extensions have been chosen to model the behaviour of Portaway sand in the current study. The determination of CASM constants is described in Chapter 4. The evaluation and verification of CASM and its extensions are presented in Chapter 6.

Chapter 3

Description of Experimental Techniques

3.1 INTRODUCTION

The focus of this chapter is to describe the necessary equipments and procedures that were used and developed in this research work. Some basic properties of the material tested are also presented. Firstly, the salient features of the NDTTS and the ADVanced stress path Triaxial Testing System (ADVTTS) are described, together with details of the calibration and modification exercises that were carried out. Secondly, the material tested and the associated index testing program are described. Thirdly, the testing procedures and data correction methods employed are introduced. Testing programs, results and interpretations are presented in Chapter 4 and Chapter 5.

3.2 EQUIPMENT EVALUATIONS AND MODIFICATIONS

3.2.1 Introduction

Since previous experimental studies were mainly focused on the testing of clays and silts, an evaluation of and necessary modifications to the equipment were made in order to carry out triaxial test on dry sands. The NDTTS was partially updated during the course of this investigation. However, the current work has paved the way for developing an advanced dynamic triaxial testing system in the future.

The key features of the NDTTS after the modification are summarised as follows:

- Two specimen sizes are available: 50 and 75 mm in diameters.
- It is fully automated with closed-loop feedback control.
- Radial strain is recorded by a newly developed ‘on-specimen’ measuring device.
- Three different wave forms are available: triangle, square, and sinusoid.
- Frequency range is between 0.1 and 10 Hz.

The ADVTTTS was supplied by GDS Ltd and used to carry out tests on saturated sand specimens. An evaluation of the system is first carried out and then a complete testing procedure is established.

The key features of the ADVTTTS are summarised as follows:

- Two specimen sizes are available: 38 and 50 mm in diameters.
- It is fully automated with closed-loop feedback control.
- The small axial and radial strains are recorded by Hall effect transducers.
- Axial force is measured by a submersible load cell inside the triaxial cell.

- The traditional U-U, C-U, C-D and more advanced stress path tests can be performed.
- One-way and two-way low speed cyclic loading tests can be performed.
- The cross-sectional area of the test specimen is continually corrected for the effects of change in volume and axial deformation.

3.2.2 Nottingham Dynamic Triaxial Testing System

3.2.2.1 Introduction

The original arrangement of the NDTTS is shown in Figure 3-1. Raybould (1992) performed extensive dynamic tests on silty clay using the NDTTS. Since then, no significant development has been carried out on this facility. During the initial phase of this study, it was found that the control system and some parts of the NDTTS could not work properly due to the lack of maintenance. Therefore, the first objective of the experimental work was to evaluate and update the NDTTS.

The system, prior to the modification, included a loading frame, a servo-hydraulic system, a triaxial cell, a load cell, two long range LVDTs, a volume-measuring device, a Dartec system for data acquisition and control and a microcomputer. This section contains the detailed evaluation and modification for each of these elements of the system.

3.2.2.2 Loading system

The loading system of the NDTTS comprises a load frame and a servo-hydraulic system. The load frame is a four-post frame with an adjustable flat plate base. Axial load is applied to the specimens by connecting the load ram in the triaxial cell directly to the actuator, which is driven by a close-loop servo-hydraulic system.

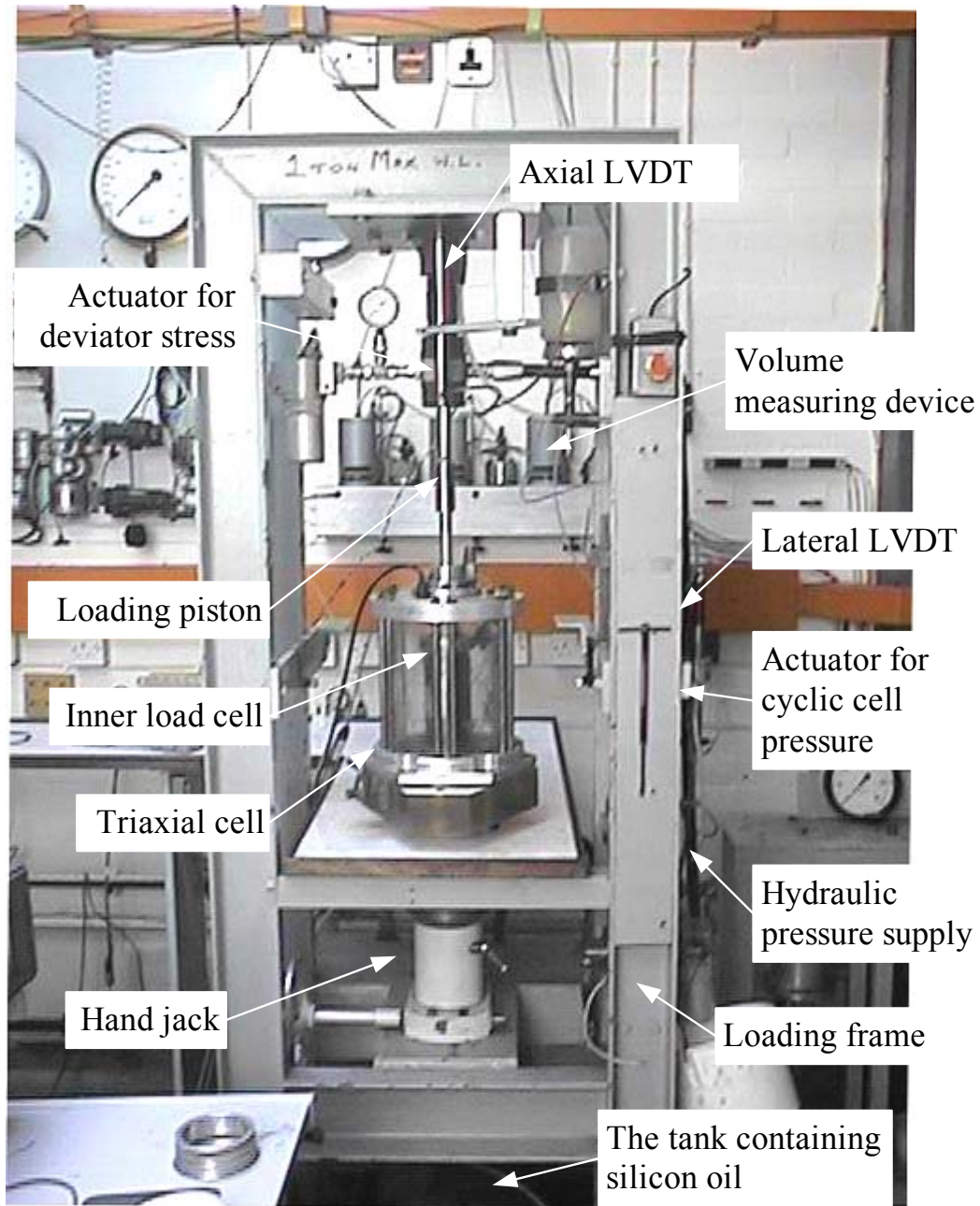


Figure 3-1. The Nottingham dynamic triaxial testing system.

Figure 3-2 shows the diagram of the hydraulic pressure source at the Nottingham Centre for Geomechanics (NCG) research laboratory.

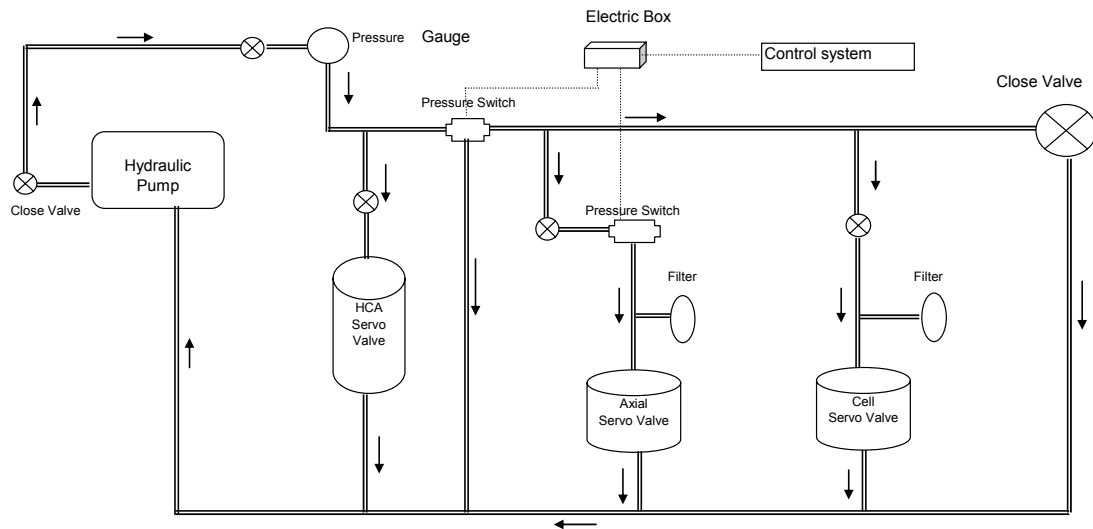


Figure 3-2. Diagram of the pressure sources at the NCG research laboratory.

The system can generate three types of waveform with frequency of 0.1Hz to 10 Hz. A series of probing tests on dummy specimens were carried out by applying various frequencies in order to investigate the responses of the load cell and external LVDT (Linear Variable Differential Transformer). Figure 3-3 shows that there is a big difference between the command signal and the response at a frequency of 5 Hz.

Cheung (1994) had carried out the similar tests on dummy specimens. He concluded that the stress measured by the load cell was lower at the peak of the sinusoidal wave and higher at the trough than expected. Therefore, the frequency response of the entire setup should be checked if cyclic load testing at higher frequencies is to be performed.

In general, the current system is able to provide a reasonable response if the loading frequency is below 2 Hz.

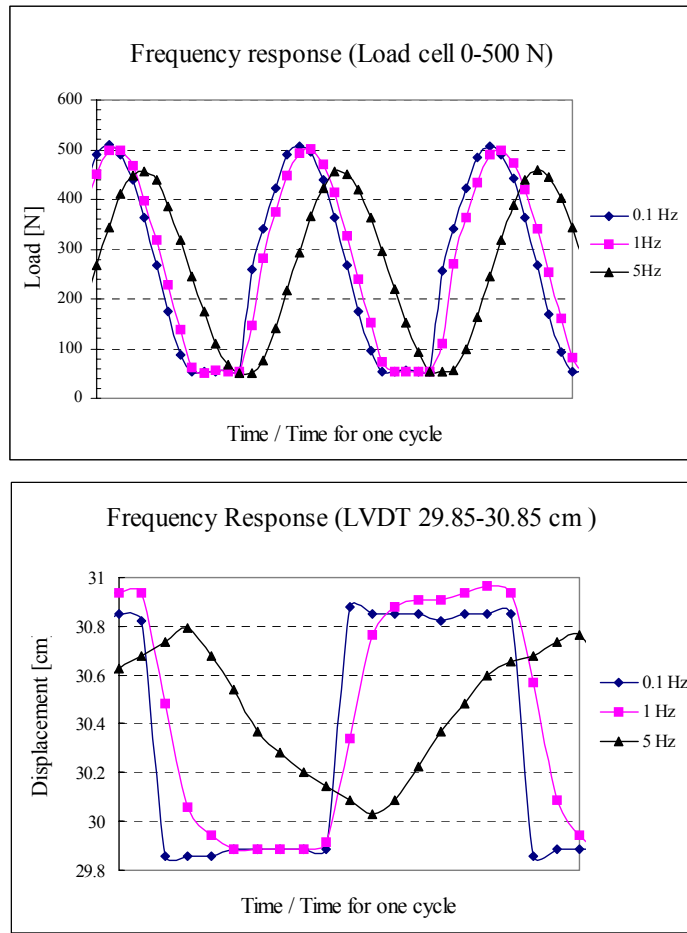


Figure 3-3. The effect of frequency on load and displacement control methods.

3.2.2.3 Triaxial cell

The existing triaxial cell was originally designed by Austin (1979) and more recently modified by Cheung (1994). During the evaluation of the NDTTS, it was found that the triaxial cell was not in good condition and the pore pressure and cell pressure transducers did not work properly. In addition, a big crack was found at the cell base. Therefore, it was decided to replace the existing cell with a new one.

In conventional triaxial cells (e.g. Bishop and Wesley, 1975), the rods or columns to support the top cap and piston are normally posted outside the triaxial cell. In this type of apparatus, after the cap is mounted on top of the specimen, the cell, the top cap and the columns are assembled together. At this stage, the specimen

stands within the cell without any side support. Then the loading piston is lowered down to touch the top cap of the specimen. In this operation, the specimen needs to stand upright in order to achieve a precise connection. To eliminate this difficulty, the internal-tie-bar triaxial cell was developed and used by many researchers (e.g. Tatsuoka, 1988; Zhang, 2002). Therefore, a new triaxial cell was built as seen in Figure 3-4. Due to the time constraints, the new cell was not incorporated into the NDTTS. A conventional triaxial cell (see Figure 3-5) was temporarily used during the course of preliminary testing on dry sand.



Figure 3-4. Triaxial cell built at the NCG.



Figure 3-5. Triaxial cell used in preliminary tests.

3.2.2.4 The transducers and calibrations

All information about the state of the specimen was measured electronically by three transducers. The cell pressure was measured pneumatically by a pressure gauge. A system of three LVDTs were used to provide feedback control and strain measurement. The ‘Nottingham’ load cell was used to measure the deviatoric stress. The existing pore pressure and cell pressure transducers were replaced by a set of corresponding transducers that had been calibrated by the manufacturers.

LVDTs

One long range LVDT (ACT 2000A) supplied by RDP Ltd was used to provide external measurement of the axial displacement. Another identical one was used to provide feedback control for cell pressure. The LVDT has an internal spring that constantly pushes the armature (the moving part of the measurement sensor) outwards. The armature of the LVDT is guided in a low friction bearing.

For radial displacement measurement, a 250 MHR LVDT supplied by Schaevitz Ltd with ± 6.35 mm stroke was incorporated into the system, giving the maximum radial strains of 12.7%. Later, a D5/200 WRA/141 (10 mm stroke) type transducer was purchased from RDT Ltd that had been used successfully to identify the *CSL* for Leighton Buzzard and Dog's Bay sands by Klotz and Coop (2002).

All relevant details of the transducers are shown in Table 3-1. Calibration of the LVDTs involved moving the LVDTs through a known distance and observing the change in the digital output. They were calibrated against a micrometer. In all cases, the output was observed to be linear, as shown in Appendix A.

Table 3-1. The LVDTs used in the NDTTS.

Type	Weight	Dimension	Linear Range	Function
ACT 2000A	398 g	280 mm	± 50.00 mm	Axial strain
250 MHR	9.9 g	47 mm	± 6.35 mm	Radial strain
D5/200 WRA/141	18 g	55 mm	± 5.00 mm	Radial strain

Load cell

The load cell was manufactured at the University of Nottingham. It consists of four gauges in a full Wheatstone bridge configuration. Its measuring range is 6 kN. The cell was calibrated against a reference load cell (40 kN / 24 mV) in the triaxial load frame. During the testing program the load cell was calibrated three times and there was insignificant zero drift.

All the transducers were powered by a SC-5B conditioning unit using a 5 Volt AC voltage. The resulting output signals were amplified by the SC-5B conditioning unit so that acceptable resolution could be obtained.

3.2.2.5 Volume measurement and back pressure

The existing volume measuring device used by Raybould (1992) was originally developed at Imperial College and supplied by Soiltech Ltd. The LVDT mounted

outside the hollow brass cylinder measures the movement of the piston caused by the volume changes in the top chamber. The capacity of this device is 100 ml.

Back pressure is supplied by compressed air and connected to the base of the volume measuring device. As mentioned earlier, the preliminary testing program centred on testing of dry sand, therefore the calibration was not carried out for this device. It should be noted that the LVDT used here is of a DC type transducer, which is not compatible with the current transducer conditioning unit (AC type). Therefore, the LVDT should be replaced by an AC type transducer before incorporating this device into the NDTTS in the future.

3.2.2.6 Data acquisition and control system

Electronic signals from devices such as pressure transducers and LVDTs are in analogue form. These signals can be recorded by analogue devices. Alternatively, digital data acquisition techniques can be employed. The existing data acquisition and control system was commissioned by Raybould (1992). Since then, no significant improvement was made.

Raybould controlled both the axial stress and confining stress independently through a digital control system supplied by Dartec Ltd. However, it was found that only one channel was available and several important parts were damaged. Many researchers at the University of Nottingham have successfully used the Automate Testing System (ATS) as the data acquisition and control system. Cheung (1994) incorporated the ATS into his repeated load triaxial apparatus with a pneumatic loading system. Later, Richardson (1999) modified the HCA and used ATS to control the axial and tensional stresses. The ATS was used in the current study in order to acquire more channels for data collection.

Figure 3-6 shows the Dartec system and the ATS. The software used in the current research program was version 3.13a, which has been described by Sousa and Chan (1991). The hardware includes:

- An IBM microcomputer and data acquisition board;
- A PG8800 servo-valve amplifier;
- A SC-5B conditioning unit.

The data acquisition board for the ATS was supplied by National Instruments Ltd. All transducers were connected to the SC-5B AC signal conditioner. Figure 3-7 shows the configuration of the connector. The transducer excitation was provided by the SC-5B conditioning unit.

A complete data acquisition and control signal flow chart is presented in Figure 3-8. The system uses two feedback loops: one for the axial actuator and the other for the lateral actuator. In this study, only the axial actuator loop was used during stress- or strain- controlled tests with the constant cell pressure. In order to allow a synchronised adjustment of the axial load (or displacement) and cell pressure, the silicon oil should be used as confining fluid in future research.

With the combination of the transducers and the data acquisition system described, the resolution of the stress and strain measurements are summarised in Appendix A.

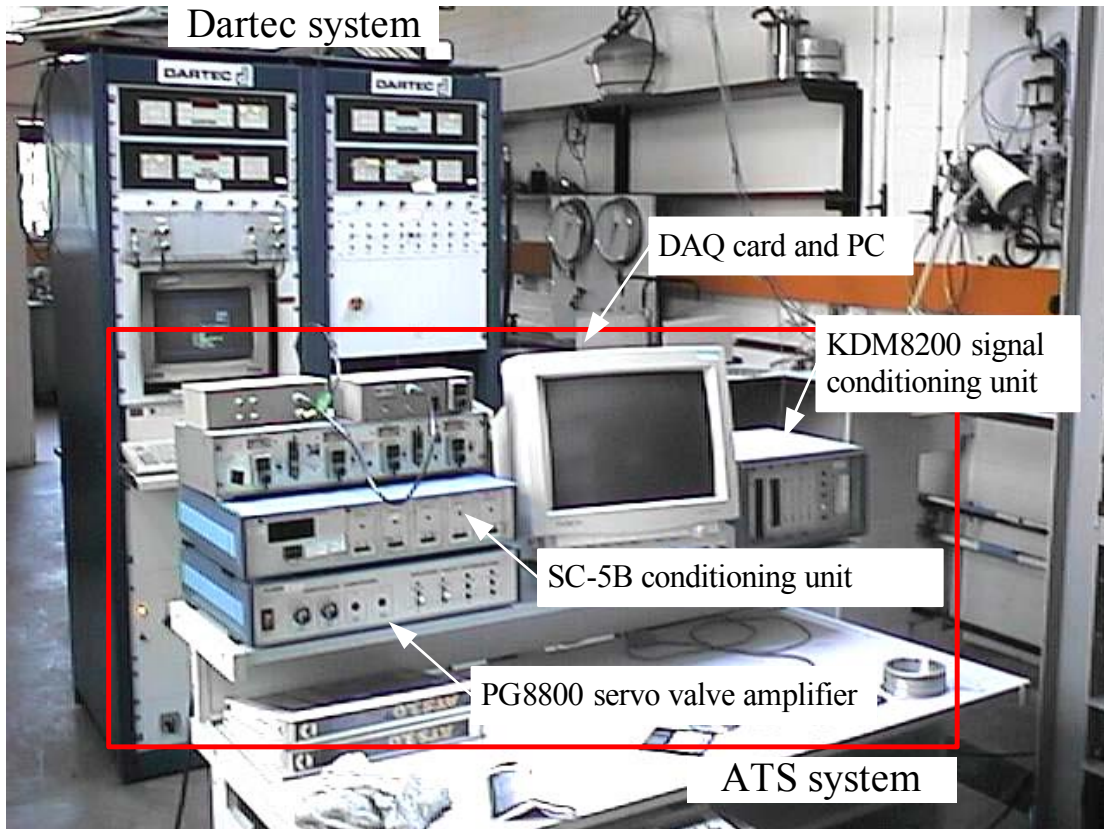


Figure 3-6. Data acquisition and control system.

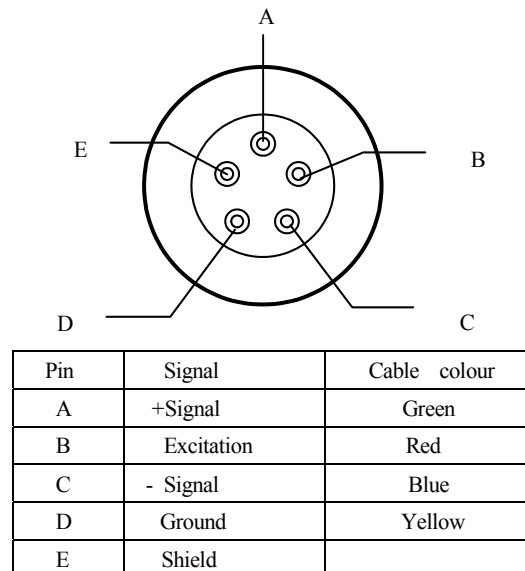


Figure 3-7. Connector of the transducers.

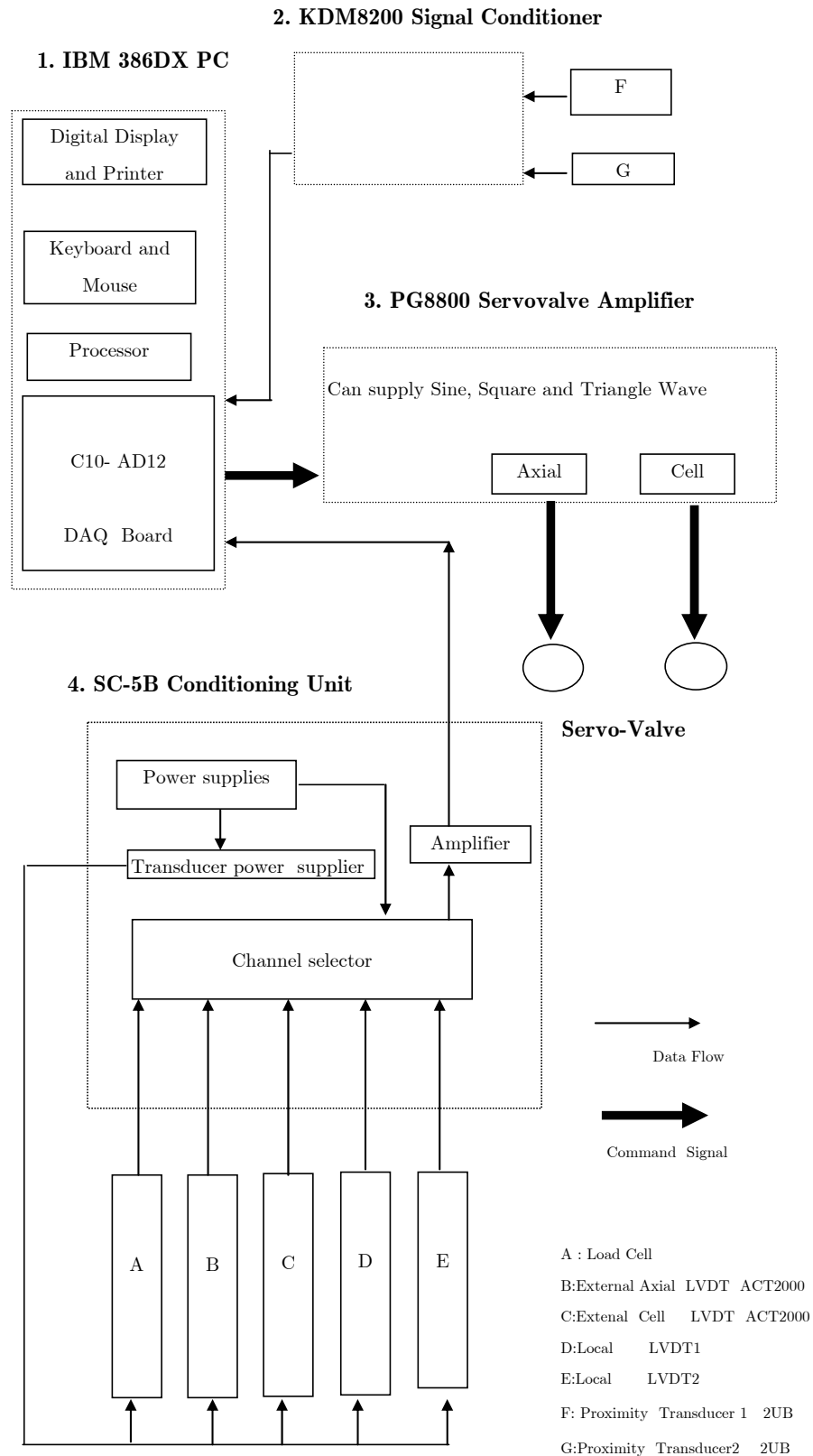


Figure 3-8. Data acquisition and control signal flow chart.

3.2.2.7 Development of a ‘on-specimen’ radial strain measuring device

Description of the device

As discussed in previous chapter, the ‘on-specimen’ techniques have been used extensively at the University of Nottingham on testing of clays and pavement base materials. To the author’s knowledge, no suitable device existed for testing sand specimens with fine grains. The need for development of this device is because the volumetric strain can only be calculated from both axial strain and radial strain for dry sands tests.

The development of a radial strain measuring device was motivated by the recent experimental works conducted at two leading geotechnical laboratories. Figure 3-9 shows the layout of a radial strain measuring device using a centrally mounted belt developed at Imperial College. A similar design was used by Zhang (2002) at MIT for axial strain measurement. Instead of using pins to attach the device, Zhang (2002) used two yokes hinged together and clamped the devices onto the specimen at three points. This arrangement is very convenient for setting up the specimens.

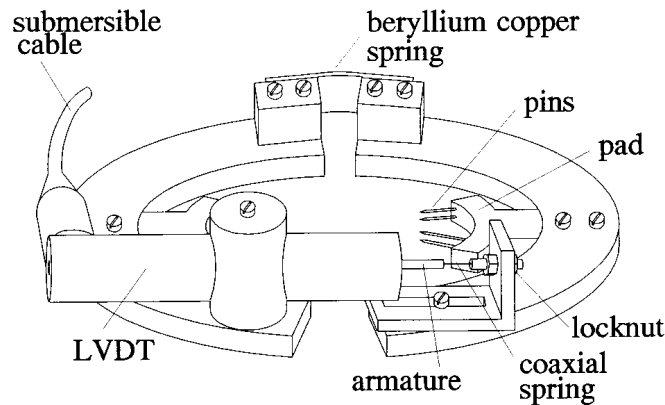


Figure 3-9. The ‘on-specimen’ measuring device used by Coop (Private communication, Appendix A).

The new design combined these two methods and is shown in Figure 3-10. The device is fabricated out of Perspex, chosen for its strength and low weight. It is

hinged and clamped onto the specimen at three points by adjustable connectors. Due to its light-weight design, the clamping force required is very small and can be adjusted through the use of a small spring placed across the hinge. This type of clamping mechanism avoids the need for a pin (or stud) to be inserted into the specimen, thus preserving the integrity of the membrane and eliminating the possibility of leakage.



Figure 3-10. ‘On-specimen’ measuring device developed at the NCG.

The key features of the newly designed ‘on-specimen’ radial strain measuring device are:

- High resolution;
- AC output for compatibility with the existing data acquisition system;
- Compact design to facilitate mounting within the limited space available inside the triaxial cell;
- Limited cost and simplicity of operation;
- Long mechanical life.

Installation onto the test specimen

After setting up the specimen, the installation of the ‘on-specimen’ device was carried out in three stages. Firstly, three connectors were smeared with quick-drying adhesive and then left for a few minutes then the device was attached to the middle height of the specimen. Secondly, the device was held by hand for a few minutes in horizontal position. Thirdly, the relative position of the core and body of the miniature LVDT was set in order to keep it within the required measuring range.

Care was taken in preventing the damage of the sand specimens during these three stages. The performance of the device will be assessed in Chapter 4.

3.2.2.8 Specimen preparation and set up for dry specimen

- (a) A 50 mm rubber membrane was sealed with two O-rings to the bottom platen of the triaxial cell.
- (b) A porous stone and a filter paper were placed on the bottom platen. Subsequently, a split mould was placed over the bottom platen and the membrane was stretched inside the mould. By applying a vacuum to the space between the mould and the membrane, the membrane was pressed against the inner side of the mould.
- (c) A tamping compaction device was then placed on the pedestal of the triaxial cell (see Appendix A).
- (d) Following six layers of tamping and levelling, the top cap was put in place and sealed with another two O-rings.
- (e) Before dismantling the split mould, a vacuum (about 15 kPa) was applied to the bottom drainage to give the specimen a small effective stress.
- (f) Finally, the triaxial cell was placed over the specimen/pedestal assembly, and air pressure was applied inside the cell. The vacuum inside the specimen was then removed, ready for testing.

The diameter and height were measured in five places with a precision of 0.01 mm and the average value was used from these measurements.

3.2.3 Advanced Stress Path Triaxial Testing System

3.2.3.1 Introduction

All the triaxial tests on the saturated sands were conducted in the ADVTTTS. A comprehensive description of the system can be found in Menzies (1988).

The ADVTTTS was previously used by Hau (2003) at the NCG research laboratory. In his research work, all the tests were carried out on clays (Speswhite kaolin). Following a brief introduction and evaluation of the ADVTTTS, the specimen preparation method and testing procedure for sands is described.

3.2.3.2 Equipment and instrumentations

Figure 3-11 shows the layout of the ADVTTTS configured with an eight-channel data acquisition pad, three pressure controllers and the Bishop and Wesley (1975) triaxial cell.

Detailed descriptions of the system elements have been given in the GDS laboratory manual (GDS Instruments Ltd, 2002). Therefore, it is unnecessary here to provide a complete introduction except for some important specifications and precautions required when handling the system, which are summarised as follows:



Figure 3-11. The arrangement of the ADVTTS at the NCG research laboratory.

- Triaxial cell:* the classical Bishop and Wesley stress path triaxial cell used in the ADVTTS could accommodate 38 mm and 50 mm diameter specimens (see Figure 3-12). The specimens with 38 mm diameter were used throughout this study. The axial force was provided by hydraulic pressure acting on a ram in the lower chamber of the triaxial cell. The maximum safe working pressure is 1700 kPa. During set up of the specimen, extreme care was taken to prevent particles of sand from entering the gap between the cell base and the pedestal. This is because the bellofram rolling diaphragm (BRD) made from rubber-like artificial materials, can easily be punctured by the sand particles. Therefore, it is suggested that the gap should be sealed by plastic tape during the specimen preparation. In addition, the saturation of the lower chamber should be checked regularly.
- Pressure controllers:* two standard pressure controllers (STDDPC) were used to control the cell pressure and lower chamber pressure. An advanced pressure controller (ADVDPCC) controlled the back pressure. All three controllers have 2 MPa capacity and 1 kPa resolution for pressure

control. As with the lower chamber, the saturation of the controllers was checked regularly.

- *Extension cap*: the extension tests could be carried out using the GDS extension cap as shown in Figure 3-12. During assembly of the triaxial cell, the specimens can easily be damaged due to the limited space between the extension cap and the cap on the top of sand specimens. Therefore, it was considered a good practice to move the pedestal down to the end of its stroke and move up the load cell as high as possible.
- *GDSLAB*: the software used for control and data acquisition system was GDSLAB v2 supplied by GDS Ltd. This package consists of several test modules that were specially designed for a particular test, such as saturation, B-check, consolidation, general triaxial testing (e.g. C-U, U-U and C-D tests) and K_0 testing. The stress path module and advanced triaxial testing module were used to carry out more complicated stress path tests. GDSLAB has a very good graphical environment, in which the transducers can easily be set up.
- *Hall effect transducers*: the Hall effect transducers were first introduced into the geotechnical laboratory for measuring small strains at the University of Surrey (Clayton et al., 1989). Two axial strain-measuring devices and one radial strain-measuring device were employed during the course of the current research work. As shown in Figure 3-13, the axial strain-measuring device consists of a spring-mounted pendulum that holds a magnet assembly, an upper mounting block and a metallic container holding the Hall effect semiconductor. The radial strain-measuring device comprises of a calliper that is mounted on the specimen by means of two diametrically opposite pads, which are attached to the membrane by pins or adhesive. The linear range is ± 3 mm for all three transducers. Assuming that the diameter of specimen tested and gauge length between the upper and lower components are 38 mm and 50 mm, this would give maximum axial strains of about 12% and radials strains of about 8%.

Therefore, the local measuring devices cannot be used to measure the critical state parameters as strains up to 25% are required. The performance of the devices are described in Chapter 4.

- *Pressure transducers:* There are four pressure transducers in the ADVTTS. Three of them are located in the pressure controllers. In addition, a pore pressure transducer is connected to the base pedestal of the cell. The system resolves pore pressure to ± 0.2 kPa over a range of 2000 kPa. De-aired water was used to ensure correct measurement.

A summary of measurement accuracy and range of the ADVTTS is given in Appendix B.

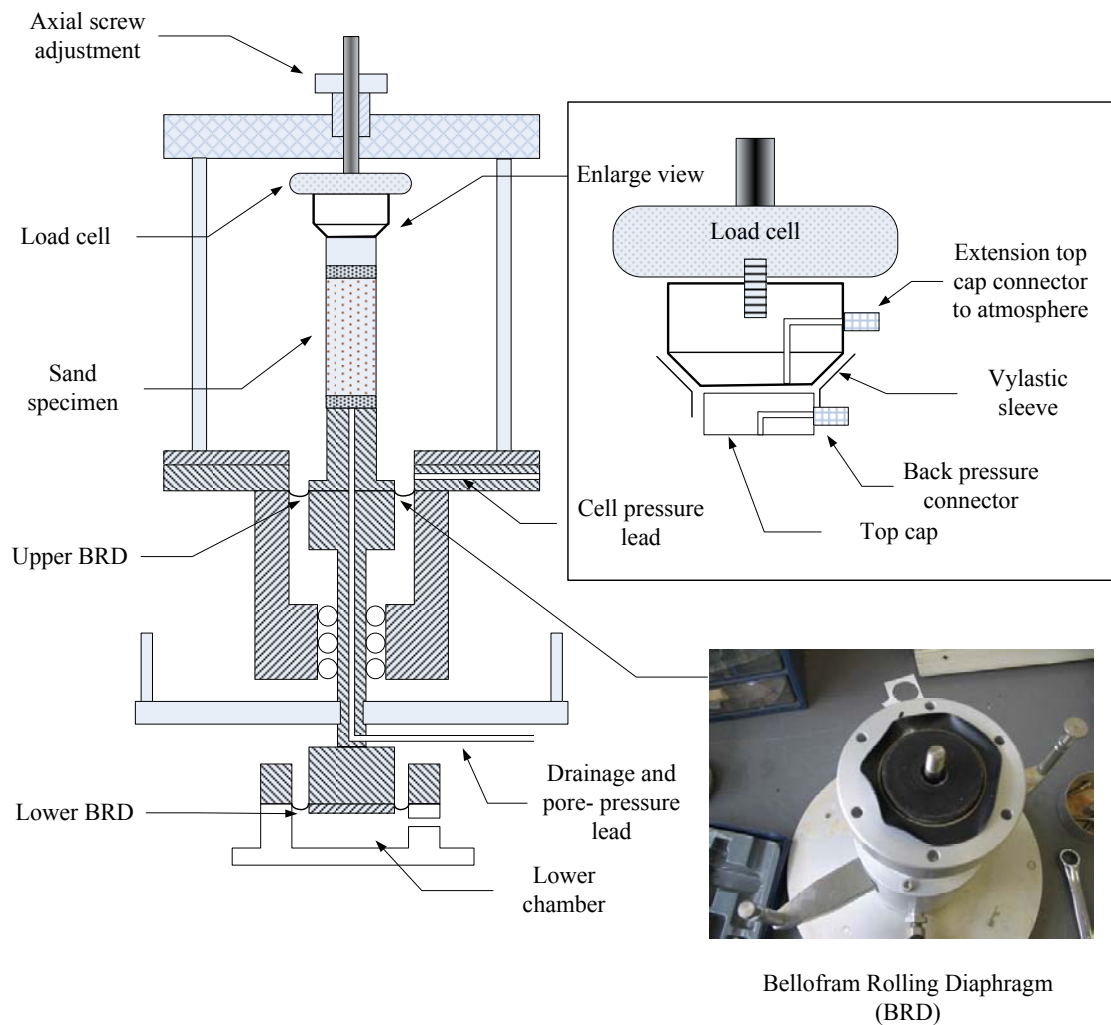


Figure 3-12. Details of the classical Bishop and Wesley stress path triaxial cell.

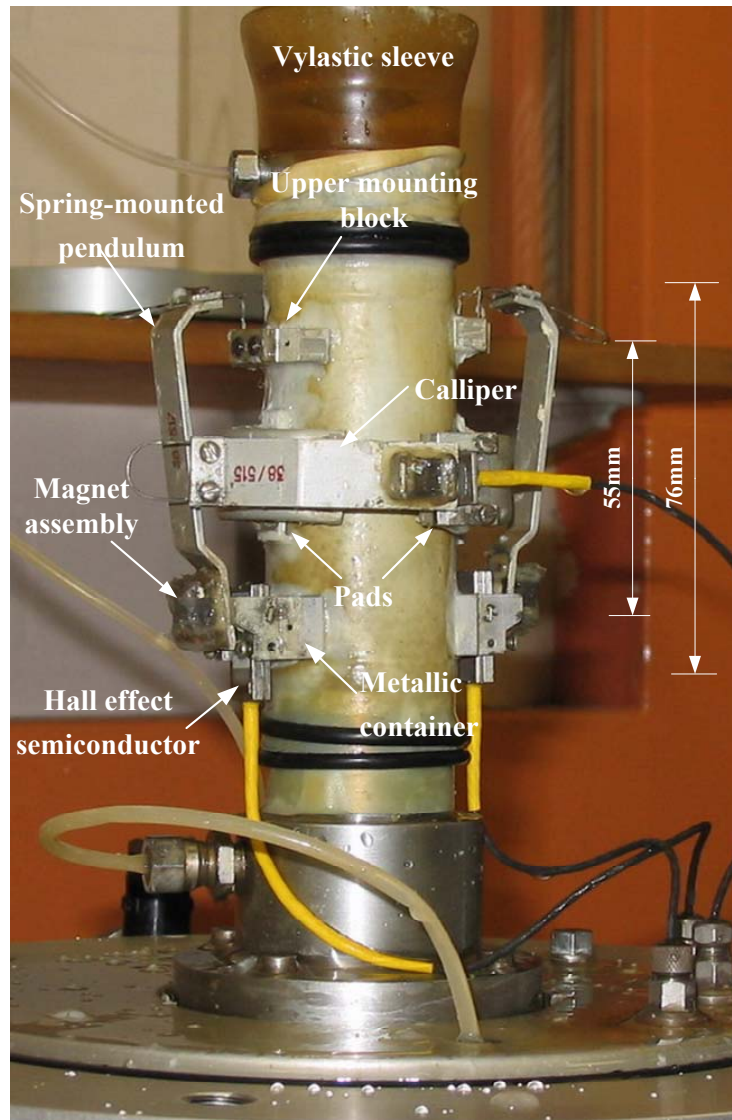


Figure 3-13. Set up of specimen in the ADVTTTS with Hall effect transducers.

3.2.3.3 Temperature control unit

During the initial phase of the testing program, it was found that the measured volumetric strain by the ADVDPCC had a large fluctuation and the actual stress path did not follow the intended direction. This was attributed to the variations of the temperatures. Without temperature control, the pressures in the triaxial cell, controllers and tubes can change. As a result, both the measured data and command signal would be incorrect.

An air conditioning unit was then installed in the NCG research laboratory. This enabled a constant temperature of $20^{\circ} \pm 0.5^{\circ}\text{C}$ to be maintained, under which the ADVTTS was found to be very stable.

3.2.3.4 Specimen preparation and set up for saturated specimen

- (a) Before the specimen was set up in the triaxial apparatus, all tubes were de-aired by flushing with water and the reading of the pore pressure and back pressure were set to zero.
- (b) A porous stone that had been soaked overnight was slid over a layer of water on the base pedestal without trapping any air. Filter paper and the specimen were then placed on the porous stone. A rubber membrane was sealed with grease and O-ring to the bottom platen of the triaxial cell.
- (c) Subsequently, a specially designed split mould was placed over the bottom platen and the membrane was stretched inside the mould. By applying a vacuum to the space between the mould and the membrane, the membrane was pressed against the inner side of the mould.
- (d) Loose and medium dense specimens were prepared by the moist tamping and wet pluviated methods, respectively (see Appendix B).
- (e) After the specimen was formed, the second filter paper and porous stone were then placed on top of it. The top cap was then put in place and sealed with two O-rings. Before removing the split mould, a partial vacuum (about 15 kPa) was applied to the bottom drainage to give the specimen a small effective stress.
- (f) After carefully measuring the height and diameter of test specimen, the internal instrumentation was installed if required. Detailed procedures for setting up Hall effect transducers are given in GDS laboratory manual (GDS Instruments Ltd, 2002). The Loctite Clear Glue adhesive was used for the attachment of the local axial and radial transducers without inserting any pins.

- (g) For the triaxial extension test, a vylastic sleeve and an extension top cap were used. The vylastic sleeve was smeared with a layer of silicone grease to prevent leakage.
- (h) The triaxial cell was then assembled and the load cell reading was set to zero.
- (i) The cell was filled with water with the air bleed open. When the water level reached the mid height of the specimen, the cell and lower chamber pressure readings were set to zero. The load cell was slowly lowered until it just made contact with the top cap. When the extension top cap was used, a very small vacuum was applied to ensure contact between the top cap and the extension cap. When the cell was completely filled with water, the air outlet valve was closed.
- (j) After each specimen was set up in the cell, the deaired water was first flushed through the bottom of the specimen and then a back pressure of 400 kPa was applied to the specimen for up to 12 hours.
- (k) During consolidation, the volume change was measured in order to obtain the initial void ratio for the condition from which the shearing test was to start. The specimen was isotropically consolidated up to the desired effective radial stress for 2 hours.

Figure 3-14 shows the different stages during preparation of the sand specimens in the ADVTTS.

- (1) Triaxial cell and accessories before setting up the specimen;
- (2) The process of forming the sand specimen using the wet pluviated method;
- (3) Triaxial specimen on pedestal after dismantling the split mould;
- (4) Triaxial specimen on pedestal after setting up the internal instrumentation.

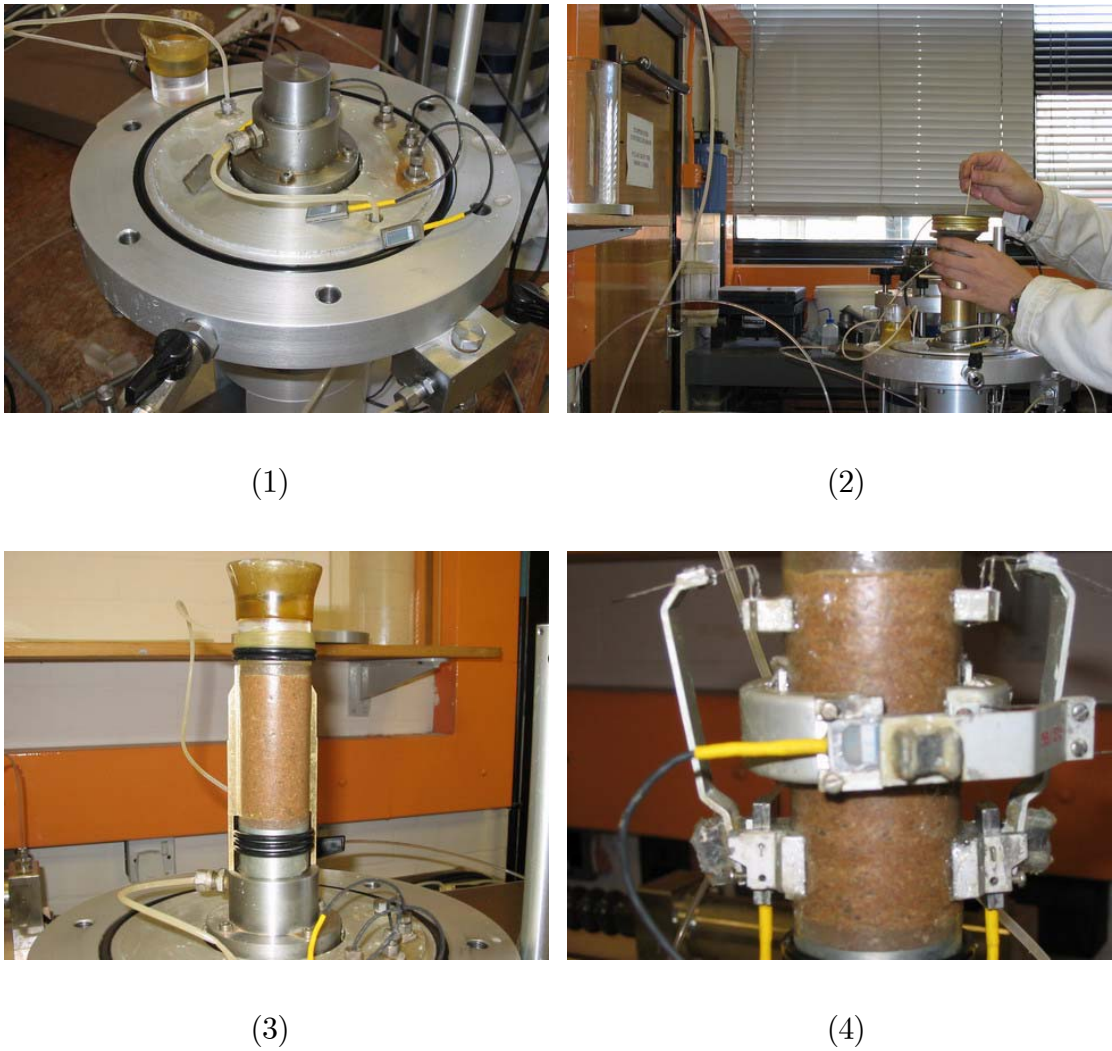


Figure 3-14. Testing setup for the ADVTTTS.

3.3 MATERIAL TESTED

3.3.1 Descriptions of Portaway Sand

The sand tested throughout the main testing program was Portaway sand, which is a well-graded, medium quartz sand from Sheffield, England. Portaway sand was chosen in this study because it was also used in another major pilot-scale experimental project on validation of the shakedown concept for pavement design

and analysis at the University of Nottingham. Element tests on the material reported in this thesis provide basic information that is needed for theoretical modelling of the deformation behaviour of pavements made of this material when subjected to moving wheel loads. A comparison of index and strength properties between Portaway sand (determined later in this thesis) and the calibration chamber sands summarised by Yu (2000) is given in Table 3-2. It can be seen that Portaway sand has very similar engineering properties to those of the calibration chamber sands.

Table 3-2. Comparison of soil properties between six sands (Yu, 2000) and Portaway sand.

Sand	Monterey No.0 sand	Hokksund sand	Kogyuk 350/2 sand	Ottawa sand	Reid Bedford sand	Ticino sand	Portaway sand
e_{\max}	0.82	0.91	0.83	0.79	0.87	0.89	0.79
e_{\min}	0.54	0.55	0.47	0.49	0.55	0.6	0.46
Γ	0.878	0.934	0.849	0.754	1.014	0.986	0.796
λ	0.013	0.024	0.029	0.012	0.028	0.024	0.025
ϕ_c	32°	32°	31°	28.5°	32°	31°	29.8°

3.3.2 Index Properties

3.3.2.1 Maximum and minimum void ratios

The maximum and minimum void ratios for Portaway sand were determined in accordance with the British Standard 1377-4 (1990). In determination of the maximum density, the test on sands was carried out in a 1 L split mould, which was placed in the watertight container on a concrete floor. The sands were compacted under water with the vibrating hammer for 2 minutes until no significant decrease in specimen height was observed. This method is considered suitable for sands containing a small amount (less than 10% by mass) of materials passing a 63 μm test sieve. Another method is specified by ASTM D4523 (1996).

This method is applicable to sands that have a maximum fines content (particles passing a No. 200, 74 μm sieve) of 15%. In determining the minimum density, a known weight of dry sand was shaken slowly in a 1 L glass cylinder. The height of the mass in the cylinder was then measured. This method is suitable for sands containing fines content less than 10%. Three methods are specified by ASTM D4524 (1996). Method A requires the use of a funnel pouring device or a hand scoop to place material in a mould. With method B, the sand is placed in a mould by extracting a soil filled tube. Method C is similar to the British Standard used here and involves inverting a graduated cylinder.

3.3.2.2 Particle size distribution

The particle size distribution for Portaway sand was determined in accordance with the British Standard 1377-2 (1990). Two methods are specified in British Standard. Wet sieving is the definitive method while dry sieving is suitable for soils containing a small amount of fines content. The latter was used for determining the mean grain size D_{50} , effective size D_{10} and the uniformity of coefficient D_u . Table 3-3 summarises the index properties of Portaway sand and Figure 3-15 shows its particle size distribution. Leighton Buzzard sand is a commercially available quartz sand and was used in the preliminary tests. A uniform grading was chosen (0.15-0.212 mm) and its index properties are also included in Table 3-3.

Table 3-3. Index properties of Portaway sand and Leighton Buzzard sand.

	Portaway Sand	Leighton Buzzard Sand (Klotz and Coop, 2002)
Mean grain size D_{50} : mm	0.40	-
Effective grain size D_{10} : mm	0.22	-
Uniformity coefficient: D_{60} / D_{10}	2.05	-
Specific gravity	2.65	2.65
Minimum void ratio	0.46	0.72
Maximum void ratio	0.79	1.01

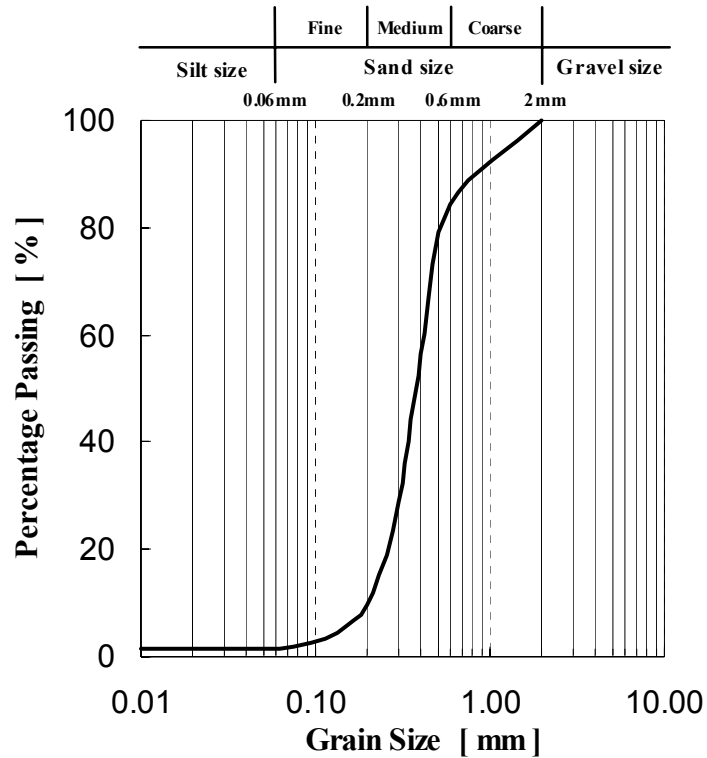
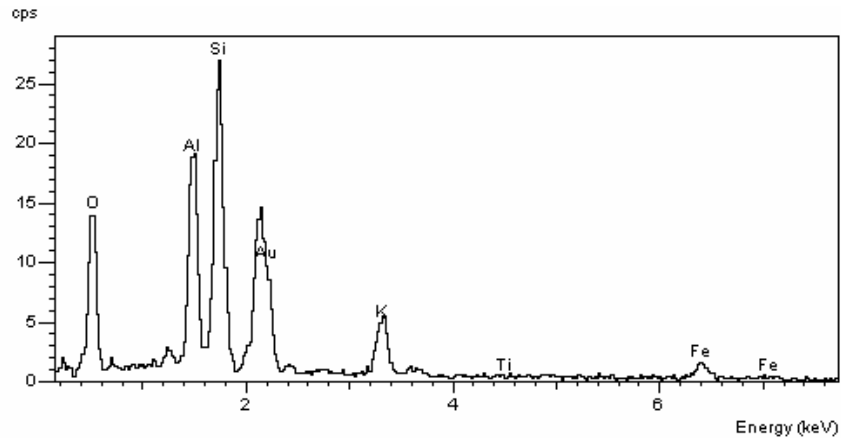


Figure 3-15. Particle size distribution of Portaway sand.

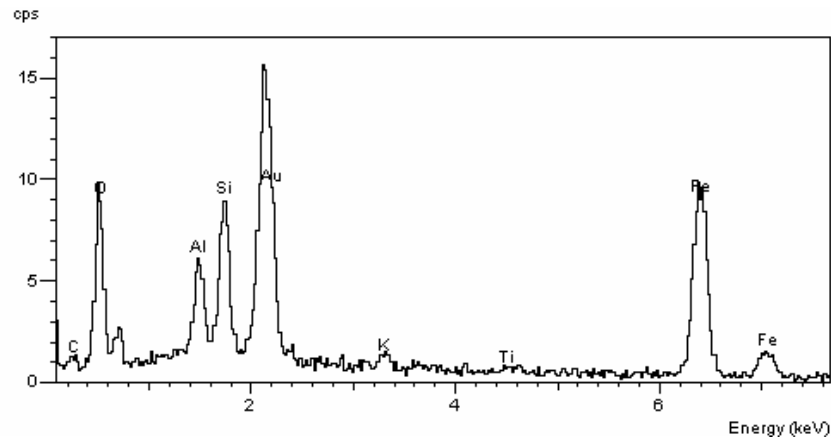
3.3.3 Minerals and Structures of Portaway Sand

It is noted that Portaway sand shows red and brown colours as seen in Figure 3-14 (4). An energy dispersive spectrum analysis (EDS) was carried out through use of a scanning electron microscopy (SEM).

Figure 3-16 (a) shows the results of EDS on a Portaway sand particle. The strong Si (silica) peak indicates that the sand particle is mainly composed of quartz. Fe-oxides are also found, which gives an explanation for the red and brown appearance. The typical clay minerals is indicated in Figure 3-16 (b) taken from fines content.



(a)



(b)

Figure 3-16. EDS analysis for Portaway sand showing: (a) a sand particle, (b) fines content.

It is widely recognised that mechanical behaviour of sands can be directly related to its microstructure. Fabric analyses are useful in showing how the stress-strain and strength characteristics of sands are dependent on particle sizes, associations and arrangements. The methods employed to characterise the microstructures of soils have been summarised by Zhang (2002) as:

- Direct visual observations;
- Examination with the aid of an SEM;

- Indirect methods: slaking, cation exchange capacity (CEC) measurements, and selective chemical dissolution (SCD) accompanied with particle size analysis.

Only the first two methods were used to characterise the structures of reconstituted Portaway sand. The third method is normally used in characterisation of clays. Careful examination of the SEM image (see Figure 3-17) reveals the existence of carbonate materials, which typically appear as bulky particles, shells, precipitates or in solution (Mitchell, 1993). Carbonate minerals are mainly composed of dolomite and calcite. However, further research is needed to quantify the elemental composition of Portaway sand using X-ray diffraction, thermal analysis and chemical analysis.

The particles of Portaway sand are subrounded to subangular in shape as illustrated in Figure 3-18 (a). With high magnification (1 μm scale), the clay platelets are clearly seen as shown in Figure 3-18 (b). In addition, small amounts of feldspar and mica have been identified in Portaway sand.

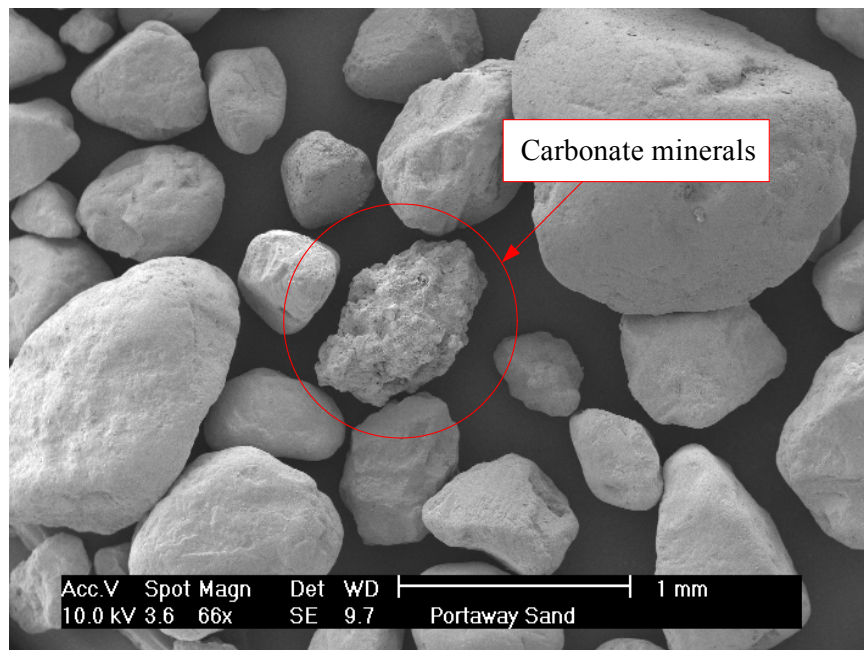


Figure 3-17. SEM micrograph of Portaway sand showing carbonate minerals.

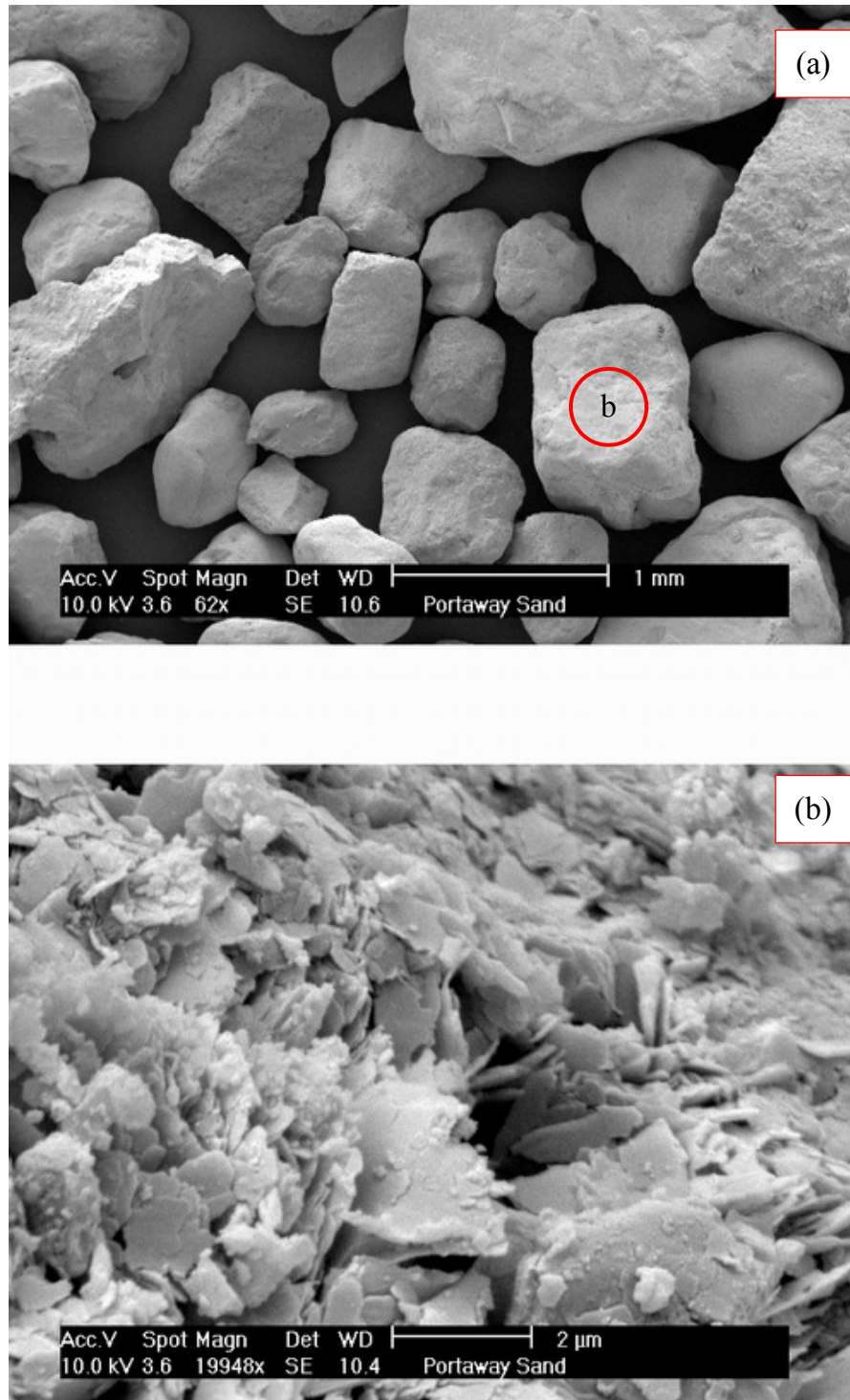


Figure 3-18. SEM micrographs of Portaway sand: (a) sand particles, (b) clays exist on the particle surface.

3.4 DATA CORRECTIONS

3.4.1 Introduction

Evaluating and correcting errors is an important aspect of any experimental investigation. Germaine and Ladd (1988) have summarised sources of problems during triaxial testing in their paper on testing of saturated cohesive soils. Some of these are also applicable to the testing of granular materials. These problems are categorised into three groups and can be evaluated or corrected during different stages as illustrated in Figure 3-19. This section is concerned with the data correction for problems shown in the first group. The problems in the second group have been addressed in previous sections. Other problems will be discussed in the following chapters.

For granular materials, most potential errors on measured parameters are due to the following factors:

- Incorrect determination of initial void ratio of specimen;
- Incorrect assumption of specimen geometry;
- Membrane penetration effect is not considered.

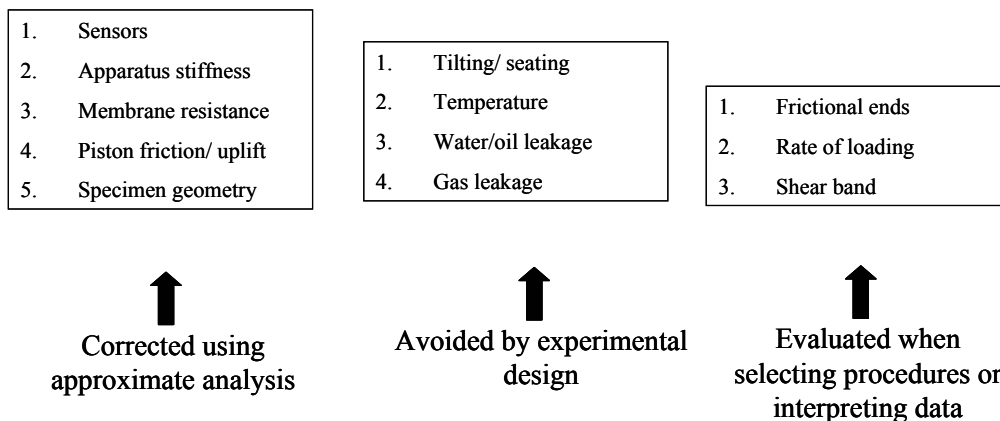


Figure 3-19. Sources of problems during triaxial testing (modified from Germaine and Ladd, 1988).

3.4.2 Determination of Initial Void Ratio

3.4.2.1 Correction after saturation

It has been well recognised by many researchers (e.g. Sladen and Handford, 1987; Been et al., 1991 and Sasitharan et al., 1993) that the potential errors in the calculated void ratio may be large if changes in specimen volume during saturation are not taken into account. Been et al. (1991) compared the void ratios determined using a freezing technique with the void ratios calculated based on the assumption of isotropic straining ($\varepsilon_p = 3\varepsilon_a$) during saturation on Erksak 330/0.7 sand. They concluded that the potential void ratio errors were very small, typically of the order of 0.01, increasing to 0.02 for very loose sands.

It was noted that the index properties of Portaway sand are very similar to Erksak 330/0.7 sand. Hence, for practical purposes the void ratio of Portaway sand specimens prior to shearing can be estimated from their initial dimensions provided that the axial strain during saturation and volume change during consolidation are carefully measured.

During back pressure saturation, the axial deformation was measured using an external LVDT transducer, while maintaining the effective radial stress at approximately 15 kPa. It can be seen from Figure 3-20 that the axial strains increase with greater in void ratios. A critical void ratio (around 0.75) appears, which suggests that significant deformation has occurred during saturation on very loose sands.

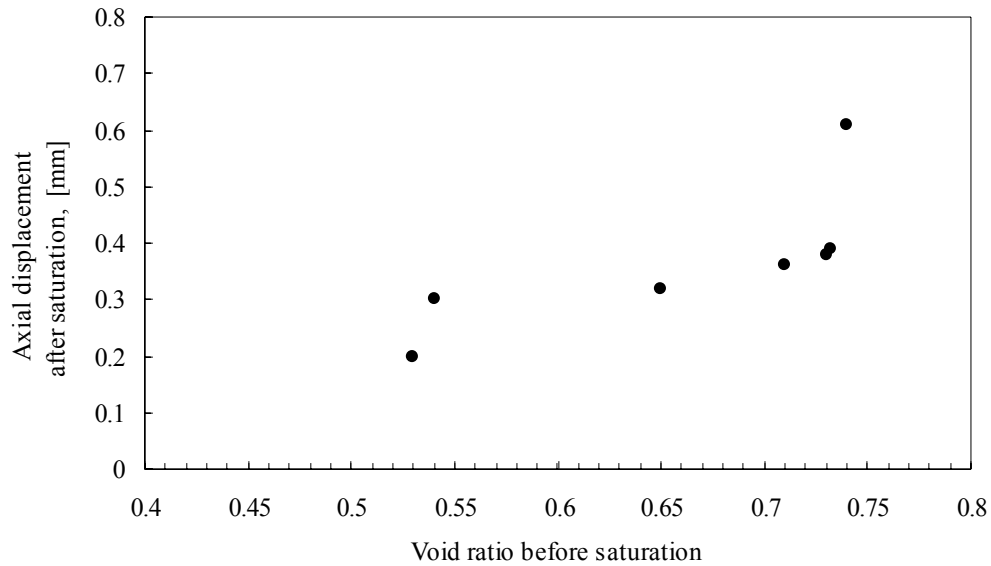


Figure 3-20. Axial displacement measured after back pressure saturation.

3.4.2.2 Correction for the membrane penetration effect

In drained tests, the volumetric strains are normally calculated based on the quantity of water expelled from or drawn into the fully saturated specimens. However, it is well known that the flexible rubber membrane may penetrate into the peripheral voids so that the measured volumetric strain can be incorrect based on the measurement of water leaving or entering the specimen. This phenomenon, known as membrane penetration, may have significant influence on the stress-strain behaviour of sands. The pore pressure is also affected by membrane penetration in undrained tests.

Several correction methods have been developed since the effect of membrane penetration was first recognised by Newland and Allely (1959). The magnitude of its effect was determined by many factors identified previously, including the properties of membrane, size of specimen, grain size distribution, grain shapes, relative density, mean grain size and effective confining pressure. The last two of these factors have more profound impacts.

An attempt has been made to evaluate the effect of membrane penetration by comparison of the results obtained from the ADVDP (global strain) and the Hall effect transducer (local strain). The difference between the results can be considered as the incorrect volumetric strain recorded by ADVDP due to membrane penetration. A similar approach was used by Baldi and Nova (1984). They stated that the use of a local measuring device was not affected by membrane penetration in the voids because the transducer attached to the specimens covered a much larger area than individual grains. A semi-empirical model developed by Baldi and Nova (1984) was then verified by the measured membrane penetration. The membrane penetration V_m is defined as:

$$V_m = \frac{1}{2} \frac{D_{50}}{D_0} V_0 \left[\frac{\sigma'_3 D_{50}}{E_m t_m} \right]^{1/3} \quad (3-1)$$

where D_{50} is the mean grain size, D_0 and V_0 are the initial diameter and volume of the specimen, respectively, E_m is the Young's modulus of membrane, and t_m is the thickness of the membrane. It was found that the errors introduced by the membrane penetration were insignificant when compared with errors introduced due to saturation. The likely errors in void ratio due to membrane penetration are smaller than 0.006, which was calculated from equation (3-1) (see Figure 3-21, when $\sigma'_3 < 500$). Hence, for practical purposes, the void correction was neglected in this study.

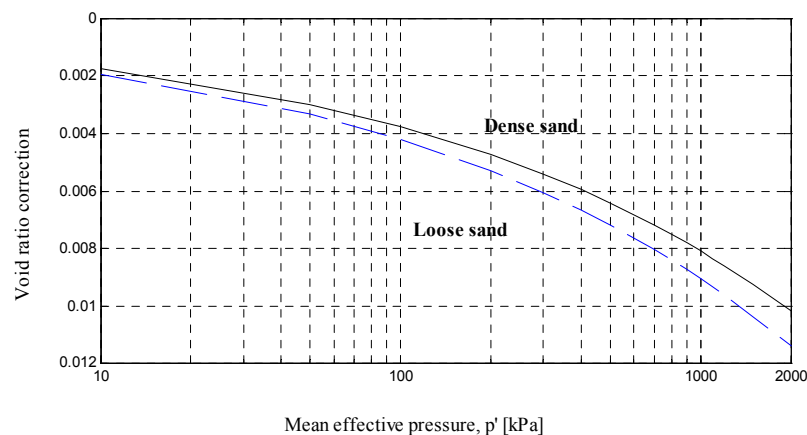


Figure 3-21. Membrane penetration effects for Portaway sand.

3.4.3 Area and Membrane Correction

3.4.3.1 Area correction

Two different methods were used in the NDTTS and the ADVTTTS for calculation of the cross-sectional area.

The ADVTTTS automatically uses volume change (recorded in the ADVDP) and axial displacement to compute the cross-sectional area of the specimen. The assumption that the specimen deforms as a right cylinder is used so that the corrected area can be expressed as (Bishop and Henkel, 1957):

$$A_c = \frac{\left(\pi \times \left(D_0/2\right)^2 \times H_0\right) + \Delta V}{H_0 - \Delta H} \quad (3-2)$$

where A_c is the corrected cross-sectional area of the specimen, D_0 and H_0 are the initial diameter and height of the specimen, respectively, and ΔH and ΔV are the changes of the height and volume of the specimen, respectively. For the undrained condition, the above equation can be written as:

$$A_c = \frac{A_0}{1 - \varepsilon_a} \quad (3-3)$$

where A_0 is the initial cross-sectional area of the specimen.

Although this assumption was seldom met in actual specimen, La Rochelle et al. (1988) has demonstrated that there is only 2–3% difference using more realistic formula for bulging type failure.

In the NDTTS, it was found that the specimen deformed in a parabolic shape. Therefore, the calculation based on the right cylindrical deformation is not really appropriate. The volume was calculated assuming a circular barrel deformation

with parabolic curvature. The volumetric strain, volume and cross-sectional area are defined as:

$$\varepsilon_p = \frac{V - V_0}{V_0} \quad (3-4)$$

$$V = \frac{1}{15} \pi (H_0 - \Delta H) (8R^2 + 4Rr_0 + 3r_0^2) \quad (3-5)$$

$$A_c = \pi \times R^2 \quad (3-6)$$

where V and V_0 are the current and initial volume respectively, R is the current radius of specimen measured by the ‘on-specimen’ device and r_0 is the initial radius of specimen.

It should be noted that the area correction method for the specimen with rupture surface is far more complicated than methods mentioned above. As shown later, this type of deformation normally occurs in drained tests on dense sands. It is well recognised that the critical state parameters measured from these tests are problematic and the correction method requires further research.

3.4.3.2 Membrane correction

The membrane correction was determined in accordance with the British Standard 1377-8 (1990).

The British Standard provides a simple membrane correction method, in which the correction is based on a chart. The membrane correction q_m can be obtained from:

$$q_m = q_{chart} \times \frac{38}{D_0} \times \frac{t_0}{0.2} \quad (3-7)$$

where q_{chart} is the value obtained from the chart, $t_0 = 0.3$ is the initial thickness of the membrane. The maximum corrections (at 20% strain) are calculated as 2.28 kPa and 3 kPa for specimens tested in the NDTTS ($D_0 = 50$) and the ADVTTTS

($D_0 = 38$), respectively. It can be seen that these corrections have insignificant effects on the calculated stress-strain and strength of the sands. Therefore, no membrane correction has been made in subsequent analyses.

3.5 SUMMARY

In this chapter, the evaluation and modification of two triaxial systems have been described. The material tested and detailed experimental procedures have also been presented. The partially updated Nottingham dynamic testing system was used in preliminary tests on dry sand. The performance of this system is evaluated in Chapter 4. The main body of the tests were carried out on an advanced stress path triaxial testing system using saturated Portaway sand. The following chapters describe the direct results and associated interpretations based on extensive monotonic and cyclic loading triaxial tests.

Chapter 4

Monotonic Loading Triaxial Tests

4.1 INTRODUCTION

Improved modelling of sand behaviour can be achieved by introducing the state parameter concept as used in the formulation of the model CASM and its extensions. Application of the models, however, requires accurate estimation of the *CSL* in the $p'-\nu-q$ space. Therefore, a laboratory testing program under monotonic loading was designed with the following objectives in mind:

- To add to the body of knowledge on the stress-strain and strength characteristics of Portaway sand.
- To evaluate the validity of the critical state concept and identify a possible *CSL* for Portaway sand.
- To investigate the applicability of state parameter concept and verify the general 'state parameter-stress ratio' relation.
- To provide triaxial test data for verifying the critical state models: CASM, CASM-b and CASM-d, which are described in Chapter 6.

This chapter is arranged in the following order: firstly, the tests on dry sands are described and the performance of the updated NDTTS is evaluated. The critical state concept is then examined based on six series of triaxial tests over a wide range of confining pressures and initial densities under both drained and undrained loading conditions. Following this, the interpretation of these results is given. Finally, some aspects of small strain behaviour of Portaway sand are introduced.

4.2 PRELIMINARY TESTS ON DRY SANDS

This section presents the preliminary finding on the triaxial shear behaviours of dry Portaway sand. As mentioned in previous chapter, the NDTTS was partially updated and only capable of testing dry materials with the current configurations. Furthermore, the newly developed ‘on-specimen’ radial strain measuring device cannot measure the deformation accurately after 10–15% axial strain. Therefore, the measurement of critical state parameters at large strain (around 25%) was not the main focus in this group of tests. The objectives of carrying out these initial tests were to evaluate the performance of the updated NDTTS and to obtain preliminary stress-strain and strength characteristics of Portaway sand under various confining pressures and densities. The results presented herein also provide some useful idea for consideration in the future designs of advanced triaxial testing systems.

4.2.1 Testing Program

Table 4-1 contains the essential information for all the triaxial tests performed in series (A) with axial strains up to 30% but without volumetric strain measurement. Table 4-2 gives details of all the triaxial tests conducted in series (B), in which a newly designed ‘on-specimen’ measuring device attached to the membrane was used for volumetric strain measurement. The tests in series (B) were terminated at

10–15% axial strains, however, because it was found that the ‘on-specimen’ measuring device would come in contact with the triaxial cell at large deformations.

All specimens were sheared monotonically under a constant effective confining pressure condition after an isotropic consolidation. A displacement-controlled method was employed with a loading rate of 10 mm/hr. The drainage valve was opened to the atmosphere during shearing so that the tests can be considered as ‘drained’ tests.

Table 4-1. Summary of tests on dry sands (series A).

Test ID#	e_0	D_r	σ'_3 (kPa)	ϕ_p Deg	$\phi_p - \phi_c$ Deg	p'_p (kPa)	I_R	$I_R + D_r \ln p'_p$
P-01	0.589	0.61	207	39.0	9.0	441.3	3.00	6.71
P-02	0.587	0.62	138	40.7	10.7	310.3	3.56	7.09
P-03	0.590	0.61	69	37.6	7.6	141.0	2.53	5.53
P-04	0.489	0.91	138	42.6	12.6	330.7	4.20	9.49
P-05	0.586	0.62	138	40.8	10.8	311.5	3.60	7.15
P-06	0.669	0.37	138	34.6	4.6	258.9	1.53	3.57
P-07	0.485	0.92	300	40.5	10.5	670.5	3.50	9.52
P-08	0.489	0.91	150	41.5	11.5	346.4	3.83	9.17
P-09	0.490	0.91	50	43.4	13.4	123.2	4.47	8.84
P-10	0.667	0.37	300	34.0	4.0	553.7	1.33	3.69
P-11	0.669	0.37	150	34.3	4.3	279.3	1.44	3.51
P-12	0.668	0.37	50	35.2	5.2	95.3	1.72	3.41
Additional tests on Leighton Buzzard sand								
L-01	0.740	0.93	300	39.3	7.3	645.5	2.43	8.45
L-02	0.740	0.93	50	44.0	12.0	125.8	4.00	8.50
L-03	0.930	0.27	300	34.1	2.1	555.2	0.70	2.41
L-04	0.900	0.37	150	34.8	2.8	282.9	0.93	3.02

Note: The values of ϕ_c shown in Table 4-1 are 30° and 32° that have determined for Portaway sand and Leighton Buzzard sand, respectively.

Table 4-2. Summary of tests on dry sands (series B).

Test ID#	e_0	D_r (%)	σ'_3 (kPa)	ε_a (%)	State at end of test
P-13	0.641	46	300	-	Equipment faulty
P-14	0.460	100	300	10	Strong dilation
P-15	0.492	90	100	8.5	Strong dilation
P-16	0.600	58	50	11	Mild dilation
P-17	0.502	87	50	10	Strong dilation
P-18	0.564	68	30	11	Mild dilation
P-19	0.636	47	100	8	Critical state
P-20	0.533	78	400	-	Equipment faulty
P-21	0.526	80	200	8	Strong dilation
P-22	0.592	60	450	9	Critical state
P-23	0.460	100	450	10	Strong dilation
P-24	0.560	70	200	10	Strong dilation

Note: ε_a = Axial strain before the 'on-specimen' device touched the triaxial cell.

Four additional triaxial tests were conducted in series (A) on Leighton Buzzard sand in order to compare the measured strength properties with published data. This sand was used extensively in the geotechnical research community and its properties have been well documented. Klotz and Coop (2002) recently carried out triaxial tests on the identification of its *CSL*. The particle size and grading selected in this testing program are similar to ones they used. Through the preliminary tests on both Leighton Buzzard sand and Portaway sand the performance of the NDTTS has been verified.

4.2.2 Results and Discussion

4.2.2.1 Shear strength

Figure 4-1 shows the typical behaviour of Portaway sand sheared under constant effective confining pressures ($\sigma'_3 = 300$ kPa) for both loose and dense states. The patterns of the sand behaviour observed agree well with those reported by Lee and

Seed (1967). The critical state was identified at constant deviatoric stress with increasing axial strain.

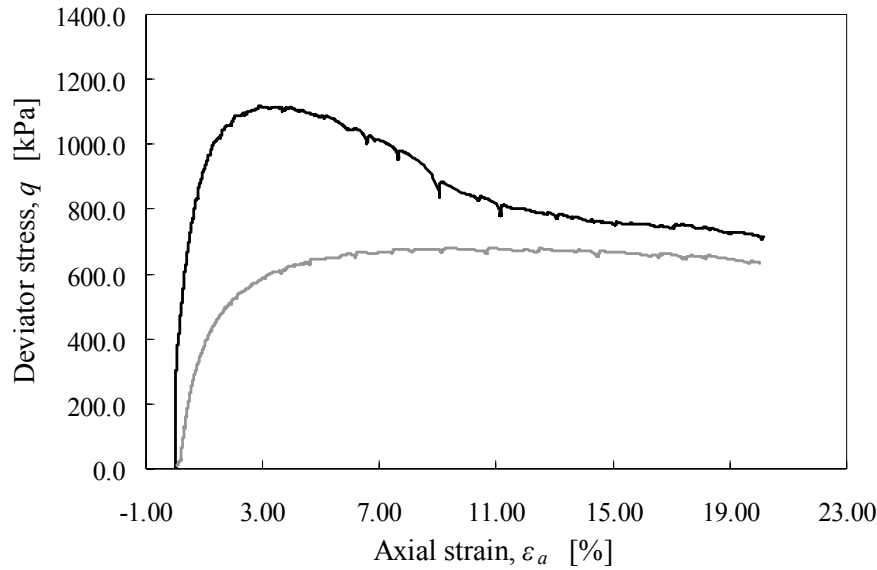


Figure 4-1. Typical stress-strain curves on dry Portaway sand.

The critical state and peak friction angles were determined according to equation (2-2) at the points of critical state and peak strength, respectively. The relationship between the critical state friction angle ϕ_c and peak friction angle ϕ_p was correlated in terms of the relative dilatancy index I_R , defined in equations (2-13)–(2-15). Figure 4-2 and Figure 4-3 show the linear regressions following equation (2-13) on the data obtained. Based on the results from the triaxial tests, the relative dilatancy index I_R can be expressed using the following equations for Portaway sand and Leighton Buzzard sand, respectively:

$$I_R = D_r(10.42 - \ln p') - 0.11 \quad (4-1)$$

$$I_R = D_r(9.4 - \ln p') - 0.28 \quad (4-2)$$

The above correlations suggest that for both Portaway sand and Leighton Buzzard sand the material constants Q and R contained in equation (2-13) are around 10 and 1, respectively. This result is consistent with Bolton's conclusion that value of Q should be equal to 10 for typical quartz sands.

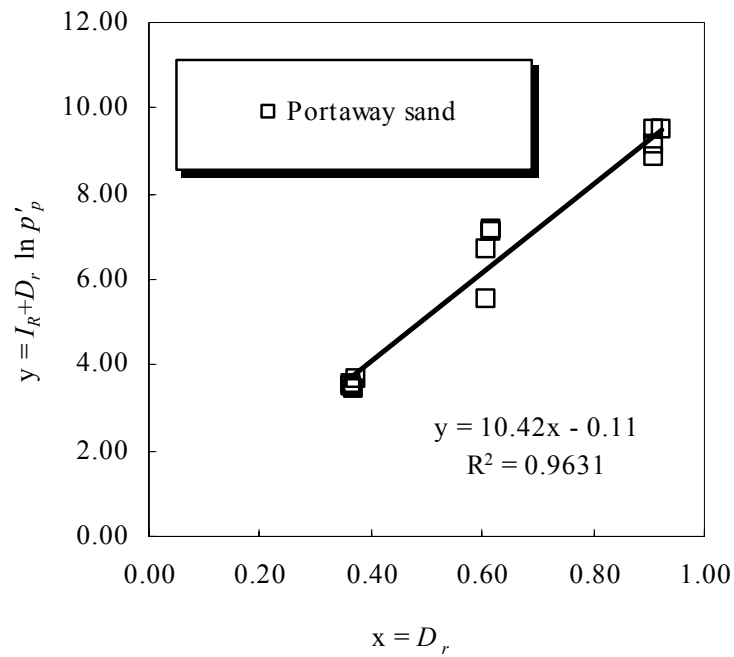


Figure 4-2. Recalibration of equation (2-13) proposed by Bolton (1986) on dry Portaway sand.

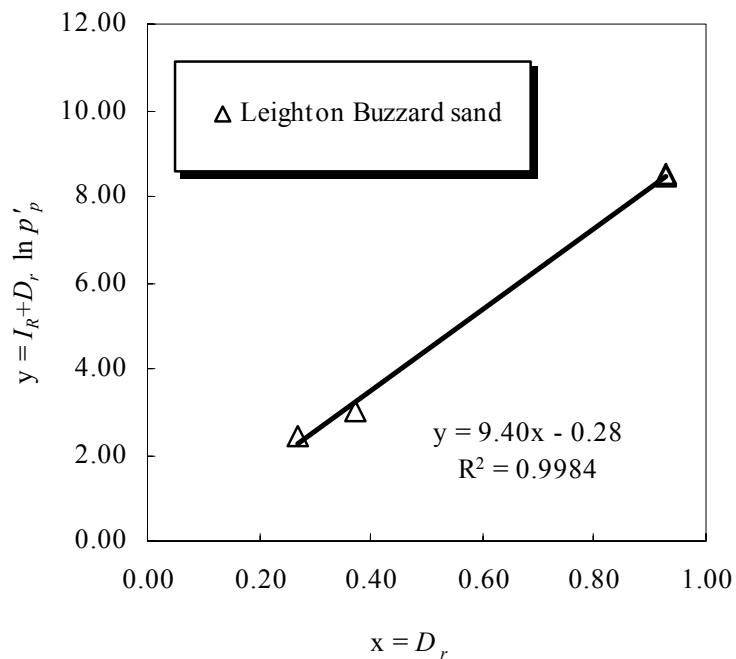


Figure 4-3. Recalibration of equation (2-13) proposed by Bolton (1986) on dry Leighton Buzzard sand.

4.2.2.2 Performance of the ‘on-specimen’ measuring device

Plotted in Figure 4-4 is the volumetric strains measured using the new ‘on-specimen’ measuring device for three dense Portaway sand specimens (P-15, 16 and 18). The method for calculating volumetric strain ε_p was based on the parabolic assumption as described in section 3.4.3.1.

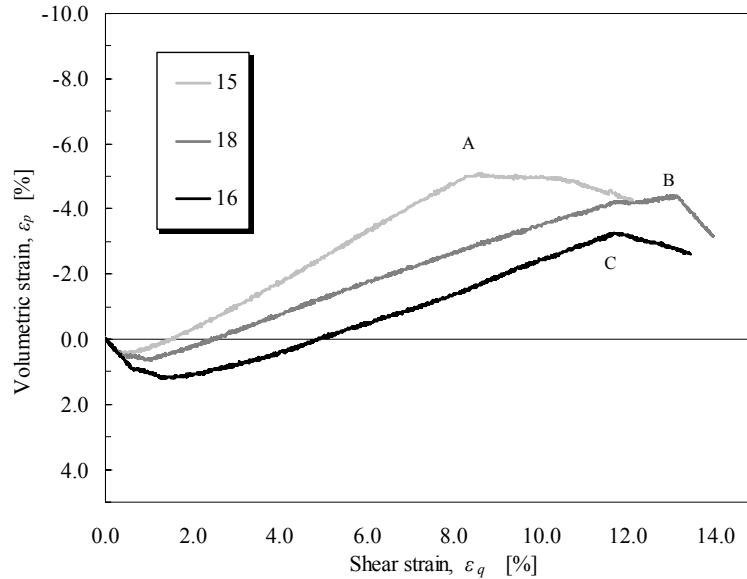


Figure 4-4. Volumetric strains obtained from ‘on-specimen’ measuring device.

It is evident that the data measured is continuous with no jumps prior to reaching medium shear strains of 8–15%. This suggests that there is no stick-slip behaviour resulting from resistance to movement of the armature. The abrupt changes of the curves at points ‘A’, ‘B’ and ‘C’ attributed to being made contact between the miniature LVDT and triaxial cell. Therefore, the data obtained afterwards was considered unreliable and discarded. The stress-dilatancy relations measured from the same set of specimens are presented in Figure 4-5. The trend suggests that Rowe’s stress-dilatancy relation can be used to describe Portaway sand behaviour very well. Plotted in Figure 4-6 are the overall stress paths in the $\ln p' - \nu$ space. Although most of the tests did not reach the critical states, the ‘possible’ *CSL* seems to lie within the shaded area indicated in Figure 4-6.

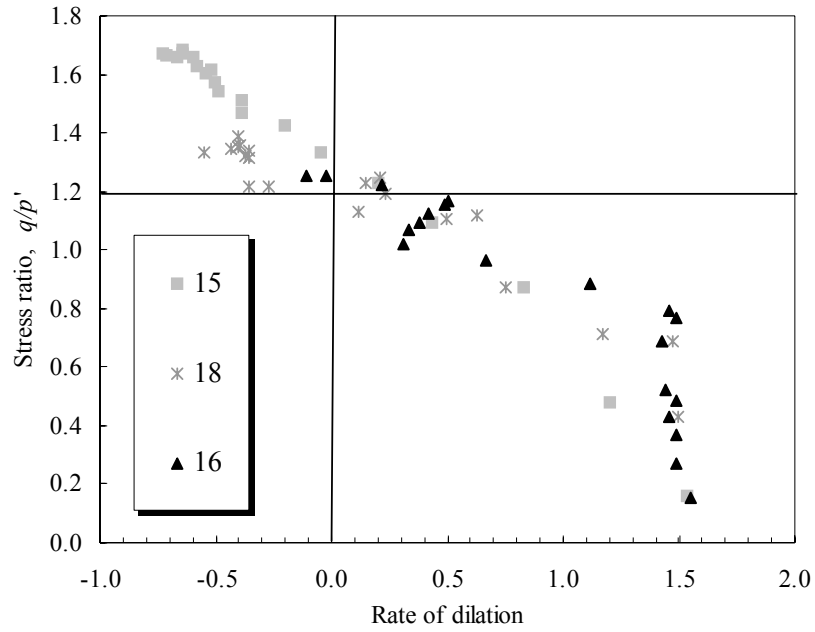


Figure 4-5. Stress-dilatancy relation of dry Portaway sand.

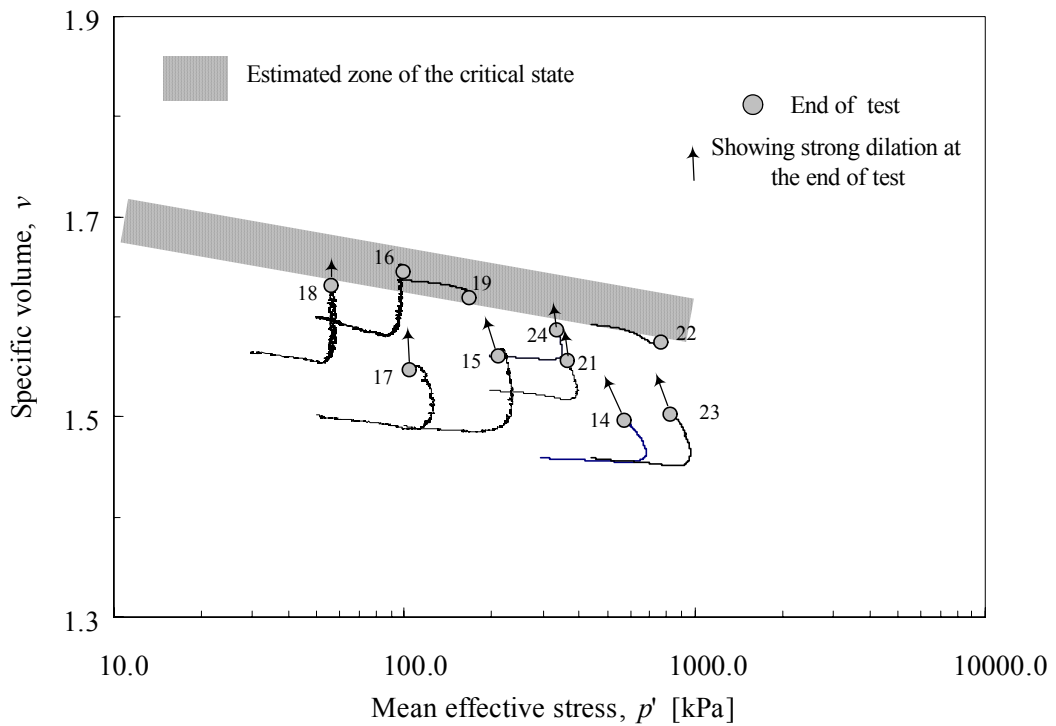


Figure 4-6. Stress paths of dry Portaway sand (up to 8-15% shear strains).

4.3 EXAMINATION OF CRITICAL STATE CONCEPT

4.3.1 Introduction

Geotechnical researchers have increasingly focused attention on the state parameter type of approach in recent years. One difficulty in the application of these methods and models is determining the correct *CSL* in the $p'-q-\nu$ space. However, since many researchers have approached this issue from different perspectives and interpreted their results in a variety of forms, it can be seen that a large number of contradictory conclusions have been reached regarding the uniqueness of the *CSL* and the factors that may or may not affect it.

One objective of the present research was to provide a consistent set of data on a quartz sand so that the validity of the critical state concept could be verified. The factors affecting the location of the *CSL* have been examined by carrying out a comprehensive and systematic testing program in light of the following conditions:

- The initial condition of the specimen;
- The drainage condition;
- The specimen preparation method;
- The stress path imposed;
- The loading mode (stress or strain controlled).

All fully saturated specimens were subjected to isotropically consolidated history before shearing. A total of 31 drained and undrained tests were grouped into six series. The designations used in this monotonic loading program are summarised in Appendix C.

The tests carried out in series A–D are known as conventional triaxial compression or extension tests, which involve holding the cell pressure constant, $\delta\sigma_3 = 0$, and

increasing or decreasing the axial load. The total stress path followed in this type of tests has a slope of 3 in the $p'-q$ stress space:

$$\delta q / \delta p' = 3 \quad (4-3)$$

The stress-strain and strength characteristics of sands have been investigated extensively using constant cell pressure (*CCP*) tests over the last five decades. Tests carried out under different stress paths are less common. This is mainly because most equipment is incapable of changing both the confining pressure and shear stress simultaneously. In most geotechnical problems, however, the stress path does not always follow this ideal stress path, as is the case shown in series A–D. Traffic loading normally involves simultaneous changing both the shear stress and confining pressure. The rotation of the principal stresses may also occur in this type of loading, in which the major principal stress does not necessarily coincide with the vertical direction. Therefore, tests carried out in series E were devised to investigate aspects of the stress-strain and strength characteristics under drained conditions with a variable confining pressure (*VCP*). The stress paths employed in these tests include:

- Constant mean effective stress, in which

$$\delta p' = 0 \quad (4-4);$$

- Constant axial shear stress, in which

$$\delta q / \delta p' = -3/2 \quad (4-5);$$

- Complex stress paths, which involved unloading, proportional loading and primary loading.

Figure 4-7 shows the stress paths carried out in the $p'-q$ stress space. In Figure 4-7 (a), the state of stress in a specimen is represented by a point 'A' after isotropic consolidation. The stress paths 1, 2 and 3 are for a conventional triaxial

compression or extension tests, a constant mean effective stress test and a constant shear stress test, respectively. In Figure 4-7 (b), stress paths 4, 5, and both 6 and 7 are defined according to Lade and Duncan (1976) as unloading, proportional loading and primary loading, respectively.

The effects of pre-shearing on the undrained behaviour of loose Portaway sand were investigated in series F.

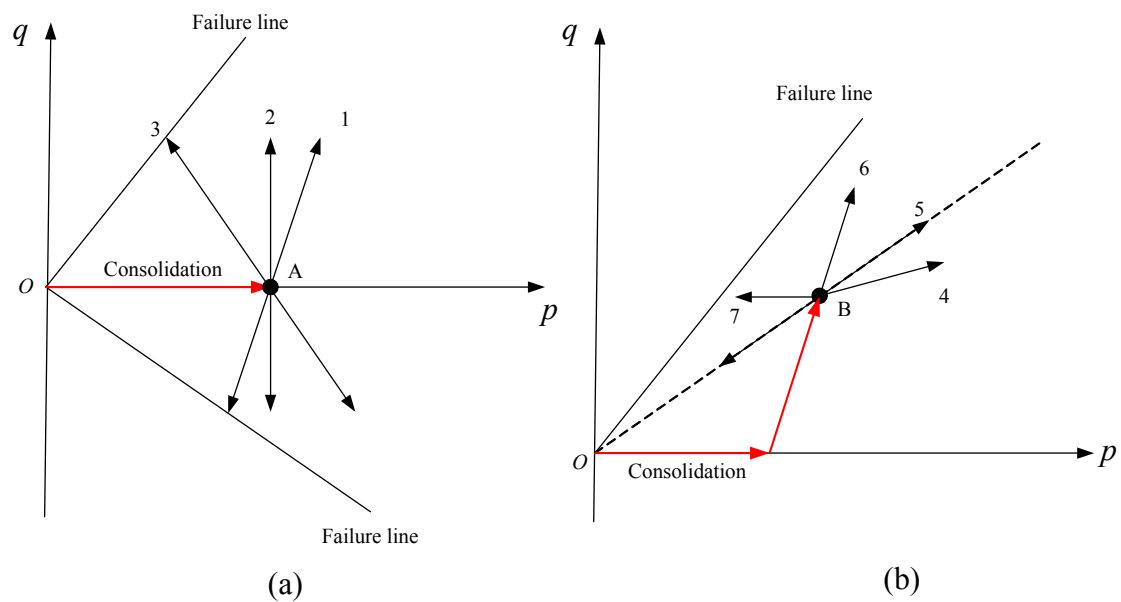


Figure 4-7. Definition of total stress paths used in triaxial tests.

4.3.2 Series A: Drained Compression Tests (CIDC-1~5)

Five drained tests were conducted for loose sand specimens (CIDC-1, CIDC-2 and CIDC-3) and dense sand specimens (CIDC-4 and CIDC-5). The specimen preparation, saturation and data correction method have been described in Chapter 3. Specimens were formed with a variety of initial void ratios using the moist tamping or wet pluviation methods. All specimens were isotropically consolidated with initial effective confining pressures ranging from 50 kPa–500 kPa. After consolidation, shearing was carried out within one hour so that the secondary compression effect could be neglected. In this series of tests, the displacement-

controlled mode was chosen, which is a conventional method that has been used by many researchers (e.g. Been et al., 1991; Coop, 1990). The initial conditions and results of tests are summarised in Table 4-3. The stress-strain relationships of these tests are presented in Figure 4-8.

Table 4-3. Summary of Series A: CIDC tests.

Initial conditions					End of test		Remarks
Test ID	e_0	D_r (%)	p'_0 (kPa)	V (%/Hr)	ε_a (%)	η_c	
Contractive behaviour							
CIDC-1	0.699	28	500	3	29	1.12	Critical state
CIDC-2	0.706	25	300	3	29	1.18	Critical state
CIDC-3	0.715	23	50	3	25	1.19	Critical state
Dilative behaviour							
CIDC-4	0.537	77	300	2	26	1.23	Critical state*
CIDC-5	0.538	76	50	2	28	1.29	Critical state*

Notes:

V = Strain rate in displacement-controlled tests

η_c = Stress ratio q/p' at the critical state

ε_a = Axial strain at the critical state

* Continuing dilation at the end of tests due to shear banding

Stress-strain and strength characteristics of loose Portaway sand

As can be seen from Figure 4-8, the three loose specimens show the behaviours of continuing strain hardening and volume contraction. The volumes of the specimens approached maximum volume contraction at a strain level of between 15-25%. The stress ratios measured at 25% axial strains were 1.12, 1.18 and 1.19 for tests CIDC -1, CIDC-2 and CIDC-3, respectively. Similar observations have been reported by Kolymbas and Wu (1990) for loose Karlsruhe sand and by Chu (1995) for Sydney sand. Chu (1995) concluded that this kind of behaviour might only occur in tests with well-prepared free ends. The occurrence of non-homogeneity in specimens can be delayed without end effects. Hence, the results obtained here indicate that boundary effects may not be critical for the current testing program.

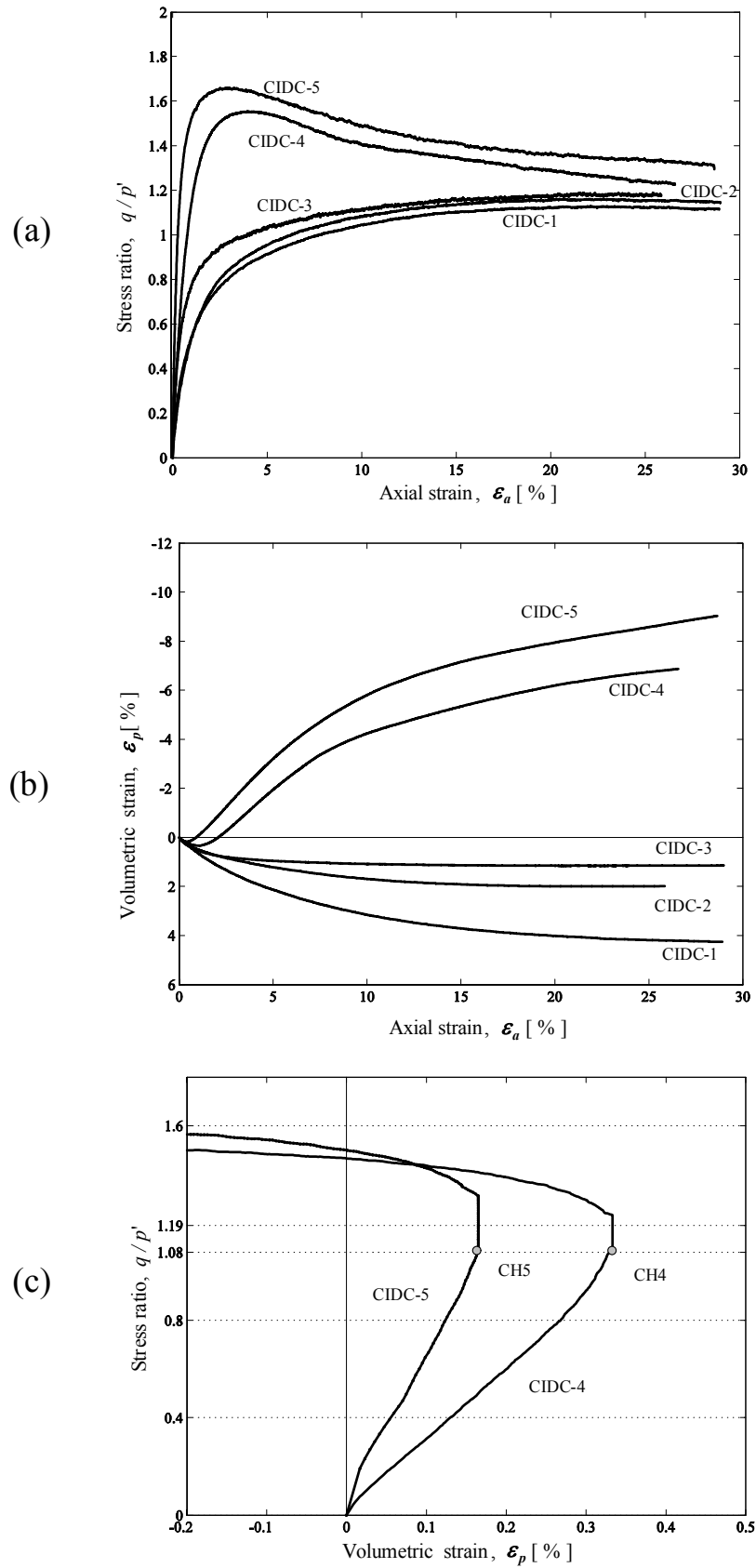


Figure 4-8. Stress-strain relationships (Series A: CIDC).

Stress-strain and strength characteristics of dense Portaway sand

Measuring the critical state parameters of dense sands by drained tests is problematic, as significant non-homogeneous deformations can develop prior to the achievement of the critical state. Two tests (CIDC-4 and CIDC-5) were run on dense sand specimens in order to evaluate such effects on Portaway sand. It is noted that the specimens exhibited strain hardening behaviour at the beginning of the tests. After reaching maximum volume contraction at strain levels of 0.45% (CIDC-5) and 1.06 % (CIDC-4), the specimens entered the second stage where they started to dilate. Strain hardening continued until the specimens reached peak strengths at 3.36% (CIDC-5) and 4.22% (CIDC-4) axial strains, when the dilatancy rate increased from zero to maximum. Through further development of the deformation, strain softening occurred together with further volume dilation. It was expected that the specimens would ultimately reach constant volumes and stress ratios at large strains. However, there was no sign of the dilation abating at large strain and the stress ratios were slightly higher than those from loose sand specimens. The stress ratios measured at the end of tests were taken as the critical state stress ratios for both tests. The ratios are 1.29 for test CIDC-5 and 1.23 for test CIDC-4.

Relationship between critical state and characteristic state

The concept of characteristic state was first introduced by Luong (1980) to refer to a stress level corresponding to the state from contraction to dilation. The relationships between critical state and characteristic state were later investigated by Chu (1995). Chu found that for loose sand showing contractive behaviour, the critical state and characteristic state coincide with each other at large strain. However, for a dense sand showing dilative behaviour, the characteristic state normally occurs at low strain level. Figure 4-8 (c) shows the stress-dilation relations for test CIDC-4 and test CIDC-5, in which the characteristic states are marked as CH4 and CH5, respectively.

Table 4-4 compares the characteristic states with the critical states for the two specimens. It can be seen that the stress ratios at CH4 and CH5 are lower than the corresponding critical states. This experimental finding is consistent with those obtained by Luong and Chu.

Table 4-4. Comparison of characteristic states and critical states.

Test ID	η at characteristic state	η at critical state
CIDC-4	1.08	1.23
CIDC-5	1.08	1.29

Stress-dilatancy relation

A fundamental issue in constitutive modelling of sands is how to describe the relationship between stress ratio η and dilatancy rate d . The classical Rowe's stress-dilatancy relation (Rowe, 1962) has been used to derive the plastic potential g used in CASM as well as many other critical state models. Therefore, it is interesting to see the performance of this well-known relation on predicting the evolution of dilatancy of Portaway sand.

Figure 4-9 shows the experimental stress-dilatancy relation of Portaway sand together with the predictions given by various theoretical stress-dilatancy relations. The plots suggest that Rowe's relation corresponds very well with the stress-dilatancy relation of Portaway sand in loose states (CIDC-1 and CIDC-2). After passing the critical state, however, Rowe's relation seems to overestimate the stress ratios for specimens packed in dense states (CIDC-4 and CIDC-5).

A similar deficiency in Rowe's and Cam-clay's stress-dilatancy relations was also reported by Li et al. (1999) on Toyoura sand. They concluded that the unique relationship between the stress ratio and dilatancy assumed in both relations did not exist and thereby rejected the use of unified modelling for sand behaviour over a wide range of densities and confining pressures.

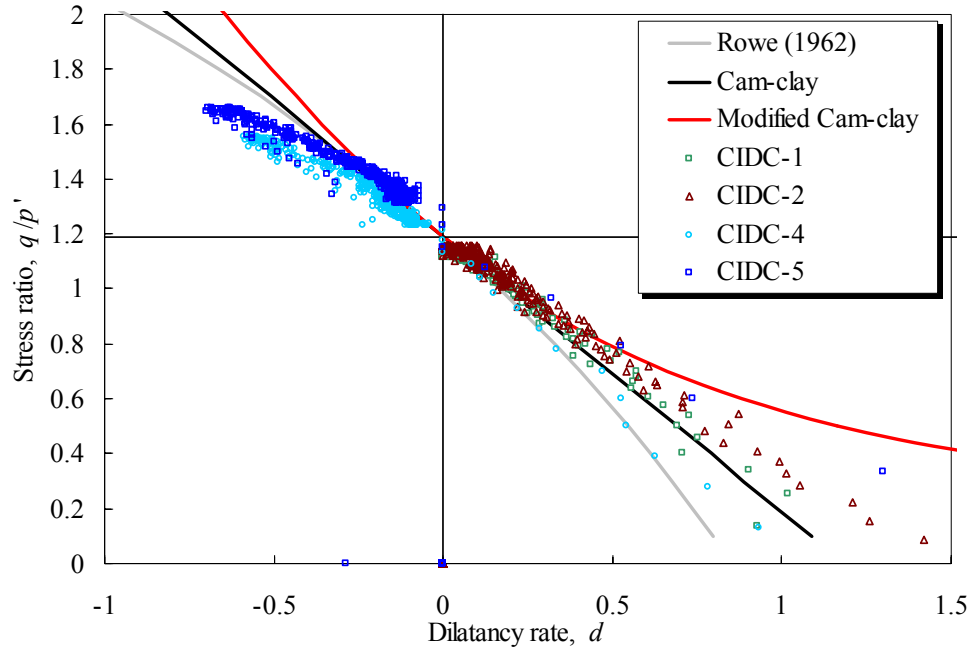


Figure 4-9. Comparison of experimental and various stress-dilatancy relations (Series A: CIDC).

As pointed out by Yu (1998), although much effort has been devoted in the past to developing a better stress-dilatancy relation for sands, such as the state-dependent dilatancy framework proposed by Li et al. (1999), very little progress have been made in this front. It is for this reason, the Rowe's stress-dilatancy relation was chosen in CASM. However, it should be noted that this flow rule is not very consistent with behaviour observed in dense Portaway sand. This may offer some explanation for the relatively poor predictions for dense sands given by CASM (see Figure 6-15) as presented in Chapter 6.

The variation in dilatancy during deformation of dense and loose sand specimens is illustrated in Figure 4-10. It can be seen that the magnitudes of dilatancy rate d of both specimens decreased as the deviatoric stresses were imposed. For dense sand (CIDC-5), a maximum dilatancy rate d_{\max} was developed at 3.36% axial strain and the magnitudes of dilatancy gradually reduced as shear continued until zero is reached at the critical state. In contrast, the loose sand test (CIDC-1) always gave a positive value of d throughout the deformation and as with dense sand, went to zero at the critical state.

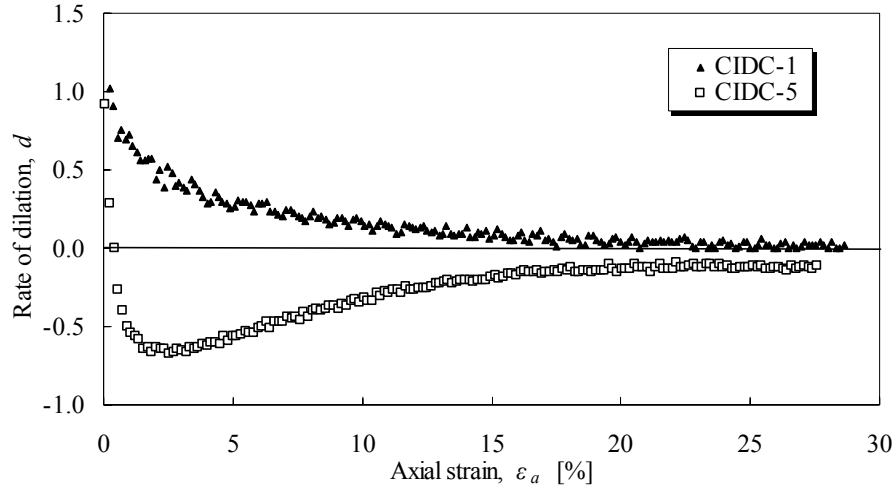


Figure 4-10. Evolution of dilatancy rate for dense and loose Portaway sand (CIDC-1 and CIDC-5).

4.3.3 Series B: Drained Extension Tests (CIDE-1~2)

The results of the drained tests loaded in extension ϵ are summarised in Table 4-5. Both loose specimen CIDE-1 and dense specimen CIDE-2 were isotropically consolidated to 200 kPa. As with the tests conducted in compression, the displacement-controlled mode was chosen. Plotted in Figure 4-11 is the measured stress-strain and volume change curves for the two specimens together with the results from compression tests CIDC-1 through CIDC-5.

Table 4-5. Summary of Series B: CIDE tests.

Initial conditions					End of test		Remarks
Test ID	e_0	D_r (%)	p'_0 (kPa)	V (%/Hr)	ϵ_a (%)	η_{peak}	
CIDE-1	0.701	27	200	3	6	-0.7	Necking
CIDE-2	0.547	74	200	3	4	-1.0	Necking

Notes: V = Strain rate in displacement-controlled tests

η_{peak} = Stress ratio q/p' at peak strength

ϵ_a = Axial strain at peak strength

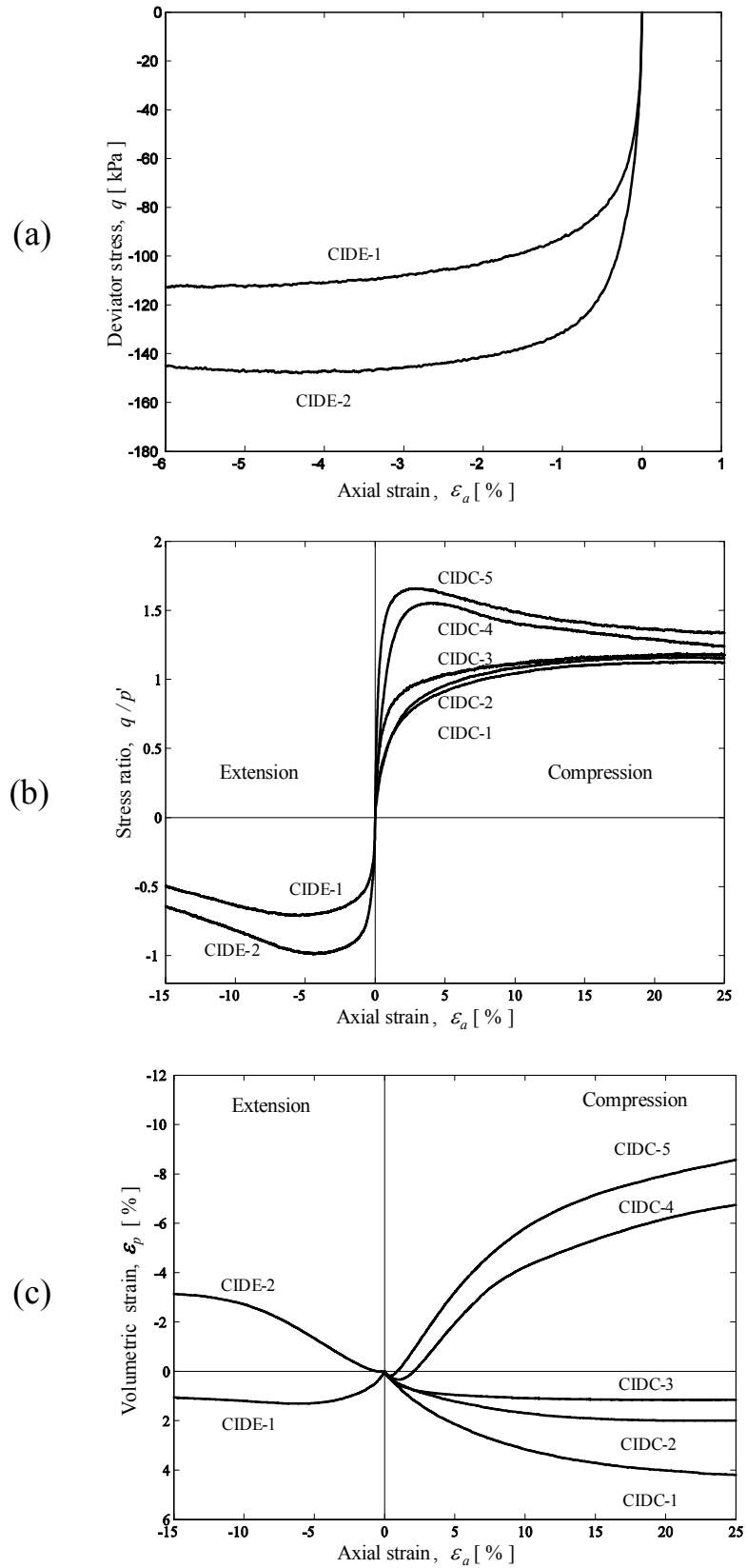


Figure 4-11. Stress-strain relationships (Series B: CIDE).

In the extension tests, necking was observed after the occurrence of the peak deviatoric stresses at 6% and 4% axial strains for tests CIDE-1 and CIDE-2, respectively (see Figure 4-12). Excessive strain localisations appeared during the post-peak stress region for the dense specimen CIDE-2. In contrast to the results obtained from compression tests, the measured critical state friction angle of the loose specimen CIDE-1 has a much lower value of 24.5° , which corresponds to a stress ratio q/p' of -0.7 . For the dense sand specimen CIDE-2, the critical state was not achieved due to strain localisation after reaching a peak stress ratio of -1.0 . These results are consistent with the studies reported by other researchers using conventional triaxial extension tests (e.g. Lade, 1982). However, Wu and Kolymbas (1991) found that friction angle in extension tests was larger than in compression tests. There are striking discrepancies in extension tests reported in the literature. Wu and Kolymbas established the factors that might cause such differences on dry Karlsruhe medium sand. The most significant of these are:

- The accuracy of the axial load measurement;
- The axial force carried by the rubber membrane;
- The effect of gravity;
- The inhomogeneous deformation.

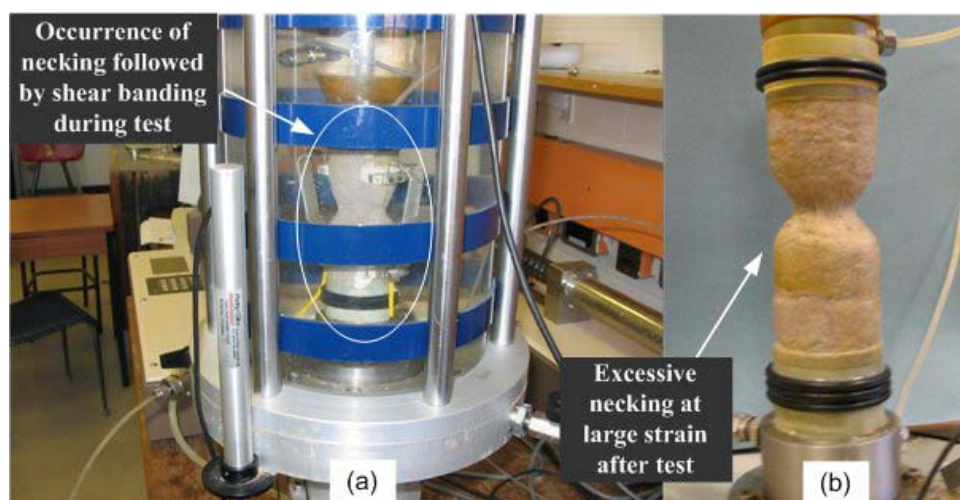


Figure 4-12. Typical specimen shape after the occurrence of necking (Series B: CIDE-1).

It is for this reason that many other researchers (e.g. Roscoe et al., 1963; Lam and Tatsuoka, 1988) have pointed out that the conventional extension test is inappropriate for determining the stress-strain and strength properties of sands. Lade et al. (1996) investigated the effects of shear band formation in triaxial extensions using different techniques and showed that significant differences would occur between the results of tests with and without strain localisation. Therefore, the determination of CASM constants, as shown later, is solely based on the results from compression tests.

4.3.4 Series C: Undrained Compression Tests (CIUC-1~12)

Twelve isotropically consolidated undrained triaxial tests in compression were conducted. The tests were carried out under either load-controlled or displacement-controlled mode in order to see the effect of the two loading modes on sand behaviour at the critical state. Seven specimens (CIUC-1 through to CIUC-6 and CIUC-12) exhibited peak shear strengths at relatively small strains, followed by subsequent reduction in these strengths as deformations continued. CIUC-7 showed a reappearance of hardening behaviour once the material had softened. Strong dilative behaviours with the development of negative excess pore pressures were observed from another four specimens (CIUC-8 through CIUC-11). Tests CIUC-10 and CIUC-11 were stopped at medium strain since the triaxial cell stress limit was reached (1700 kPa). The results of all CIUC tests are summarised in Table 4-6.

Table 4-6. Summary of Series C: CIUC tests.

Initial conditions					End of test		Remarks
Test ID	e_0	D_r (%)	p'_0 (kPa)	Control method	ε_a (%)	η_{peak}	
CIUC-1	0.712	24	300	D	20	0.68	Steady state
CIUC-2	0.699	27	500	L	18	0.68	Steady state
CIUC-3	0.687	31	800	L	20	0.68	Steady state
CIUC-4	0.664	38	500	D	14	0.91	Steady state

CIUC-5	0.740	20	300	L	25	0.5	-
CIUC-6	0.705	30	300	L	20	0.75	Steady state
CIUC-7	0.710	24	100	L	25	0.85	Quasi-steady state
CIUC-8	0.655	41	100	L	20	-	Steady state
CIUC-9	0.648	43	100	L	18	-	Steady state
CIUC-10	0.638	46	300	L	-	-	-
CIUC-11	0.620	52	500	L	-	-	-
CIUC-12	0.739	15	100	L	25	0.68	Steady state

Notes: L = Load control; D = Displacement control

η_{peak} = Stress ratio q/p' at peak strength

ε_a = Axial strain at steady state

The effective stress paths for the following undrained tests are interpreted in terms of the deviatoric stress $q = \sigma'_1 - \sigma'_3$ and the mean effective stress $p' = (2\sigma'_3 + \sigma'_1)/3$. This so-called critical state convention is commonly used in many constitutive models within the critical state soil mechanics framework.

Stress-strain and strength characteristics of very loose Portaway sand

The term ‘very loose’ is used here to refer to sand in a state which is much looser than its critical state (Sladen et al., 1985; Yu, 1998). Very loose sand exhibits a peak strength at a small strain and then has a large reduction of stresses due to the continuous generation of excess pore pressure. This phenomenon is known as static liquefaction (Castro, 1969; Poulos, 1981). Owing to its dramatic effects and complex nature, considerable efforts have been made in the past to understand and characterise this behaviour.

Figure 4-13 shows the stress-strain relationships of four very loose specimens CIUC-2, 4 and CIUC-5, 6 sheared after being isotropically consolidated to 500 kPa and 300 kPa, respectively. It is evident that all four specimens reached their peak stresses at about 1% axial strains and subsequently had a sharp drop of deviatoric stresses until the constant stresses and the excess pore pressures were obtained at large axial strains of 10–15%.

It can be seen from Figure 4-13 that the peak values of deviatoric stresses depend on both the densities and consolidation pressures. The strengths at steady state seem solely to be a function of the void ratios, regardless of the initial confining pressures. As would be expected, the identical stress ratio q/p' of 1.19 was obtained during steady state for tests CIUC-2, CIUC-4 and CIUC-6, which corresponds to a friction angle of 29.8° . This value is consistent with the average value obtained from drained tests in compression.

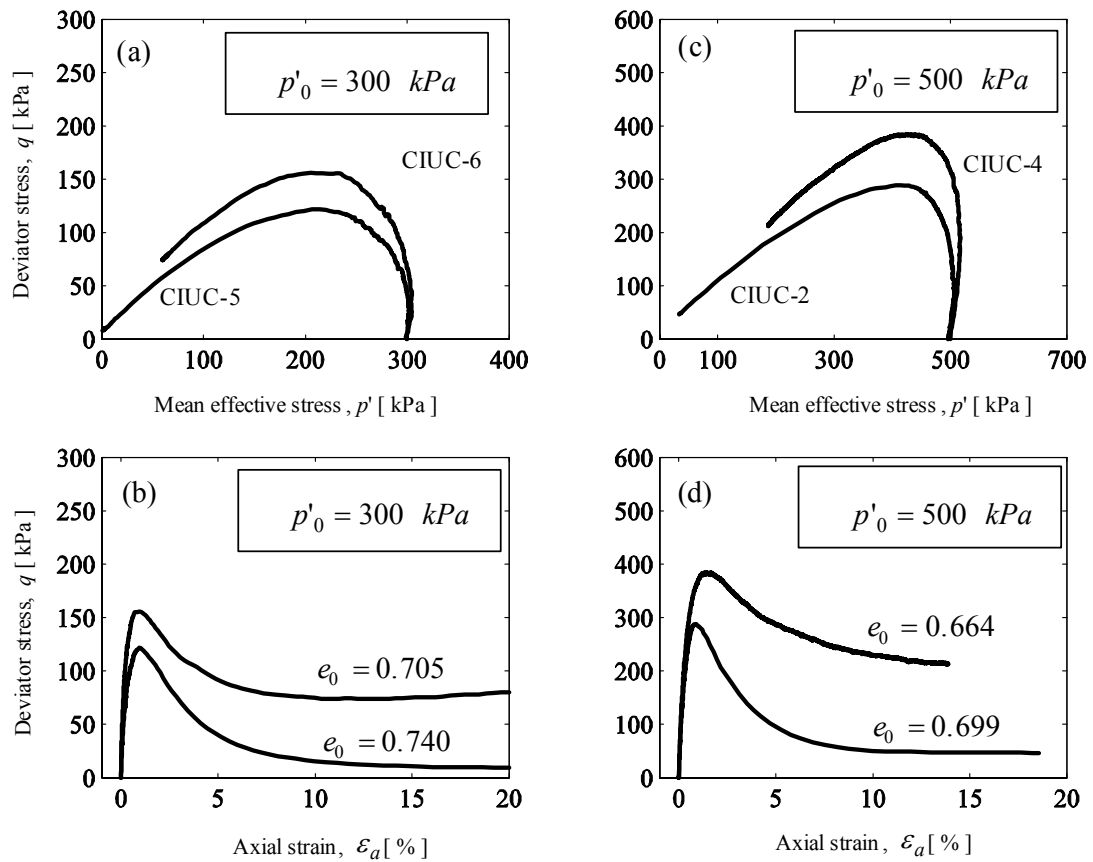


Figure 4-13. Stress-strain relationships and stress paths (A) (Series C: CIUC).

It is noted that CIUC-5 with the highest void ratio of 0.740 shows zero residual stress. Ishihara (1993) found the same behaviour for Toyoura sand when the void ratios were in excess of 0.93. He concluded that there was a ‘threshold’ void ratio at which the residual strength became zero and the behaviour of sand was less tenable. He further pointed out that the state parameter ξ was not useful in quantifying sand behaviour looser than this threshold void ratio. It is for this

reason that the reference state parameter ξ_R was chosen as 0.06, as shown in section 4.4.2.3.

Instability of Portaway sand

Plotted in Figure 4-14 are the stress paths, stress-strain relationships and excess pore pressure changes of two very loose specimens (CIUC-3 and CIUC-6) and a loose specimen (CIUC-7). It is evident that the peak points in the stress paths do not lie on a single line through the origin, but rather, the line varies with the state of the sand tested. The slopes of the lines are 0.68, 0.75 and 0.85 for CIUC-3, CIUC-6 and CIUC-7, respectively. This finding on Portaway sand is consistent with published data on various sands, such as Leighton Buzzard sand, Nerlerk sand, Banding sand (Sladen et al., 1985) and Toyoura sand (Ishihara, 1993). This line is termed as the flow liquefaction line (Ishihara, 1993; Yang, 2002).

Relationships between quasi-steady, steady and phase transformation states

The definitions of quasi-steady state, steady state and phase transformation state have been briefly introduced in Chapter 2. Figure 4-15 shows these typical behaviours for four specimens (CIUC-7, 8, 9 and 12) of Portaway sand, which were isotropically consolidated to the same effective confining pressure of 100 kPa.

CIUC-12 shows zero residual strength at 5% axial strain with a void ratio of 0.739, which is close to the ‘threshold’ value defined previously for test CIUC-5. The static liquefaction was initiated at 0.5% axial strain and after that, ‘runaway’ deformation (Chu and Leong, 2001) appeared due to the instability of the specimen. It is noted that the excess pore pressure of test CIUC-12 (see Figure 4-15 (c)) exceeded the initial effective confining pressure of 100 kPa at 2% axial strain. The reason for this is the constant confining pressure could not be maintained by the triaxial controller due to the sudden increase in axial strain at a large deformation rate.

The quasi-steady state (labelled ‘A’ in Figure 4-15 (b)) occurred for test CIUC-7 at about 8% axial strain, which corresponds to a stress ratio q/p' of 1.19, at which the excess pore pressure started to decrease (see Figure 4-15 (c)). It can be seen that steady state was not reached even at an axial strain of 25% and the deviatoric stress was still increasing. This type of behaviour is termed as flow type with limited liquefaction (Ishihara, 1993).

The dilative behaviour was exhibited in tests CIUC-8 and CIUC-9. After the phase transformation state ‘B’, the excess pore pressures were decreased at about 0.5% axial strain. The denser specimen CIUC-9 reached steady state ‘C’ with an excess pore pressure of -130 kPa.

As shown in Figure 4-15, the steady state and phase transformation state were the same for flow type specimen CIUC-12. For limited flow type specimen CIUC-7, the quasi-steady state coincided with the phase transformation state at point ‘A’. It can also be seen from Figure 4-15 that the phase transformation state and steady state are apparently different for dilative specimens CIUC-8 and CIUC-9. Table 4-7 compares the stress ratios at different states for the two specimens. It is evident that the stress ratios at steady state and phase transformation are not the same.

Table 4-7. Comparison of the phase transformation states and steady states.

Test ID	η at phase transformation state	η at steady state
CIUC-8	1.10	1.19
CIUC-9	1.26	1.19

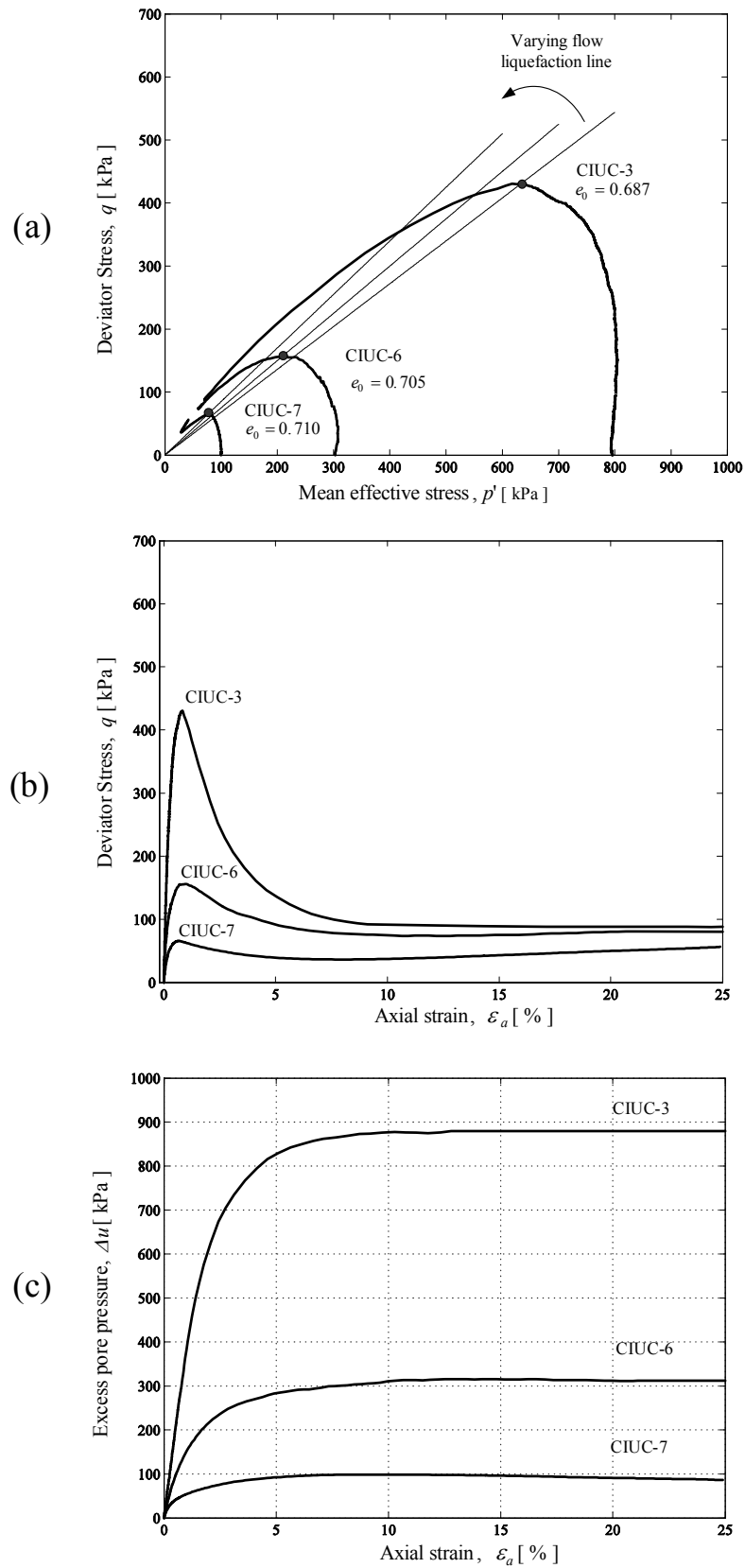


Figure 4-14. Stress-strain relationships, stress paths and excess pore pressure changes (B) (Series C: CIUC).

The stress-strain and strength characteristics of Portaway sand

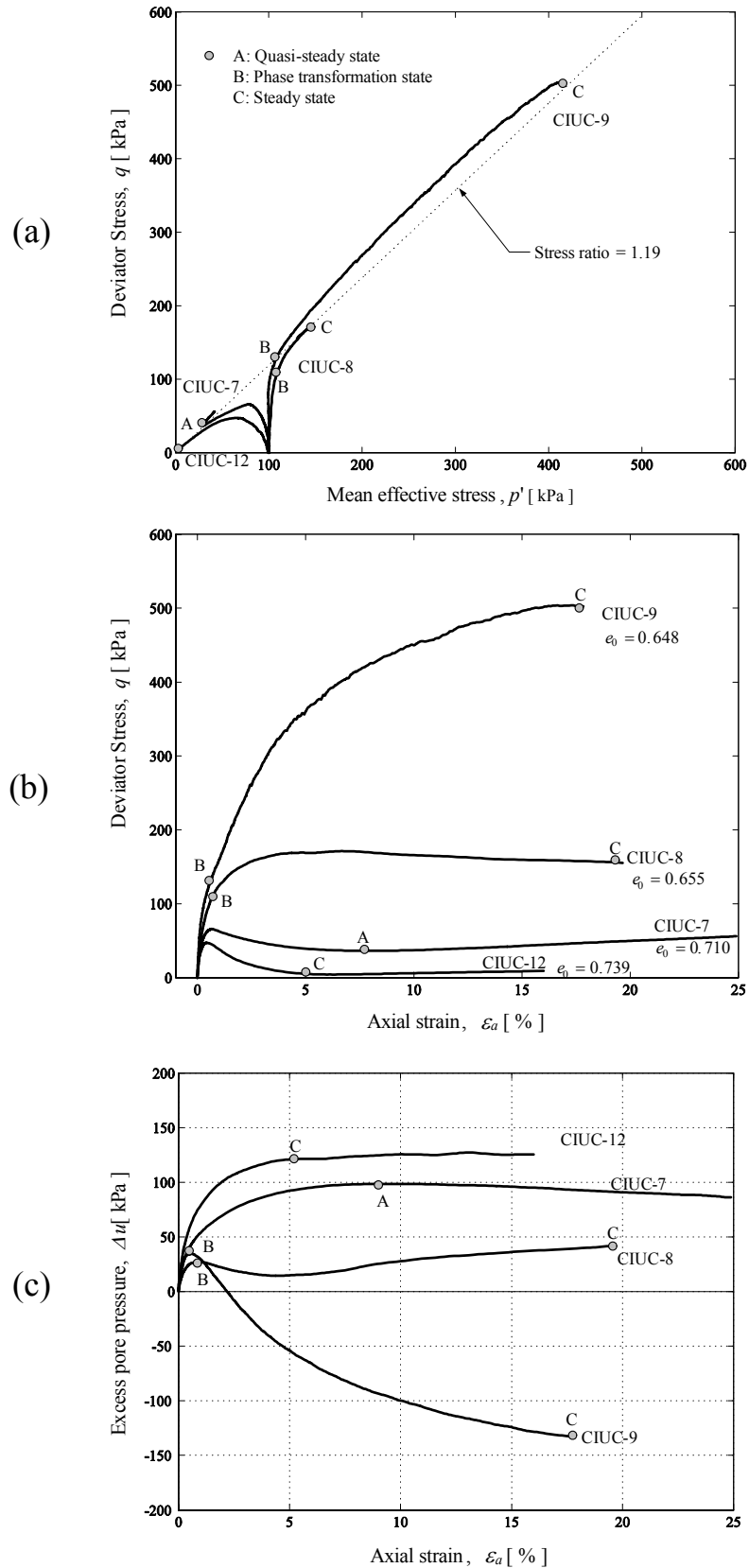


Figure 4-15. Stress-strain relationships, stress paths and excess pore pressure changes (C) (Series C: CIUC).

4.3.5 Series D: Undrained Extension Tests (CIUE-1~4)

Four isotropically consolidated undrained triaxial tests in extension were conducted on very loose sand specimens. All specimens were sheared under load-controlled mode. The results of four CIUE tests are summarised in Table 4-8.

Table 4-8. Summary of Series D: CIUE tests.

Initial conditions				Control method	End of test		Remarks
Test ID	e_0	D_r (%)	p'_0 (kPa)		ε_a (%)	$ \eta_{peak} $	
CIUE-1	0.722	21	200	L	-5	0.50	Necking
CIUE-2	0.693	23	500	L	-4	0.55	Necking
CIUE-3	0.664	38	800	L	-4	0.60	Necking
CIUE-4	0.661	36	1200	L	-4	0.58	Necking

Notes: L = Load control

η_{peak} = Stress ratio q/p' at peak strength

ε_a = Axial strain at peak strength

Figure 4-16 shows the stress-strain relationship of CIUE-1 with an initial consolidation pressure of 200 kPa. It is evident that the deviatoric stress reached peak strength (point 'A') of -65 kPa at an axial strain of -0.45% . After point 'A', 'runaway' deformation occurred due to the instability of CIUE-1 to sustain a given stress. This behaviour is similar to the CIUC test series on loose Portaway sand and has been termed as static liquefaction. Visible necking was observed at about 7% axial strain at point 'B' on the specimen. The stress-strain relation is not considered as real material behaviour after point 'B' with a stress ratio q/p' of -0.7 due to the appearance of excessive non-homogeneous deformation.

The complete stress-strain relationships and stress paths for all four tests are presented in Figure 4-17 (a) and (b). In contrast to the compression tests, the consolidation pressure has a significant effect on the ultimate state that the specimen can reach in extension. It can be seen that tests CIUE-2, 3 and 4 reached the same stress ratio q/p' of -0.7 and then collapsed dramatically. The expected

steady states were not reached for all three specimens. The developments of excess pore pressures in tests CIUE-1 and CIUC-3 are presented in Figure 4-17 (c). Both tests exhibited continuous increases in excess pore pressures.

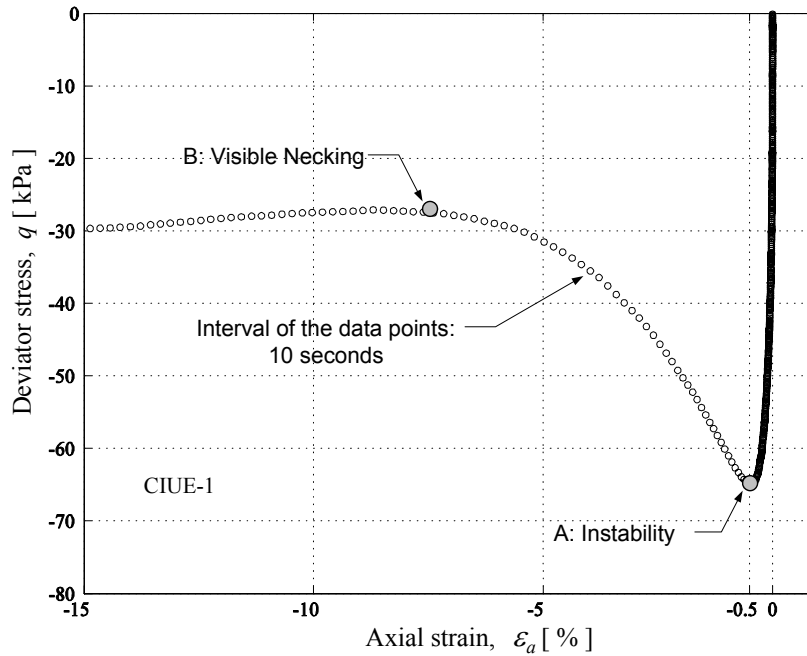


Figure 4-16. Instability of load-controlled test (Series D:CIUE-1).

Vaid et al. (1990) found that the strength of sand was smaller in extension than in compression and attributed this to the inherent anisotropy. The results obtained by the author from Portaway sand reconstituted by the moist tamping method indicate the same conclusion. As pointed out by Lade et al. (1996), however, the stress-strain and strength characteristics obtained from conventional triaxial extension tests are usually incorrect due to the excessive influence of necking in the hardening regime followed by shear banding. Consequently, data obtained from this series of tests are not used for determining model parameters discussed in Chapter 6.

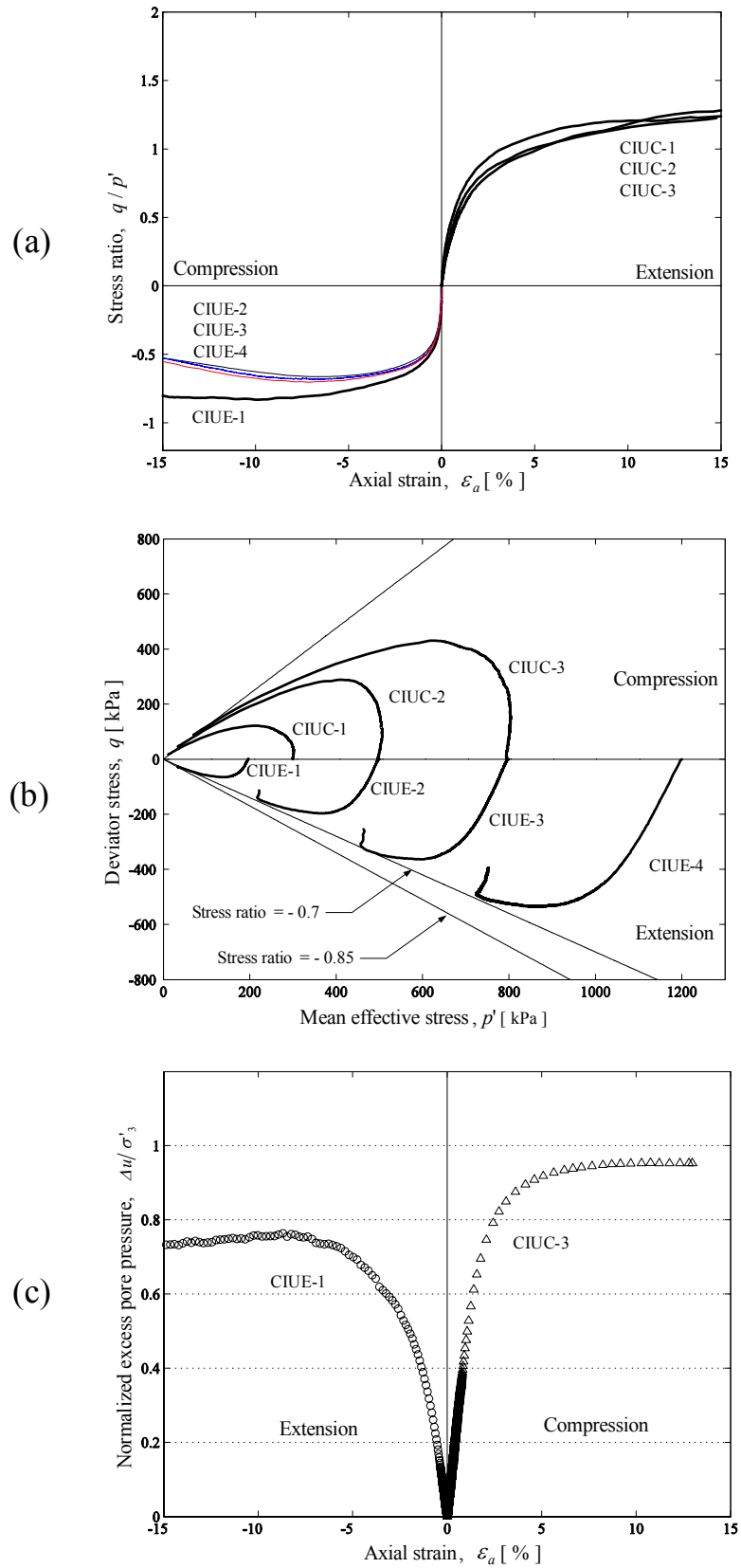


Figure 4-17. Stress-strain relationships, stress paths and excess pore pressure changes (Series D: CIUE).

4.3.6 Series E: Drained Tests with Variable Confining Pressures

The effects of stress path and loading direction on the stress-strain and strength characteristics of Portaway sand are presented in this section. Six drained triaxial tests, which were isotropically consolidated, were conducted on Portaway sand with variable confining pressures. All specimens were sheared under load-controlled mode. The test conditions are summarised in Table 4-9.

Table 4-9. Summary of Series E: drained tests with variable confining pressures.

Initial conditions					End of test		Effective stress path
Test ID	e_0	D_r (%)	p'_0 (kPa)	Control method	ε_a (%)	η_c	Defined in Figure 4-7
CIDCP-1	0.520	82	500	L	25	1.19	2 (compression)
CIDCP-2	0.702	27	200	L	25	1.15	2 (compression)
CIDCA-3	0.512	84	900	L	25	1.19	3 (compression)
CIDEA-4	0.704	26	200	L	-7	-0.7	3 (extension)
CIDCC-5	0.690	30	100	L	24.5	1.19	1, 4, 5 and 6 (compression)
CIDCC-6	0.665	38	400	L	24.5	1.19	1, 6 and 7 (compression)

Notes: η_c = Stress ratio q/p' at the critical state

ε_a = Axial strain at the critical state

Plotted in Figure 4-18 are the stress-strain relationships and stress paths of four tests (CIDCP-1, CIDCP-2, CIDCA-3 and CIDEA-4). The results from the CIUC tests are included for comparisons. It is clear that the critical states obtained from these tests also lie on the possible *CSL* defined in these tests from series A–D. Figure 4-19 compares the stress-strain relationships and stress paths between test CIDCC-5 and CIDCC-6 loaded with complex stress paths. It is evident that the identical critical state stress ratio ($\eta = 1.19$) was found for both tests, although the stress-strain relationships were quite different before 15% shear strain.

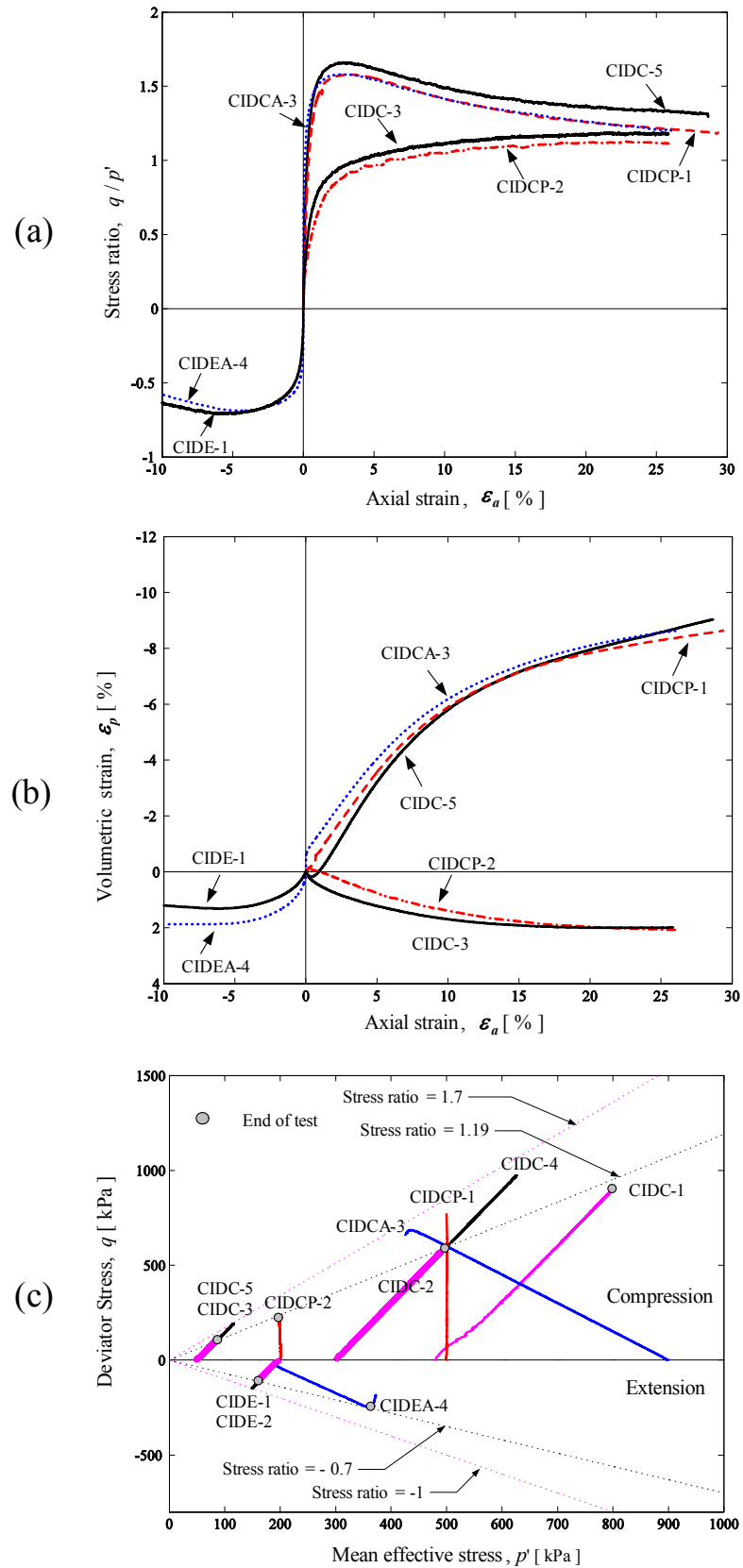


Figure 4-18. Stress-strain relationships and stress paths (A) (Series E: CID tests with variable confining pressures).

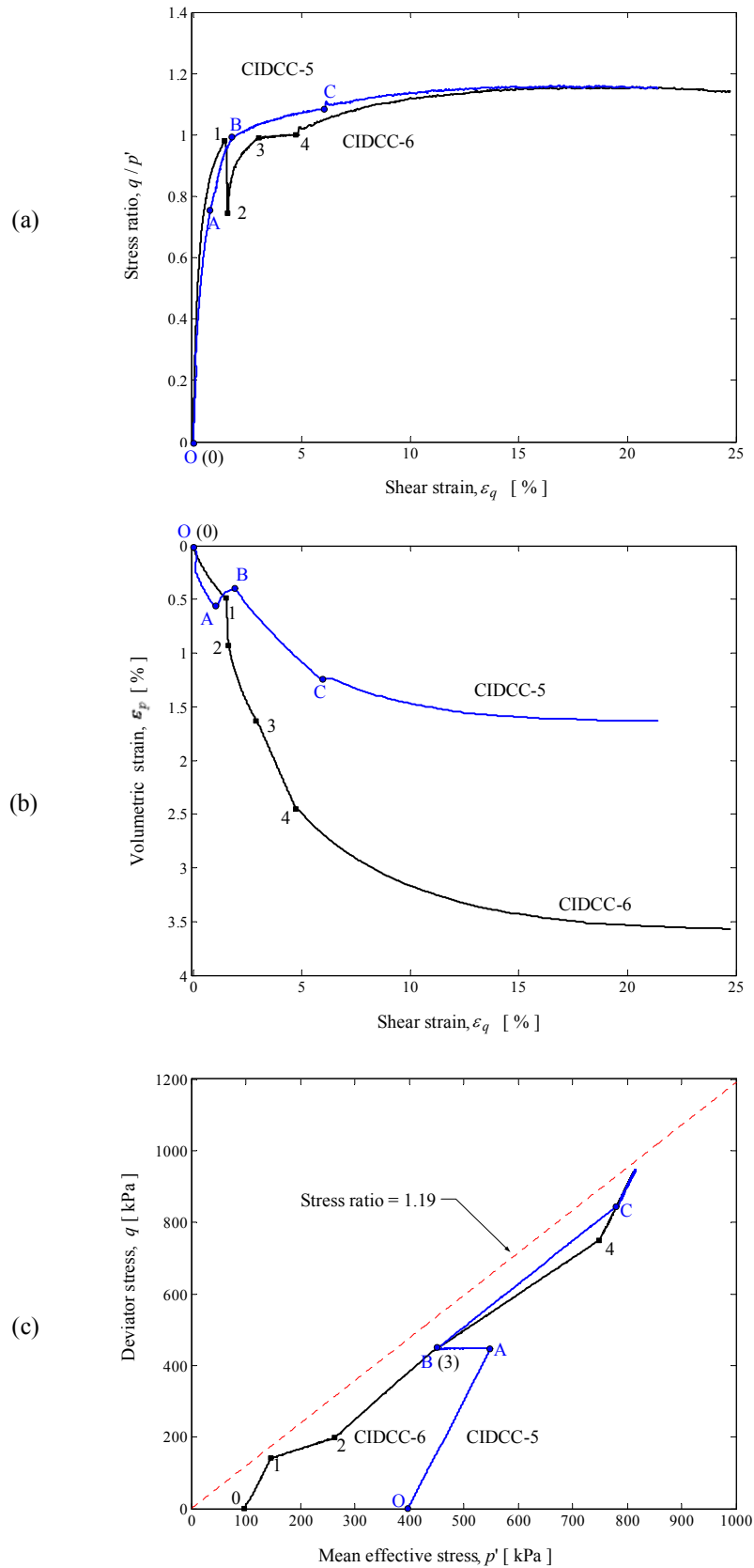


Figure 4-19. Stress-strain relationships and stress paths (B) (Series E: CID tests with variable confining pressures).

The stress-strain and strength characteristics of Portaway sand

4.3.7 Series F: Pre-sheared Undrained Tests (CIPU-1~2)

The purpose of carrying out these tests was to investigate the effect of pre-shearing history on the undrained behaviour of loose Portaway sand. Two isotropically consolidated pre-sheared undrained triaxial tests were conducted. The tests were carried out under displacement-controlled mode. The undrained shearing was conducted after the specimen was pre-sheared to a sufficiently high stress ratio ($\eta = 0.9$). The two specimens tested had essentially the same initial void ratio ($e_0 = 0.690 \pm 0.003$) but with different pre-shearing paths. Figure 4-20 shows the stress paths experienced by the two specimens.

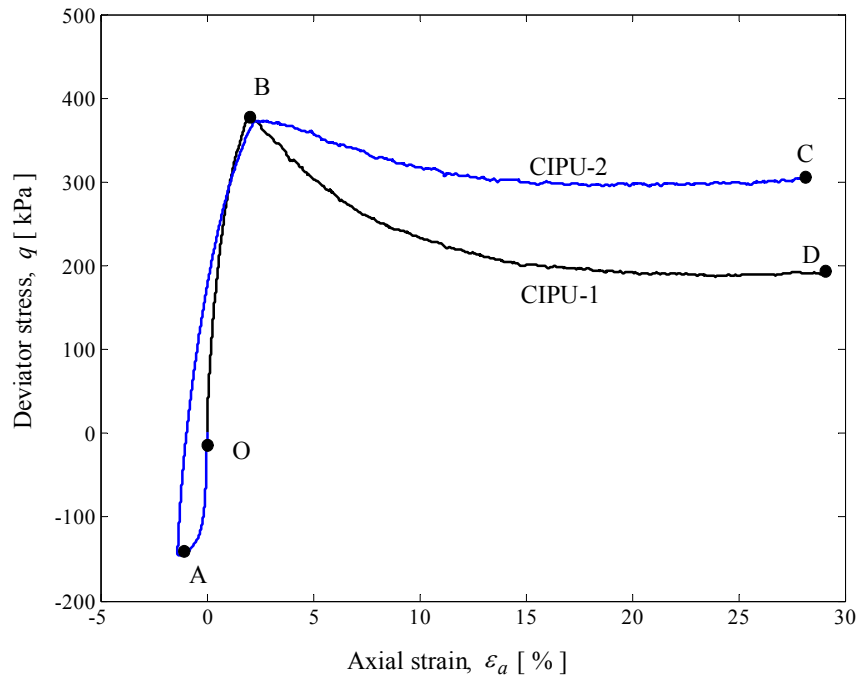
Test CIPU-1 follows paths OB (conventional drained shearing in compression) and BD (undrained shearing). Test CIPU-2 follows paths OA (conventional drained shearing in extension), AB (conventional drained shearing in compression) and BC (undrained shearing). The test conditions are summarised in Table 4-10.

Table 4-10. Summary of Series F: CIPU tests.

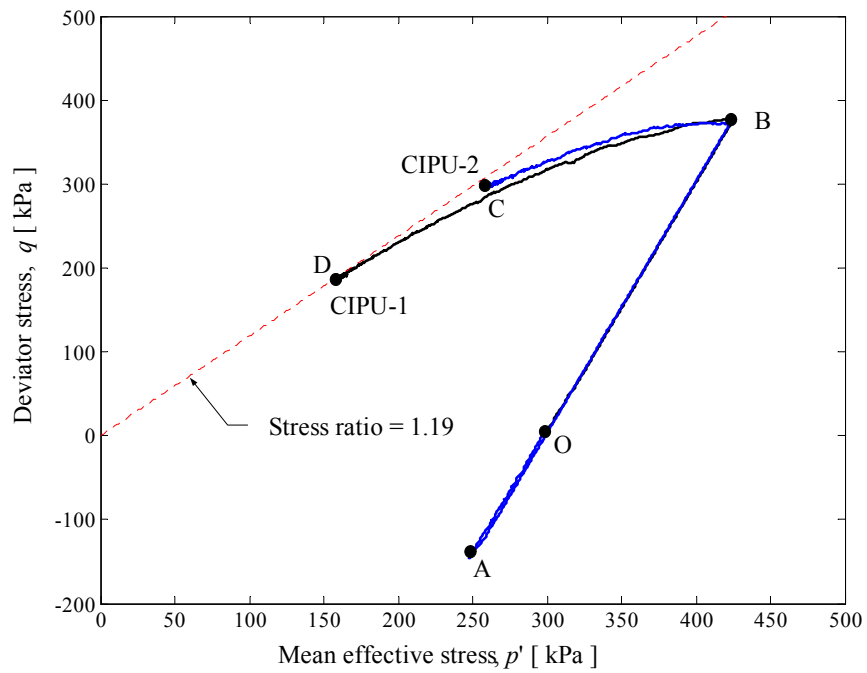
Initial conditions				Control method	End of test		Remarks
Test ID#	e_0	D_r (%)	p'_0 (kPa)		ε_a (%)	η_c	
CIPU-1	0.687	31	300	D	27	1.19	Steady state
CIPU-2	0.693	29	300	D	29	1.18	Steady state

Notes: D = Displacement control
 η_c = Stress ratio q/p' at critical state
 ε_a = Axial strain at critical state

Figure 4-20 and Figure 4-21 compares the stress-strain relationships, effective stress paths and excess pore pressure changes between these two tests. It is noted that the pre-shearing paths have a profound effect on the sand behaviour. The initially loose sand specimen (CIPU-2) exhibited higher strength at steady state due to drained extension path OA.



(a)



(b)

Figure 4-20. Stress-strain relationships and stress paths (A) (Series F: CIPU).

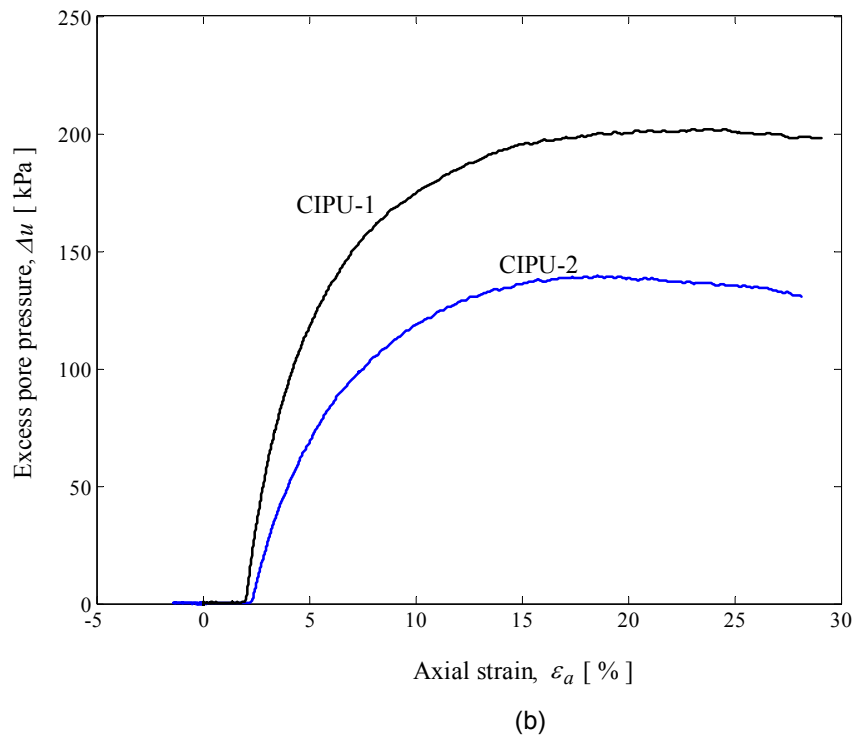
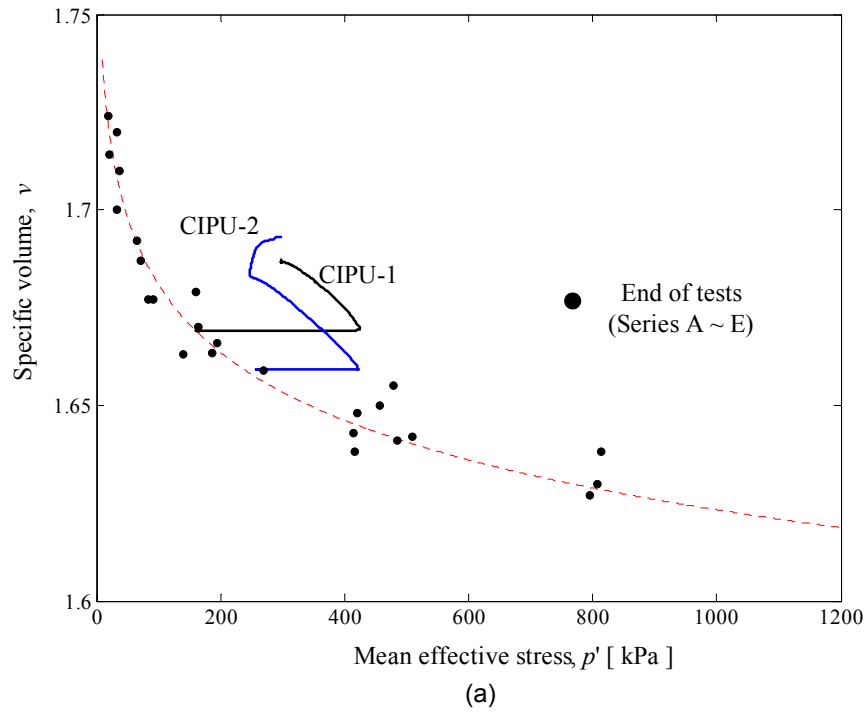


Figure 4-21. Stress paths and excess pore pressure changes (B) (Series F: CIPU).

4.4 INTERPRETATION AND DISCUSSION

4.4.1 Identification of the Critical State Line

The determination of the *CSL* is an important aspect in modelling the stress-strain and strength characteristics of sands within the framework of critical state soil mechanics. Researchers have generally relied on drained, strain-rate-controlled tests on dilatant specimens to determine the *CSL* (e.g. Been et al., 1991; Klotz and Coop, 2002). On the other hand, some researchers have used undrained stress-controlled tests on loose specimens to determine the *SSL* (e.g. Castro, 1969; Poulos, 1981; Ishihara, 1993).

Critical state and steady state

Figure 4-22 shows the stress paths for all compression tests that apparently reached the critical (or steady) state. It is evident that the critical (or steady) states were clearly identified for most of these tests at large strains. Only compression tests were used in determining the critical (or steady) state. The reason for this has been given in sections 4.3.3 and 4.3.5. It can be seen that the critical state and steady state coincide and are not affected by the drainage condition. It is therefore acceptable to use a single term, the critical state, for both critical state and steady state, which has been used in the rest of this thesis. The *CSL* of Portaway sand as seen in Figure 4-23 may be expressed using the following equation in the $\nu - \ln p'$ space:

$$\nu = 1.796 - 0.0253 \ln p' \quad (4-6)$$

It should be noted that the above linear relationship of ν and $\ln p'$ is only valid when mean effective pressure p' is less than 1000 kPa.

Figure 4-24 shows the *CSL* in the $p'-q$ stress space. According to equation (2-10), a critical state friction angle of 29.8° is obtained in compression.

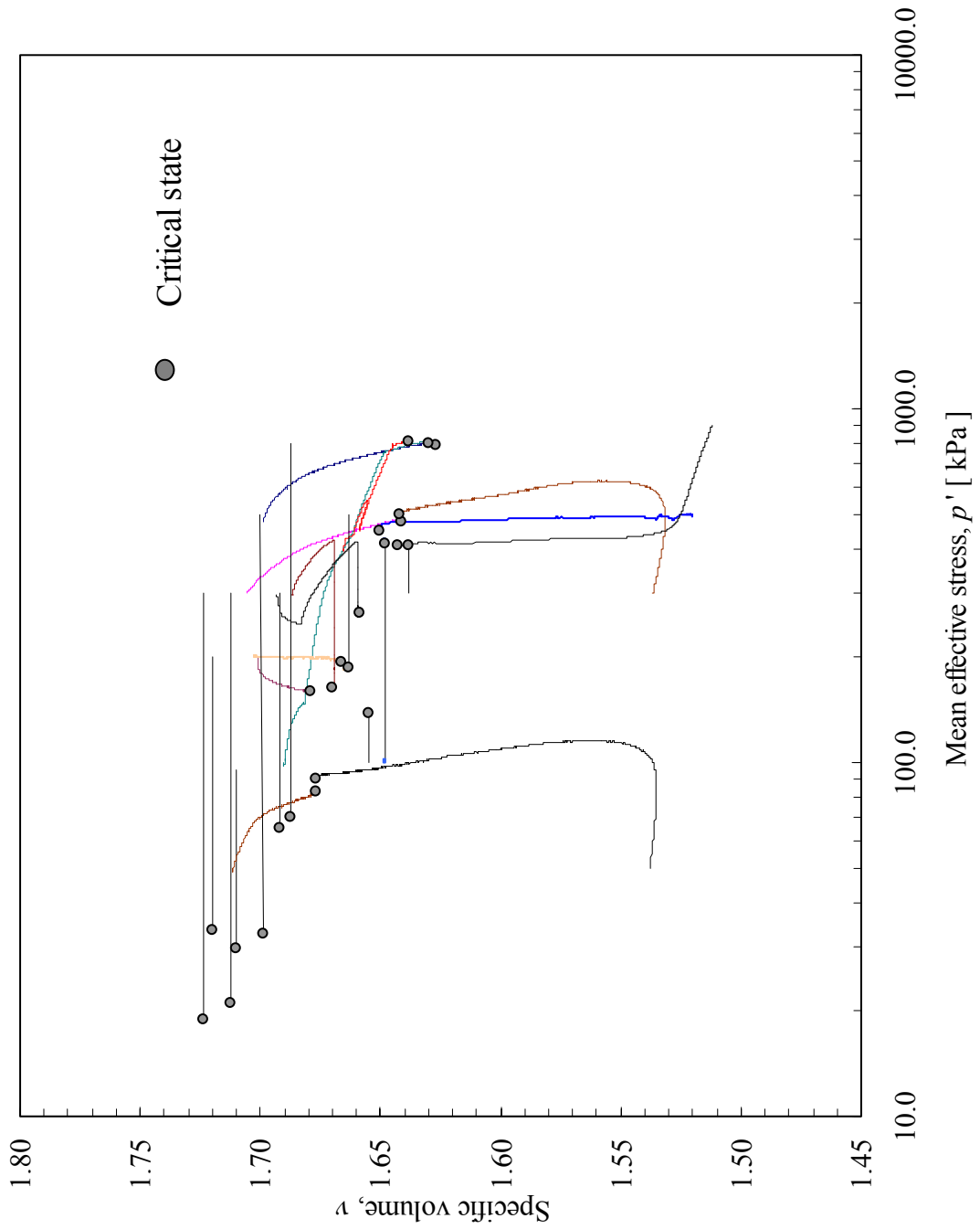
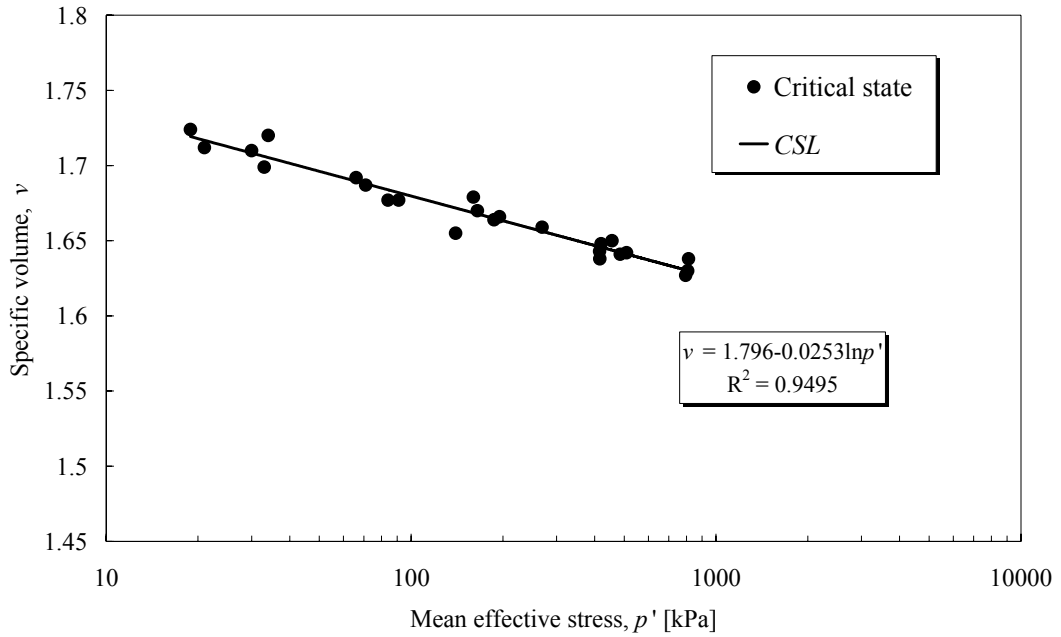
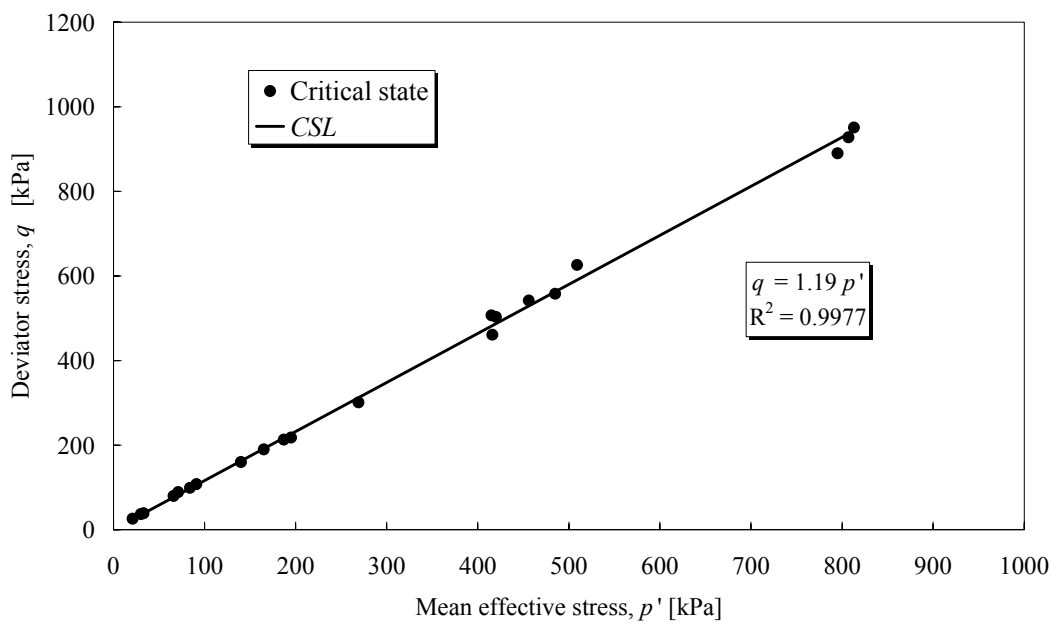
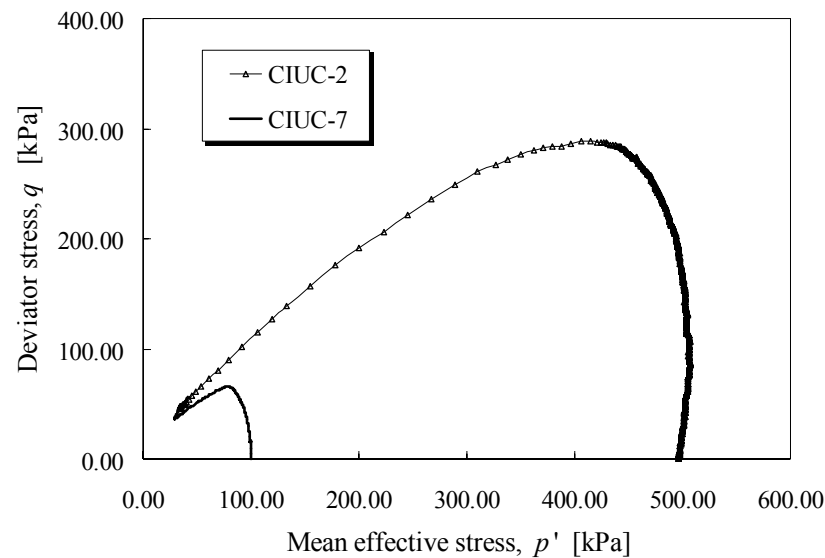


Figure 4-22. Overall stress paths (Series A-F).

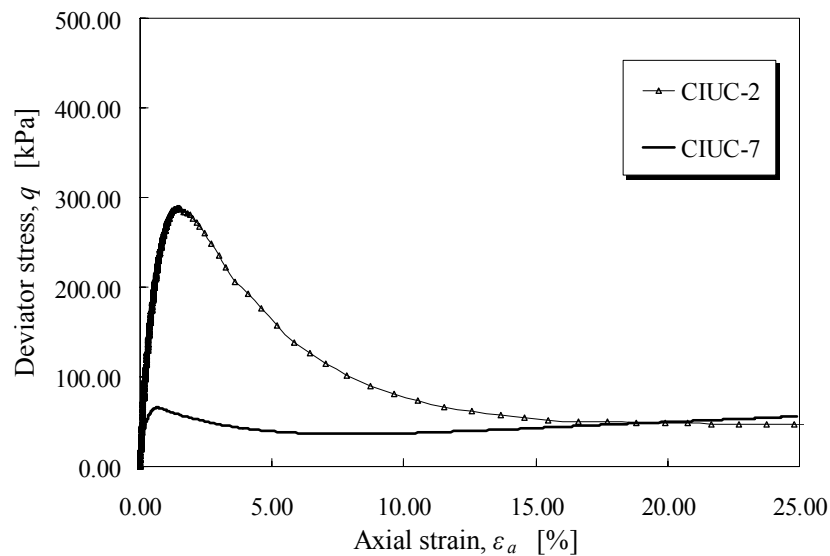
Figure 4-23. *CSL* in the $\ln p' - v$ space.Figure 4-24. *CSL* in the $q - p'$ stress space.

Effect of consolidation pressure and density on the critical state

Figure 4-25 illustrates the effect of consolidation pressure on the critical state in undrained tests. Two specimens (CIUC-2 and CIUC-7) were carefully prepared and consolidated to different consolidation pressures at essentially the same void ratio. The results indicate that the critical state is independent of the initial consolidation pressure.



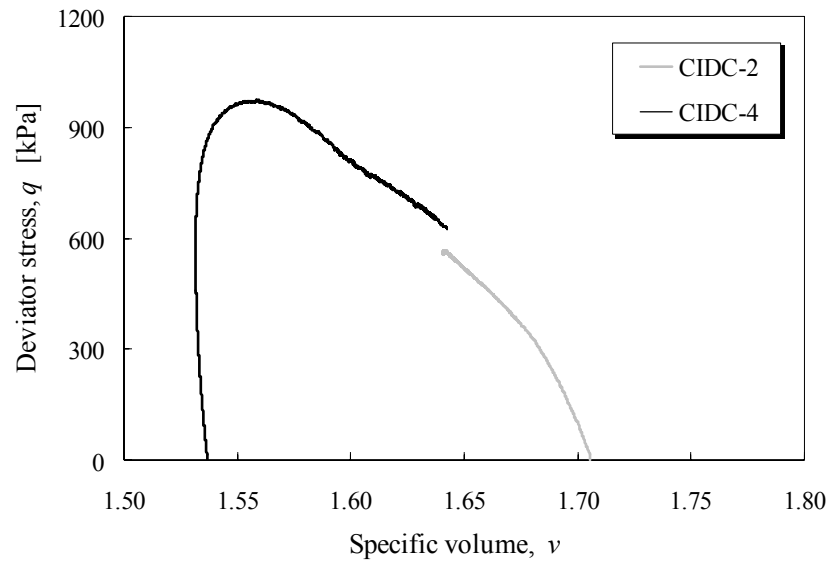
(a)



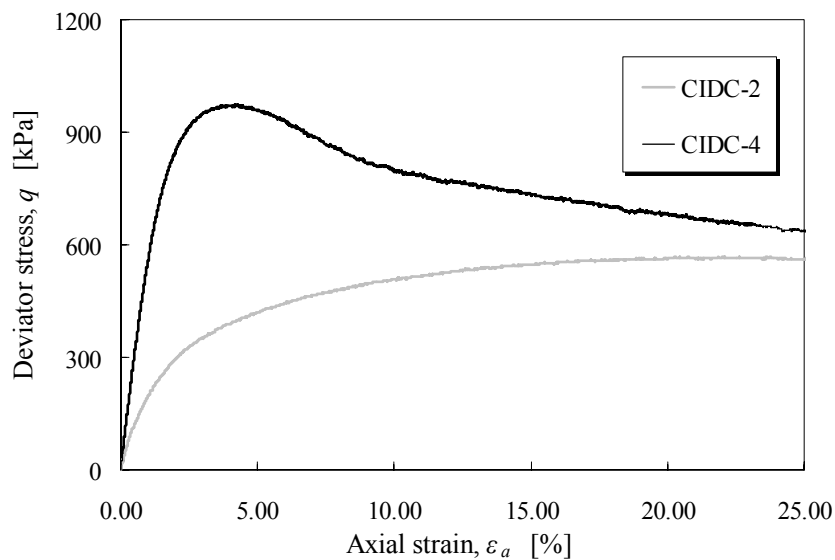
(b)

Figure 4-25. Specimens sheared at the same void ratio ($e_0 = 0.705 \pm 0.006$) but from different consolidation pressure levels.

Figures 4-26 and 4-27 show the influence of density on the critical state in drained tests. Although the friction angle at critical state is slightly higher in dense sand specimens, essentially the same critical state can be assumed. The slight differences observed may be attributed to the occurrences of shear band and non-uniform deformation in the dense specimen as discussed previously.

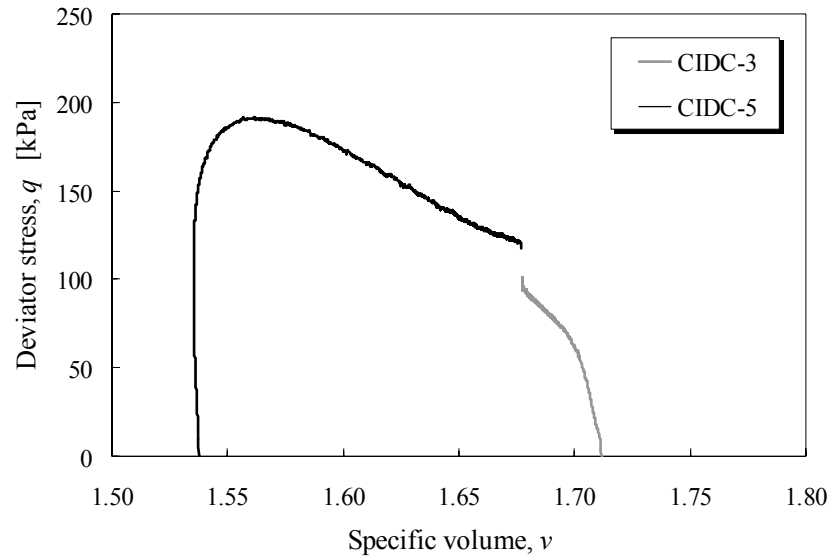


(a)

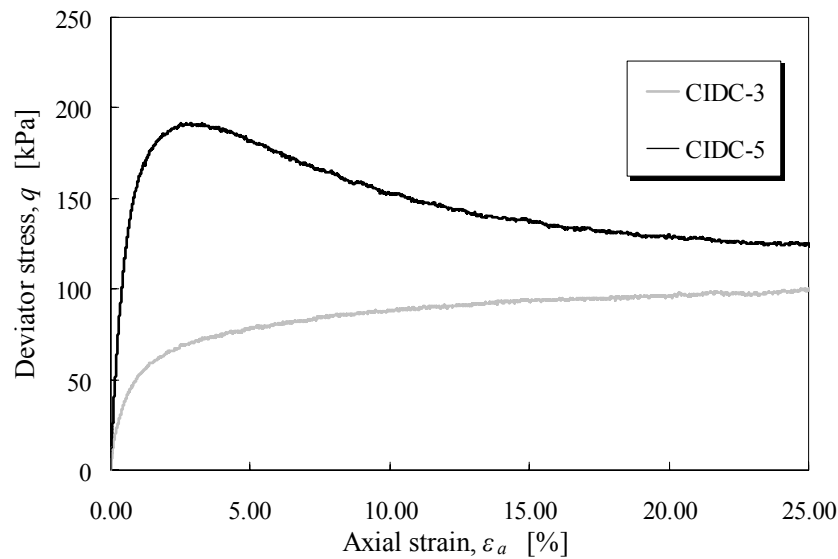


(b)

Figure 4-26. Specimens sheared at the same effective confining pressure (300 kPa) but with different initial densities.



(a)



(b)

Figure 4-27. Specimens sheared at the same effective confining pressure (50 kPa) but with different initial densities.

Shape of the critical state line

Several functions have been proposed in the past for sands to define the *CSL* in the $\nu - \ln p'$ space based on experimental observations, which include:

- Two linear functions (bilinear shape) for Erkask sand (see Figure 2-8, Been et al., 1991);

- An exponential function at low pressure and a linear function at high pressure for Dog's Bay sand (see Figure 4-28 (a), Klotz and Coop, 2002);
- An exponential function (curved shape) for Toyoura sand (see Figure 4-28 (b), Li et al., 1999).

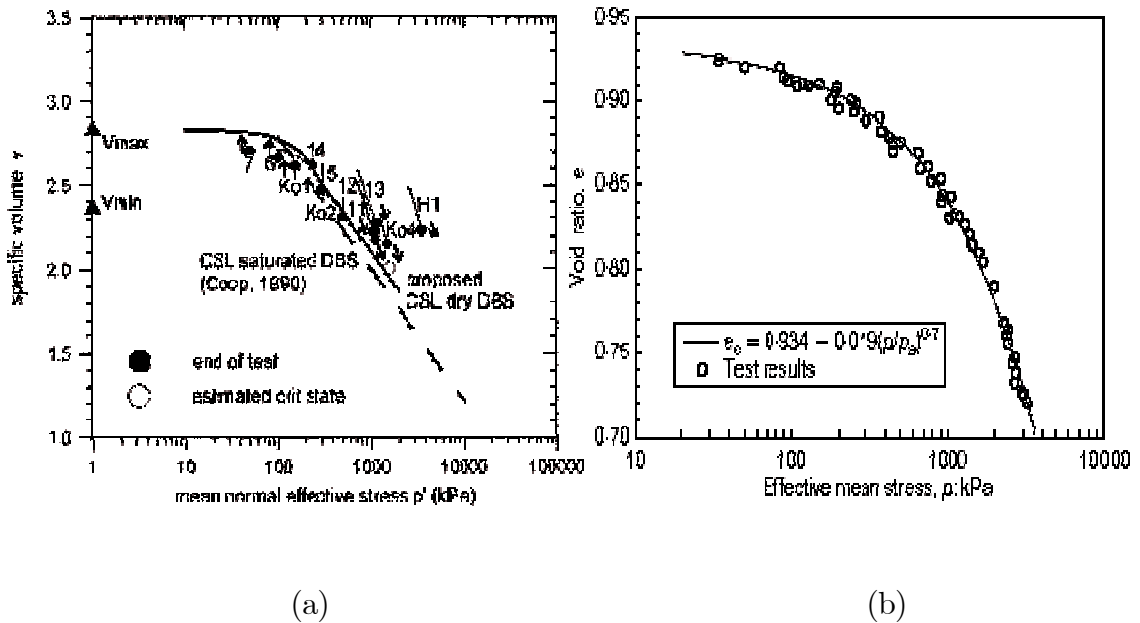


Figure 4-28. *CSLs*: (a) Dog's Bay sand (Klotz and Coop, 2002), (b) Toyoura sand (data from Verdugo and Ishihara, 1996).

Semi-logarithmic plots are usually used by most researchers so that a kind of break point can be identified (typically around 1000 kPa). For lower pressures, a linear relation is used for practical purpose.

The *CSL* of Portaway sand defined previously is shown in Figure 4-29, together with the *CSL* of Erksak 330/0.7 sand. It is evident that the *CSL* for both sands has relatively linear shape at low pressure.

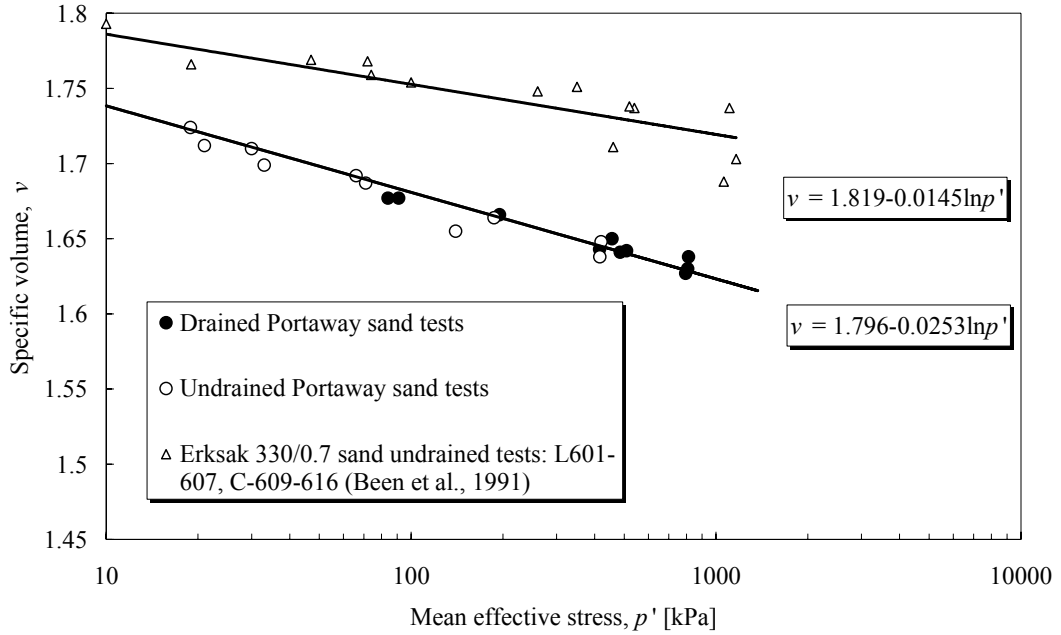


Figure 4-29. Comparison of the *CSLs* between Portaway sand and Erksak 330/0.7 sand.

Verdugo (1992) argued that the curvature of the *CSL* is dependent on the scale of axis chosen. He found that the break point at $p' = 1000$ kPa for Erksak sand (see Figure 2-8) was not manifested in an arithmetic plot. The critical states shown in Figure 4-29 have been re-plotted in this way in Figure 4-30. It is noted that a kind of break point exists for both sands at $p' = 200$ where the *CSL* changes from a non-linear to a linear relationship. These results are in good agreement with findings reported by Verdugo (1992).

More recently, an exponential function for the *CSL* under a wide range of stresses was adopted by some researchers in the development of the critical state models. For example, Li et al. (1999) proposed the following expression for the curved *CSL*:

$$\nu = (1 + e_T) - \lambda_c \left(\frac{p'}{p_a} \right)^\chi \quad (4-7)$$

where e_T , λ_c and χ are model parameters and p_a is set to equal the atmosphere pressure (101 kPa).

Figure 4-31 shows the *CSLs* for Portaway sand and Erksak 330/0.7 sand predicted by equation (4-7). Table 4-11 summarises the constants used in predictions for the sands together with data for Toyoura sand.

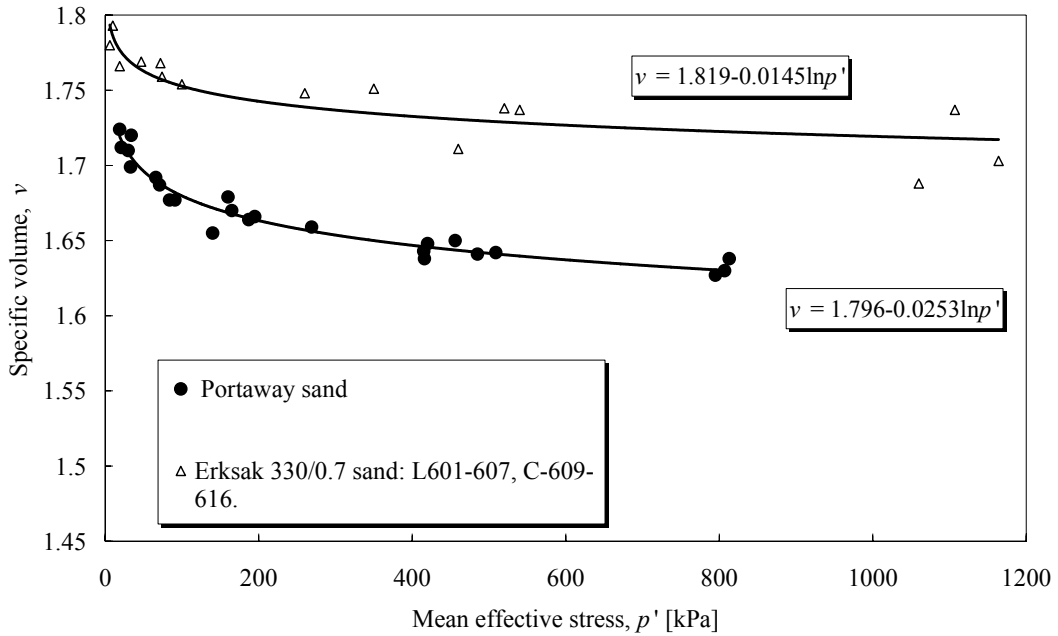


Figure 4-30. *CSLs* of Portaway sand and Erksak 330/0.7 sand in arithmetic plot.

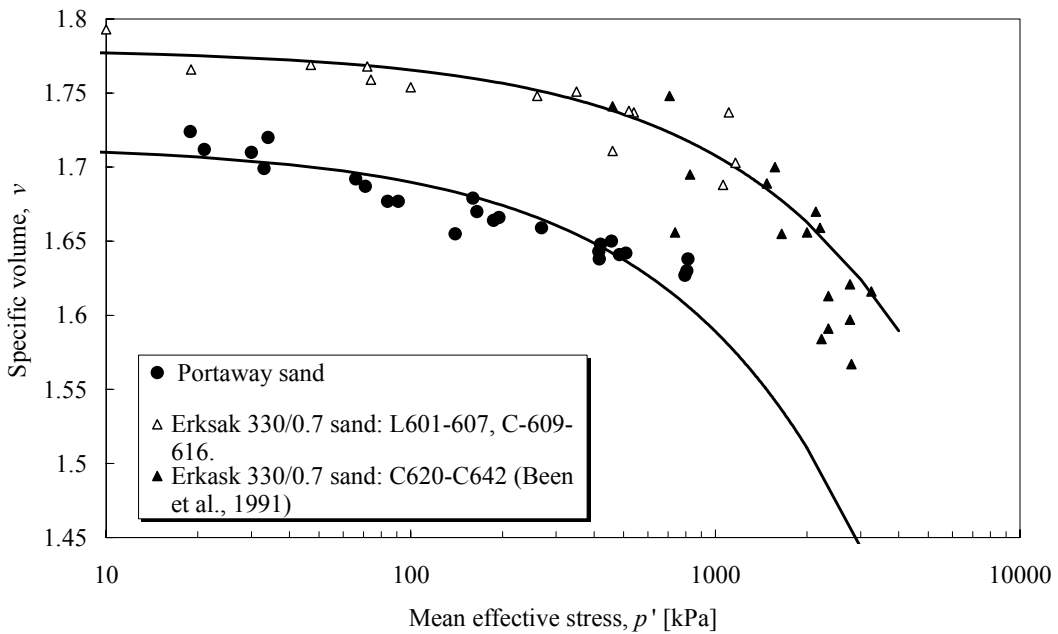


Figure 4-31. Predicted *CSLs* of Portaway sand and Erksak 330/0.7 sand.

Table 4-11. Material constants of sands used in equation (4-7).

Sand	Toyoura sand (Li et al., 1999)	Erksak 330/0.7 sand	Portaway sand
e_{\max}	NA	0.75	0.79
e_{\min}	NA	0.53	0.46
e_{Γ}	0.934	0.78	0.715
λ_c	0.019	0.145	0.025
χ	0.7	0.7	0.7
ϕ_c	31.1°	31°	29.8°

It is evident from Figure 4-31 that equation (4-7) can be satisfactorily used to predict measured *CSLs* for both Portaway sand and Erksak 330/0.7 sand. However, this correlation should be further verified by conducting triaxial tests at high pressure for Portaway sand.

In the remainder of this thesis, the linear *CSL* shown in Figure 4-23 is adopted for the following interpretation and modelling works on Portaway sand.

4.4.2 Determination of CASM Constants

There are a total of seven material constants required in CASM. They are μ , κ , λ , Γ , M , r (or ξ_R) and n . In the following sections, the role of each of these seven constants and the methods for determining them are described.

Figure 4-32 shows a definition of the state parameter, the reference state parameter and the critical state constants. Table 4-12 summarises the typical values of the CASM constants and their physical meanings for both clay and sand.

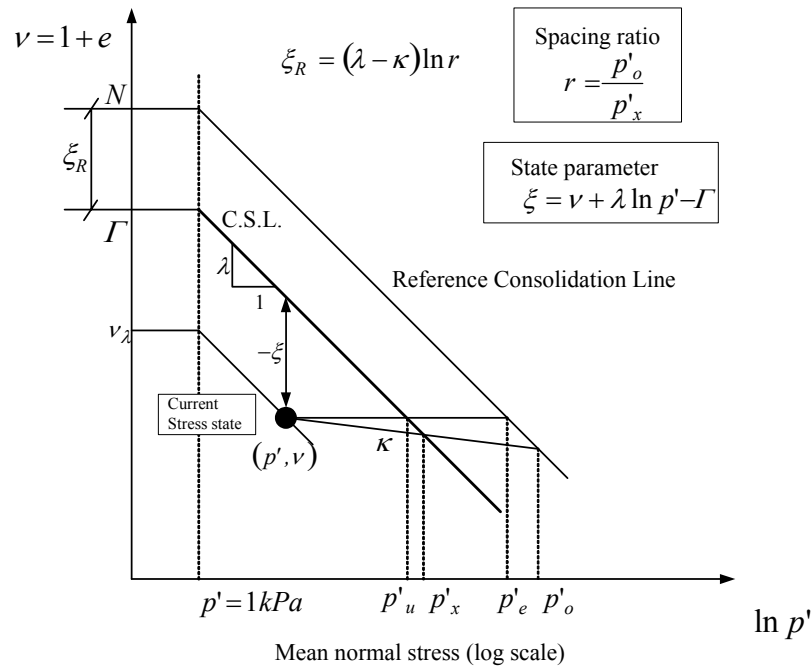


Figure 4-32. State parameter, reference state parameter and critical state constants (Yu, 1998).

Table 4-12. CASM constants and their physical meanings (Yu, 1998).

	Symbol	Typical value		Physical meaning
		Clay	Sand	
Elastic constants	μ	0.15–0.35	0.15–0.35	Poisson's ratio
	κ	0.01–0.06	≤ 0.01	Slope of overconsolidation (swelling) line
Critical state constants	λ	0.1–0.2	0.01–0.05	Slope of the <i>CSL</i> (<1000 kPa)
	Γ	1.8–4.0	1.8–4.0	Specific volume at critical state with $p' = 1$ kPa
	M	0.8–1.0	1.1–1.4	Slope of the <i>CSL</i> in the $p' \sim q$ space under compression
New material constants	r	1.5–3.0	$1 - \infty$	Spacing ratio to control the intersection point of the <i>CSL</i> and the yield surface
	n	1–5	1–5	Stress-state coefficient to specify the shape of the yield surface

4.4.2.1 Elastic Constants μ and κ

The elastic behaviour is modelled by the Poisson's ratio μ and the slope of the swelling line κ . To determinate the values of μ and κ , loading and unloading of a specimen to the *NCL* is needed. Locating the *NCL* for sands, however, seems to be very difficult as a test device able to supply very high pressure is required, which is not normally available in geotechnical laboratories. Other methods to obtain the elastic properties of soils include:

- Resonant column devices and triaxial tests equipped with piezo-crystals or bender elements;
- High-quality measurements of small stress and strain of soils using 'on-specimen' instrumentation.

The first method uses the equipments to measure the shear wave velocity V_s and longitudinal wave velocity V_p , which can be used to calculate the Poisson's ratio μ and maximum shear modulus G_0 with the following equations:

$$\mu = \frac{1 \left(\frac{V_p}{V_s} \right)^2 - 2}{2 \left(\frac{V_p}{V_s} \right)^2 - 1} \quad (4-8)$$

$$G_0 = \rho V_s^2 \quad (4-9)$$

where ρ is the density of the specimen.

The elastic constants determined in this study are based on the second method. The Poisson's ratio μ was obtained by performing several conventional drained triaxial compression tests as shown in Figure 4-33. The initial gradient of the volume change curve is given by:

$$\frac{\delta \varepsilon_p}{\delta \varepsilon_q} = \frac{G}{K} = \frac{3(1 - 2\mu)}{2(1 + \mu)} \quad (4-10)$$

Hence,

$$\mu = \frac{3 - 2\frac{G}{K}}{6 + 2\frac{G}{K}} \quad (4-11)$$

Four isotropically consolidated drained tests were conducted. A resolution of 10^{-4} % for the axial and radial strains can be achieved by employing the ‘on-specimen’ measuring device described in Chapter 3. Figure 4-33 shows the initial void ratios and test conditions of these four specimens, giving an average value of $\mu \approx 0.13$ ($G_{\max}/K_{\max} = 1.0$).

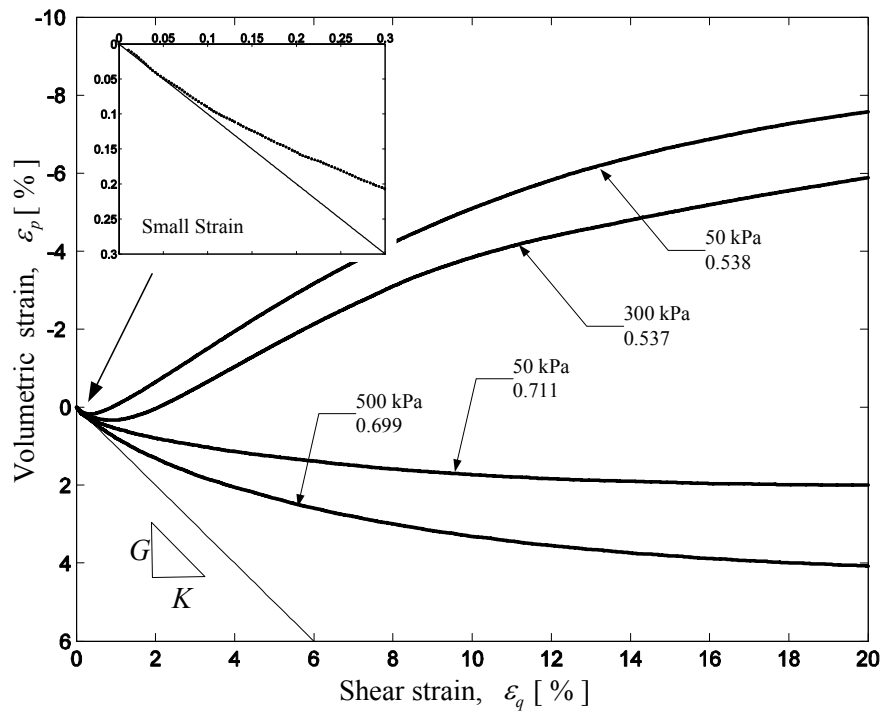


Figure 4-33. Determination of Poisson's ratio μ by drained triaxial tests.

For uncemented sands, several researchers (e.g. Lade and Duncan, 1975; Lade, 1977) recommended a constant value of 0.20. Jamiolkowski and co-workers (1994) reported values of Poisson's ratio at low stresses ranging from 0.12 to 0.15 based on local strain measurements, and from 0.20 to 0.25 based on external measurement of the axial strain. A constant value of 0.16 was found to be an optimum value for the current study.

As mentioned earlier, locating the *NCL* for sands may be more difficult since a test device able to supply very high pressure is required. Without such equipment, direct measurement of the slope of the swelling line for sands in the $\nu - \ln p'$ space cannot be done. However, in CASM, using a reference consolidation line (*RCL*) eliminates such difficulty and therefore κ can satisfactorily be measured, which corresponds to a reference state parameter ranging between 0.05–0.07 that is unlikely to be encountered in practice (Yu, 1998).

κ is measured from the slope of the unloading-reloading loop BC in isotropic compression tests (see Figure 4-34). For uncemented sands, a typical value of κ is 0.005 (Yu, 1998), which was found to fall within the measured data range. The value of κ was taken as 0.005 for this study.

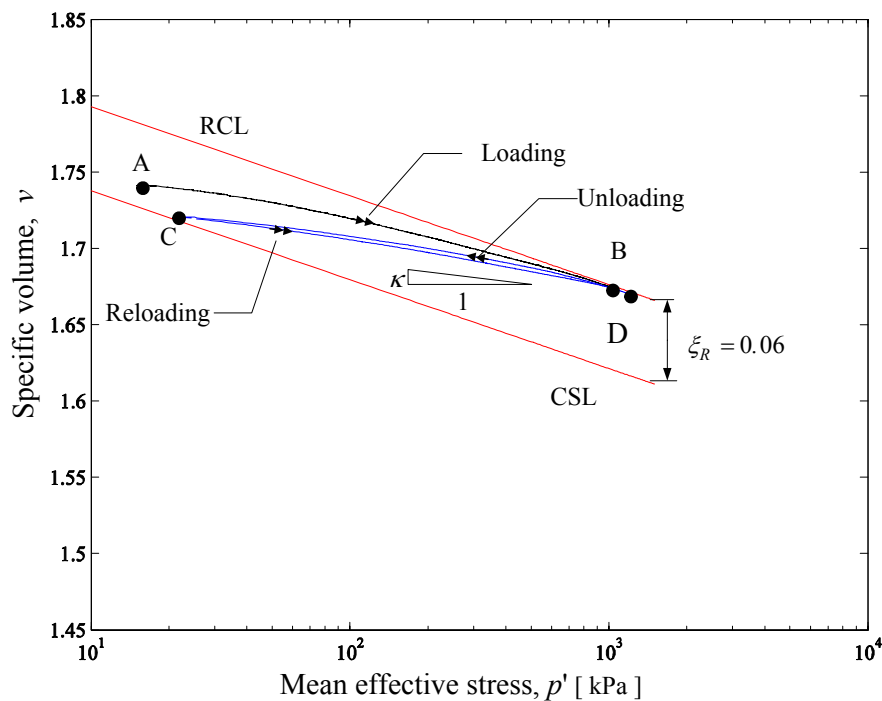


Figure 4-34. Determination of slope of swelling line κ by isotropic compression tests.

4.4.2.2 Critical State Constants λ , Γ and M

The values of the critical state constants for Portaway sand have been established in the previous section as:

$$\lambda = 0.025, \Gamma = 1.796, M_c = 1.19$$

4.4.2.3 Spacing Ratio r and Stress-State Coefficient n

The spacing ratio r is used to estimate the reference state parameter ξ_R , which corresponds to the loosest state a specimen may reach. After saturation and consolidation in the current testing program on Portaway sand, r was found to be 19.2 equivalent to a reference state parameter of $\xi_R = 0.06$. The reason for using this value is given in section 4.3.4.

To determine the stress-state coefficient n , it is necessary to plot the stress paths from both drained and undrained tests, where the specimens are subjected to different initial conditions in terms of the stress ratio η against the state parameter ξ . Using the general stress-state relation adopted in CASM (see equation (2-41)), the experimental state boundary surface can be regarded as a straight line in the plot of $\ln\left(1 - \left(\xi/\xi_R\right)\right)$ against $\ln\left(\eta/M\right)$.

The stress-state coefficient n is the slope of the state boundary surface in this particular log-log plot. Plotted in Figure 4-35 are the relationships between stress ratios and state parameters on loose and dense Portaway sand. Based on the data obtained, the parameter n for Portaway sand was taken to be 3.5.

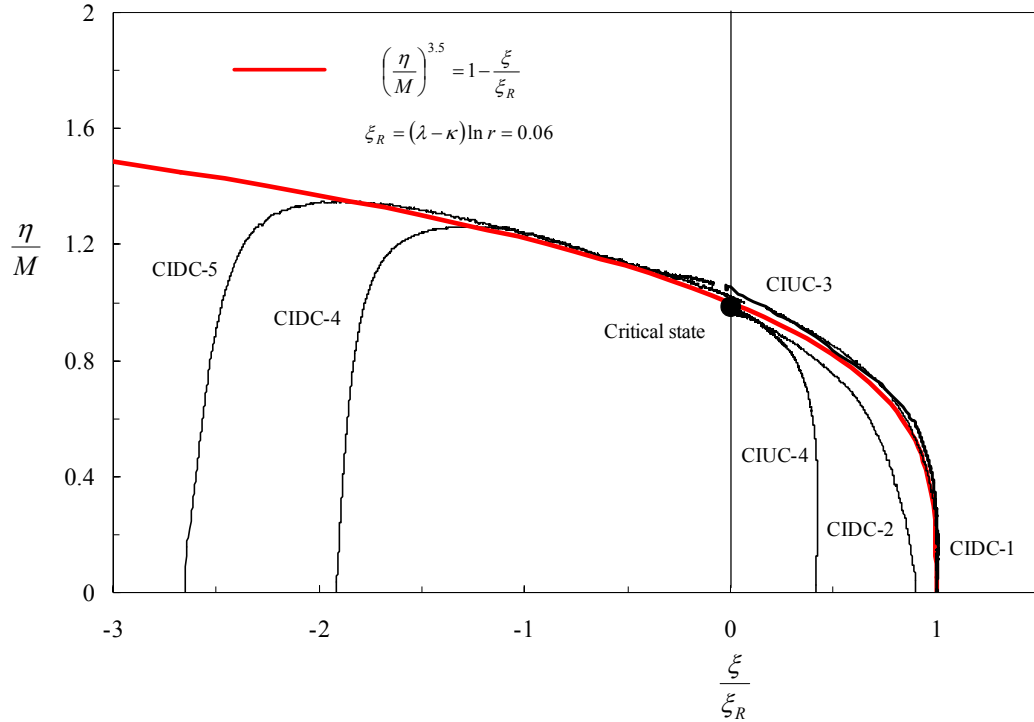


Figure 4-35. Determination of stress-state coefficient n from drained and undrained tests.

4.4.3 Undrained Instability

It has been shown in section 4.3.4 that very loose Portaway sand can collapse and strain soften during monotonic undrained loading and ultimately reach the critical state. Figure 4-36 shows the effective stress paths of three very loose specimens (CIUC-1–3) in the $p'-\nu-q$ space. Based on the *CSL* established previously for Portaway sand, the initial state parameter can be determined for test specimens according to equation (4-12):

$$\xi_0 = \nu + \lambda \ln p' - \Gamma = \nu + 0.025 \ln p' - 1.796 \quad (4-12)$$

It should be noted that the three specimens have an identical initial state parameter of 0.06. Projections of their effective stress paths in the $p'-q$ space are shown in Figure 4-37. It can be seen that a unique instability line (Lade et al., 1988) exists, which connects different peak-deviatoric stresses and passes through the origin. This line is also known as the flow liquefaction line.

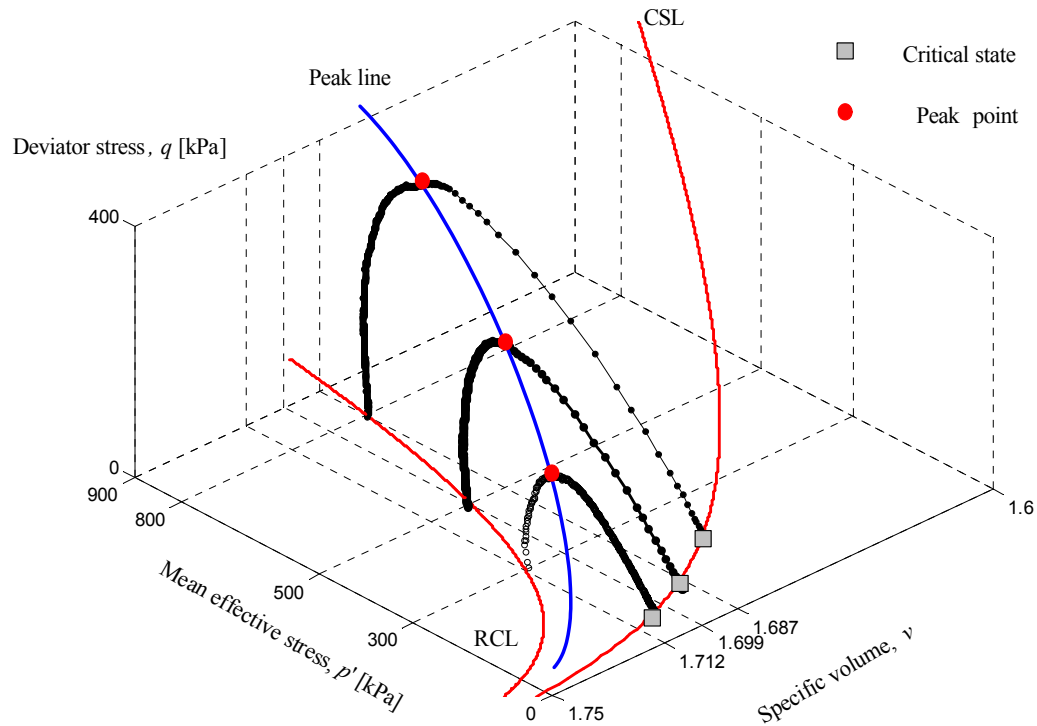


Figure 4-36. Effective stress paths of three normally consolidated specimens in the $p' - \nu - q$ space.

Lade et al. (1988), Vaid et al. (1990) and recent experimental investigations have suggested that the flow liquefaction line is uniquely related to the material tested regardless of the initial conditions. However, the results obtained for Portaway sand indicate that the slope of the flow liquefaction line is strongly dependent on the initial state of the specimens. Figure 4-38 compares the stress paths between tests CIUC-1-3 and test CIUC-4 with initial state parameters of 0.06 and 0.025, respectively. It is evident that the peak point of test CIUC-4 (solid line) does not lay on the flow liquefaction surface for specimens with an initial state parameter equal to 0.06.

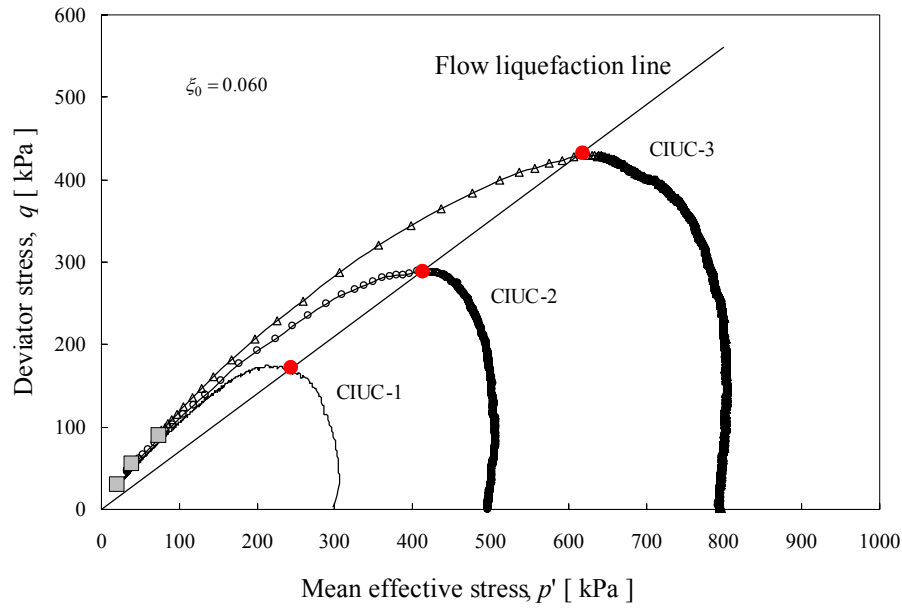


Figure 4-37. Definition of flow liquefaction line.

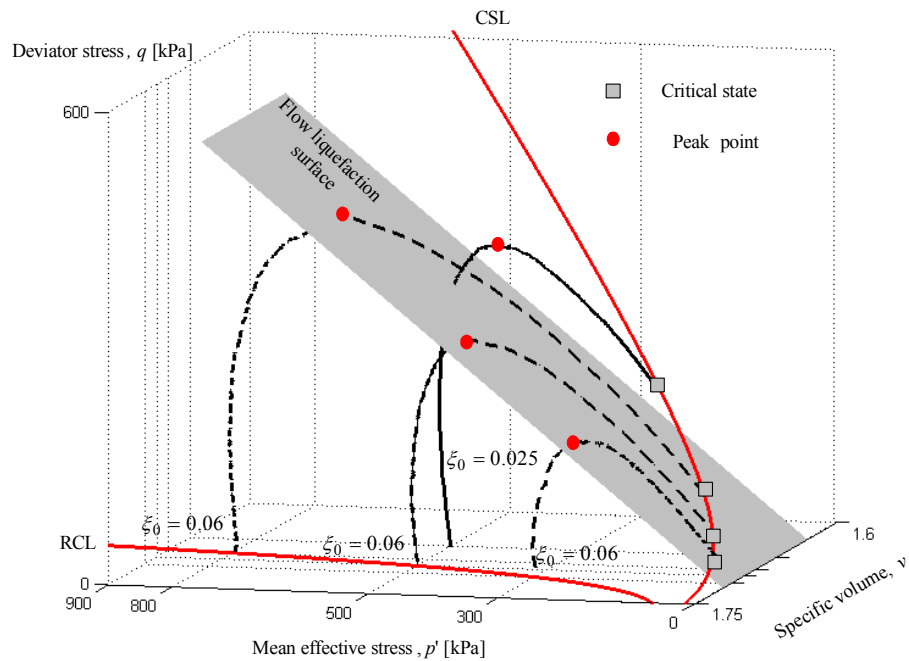


Figure 4-38. State-dependent flow liquefaction line.

Figure 4-39 shows three undrained effective stress paths normalised by the equivalent critical state pressure p'_u (mean effective stress at the critical state with the same void ratio). It suggests that the slope of the flow liquefaction line increases with a decrease in the initial state parameters.

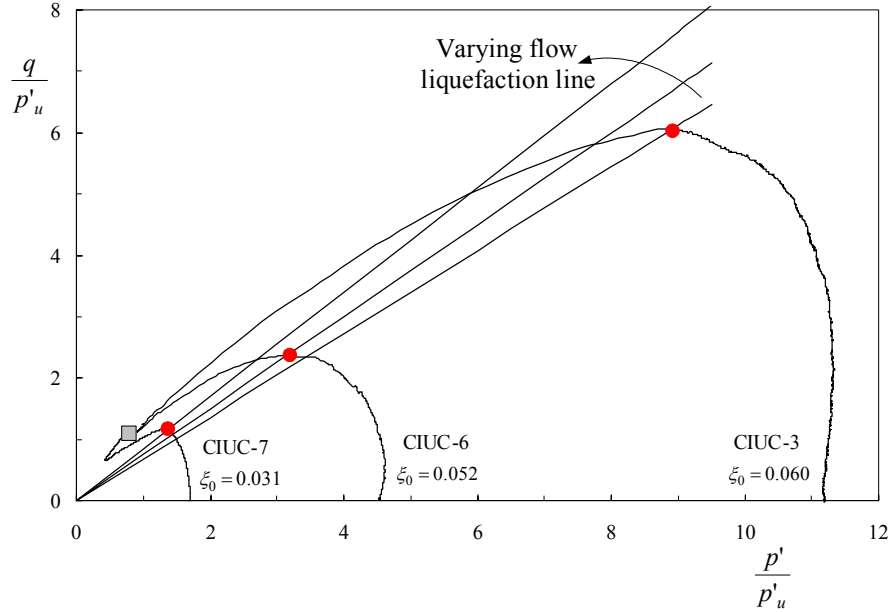


Figure 4-39. Effective stress paths normalised by equivalent critical state pressure.

Yang (2002) proposed an empirical relationship between the stress ratio $\eta_{peak} = \left(q/p' \right)_{peak}$ at the peak point and the initial state parameter ξ_0 based on the published data of Leighton Buzzard sand (Sladen et al., 1985) and Toyoura sand (Ishihara, 1993). The relationship is expressed as:

$$\eta_{peak} = \frac{M}{B} \exp(A\xi_0) \quad (4-13)$$

where M is the critical state stress ratio, and A and B are the two parameters that depending on the material tested.

The above relationship was only verified in the compression space by Yang (2002) (see Figure 4-40) for Leighton buzzard sand and Toyoura sand. The validity of this correlation was re-examined using results obtained from both compression and extension tests on Portaway sand in the current experimental investigations.

Jefferies and Been (2004) argued that the state parameter ξ is a variable in the constitutive models, not an initial index parameter, therefore, the following interpretations are based on the current state parameter. The state parameter at

the peak point is denoted ξ_{peak} . The tests used in the analysis are summarised in Table 4-13.

Table 4-13. Initial and peak parameters for loose specimens.

Test ID	e_0	p'_0	p'_{peak}	$\eta_{peak} = \left q/p' \right _{peak}$	ξ_0	ξ_{peak}
CIUC-2	0.699	500	400	0.68	0.060	0.055
CIUC-3	0.687	800	600	0.68	0.060	0.055
CIUC-6	0.705	300	200	0.75	0.052	0.048
CIUC-7	0.710	100	80	0.85	0.031	0.025
CIUE-1	0.722	200	135	0.50	0.060	0.050
CIUE-2	0.693	500	360	0.55	0.054	0.046
CIUE-3	0.664	800	600	0.60	0.037	0.030
CIUE-4	0.661	1200	900	0.58	0.044	0.037

It is evident from Figure 4-41 that the stability of Portaway sand in triaxial compression and extension are not equivalent. The extension loading shows a more critical response than compression loading does. It also shows that the general function proposed by Yang (2002) that correlates the state parameter and corresponding stress ratio at the peak point works very well.

The following two specific correlations were obtained for Portaway sand in compression and extension, respectively:

$$\eta_{peak} = \frac{1.19}{1.16} \exp(-7.1\xi_{peak}) \quad (\text{Compression}) \quad (4-14)$$

$$\eta_{peak} = \frac{0.7}{0.9} \exp(-8.3\xi_{peak}) \quad (\text{Extension}) \quad (4-15)$$

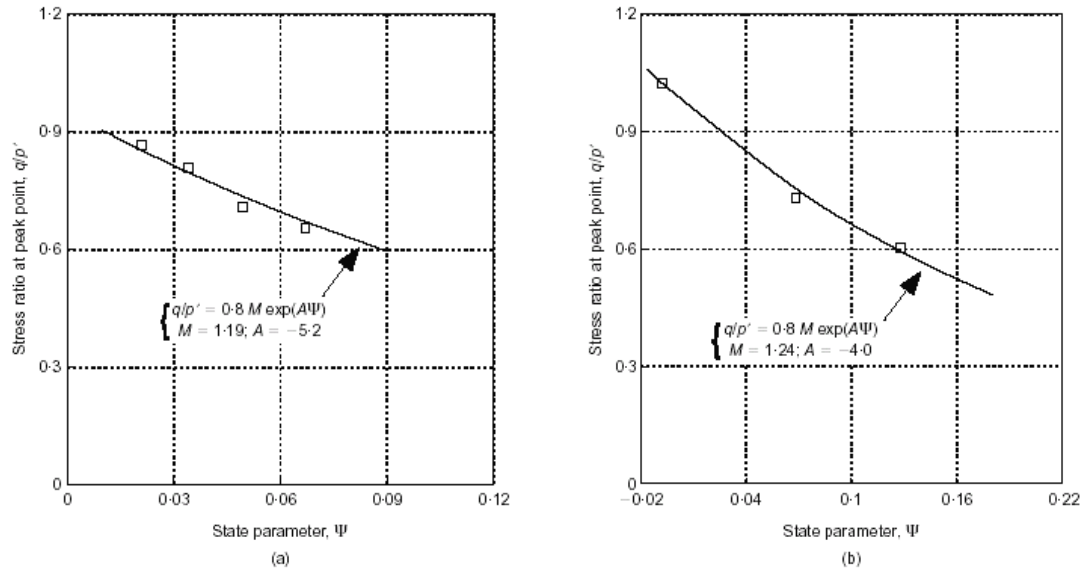


Figure 4-40. The relationship between peak stress ratio and initial state parameter in compression tests: (a) Leighton buzzard sand, (b) Toyoura sand (Yang, 2002).

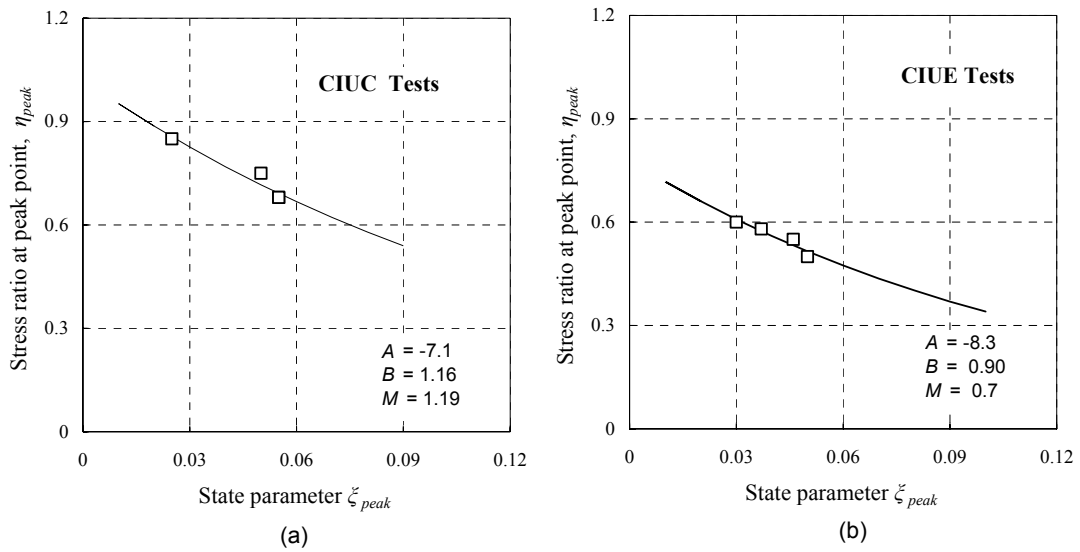


Figure 4-41. The relationships between peak stress ratio and the current state parameter on Portaway sand: (a) compression tests (CIUC), (b) extension tests (CIUE).

4.4.4 Experimental State Boundary Surface

The experimental state boundary surface shown in Figure 4-35 can be expressed using the following equation in the stress-state space:

$$\left(\frac{\eta}{1.19}\right)^{3.5} = 1 - \frac{\xi}{0.06} \quad (4-16)$$

Figure 4-42 shows the effective stress paths normalised with respect to the current preconsolidation pressure p'_o (the state boundary surface along the elastic wall), which is defined as:

$$p'_o = \exp\left[\frac{\Gamma + \xi_R - \nu - \kappa \ln p'}{\lambda - \kappa}\right] \quad (4-17)$$

The theoretical state boundary surface is defined by:

$$\left(\frac{\eta}{M}\right)^{3.5} = -\frac{\ln(p'/p'_o)}{\ln 19.2} \quad (4-18)$$

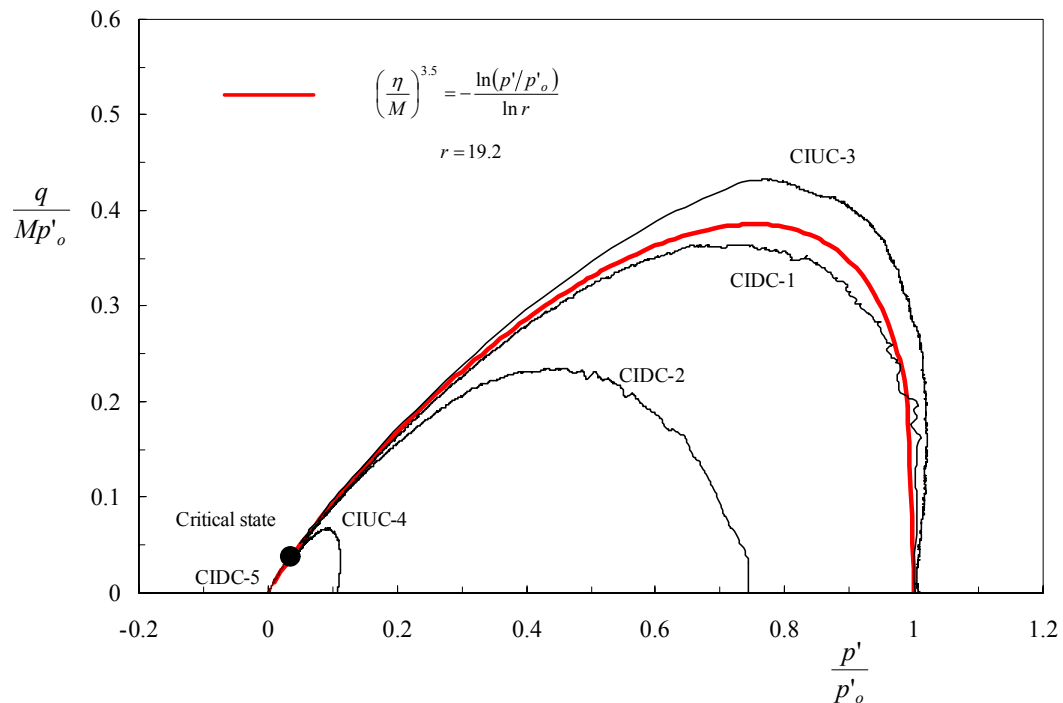


Figure 4-42. Stress paths and state boundary surface normalised with respect to the preconsolidation pressure.

It can be seen that the critical state is to the left of the apex of the theoretical and experimental state boundary surfaces. This result is in good agreement with the observations reported by Coop and Lee (1993) and McDowell et al. (2002), and supports their conclusions that, for sands, the value of spacing ratio r is much larger than for clays.

To compare the triaxial data it is also convenient to present the effective stress paths normalised with respect to the equivalent critical state pressure p'_u (the state boundary surface at constant ν). This technique of normalising triaxial data has been used by many researchers to investigate the undrained instability of loose sands (e.g. Sladen and Oswell, 1989; Yang, 2002). The equivalent critical state pressure p'_u is defined according to the following equation:

$$p'_u = \exp\left[\frac{\Gamma - \nu}{\lambda}\right] \quad (4-19)$$

The theoretical state boundary surface is expressed as:

$$\left(\frac{\eta}{M}\right)^{3.5} = 1 - \frac{\ln(p'/p'_u)}{\Lambda \ln 19.2} \quad (4-20)$$

where Λ is known as the plastic volumetric strain ratio (Schofield and Wroth, 1968) and is calculated for Portaway sand using:

$$\Lambda = \frac{\lambda - \kappa}{\lambda} = \frac{0.0253 - 0.005}{0.0253} = 0.802 \quad (4-21)$$

The value of Λ is between 0 and 1 and is typically about 0.8 (Wroth and Houlsby, 1985). It is evident from Figure 4-43 that the experimental state boundary surface for Portaway sand has a very similar shape compared to those obtained for various sands (see Figure 2-21).

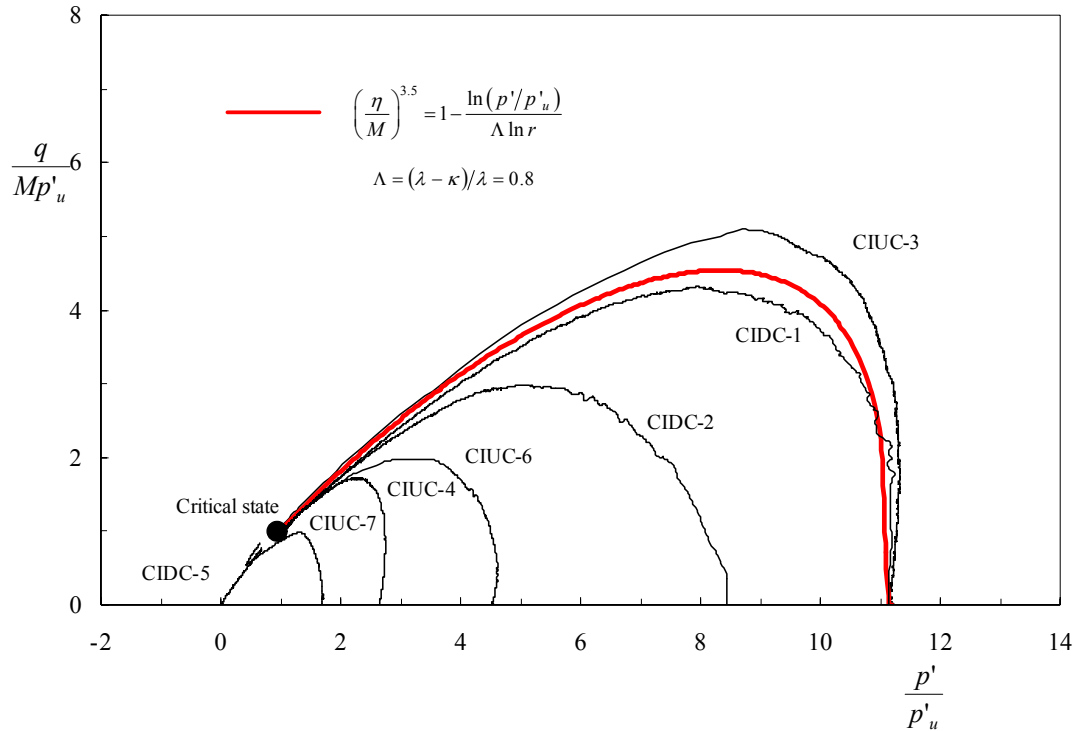


Figure 4-43. Stress paths and state boundary surface normalised by equivalent critical state pressure.

4.5 SMALL STRAIN BEHAVIOUR

4.5.1 Series G: Tests Measured with Hall Effect Transducers (S-1~S-6)

The purposes of carrying out these tests were to investigate some aspects of small strain behaviour of Portaway sand and to evaluate the performance of the Hall effect transducers.

Proper understanding of small strain behaviour of soils is very important, since many elastic properties, such as initial shear modulus and Poisson's ratio are critical parameters in the analysis of many geotechnical engineering problems. However, external strain measurements are well known to be inadequate due to the unreliable displacement measurement as reviewed in section 2.3.1.2. The Hall effect

transducers described in Chapter 3 (see Figure 3-13) were used throughout the following investigations. The tests reported in this section consist of eight specimens comprising dense and loose specimens, which were sheared under various stress paths. A summary of the testing program is shown in Table 4-14.

Table 4-14. Summary of Series G: tests with small strain measurement.

Initial conditions				Control method	End of test		Remarks
Test ID	e_0	D_r (%)	p'_0 (kPa)		ε_a (%)	G_0 (MPa)	
S-1	0.540	76	300	L	23	125	Drained
S-2	0.580	64	100	L	5	43	Drained
S-3	0.538	76	50	D	28	17	Drained
S-4	0.699	28	500	D	29	71	Drained
S-5	0.678	34	300	L	25	28	Drained
S-6	0.715	23	50	D	25	12	Drained
S-7	0.710	24	100	L	25	-	Undrained
S-8	0.610	55	50	D	4.3	-	Drained

Note: L = Load control; D = Displacement control

4.5.2 Results and Discussion

Figure 4-44 illustrates the typical stress-strain curves measured from the external LVDT and two Hall effect transducers on specimen S-2 being sheared under an initial consolidation pressure of 100 kPa with drained condition. It is noted that the externally measured value is about 1.8 times higher than those measured internally. The average value of internal measurements and corrected external measurements match each other very well. Cuccovillo and Coop (1997) pointed out that stress-strain data with highly non-uniform strain might be obtained using conventional apparatus and specimen preparation methods, and the measured parameters based on the average axial strain were incorrect. It is for this reason that the extension cap was used for all the tests conducted to ensure the accurate coaxiality of the specimen and apparatus. The discrepancy obtained from two local measurements

may be attributed to the installation method adopted. This needs further investigation.

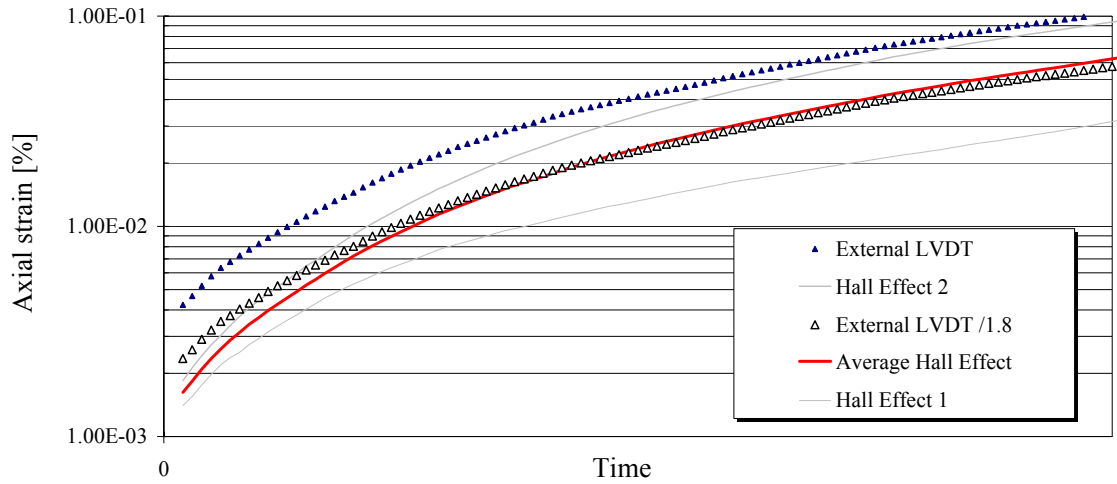


Figure 4-44. Comparison of internal and external measurements (S-2).

Figure 4-45 shows typical results of stress-strain curves measured by two axial Hall effect transducers. It is noted that the measured non-uniform strains were increased before the axial strain reached 0.15%. After that, the two measurements approached each other. It is believed that the observed non-uniformity was caused by bedding and/or seating errors. Generally speaking, the small strain measuring technique employed in this study can obtain reasonable results for Portaway sand.

Figure 4-46 evaluates the performance of the Hall effect transducers subjected to an undrained loading condition. The results from the internal and external measurements indicate that the transducers function very well from small strain to large strain regions.

The yielding of Portaway sand is clearly identified in Figure 4-47 for two specimens (S-1 and S-2) with different initial conditions. It can be seen that the yielding strains are $\varepsilon_q \approx \varepsilon_a = 0.001 - 0.0015\%$ for both specimens. The results agree well with the elastic limit axial strains for various soils summarised by Lo Presti (1995) as shown in Table 4-15.

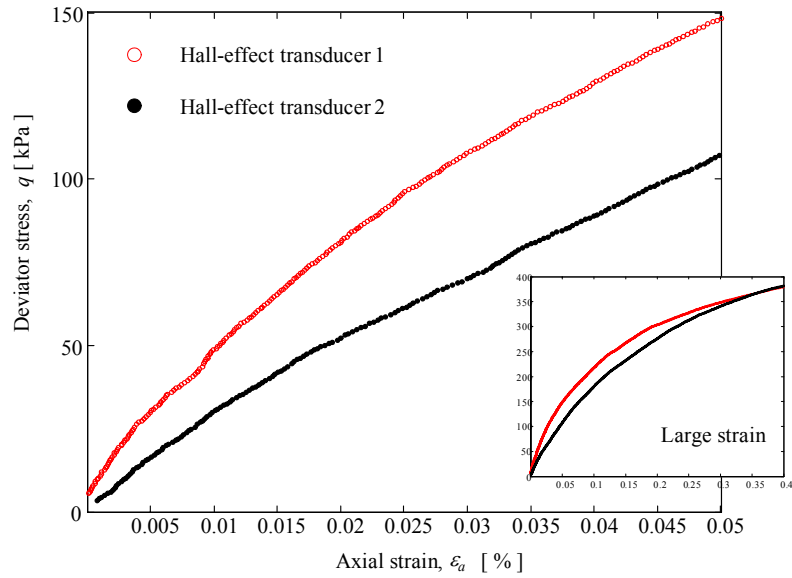


Figure 4-45. Typical stress-strain curves measured from two Hall effect transducers (S-1).

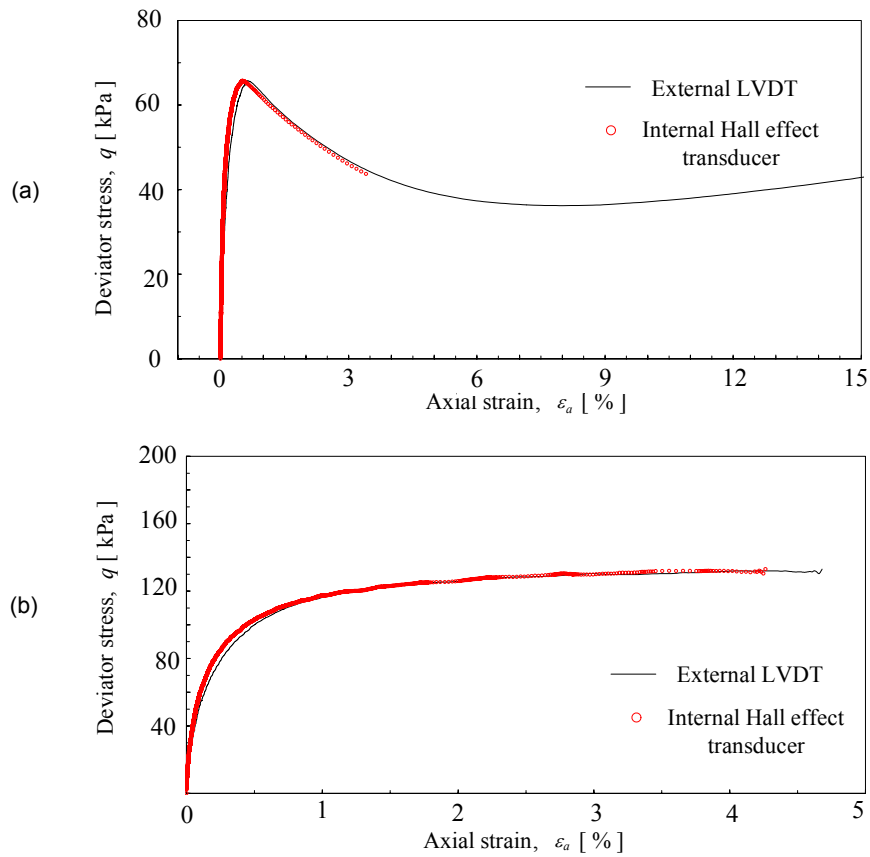
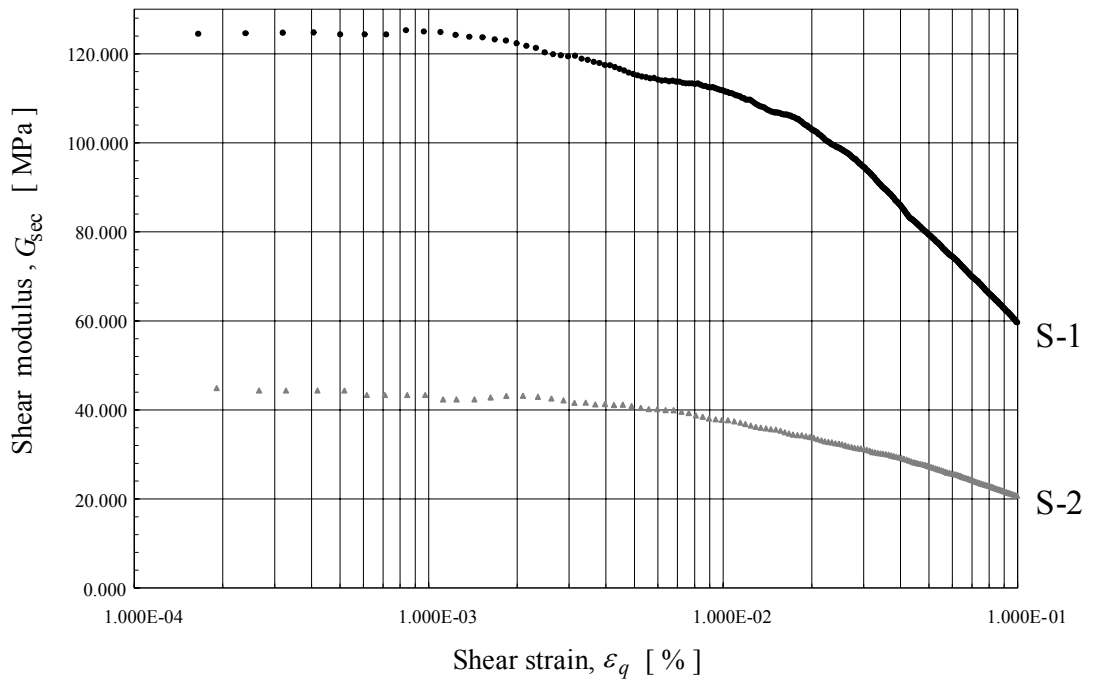
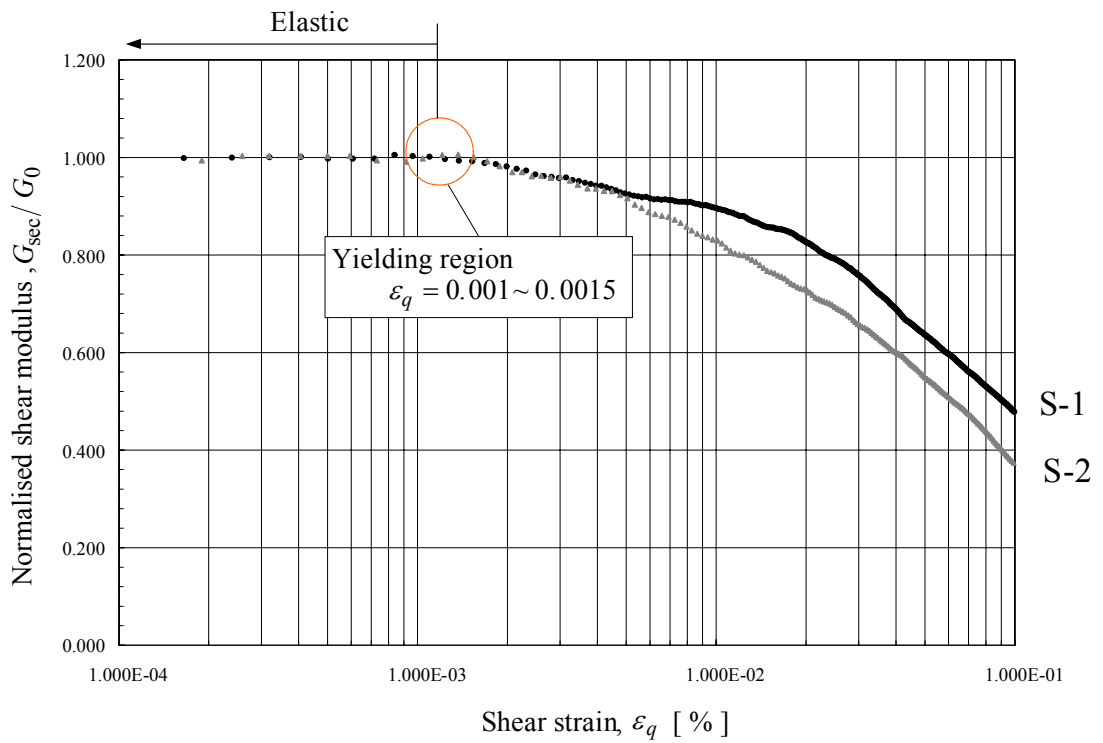


Figure 4-46. Comparisons of external and internal measurements: (a) undrained (S-7), (b) drained (S-8).



(a)



(b)

Figure 4-47. Degradation in the stiffness of Portaway sand.

The small strain shear modulus G_0 ($= \delta q / 3 \delta \varepsilon_s$) for uncemented sands was found to have the following relationship proposed by Hardin and Richard (1963):

$$G_0 = A \cdot F(e) (\sigma'_0)^n \quad (4.23)$$

where A is a material constant that depends on the mineral composition, size, shape, grading and surface texture of particles. $F(e)$ is a void ratio function, which can be taken as $(2.17 - e)^2 / (1 + e)$ for round particles or $(2.97 - e)^2 / (1 + e)$ for angular particles. Lo Presti (1995) suggested that $F(e) = e^{-1.3}$ proved satisfactory for various kinds of soils. σ'_0 is the initial effective confining pressure and n has an average value of 0.5.

Figure 4-48 plots the measured and predicted initial shear modulus for six specimens (S-1~6) at various initial conditions. The measured value of G_0 was obtained from the small strain level ($\varepsilon_q = 0.0001 - 0.0015\%$). The dependence of the small strain stiffness on the initial stress and void ratio is evaluated by these tests. It can be seen from the comparisons that the empirical relationship proposed by Lo Presti (1995) correlated better with the measured data than one proposed by Hardin and Richard (1963). However, different values of constant A were found for dense specimens and loose specimens, respectively.

Table 4-15. Elastic limit axial strain (Lo Presti, 1995).

ε_a^{et} [%]	Soils	Reference
0.001–0.0015	Reconstituted sands and gravel	Kohata et al., Dong et al.
0.002	Artificial and natural soft rocks	Kohata et al.
0.001	Osaka Bay clay ($OCR = 1.2-3.2$)	Mukabi et al.

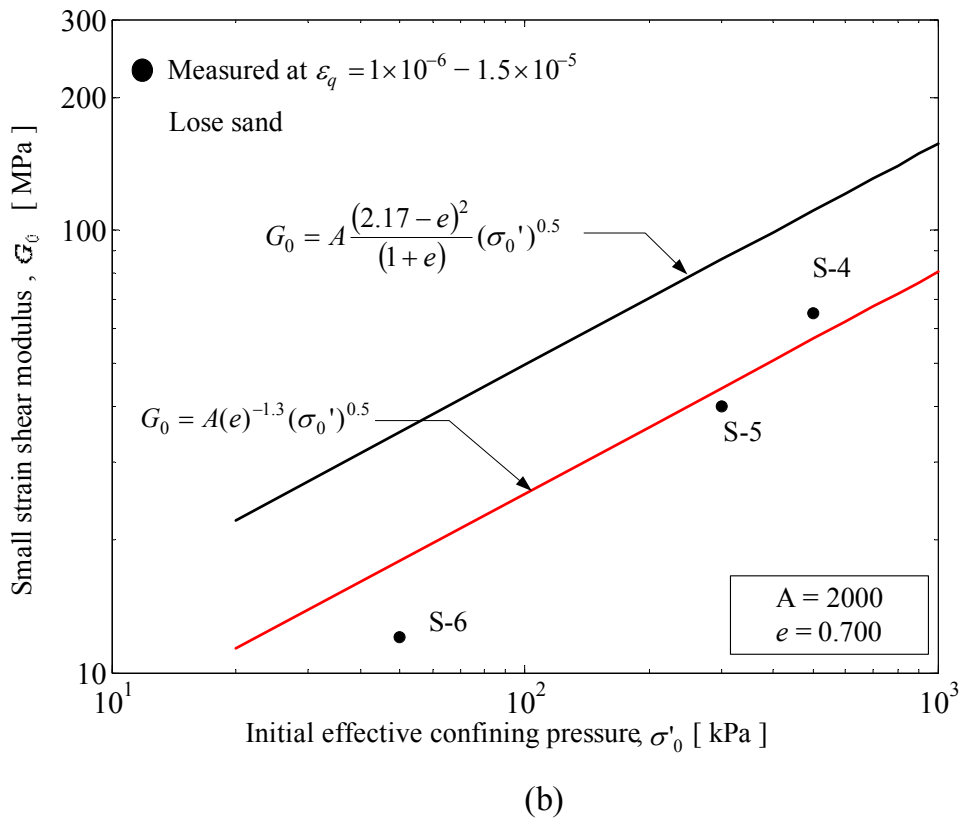
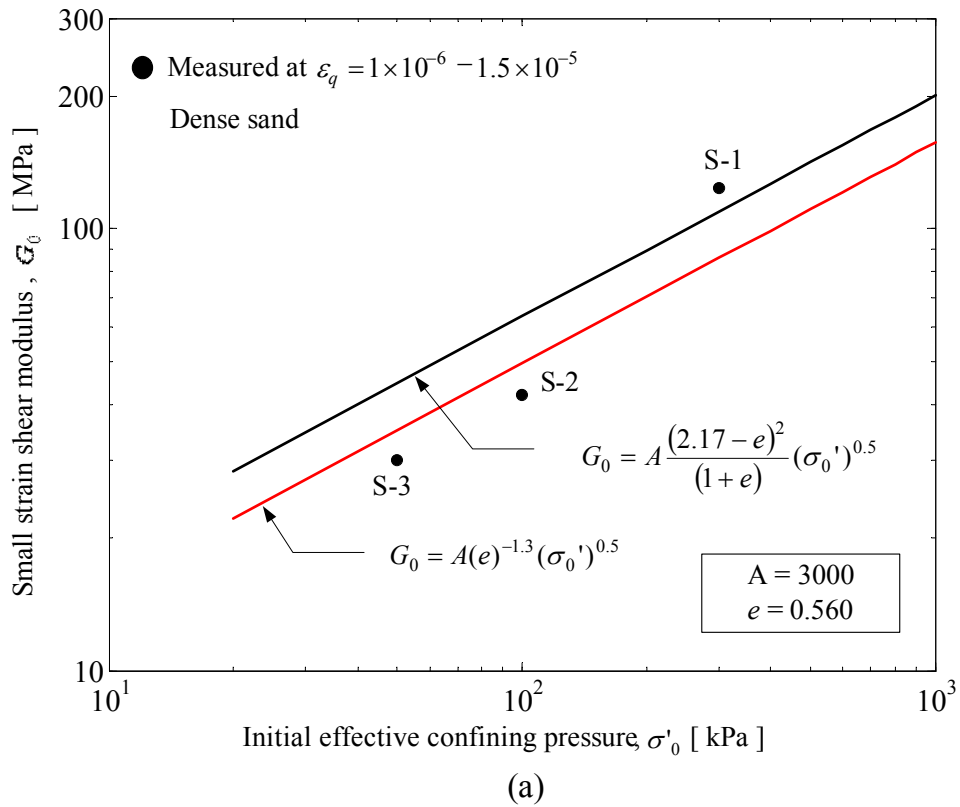


Figure 4-48. Effects of effective confining pressure and density on small strain shear modulus: dense sand (S-1-S-3), (b) loose sand (S-4-S-6).

4.6 SUMMARY

The preliminary tests on dry Portaway sand and Leighton Buzzard sand were carried out on the updated NDTTS. The results show that the system is capable of performing conventional triaxial tests on dry materials.

The stress-strain and strength characteristics of saturated Portaway sand under various monotonic stress paths have been investigated on the ADVTTS. The results suggest that the critical state concept is valid for Portaway sand and a unique *CSL* exists that is independent of the stress path, specimen preparation method, initial condition and loading mode. The different states undergone during shearing, such as the critical state, steady state, characteristic state, phase transformation state and quasi-steady state have been clarified and evaluated. The state parameter, that combines the influence of void ratio and stress level, has been used successfully to characterise most of the behaviours observed in the laboratory. A simple procedure for determining the CASM constants has also been demonstrated. By using a local measurement technique, some characteristics of the small strain behaviour of Portaway sand were identified.

Chapter 5

Cyclic Loading Triaxial Tests

5.1 INTRODUCTION

In the previous chapter, the stress-strain and strength characteristics of Portaway sand under monotonic loading condition have been given. A unique *CSL* was found and defined in the $q - p' - \nu$ space ($p' < 1000$ kPa). The experimental results suggest that the general ‘stress ratio-state parameter’ relation (see equation (2-41)) describes the experimental state boundary surface of Portaway sand very well. This finding supports the basic assumption made in the unified critical state model CASM, which was formulated in terms of the state parameter concept. It was also found that the sand behaviour is controlled by the state parameter prior to the reaching of the critical state.

During the course of this experimental study, a theoretical investigation on cyclic loading behaviour of both clay and sand was undertaken by Khong (2004) based on the CASM framework. Several assumptions have been introduced into the new cyclic bounding surface model CASM-c in order to capture the hysteretic loops, accumulated plastic deformations and pore pressure developments of soils under

cyclic loading. Although some published cyclic triaxial data on sands exists, a complete set of CASM constants is not available. The main objectives of carrying out this series of tests are as follows:

- To further investigate the stress-strain and strength characteristics of Portaway sand under cyclic loading.
- To correlate the monotonic and cyclic behaviours of Portaway sand.
- To provide typical drained and undrained cyclic loading data for verifying cyclic model CASM-c described in Chapter 6.

The data presented in this chapter was obtained from cyclic loading triaxial tests performed using the ADVTTTS with saturated Portaway sand. The test series consisted of several specimens subjected to one-way, two-way and moving wheel loading stress paths.

This chapter is arranged in the following order: firstly, an overview of the cyclic testing method is described. Three series of testing programs and direct experimental results are then presented. Finally, the interpretation of the results and the correlations between cyclic and monotonic loading behaviours are given.

5.2 OVERVIEW OF THE TESTING METHOD

Cyclic triaxial testing is commonly used to evaluate cyclic characteristics and measure the liquefaction resistance of soils. The literature contains numerous well-documented reports of tests on sands with emphasis on earthquake engineering (e.g. Ishihara, 1993). It has long been recognised, however, that there is no standard procedure to characterise the cyclic behaviour of sands within the geotechnical engineering community. Silver et al. (1976) initiated a cooperative soil testing programme that involved eight laboratories in order to define the cyclic strength characteristics of a clean uniform sand. Their findings indicate three factors that

are more critical than others when trying to reproduce meaningful and comparable results:

- Specimen preparation method;
- Shape of the loading pattern;
- Initial state of sand tested.

Specimen preparation method

In this experimental work, the same specimen preparation technique was used for both the monotonic and cyclic testing programs so that a meaningful correlation between the two types of tests could be made.

Shape of the loading pattern

Three wave forms are commonly used in geotechnical research laboratories including triangular, square-shaped and sinusoidal. Silver et al. (1976) concluded that the sinusoidal wave form could produce 10% higher cyclic strength than those from the square wave form. The reason for this is due to the severe velocity changes that occur during loading with a square wave form and their effects on pore pressure. The sinusoidal wave form was recommended by Silver et al. (1976) and has been used in most tests conducted in this research work.

Loading rate

Slow cyclic loading rate was employed for all the tests performed with a rate of around 10 minutes per cycle, which can be considered as quasi-static loading. The reason for choosing this type of loading rate instead of fast one is that, given by Wood (1982):

‘Slow cyclic tests in which one can be certain of the reliability of the measured pore water pressures are to be preferred to fast tests, and are more likely to provide the necessary clues for modelling cyclic behaviour of soils’.

It is also well accepted that the rate of loading has significant influence on clays. Conversely, no obviously time-dependent behaviour is found for sands due to its higher permeability.

Definition of the cyclic stress ratio (*CSR*)

In view of literature on characterising the behaviour of saturated sands under undrained cyclic loading, the main influencing factors were identified as the initial effective confining pressure σ'_0 , the amplitude of cyclic shear stress q_{cyc} and the number of cycles N_{cyc} . It has been recognised as reasonable and become a routine to combine the first two parameters as one parameter named as the *CSR* to describe different cyclic loading tests, which is defined as:

$$CSR = \frac{q_{cyc}}{2\sigma'_0} \quad (5-1)$$

It has also become common to take the *CSR* required to cause 5% double amplitude axial strain under 20 cycles as a factor to quantify cyclic strength under a given state of specimens (Ishihara, 1996). It is well known that the cyclic strength of reconstituted sand is uniquely related with the density and specimen preparation methods. Therefore, in order to isolate various factors from each other, specimens tested under undrained cyclic loading have essentially the same density ($e_0 = 0.711 - 0.712$) and the same initial confining pressure ($\sigma'_0 = 300$ kPa).

5.3 ONE-WAY CYCLIC LOADING

This series of tests were used to investigate the effects of the initial state parameter ξ_0 , cyclic shear stress q_{cyc} , and the stress path on the stress-strain and strength characteristics of Portaway sand cycled in compression or in extension stress spaces. The magnitude of the cyclic shear stress concerned was in excess of the stress at elastic limit but lower than that at failure, which is defined from monotonic loading

as shown in Chapter 4. The four drained and two undrained one-way cyclic loading tests were carried out and are summarised in Table 5-1.

Table 5-1. Summary of one-way cyclic loading program.

Test ID	e_0	p'_0 (%)	ξ_0	Stress path	CSR
OWDC-1	0.678	300	0.026	Constant $q_{cyc} = 200$ kPa	-
OWDC-2	0.560	50	-0.137	Shear amplitude q_{cyc} increased	-
OWDC-3	0.512	300	-0.140	Shear amplitude q_{cyc} increased	-
OWDC-4	0.518	100	-0.161	Shear amplitude q_{cyc} increased	-
OWUC-5	0.711	300	0.06	Constant $q_{cyc} = 120$ kPa	0.20
OWUE-6	0.712	300	0.06	Constant $q_{cyc} = -90$ kPa	0.15

Notes:

OWDC = One-way drained loading in compression

OWUC = One-way undrained loading in compression

OWUE = One-way undrained loading in extension

5.3.1 Drained Tests (OWDC-1-4)

Figure 5-1 shows the typical result of one-way cyclic loading in compression (OWDC-1) performed at a constant effective confining stress σ'_3 of 300 kPa. For comparison purposes, the results of the two monotonic tests CIDC-2 and CIDC-3 are indicated in the figure. After three cyclic loadings, test OWDC-1 was sheared monotonically until the critical state was reached. As expected, at the first loading condition, the stress-strain relationships of the three specimens were strongly dependent on the initial state parameter ξ_0 . It is evident that test OWDC-1 was undergoing dilation continuously during cyclic loads. As soon as monotonic loading started, the specimen immediately showed signs of contraction. The results of three dense specimens are shown in Figure 5-2. It can be seen that cyclic loading patterns had a profound effect on the developments of the volumetric strains.

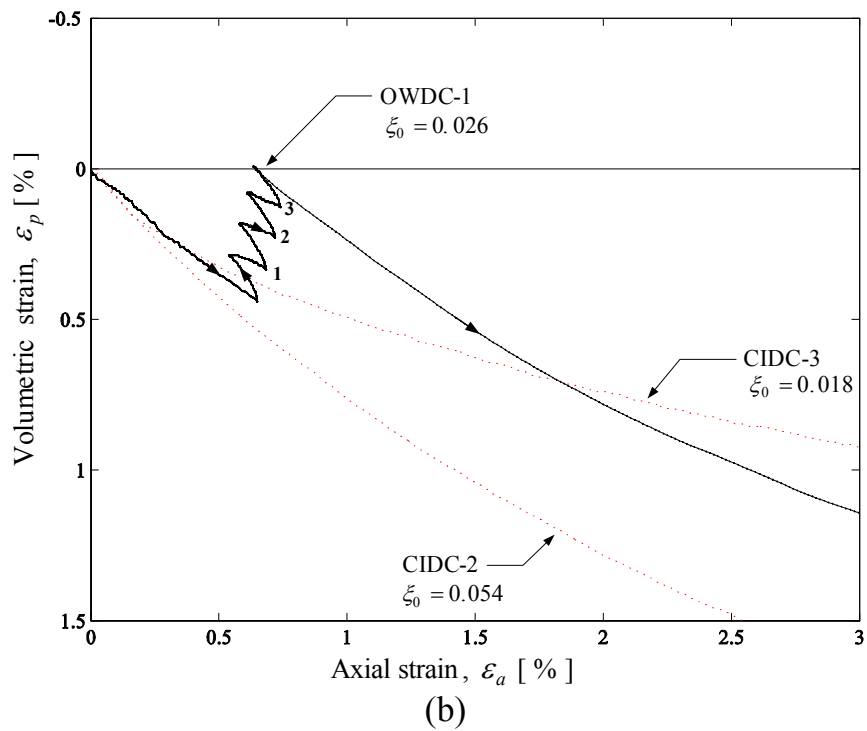
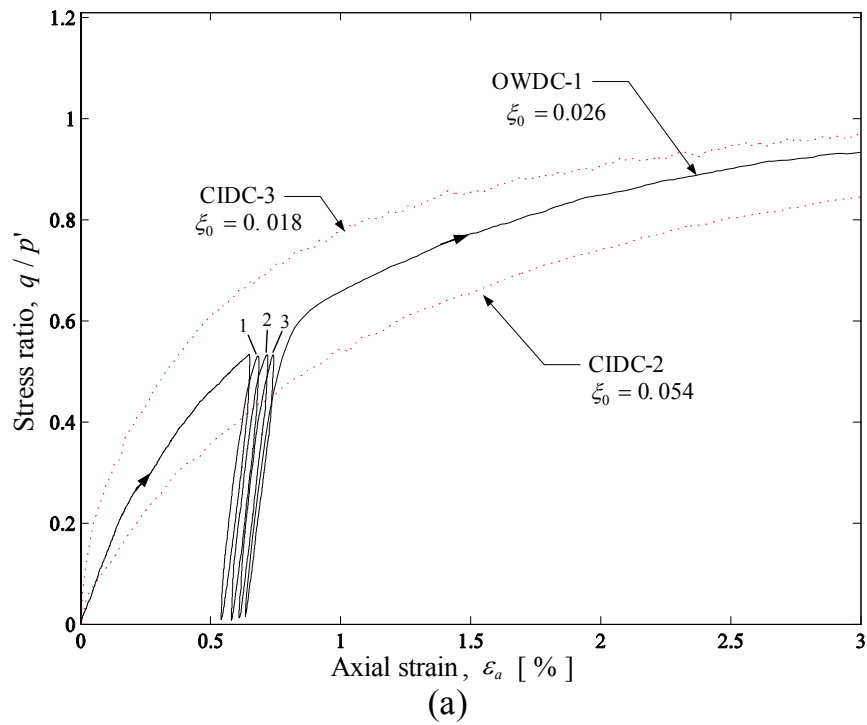


Figure 5-1. One-way drained cyclic loading in compression ($\xi_0 = 0.026$, OWDC-1).

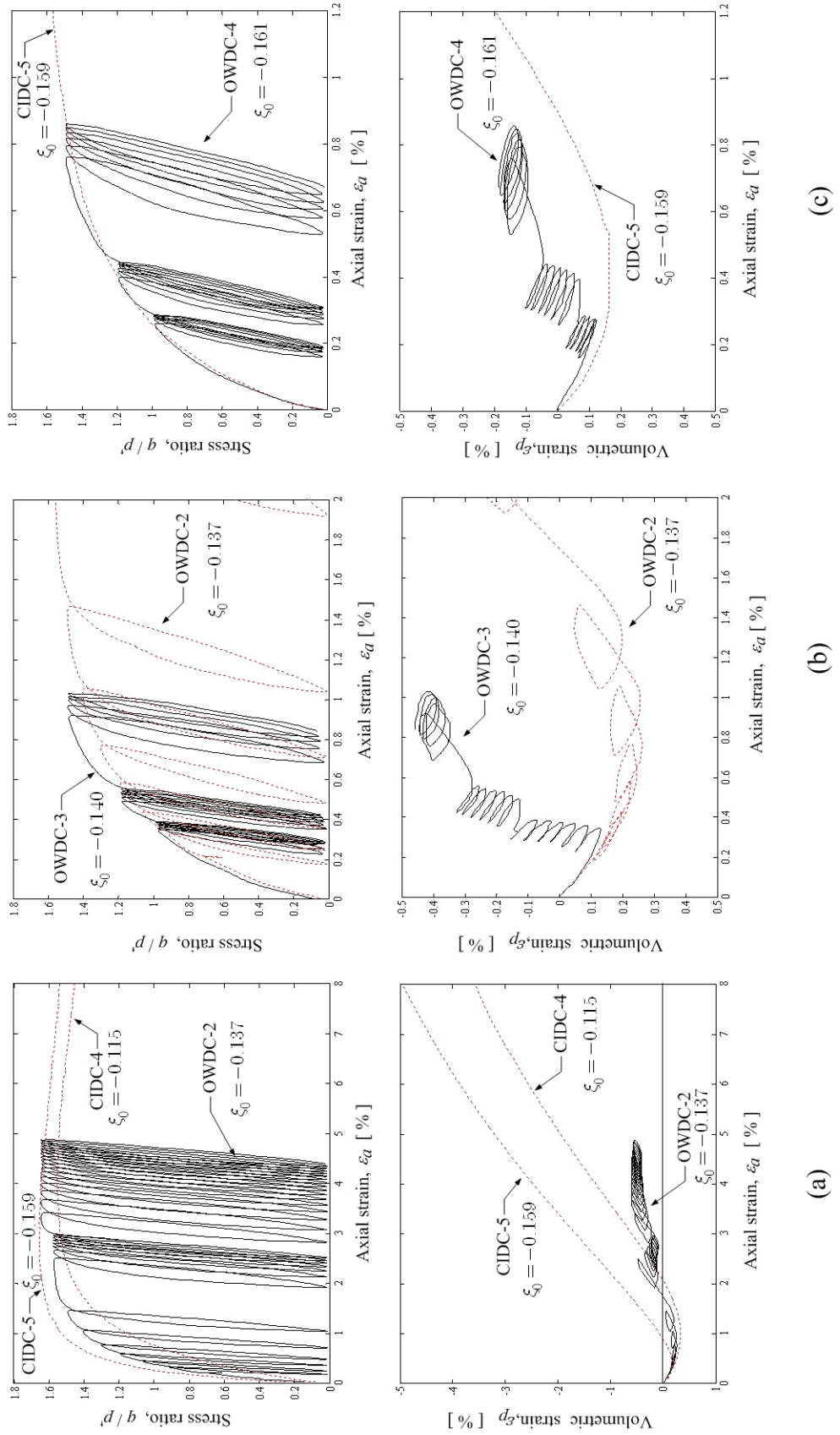


Figure 5-2. One-way drained cyclic loading in compression (OWDC-2-4).

5.3.2 Undrained Tests (OWUC-5 and OWUE-6)

Figure 5-3 shows the results obtained during one-way cyclic undrained loading on two specimens OWUC-5 and OWUE-6 with the same initial state parameter. Before the undrained shearing, both specimens were placed on the *RCL* ($\xi_0 = \xi_R = 0.06$) so that they could be considered as normally consolidated specimens.

Test OWUC-5 was sheared in compression with a *CSR* of 0.2. The variations of axial strain ε_a , deviatoric stress q and excess pore pressure Δu versus number of cycles N_{cyc} are shown in Figure 5-3. It can be seen that Δu built up steadily and ε_a increased slightly while amplitude of cyclic shear stress q_{cyc} was unchanged. However, after 42 cycles, the sudden generation of large excess pore pressure occurred with a large axial strain accumulation and reduction of cyclic shear strength. At about the 47th cycle, the specimen lost most strength and reached liquefied state. Figure 5-4 presents the stress path, stress-strain relation and excess pore pressure-strain relation. Test OWUC-5 shows the typical behaviour of loose sand subjected to cyclic loading in compression. Similar results have been reported by many other researchers (e.g. Ishihara et al., 1975; Polous, 1981).

As summarised by Ghaboussi and Momen (1982), three distinct stages are observed in the effective stress paths of this type of tests, which are clearly indicated in Figure 5-4 (a):

- 1) 1st cycle: Significant mean effective stress reduction and excess pore pressure generation occurred.
- 2) 1st–42nd cycles: The increment of excess pore pressure per cycle remained constant. The decrease of the mean effective stress occurred in the unloading segment.

- 3) After 42nd cycle: When the stress path was closed to the *CSL*, liquefaction was initiated. The stage was characterised by rapid changes in the mean effective stress.

In contrast to the compression test, the behaviour of specimen in test OWUE-6 was less stable. It can be seen from Figure 5-3 that liquefaction was only reached after 20 cycles with *CSR* equal to 0.15. According to the definition introduced in section 5.2, the cyclic strength of Portaway sand can be represented as $\left[q_{cyc} / (2\sigma'_{0}) \right]_{20} = 0.15$ with a void ratio equal to 0.712 in the one-way extension test.

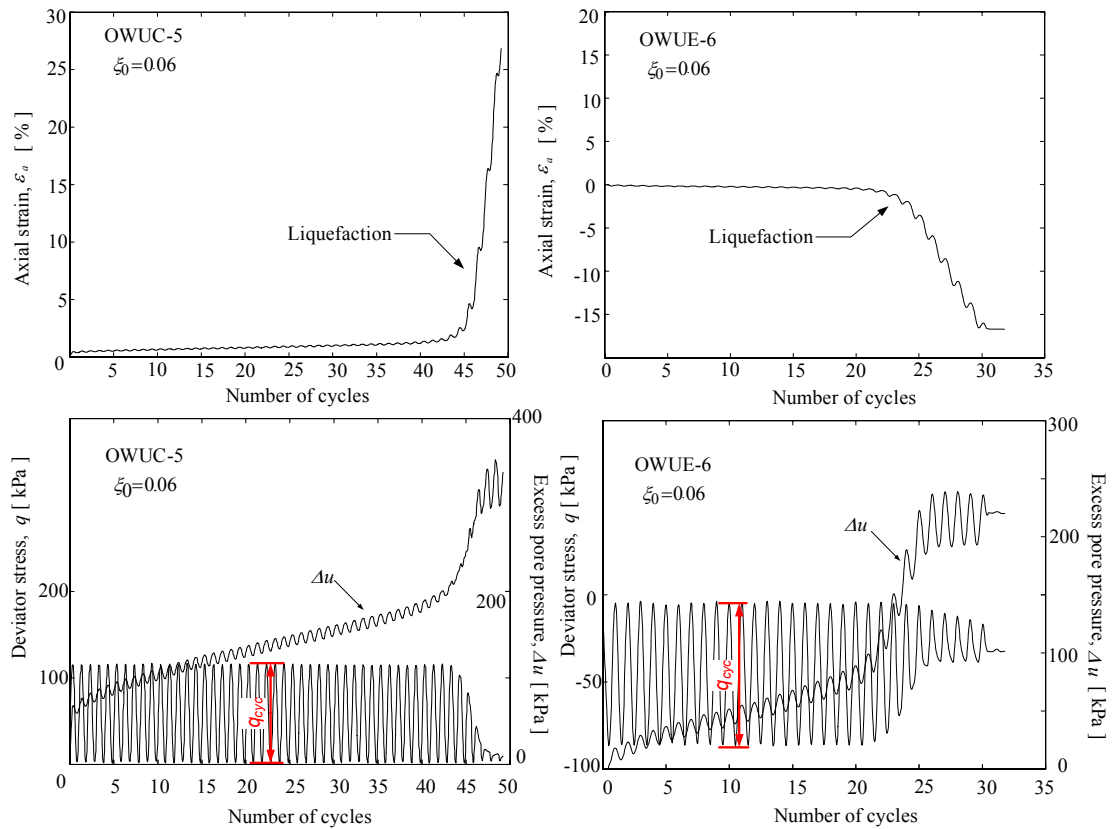


Figure 5-3. One-way undrained cyclic loading (A) ($\xi_0 = 0.06$, OWUC-5; $\xi_0 = 0.06$, OWUE-6).

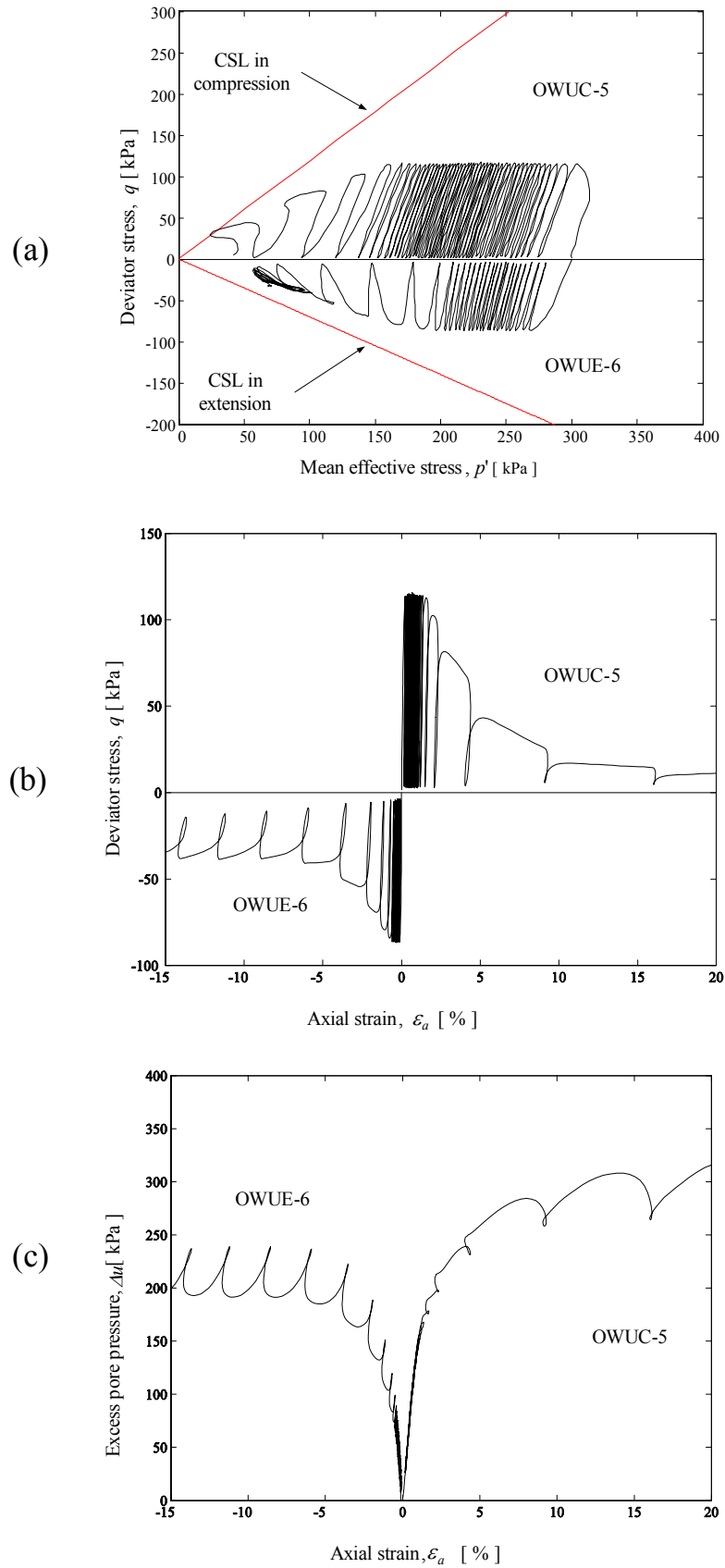


Figure 5-4. One-way undrained cyclic loading (B) ($\xi_0 = 0.06$, OWUC-5; $\xi_0 = 0.06$, OWUE-6).

5.4 TWO-WAY CYCLIC LOADING

As before, the magnitude of the cyclic shear stress concerned was in excess of stress at the elastic limit but lower than that at failure. Six drained and two undrained two-way cyclic loading tests were carried out as summarised in Table 5-2.

Table 5-2. Summary of two-way cyclic loading program.

Test ID	e_0	p'_0 (kPa)	ξ_0	Stress path	CSR
TWD-1	0.540	300	-0.112	Constant p' , $\eta_{cyc} = +1.4 \sim -0.7$	-
TWD-2	0.581	100	-0.098	Constant p' , $\eta_{cyc} = +1.4 \sim -0.7$	-
TWD-3	0.711	300	0.060	Constant p' , $\eta_{cyc} = +0.6 \sim -0.45$	-
TWD-4	0.570	100	-0.109	Constant p' , deviatoric stress amplitude increased with cyclic loading	-
TWU-5	0.712	300	0.060	Constant σ_3 , $q_{cyc} = -75 \sim +80$ kPa	0.26
TWU-6	0.711	300	0.060	Constant σ_3 , $q_{cyc} = -60 \sim +60$ kPa	0.2
TWDS-7	0.500	300	-0.152	Constant p' , $\eta_{cyc} = +1.5 \sim -0.7$	-
TWDS-8	0.530	100	-0.149	including small unloading and reloading loops	-

Notes:

TWD = Two-way drained loading with constant mean effective stress

TWU = Two-way undrained loading

TWDS = Two-way drained loading with small cyclic loops

Figure 5-5 shows the intended stress paths for all the drained tests (TWD-1~4 and TWDS-7~8). The path OA indicates the stage of isotropic consolidation. After consolidation, cyclic shearing was started while keeping the mean effective stress constant. The path BC is the direction that cyclic shear stress was applied. Tests TWD-1, 2 and 3 maintained constant shear stress amplitude, whilst in test TWD-4, the shear stress amplitude was increased with cycles. After 7–8 cyclic loadings, the specimens were subjected to monotonic loading in compression until the critical states was reached.

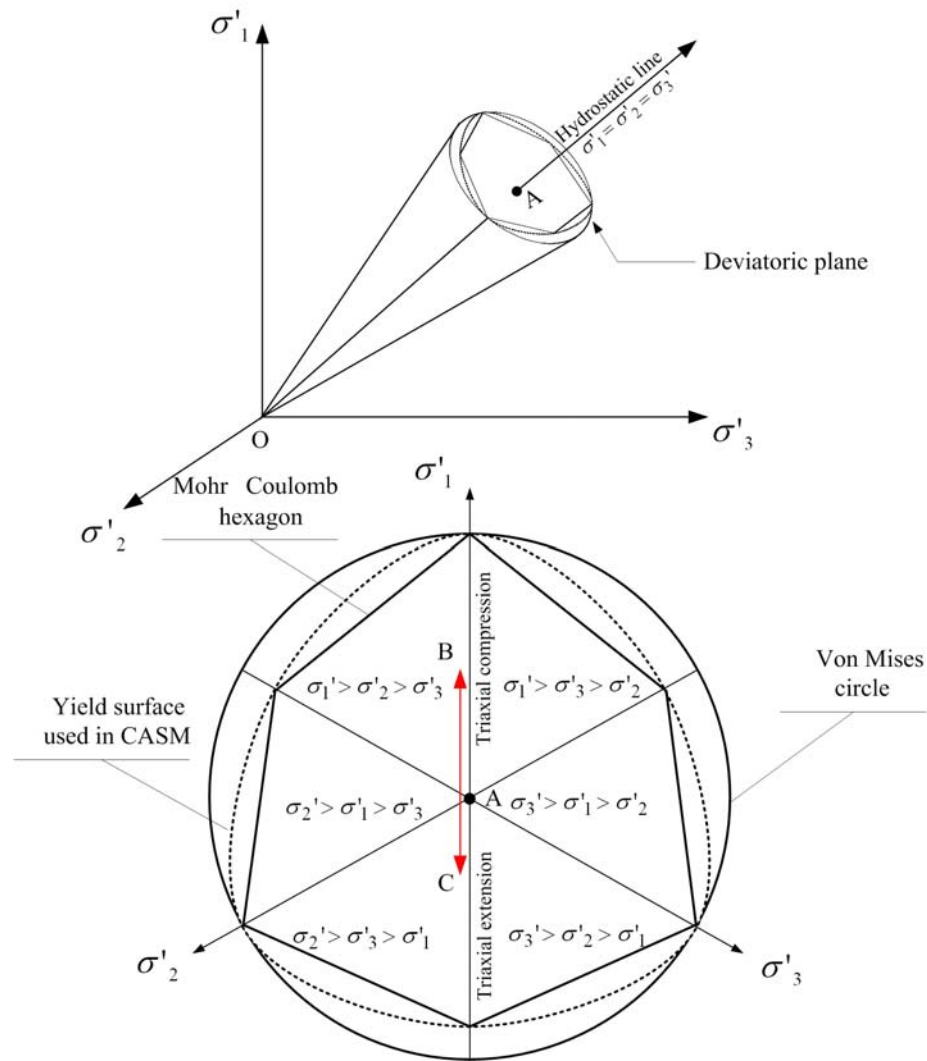


Figure 5-5. The deviatoric-plane view of the applied stress paths for tests TWD-1-4.

Specimens TWU-5 and TWU-6, with the same initial density, were isotropically consolidated on to the *RCL* with $p'_0 = 300$ kPa. Two different cyclic shear stress amplitudes were then applied, while maintaining constant confining pressure until liquefaction occurred.

The elastic behaviour of Portaway sand under various stress states were evaluated in tests TWDS-7 and TWDS-8, which includes five small loops of unloading and reloading. The differences in the measurements obtained from the external LVDT and internal Hall effect transducers were assessed.

5.4.1 Drained Tests (TWD-1~4)

The actual stress paths that the specimens followed are plotted in Figure 5-6. The solid and dotted lines are failure lines and *CSLs* determined from monotonic loading tests, respectively. It is clear that constant mean effective stresses were maintained throughout the cyclic loadings.

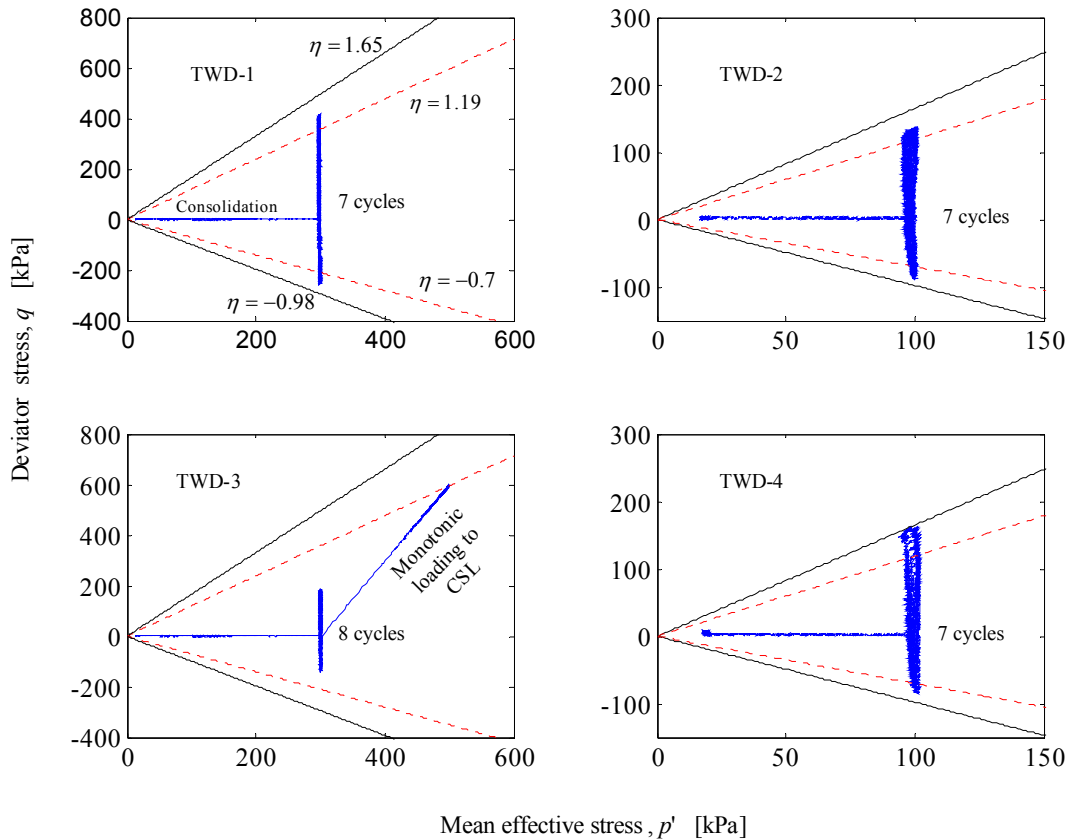


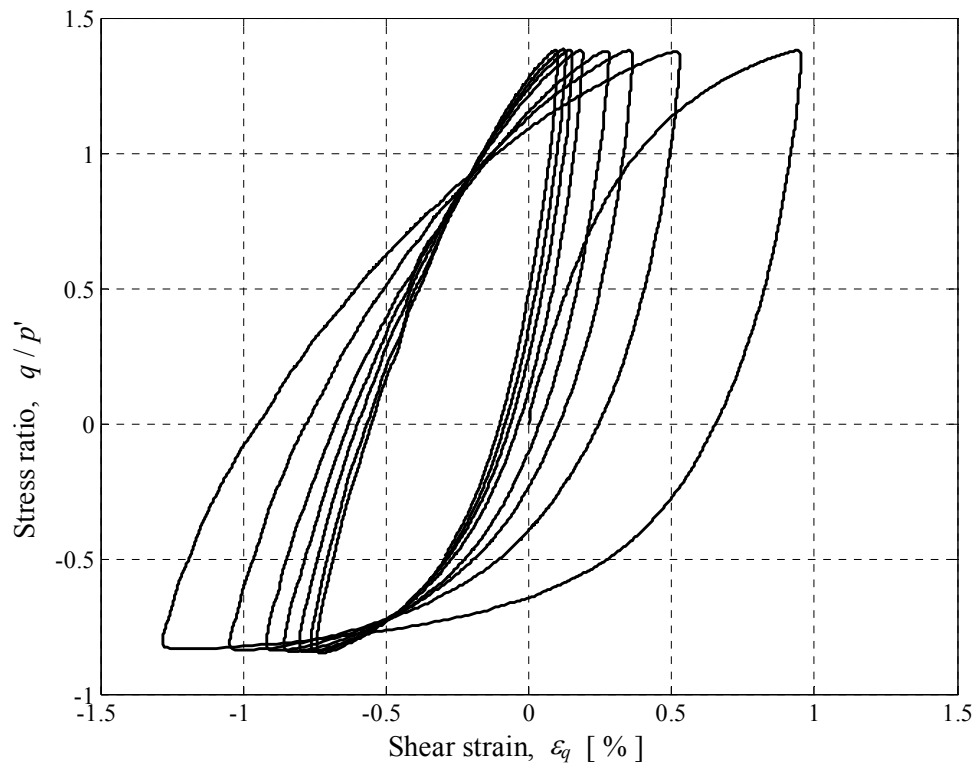
Figure 5-6. Applied stress paths in the p' - q stress space (TWD-1~4).

In this group of tests, the magnitude of the induced cyclic shear strains are around $\pm 1.5\%$. After cyclic loading, all specimens were loaded monotonically to the critical states under a constant mean effective stress path (TWD-1, 2 and 4) or constant effective radial stress path (TWD-3).

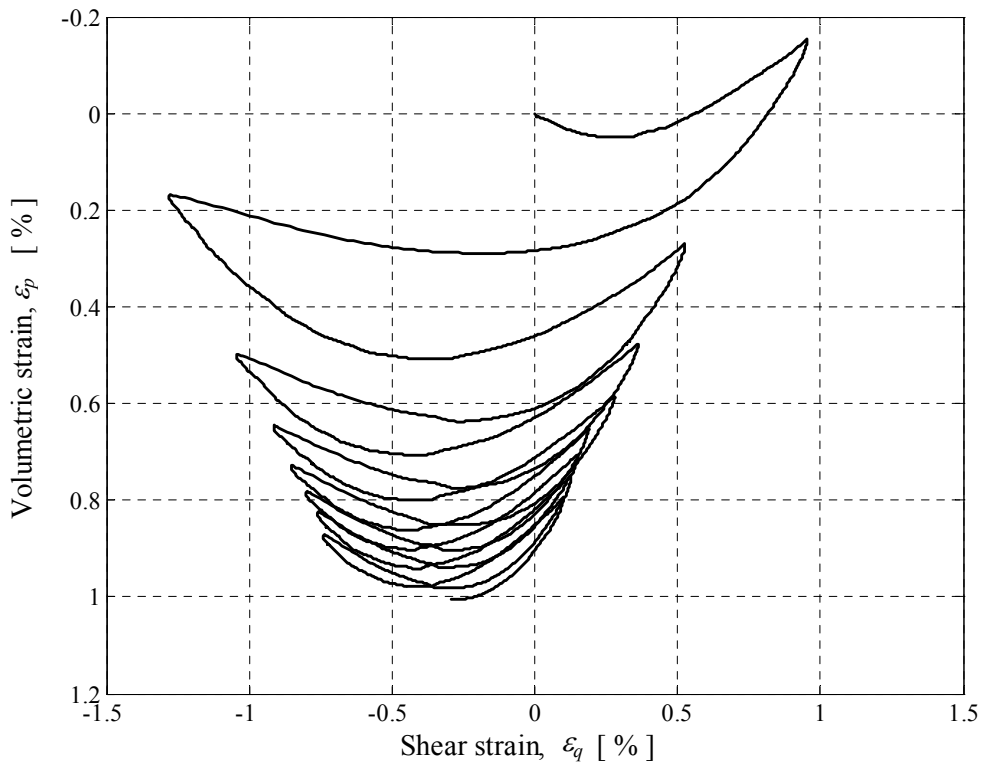
Plotted in Figure 5-7 and Figure 5-8 are the stress-strain relationships of the two drained tests TWD-1 and TWD-3 with constant shear stress amplitude ($\xi_0 = -0.112$ and $\xi_0 = 0.06$, respectively). It can be seen that stress-strain

hysteretic loops of the specimens become smaller with increasing number of loading cycles, although with different initial state parameters. The volumetric contractions initiated immediately after imposing the shear stresses, while the overall pattern of the curves is strongly dependent on the initial conditions of the specimens. The widths of the hysteretic loops are decreasing continuously, which might be attributed to the densification of the specimens during cyclic loadings. The typical behaviour of Portaway sand, subjected to incremental cyclic shear stress, is shown in Figure 5-9.

Figure 5-10 shows the behaviour of Portaway sand (TWD-1) under cyclic loading and then loaded to the critical state monotonically. In order to see the effect of pre-cyclic loading on the sand behaviour, a comparison was made between the tests TWD-1 and CIDCP-1 with essentially the same initial state parameter ($\xi_0 = -0.112$ and $\xi_0 = -0.119$, respectively). It can be seen from Figure 5-10 that test TWD-1 reached a higher stress ratio at peak strength, but the difference of the mobilised strengths between the two specimens became smaller during the softening stage. Finally, they showed the same shear strength after reaching 8% axial strain.



(a)



(b)

Figure 5-7. Two-way drained cyclic loading ($\xi_0 = -0.112$, constant $p' = 300$ kPa, TWD-1).

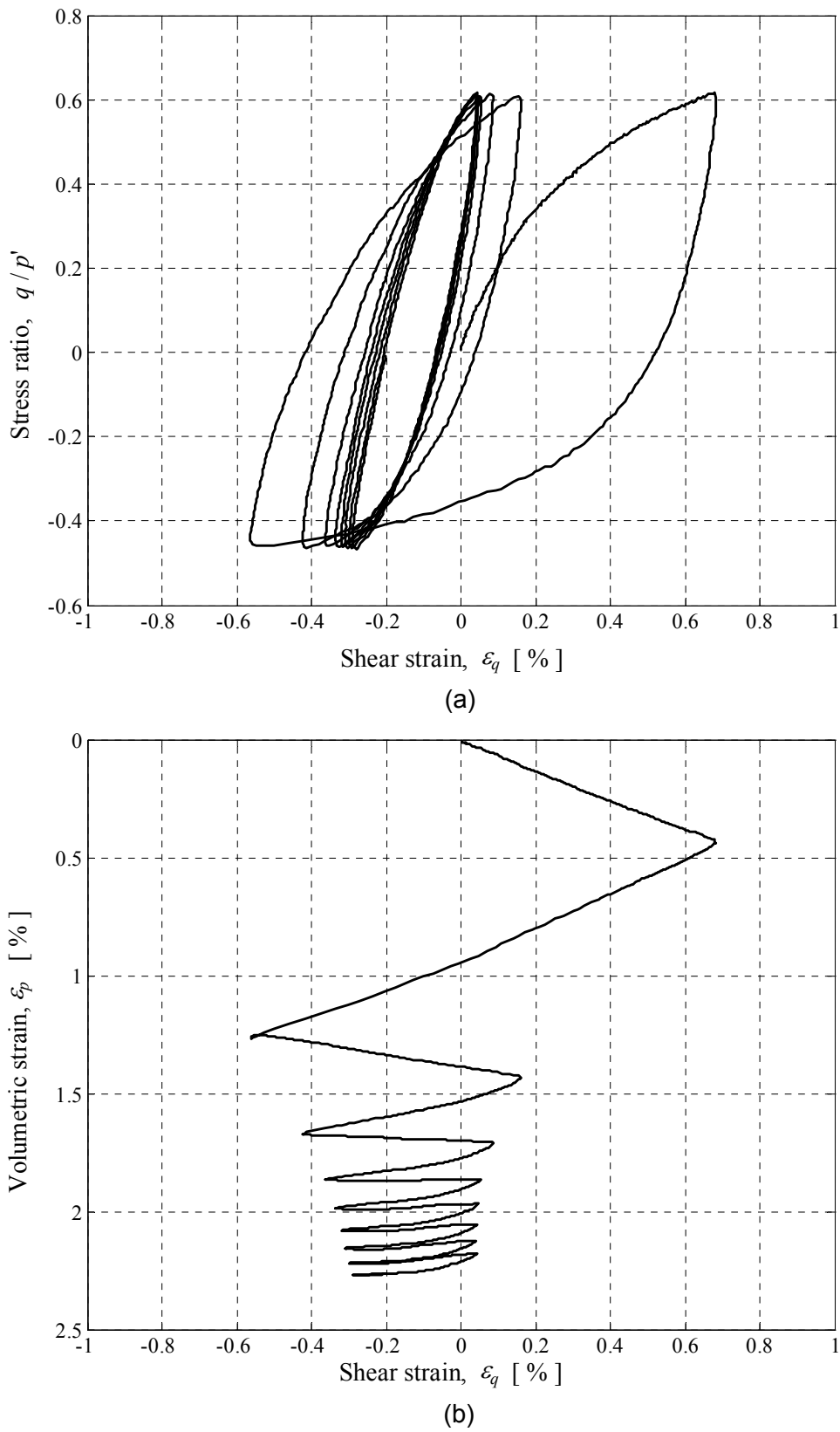


Figure 5-8. Two-way drained cyclic loading ($\xi_0=0.060$, constant $p'=300$ kPa, TWD-3).

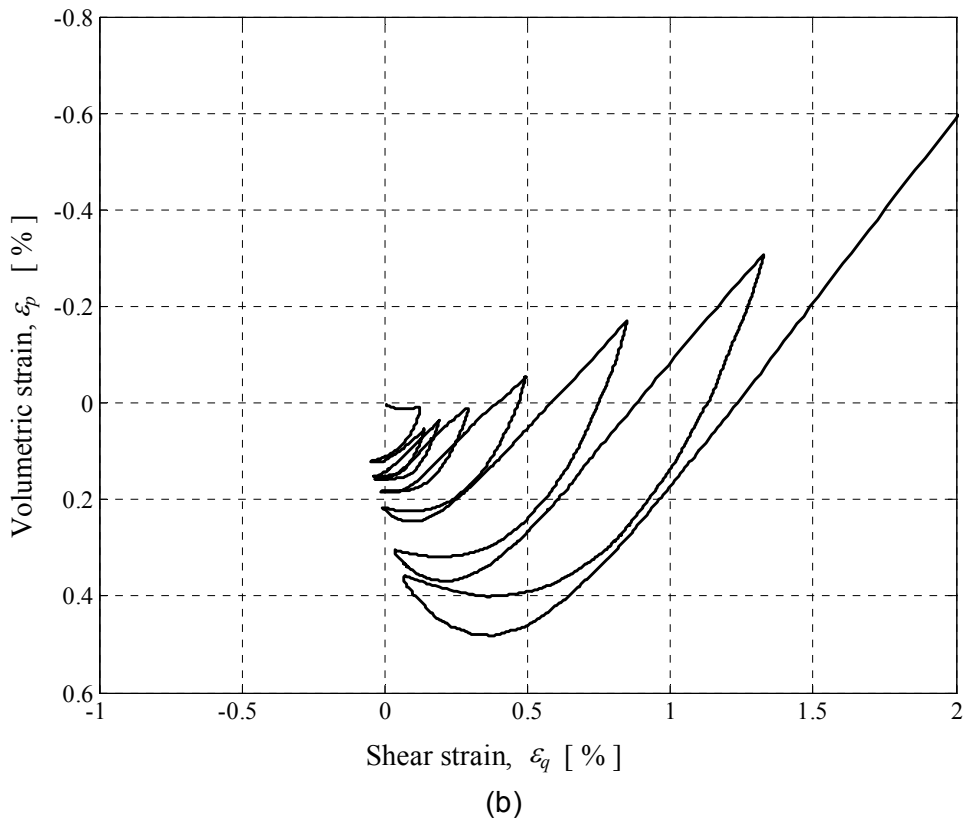
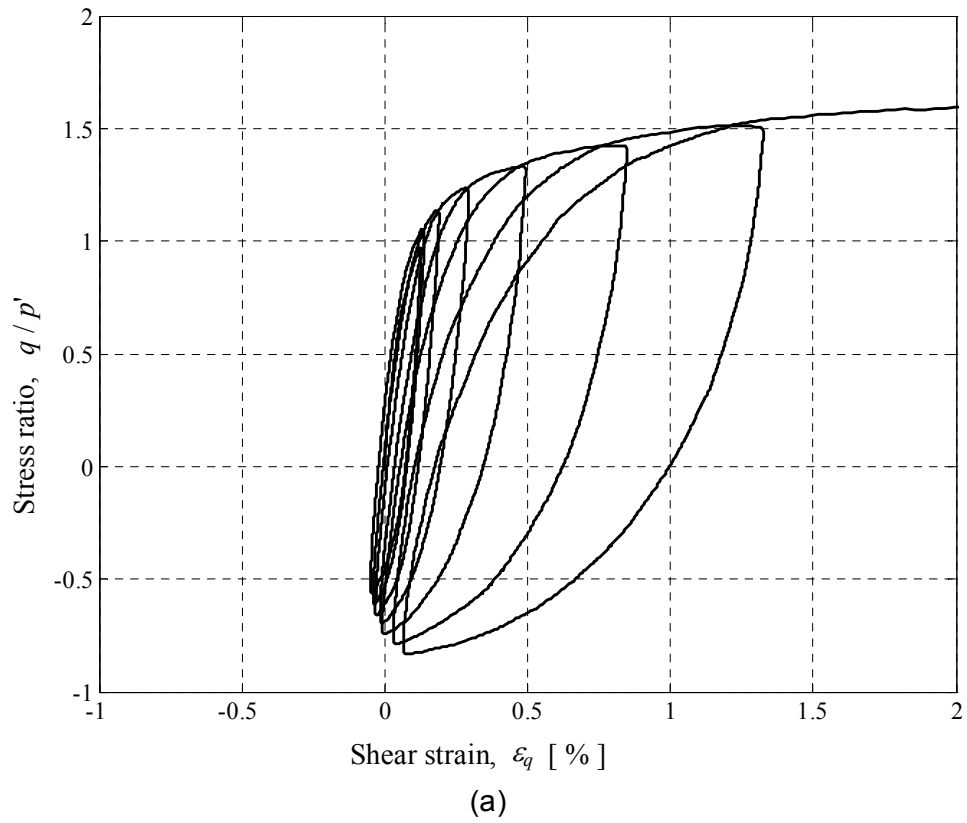


Figure 5-9. Two-way drained cyclic loading ($\xi_0 = -0.109$, constant $p' = 100$ kPa, TWD-4).

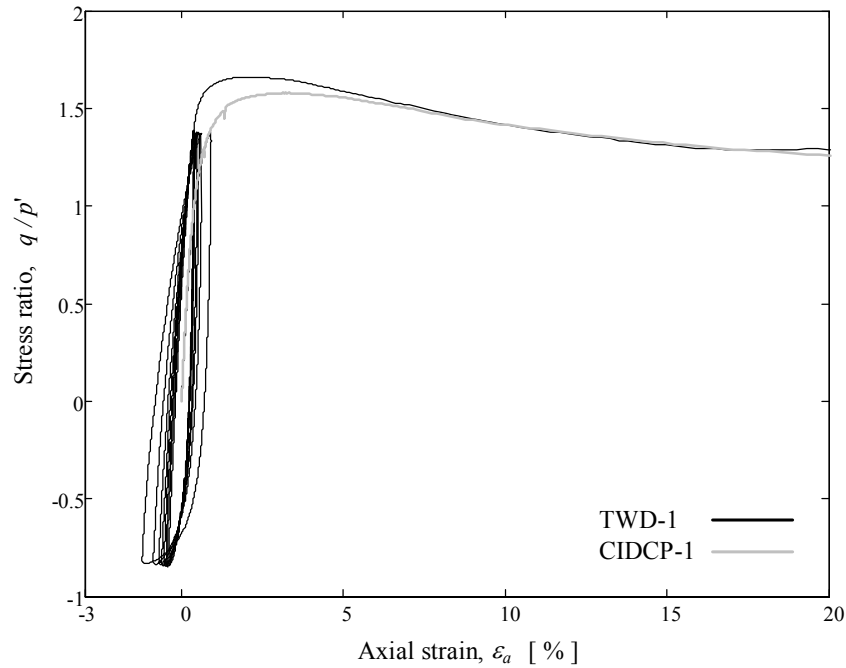


Figure 5-10. Comparison of strength characteristics ($\xi_0 = -0.112$, TWD-1; $\xi_0 = -0.119$, CIDCP-1).

Pradhan et al. (1989) have investigated the stress-dilatancy relations of Toyoura sand systematically using cyclic triaxial apparatus and cyclic torsional shear apparatus. Similar results were obtained on Portaway sand as seen in Figure 5-11. It is observed that by reversing the direction of loading, two slightly curved stress-dilatancy relations exist. The rate of dilatancy changes discontinuously when the loading direction is changed. The modified Rowe's relations proposed by Pradhan and Tatsuoka (1989) are shown as solid lines.

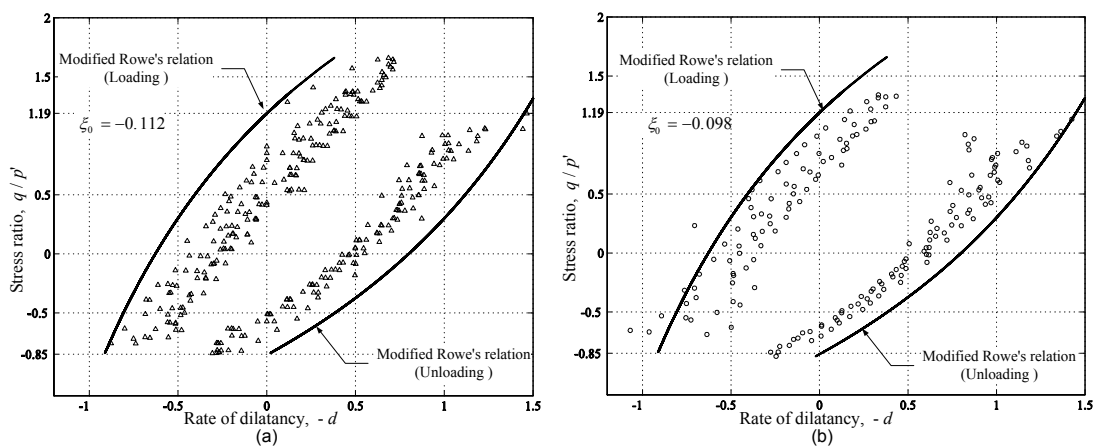


Figure 5-11. Stress-dilatancy relations of two-way cyclic loading (TWD-1 and TWD-2).

5.4.2 Undrained Tests (TWU-5 and TWU-6)

Plotted in Figure 5-12 and Figure 5-13 are the results obtained from two-way cyclic undrained loading on two specimens TWU-5 and TWU-6.

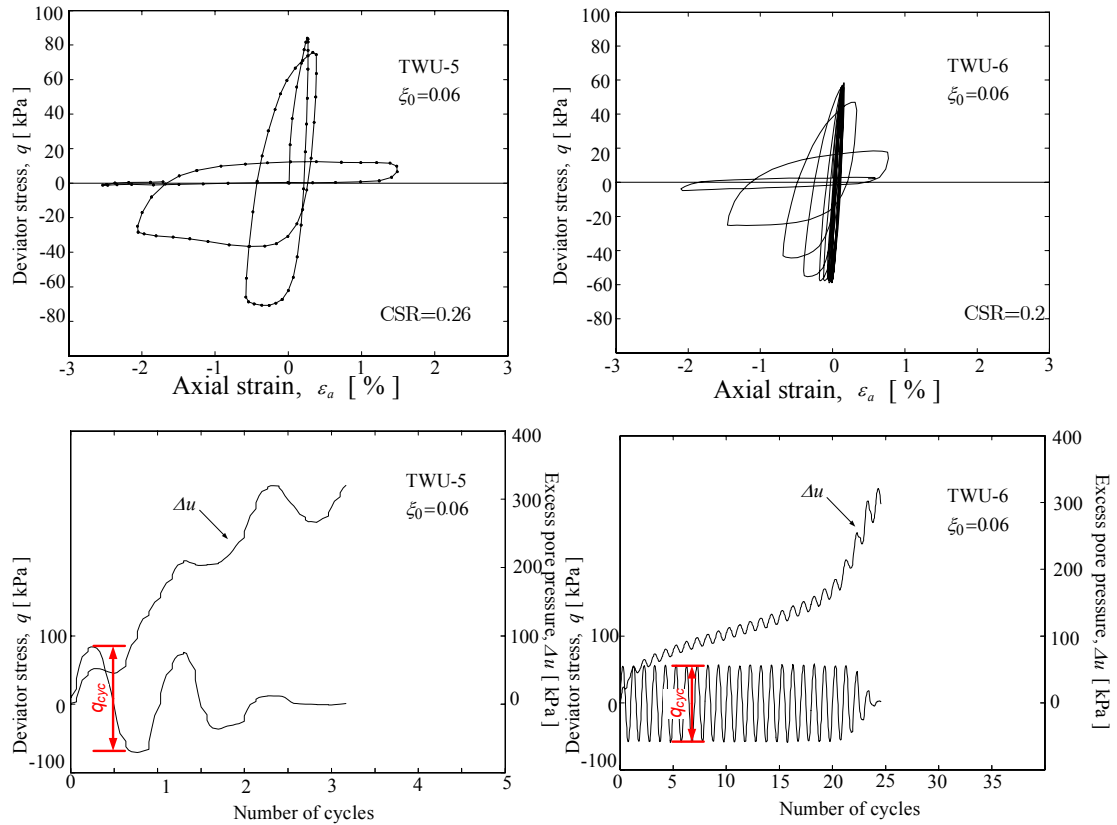


Figure 5-12. Two-way undrained cyclic loading (A) ($\xi_0 = 0.06$, TWU-5; $\xi_0 = 0.06$, TWU-6).

It can be seen that with a slightly higher value of CSR (TWU-5: $CSR = 0.26$ and TWU-6: $CSR = 0.2$), the generation of excess pore pressure is much faster in test TWU-5 than in test TWU-6. Test TWU-5 reached liquefied state only after two cycles. In contrast, the excess pore pressure of test TWU-6 built up steadily and the liquefaction was initiated after 20 cycles. The cyclic strength of Portaway sand can be represented as $0.2 < \left[q_{cyc} / (2\sigma'_0) \right]_{20} < 0.26$ with a void ratio equal to 0.711 in the two-way test.

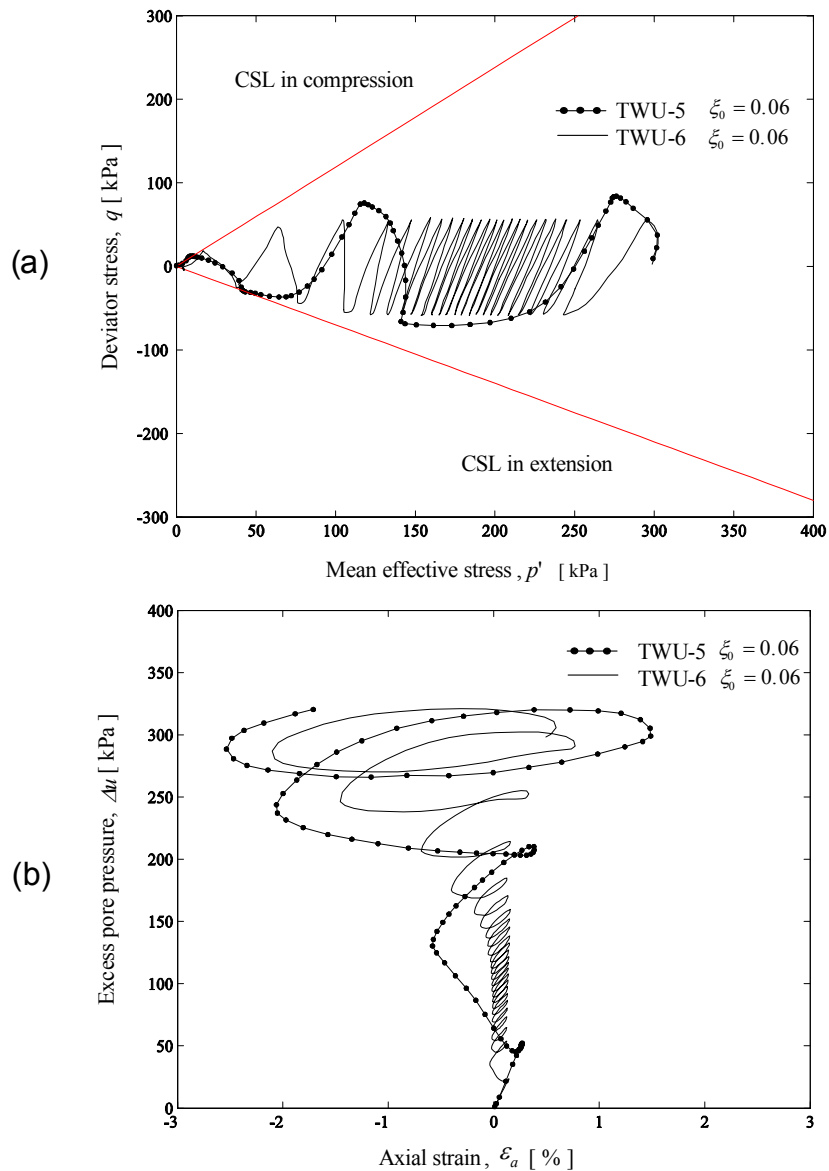


Figure 5-13. Two-way undrained cyclic loading (B) ($\xi_0 = 0.06$, TWU-5; $\xi_0 = 0.06$, TWU-6).

5.4.3 Drained Tests with Small Cyclic Loops (TWDS-7 and TWDS-8)

The performances of small strain behaviour under monotonic loading condition have been evaluated in the previous chapter. Monitoring small strain behaviour, however, is more difficult in cyclic loading than in monotonic loading. As found by Raybould (1992), the displacement recorded by the internal measuring device was sometimes incorrect due to various reasons, including friction and the attaching method. The method of attachment used for the Hall effect transducers in this

study is the so-called ‘glue-on’ technique. Therefore, the major concern is whether relative movement between the Hall effect transducers and the specimen would occur during cyclic loading.

Figure 5-14 compares the stress-strain curves of test TWDS-7 recorded by both the external LVDT and the Hall effect transducers. As expected, the stiffness obtained from the external LVDT is lower due to the bedding error and the system compliance. It is noted though that the shapes of two curves are very similar and there is no sign to indicate that unreliable measurements were recorded with the Hall effect transducers.

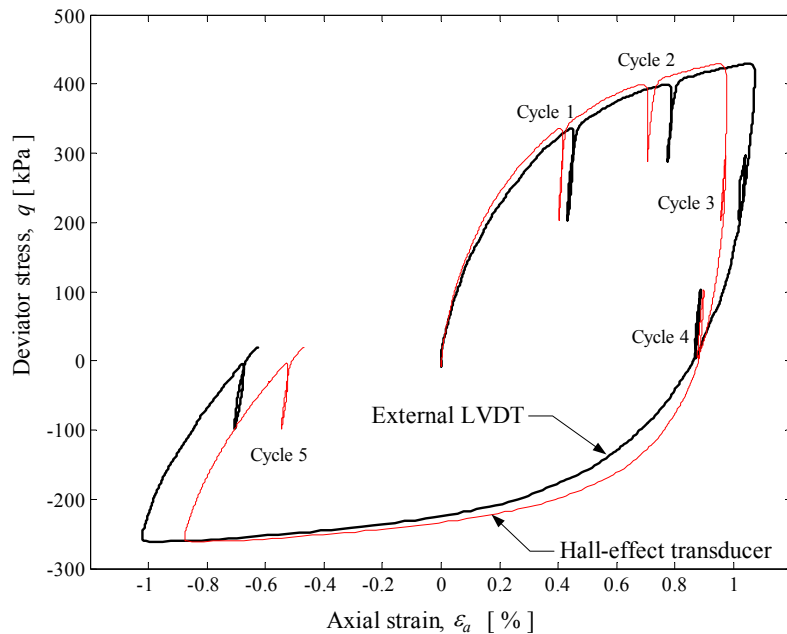


Figure 5-14. Comparison of external and internal measurements (TWDS-7).

5.5 MOVING WHEEL LOADING

The cyclic stress paths used in characterising the behaviour of Portaway sand subjected to moving wheel load were of three types. The testing program adopted in this series of tests was similar to those used by Mcvay and Taesiri (1985). The

first stress path BC, commonly used in characterising resilient modulus is shown in Figure 2-15 (c). The tests with this kind of stress path have been investigated using one-way drained cyclic loading in compression tests (OWDC-1–4). Another two stress paths BC and BCD were performed on tests MW-1 and MW-2, respectively, which involved a 90° jump rotation of principal stress. In order to investigate the effect of stress paths on the behaviour of Portaway sand, path CD in the p' – q space was kept the same for all three tests. After five cycles, the resilient modulus were measured. The detailed information of the tests is summarised in Table 5-3 together with a test OWDC-4 selected from the one-way cyclic loading series.

Table 5-3. Summary of moving wheel loading program.

Test ID	e_0	p'_0 (kPa)	ξ_0	q_{cyc} (kPa)	Stress path	M_r (MPa)
OWDC-4	0.518	100	-0.161	$q_{cyc} = 0 \sim +145$	CD	145
MW-1	0.520	100	-0.159	$q_{cyc} = -10 \sim +145$	BCD	132
MW-2	0.519	100	-0.160	$q_{cyc} = -20 \sim +145$	ABCD	88

Notes: M_r = Resilient modulus measured at 5th cycle
 Stress path: see Figure 2-15 (c)

Figure 5-15 shows the cyclic deviatoric stress, the effective confining pressure and the actual stress path followed in test MW-2. The stress-strain relationships of three tests are shown in Figure 5-16, Figure 5-17 and Figure 5-18, respectively. It is evident that the cyclic hysteretic loops were much stiffer in test OWDC-4 with less permanent strain build up. A large permanent deformation was developed in test MW-2 and the resilient modulus M_r was only 88 MPa on the 5th cycle. The results agree with the conclusions drawn by Mcvay and Taesiri (1985) that:

- Excursions of applied loads from extension into compression stress space will result in material anisotropy.
- The anisotropy produced greater cyclic permanent strain build-up and a lower resilient modulus in the test with stress path ABCD than one with stress path CD.

In addition, the current testing program revealed that the effect of anisotropy has much more influence on test MW-2 than test MW-1. Therefore, it implies that the conventional method of characterising resilient and permanent behaviour, such as in pavement engineering, may give unsafe results using stress path CD or BCD.

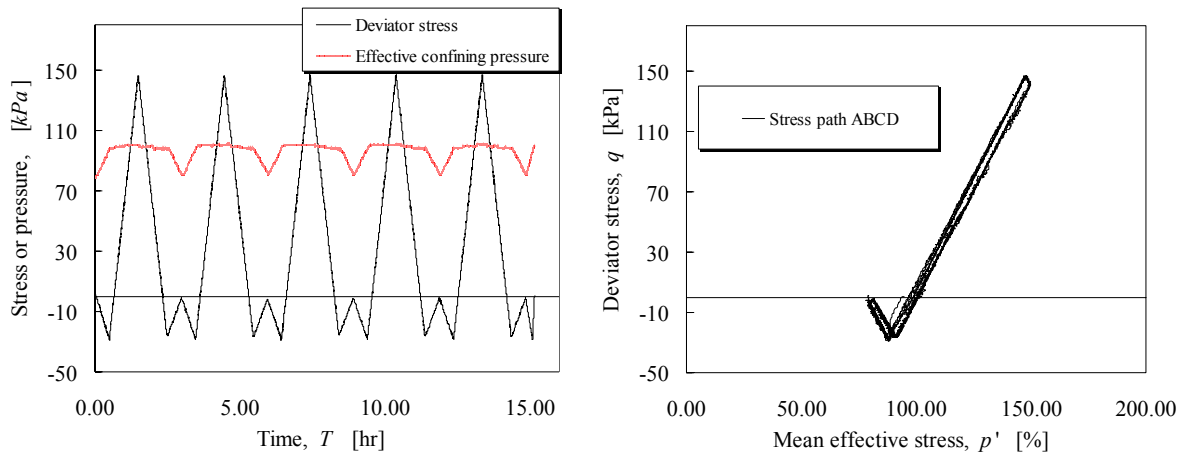


Figure 5-15. Cyclic deviatoric stress, effective confining stress and moving wheel loading stress path (MV-2).

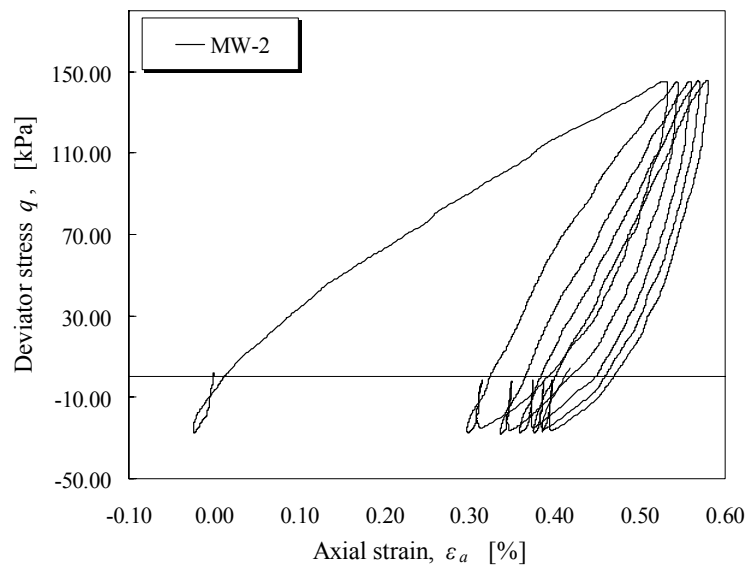


Figure 5-16. Stress-strain curve of moving wheel loading path ABCD (MW-2).

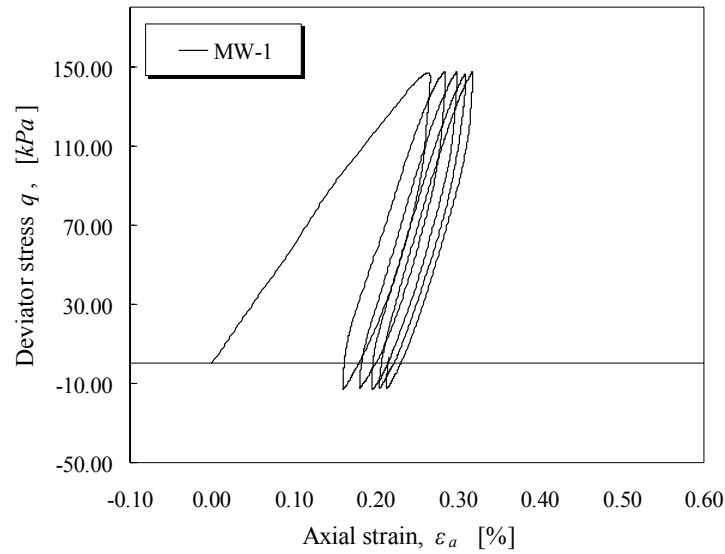


Figure 5-17. Stress-strain curve of moving wheel loading path BCD (MW-1).

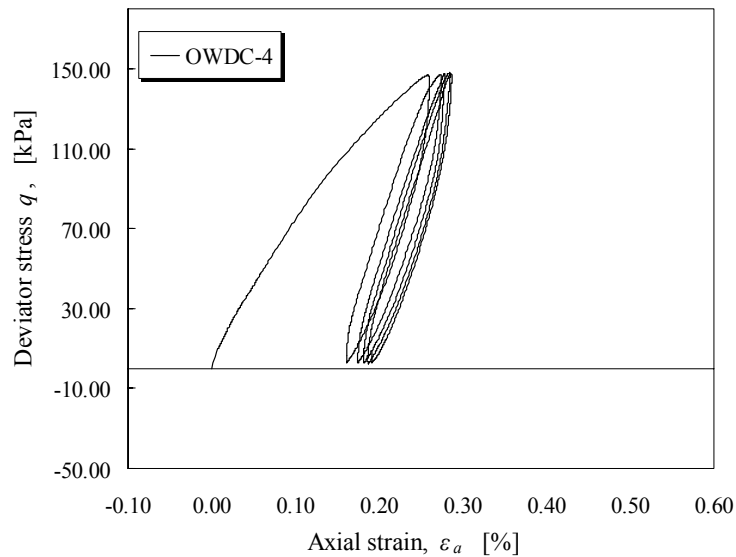


Figure 5-18. Stress-strain curve of moving wheel loading path CD (OWDC-4).

5.6 INTERPRETATION AND DISCUSSION

The direct experimental observations presented so far have indicated that there are some correlations between monotonic loading and cyclic loading behaviours. It is important that these results are interpreted within an appropriate theoretical

framework. It has been demonstrated in Chapter 4 that the monotonic behaviour of Portaway sand is controlled by the state parameter prior to the achievement of the critical state. As with CASM, the new cyclic bounding surface cyclic model CASM-c was formulated in terms of the state parameter concept. Therefore, it is interesting to see the effect of the state parameter on Portaway sand under cyclic loading. In the following sections, some aspects of the stress-strain and strength characteristics of Portaway sand are interpreted within the state parameter concept.

5.6.1 Stress Ratio – State Parameter Relation

Figure 5-19 through to Figure 5-23 compare the stress-state relations between cyclic loading and monotonic loading conditions. It can be seen that the stress paths of monotonic tests in compression and extension form a boundary surface that contains cyclic loading paths. The state boundary surface in compression has been defined in equation (4-16).

Figure 5-19 shows that drained loading paths always travel along (or close to) the state boundary surface after the initial cyclic loadings. This implies that the effect of cyclic loading diminishes with increases of strain in drained conditions. In contrast, the behaviour of undrained cyclic loading depends strongly on the type of loading. Presented in Figure 5-20 is the stress-state relation of test OWUC-5 together with the flow liquefaction line obtained for Portaway sand in compression discussed in section 4.4.3. It is evident that the behaviour of the specimen becomes unstable when the cyclic loading path reaches the flow liquefaction line. After this line, the peak points for each cycle follow the boundary surface defined by test CIUC-1. Test OWUE-6, however, indicates that cyclic loading in extension was more critical than in compression as shown in Figure 5-21. The stress paths for two-way undrained tests are illustrated in Figure 5-22 and Figure 5-23.

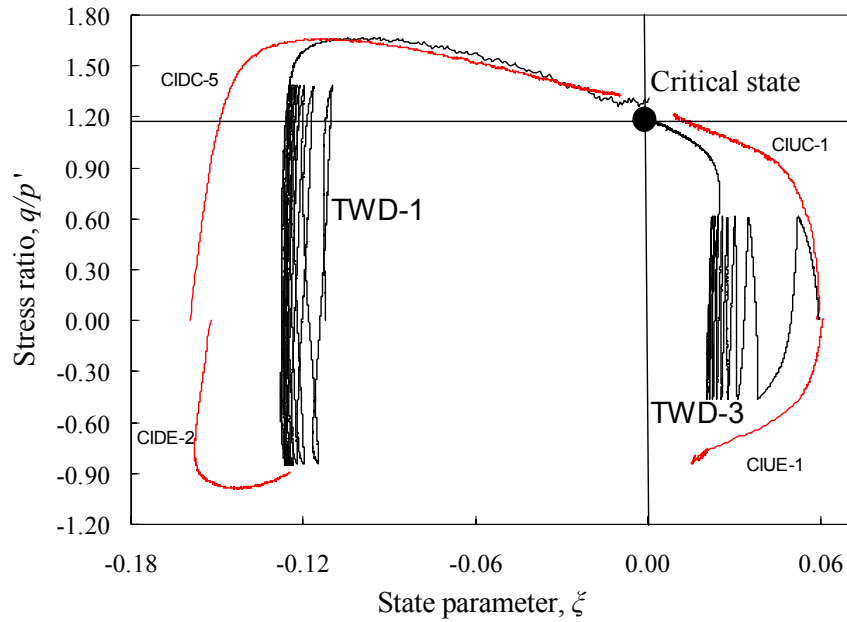


Figure 5-19. Stress ratio-state parameter relations (TWD-1 and TWD-3).

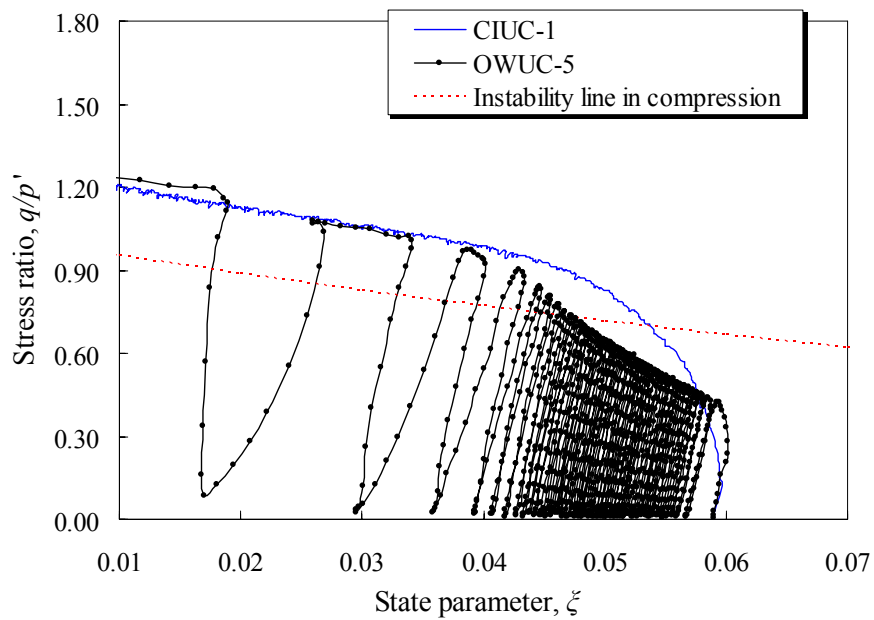


Figure 5-20. Stress ratio-state parameter relations (OWUC-5 and CIUC-1).

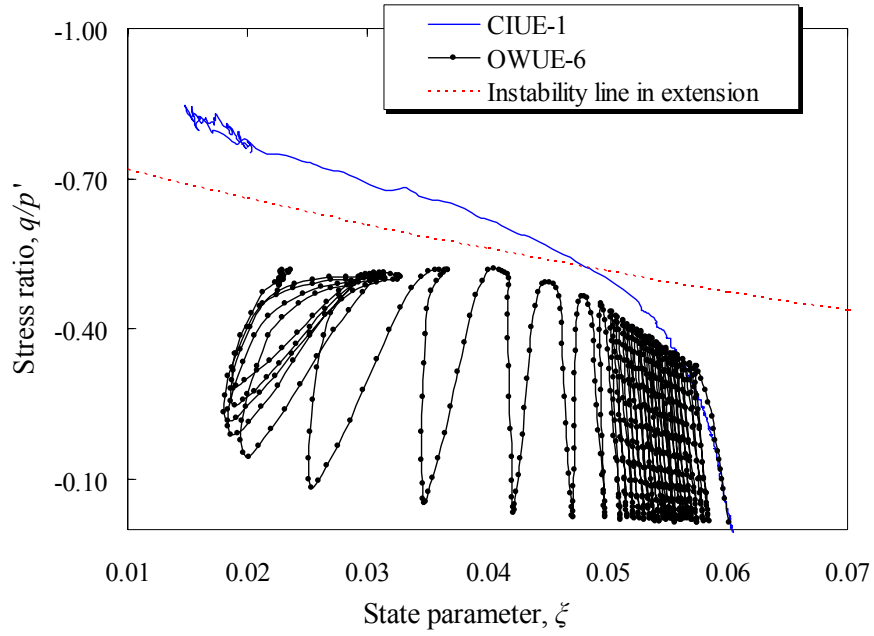


Figure 5-21. Stress ratio-state parameter relations (OWUE-6 and CIUE-1).

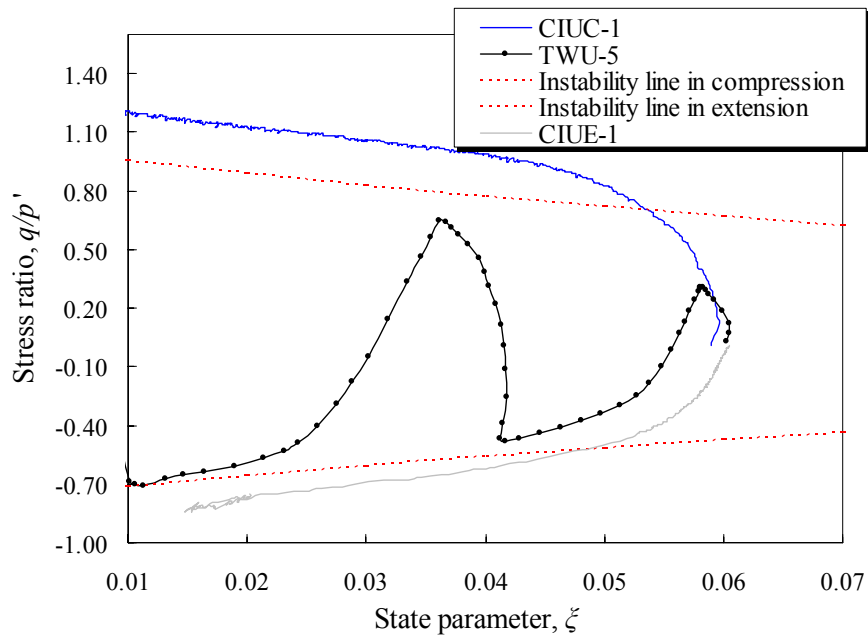


Figure 5-22. Stress ratio-state parameter relations (TWU-5, CIUC-1 and CIUE-1).

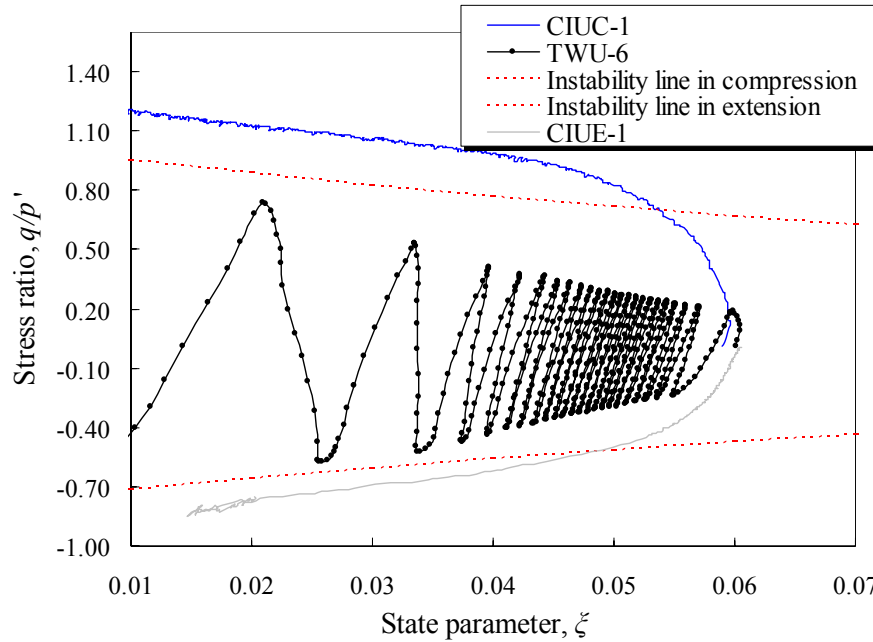


Figure 5-23. Stress ratio-state parameter relations (TWU-6, CIUC-1 and CIUE-1).

5.6.2 Shear Strength – State Parameter Relation

5.6.2.1 Drained shear strength

The critical state friction angles determined from drained and undrained monotonic tests are about 29.8° and 24.5° in compression and extension, respectively. The experimental results from combined cyclic and monotonic loading show that the loading paths have no significant effect on the critical state friction angles. It is evident, however, that the value of the peak friction angle is stress path dependent for dense sands. For example, Figure 5-10 shows that the cyclic test TWD-1 reached much higher peak strength than the monotonic test CIDCP-1, although the two specimens have essentially the same initial state parameters ($\xi_0 = -0.112$ and $\xi_0 = -0.119$, respectively). This is attributed to the continuing densification of the specimen in test TWD-1 during two-way cyclic loading. Its state parameter was about -0.128 after 7 cycles as can be seen in Figure 5-19.

The experimental correlations between the various strength properties of sands and the initial state parameter have been investigated by Been and Jefferies (1985). Following their work, Collins et al. (1992) and Yu (1994) proposed various plasticity models, in which the angle $\phi_m - \phi_c$ was assumed to be an exponential function of the state parameter as follows:

$$\phi_m - \phi_c = A[\exp(-\xi) - 1] \quad (5-2)$$

where ϕ_m is the mobilised friction angle, ϕ_c is the critical state friction angle and A is a curve-fitting parameter, which ranges from 0.6 to 0.95 depending on the type of sand. Note that angles ϕ_m and ϕ_c expressed in radians. According to equation (2-12) proposed by Bolton (1986), the mobilised dilation angle ψ_m can be expressed as a function of the state parameter using:

$$\psi_m = 1.25(\phi_m - \phi_c) = 1.25A[\exp(-\xi) - 1] \quad (5-3)$$

The above equations implies a non-associated flow rule, because the angles of friction and dilation are not the same. Figure 5-24 shows a comparison of the measured peak friction angles of Portaway sand and those estimated from equation (5-2). The value of parameter A was calibrated as 1.1 using a critical state friction angle equal to 29.8° , which is slightly higher than the value suggested by Yu (1994) (which ranges from 0.65 to 0.95). It is believed that this may be due to the occurrence of strain localisation at large strains in the specimens.

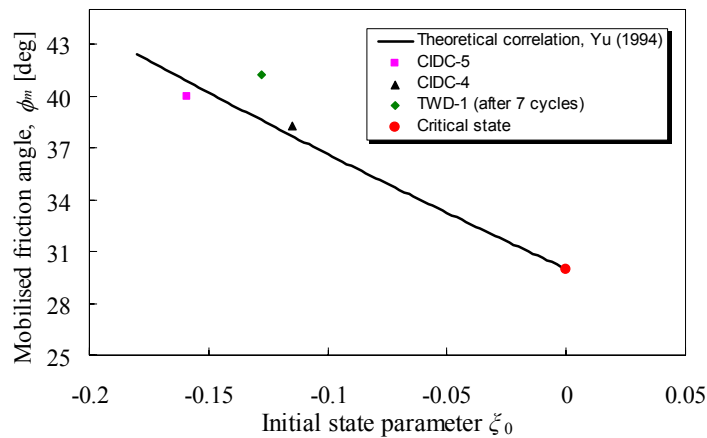


Figure 5-24. Predicted and measured peak friction angles on dense sands.

5.6.2.2 Undrained cyclic shear strength

Figure 5-25 compares the curves of axial strains versus number of cycles for three tests carried out under various loading paths. For comparison purposes, the same initial conditions of the three specimens were set up ($\xi_0 = 0.06$). Tests OWUC-5 and TWU-6 have the same cyclic stress ratio ($CSR = 0.2$) while test OWUE-6 has a slightly lower value ($CSR = 0.15$). It is clear that the cyclic strength of Portaway sand is stress path dependent. The test OWUC-5 has highest cyclic shear strength ($\left[q_{cyc} / (2\sigma'_0) \right]_{20} > 0.2$), whilst OWUE-6 shows lowest cyclic shear strength ($\left[q_{cyc} / (2\sigma'_0) \right]_{20} = 0.15$). These results are consistent with the conclusion drawn previously from undrained monotonic loading tests that the behaviour of Portaway sand is weaker in extension than in compression. Vaid et al. (1990) have investigated the effect of the stress path on the *SSL* of a liquefiable sand under monotonic loading. The explanation of this behaviour was given in terms of inherent and induced anisotropy. The former is defined as the physical characteristic, inherent in the material before any deformations are imposed, and is caused mainly by the specimen preparation method. The latter is associated with the principal stress rotation. In triaxial testing, induced anisotropy can be produced in two-way cyclic loading with a 90° jump rotation of the principal stress from extension to compression.

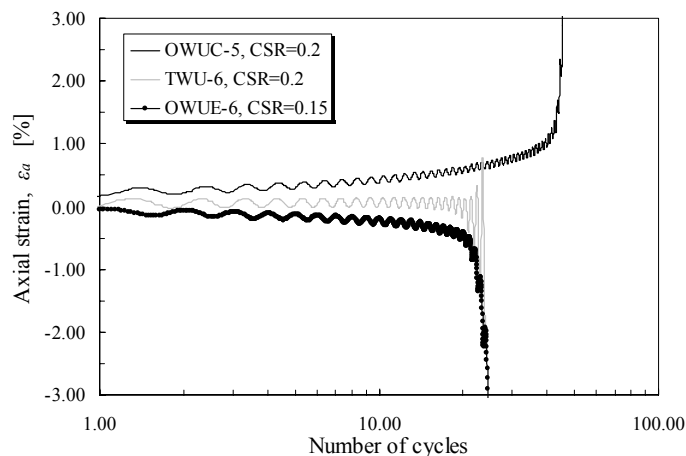


Figure 5-25. Comparison of cyclic shear resistance of Portaway sand under different loading paths ($\xi_0 = 0.060$, OWUC-5, OWUE-6 and TWU-6).

5.6.3 Volumetric Strain – State Parameter Relation

Plotted in Figure 5-26 is the volumetric strain-state parameter response of Portaway sand under drained monotonic loading (CIDC-1~5) and cyclic loading (TWD-1) conditions. It is interesting to note that the plots of volumetric strain against state parameter may be regarded as a series of straight lines with the same slope. It is clear that a correlation exists between the two variables. For the data analysed, a linear function, as suggested below, can be used to describe the relationship between ε_p and ξ reasonably well for Portaway sand:

$$\varepsilon_p = \Omega\xi + \Pi \quad (5-4)$$

where Ω is the slope of the line, which has a negative value, and Π is a constant that depends on the initial state parameter ξ_0 and the stress path. An appropriate value for Ω is found to be -65 in this study and can be expressed as:

$$\Omega = \frac{\delta\varepsilon_p}{\delta\xi} = -65 \quad (5-5)$$

Equation (5-4) suggests that the development of the volumetric strain is directly controlled by the state parameter. This finding supports the assumption made in CASM and its extensions.

It is well known that dilatancy is a key issue in constitutive modelling of sand behaviour. Figure 5-27 presents the relationship between the dilatancy rate d and the normalised state parameter ξ/ξ_R . It is clear from the figure that a state boundary surface of Portaway sand appears and its theoretical relation is derived here.

Since Rowe's stress-dilatancy relation (Rowe, 1962):

$$d = \frac{\delta\varepsilon_p^p}{\delta\varepsilon_q^p} = \frac{9(M - \eta)}{9 + 3M - 2M\eta} \quad (5-6)$$

Substituting the above equation into Yu's general stress-state relation (Yu, 1998):

$$\left(\frac{\eta}{M}\right)^n = 1 - \frac{\xi}{\xi_R} \quad (5-7)$$

leads to a generalised dilatancy-state relation, which takes the following form:

$$\left(\frac{\frac{9d}{M} + 3d - 9}{2Md - 9}\right)^n = 1 - \frac{\xi}{\xi_R} \quad (5-8)$$

where $M = 1.19$, $n = 3.5$ and $\xi_R = 0.06$ for Portaway sand.

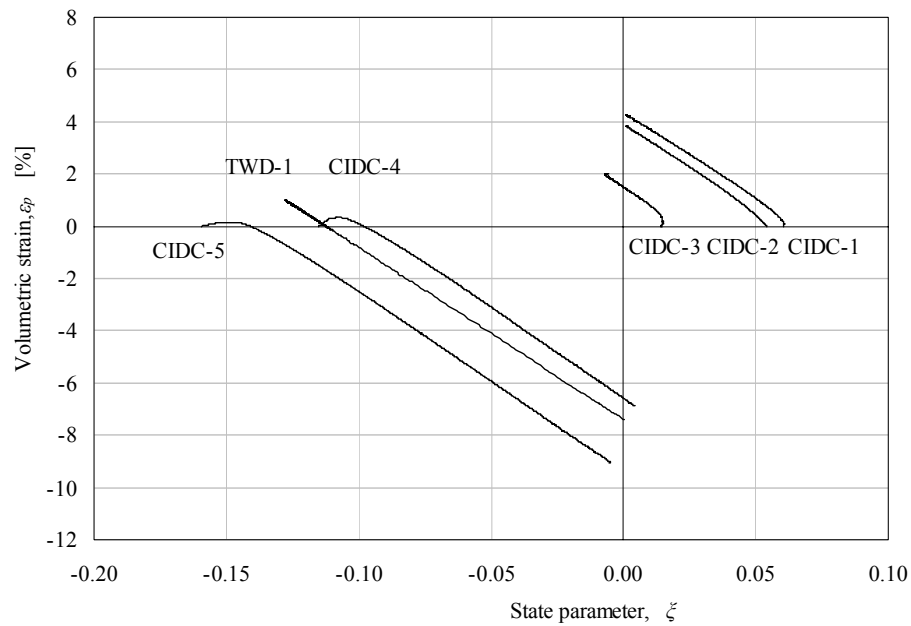


Figure 5-26. Volumetric strain-state parameter relations (CIDC-1-5, TWD-1)

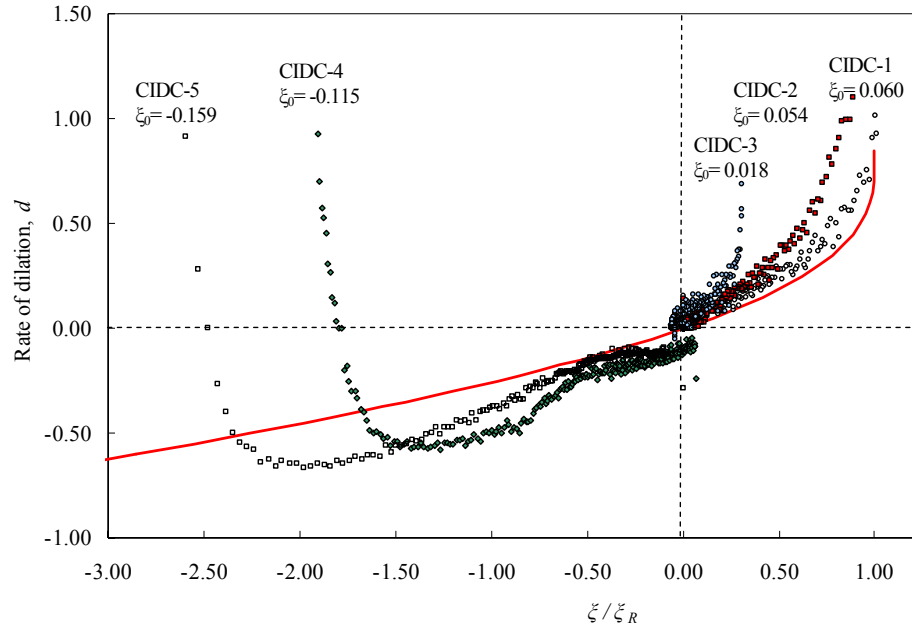


Figure 5-27. Dilatancy-state relations with $\xi_R = 0.06$.

From Figure 5-27, it can be shown that equation (5-8) slightly underestimates the dilatancy rate of the two dense specimens (CIDC-4 and CIDC-5). This may be due to:

- the occurrence of excessive shear band in dense sands as discussed in section 4.3.2;
- the deficiency of the classical Rowe's and Cam-clay's dilatancy relations (Li et al. 1999).

5.6.4 Excess Pore Pressure – State Parameter Relation

It has been shown previously that saturated sands subjected to both monotonic and cyclic undrained loading will experience changes in excess pore pressure Δu . Loose sands normally develop positive pore pressure (e.g. CIUC-1 and TWU-6), whilst medium dense sands develop negative pore pressures (e.g. CIUC-9).

The results of monotonic and cyclic triaxial testing on specimens prepared in a very loose state ($\xi_0 = 0.06$) are presented in Figure 5-28 through to Figure 5-30.

The normalised excess pore pressure is defined as the ratio of the excess pore pressure to the initial effective confining pressure.

A similar tendency in developing excess pore pressure has been observed in different undrained tests with the same initial state parameter. This finding implies that excess pore pressure is also controlled by the state parameter prior to reaching the critical state.

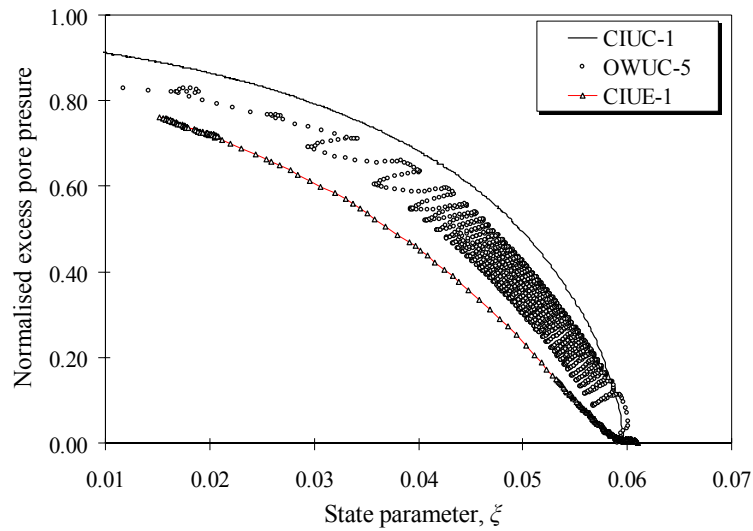


Figure 5-28. Excess pore pressure-state parameter relations (CIUC-1, OWUC-5 and CIUE-1).

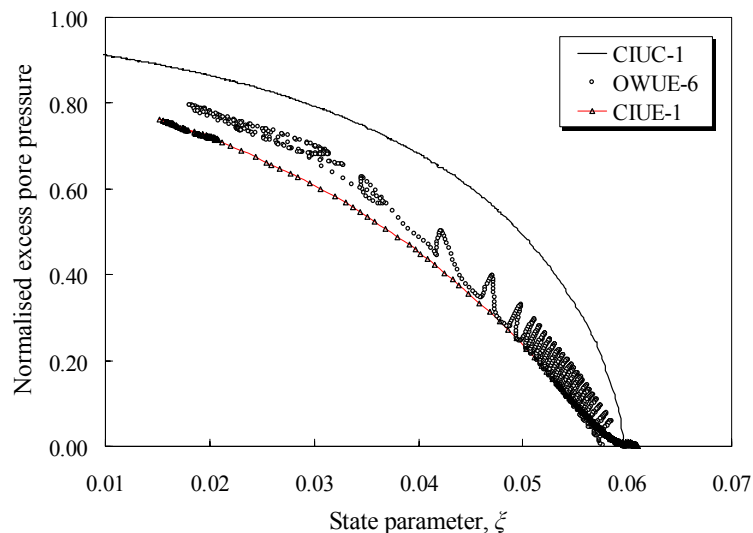


Figure 5-29. Excess pore pressure-state parameter relations (CIUC-1, OWUE-6 and CIUE-1).

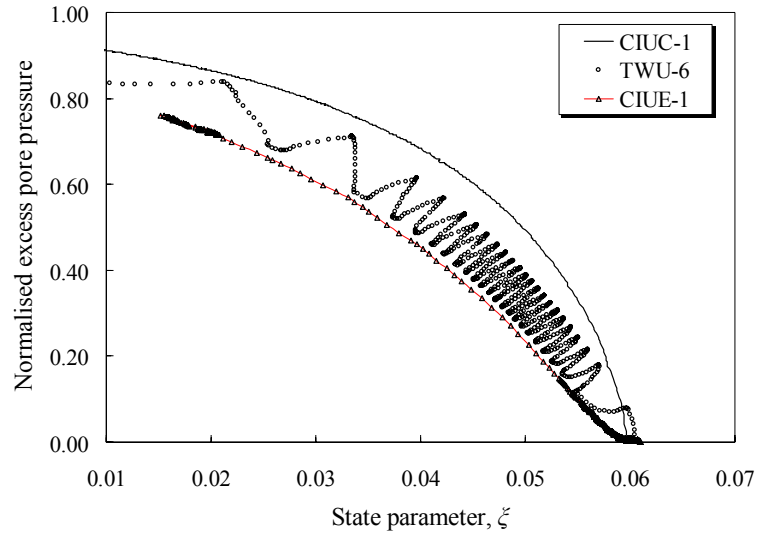


Figure 5-30. Excess pore pressure-state parameter relations (CIUC-1, TWU-6 and CIUE-1).

5.7 SUMMARY

This chapter has presented results from drained and undrained cyclic triaxial tests of sand subjected to various stress paths and initial conditions. It has been shown that the initial state parameter and loading method have significant impacts on the cyclic stress-strain behaviour of Portaway sand. The state boundary surface determined in the monotonic loading tests is also applicable to the cyclic loading condition and there is close correlation between the different loading types in terms of the state parameter. It has also been demonstrated that many aspects of Portaway sand behaviour can be characterised with the state parameter in a unique way to combine the influences of density and stress level.

The results of one-way and two-way cyclic tests indicate that the permanent and the resilient behaviours of Portaway sand are strongly dependent on the stress paths imposed. In drained conditions, conventional resilient modulus tests with only cyclic loading in compression lead to a higher value of stiffness than those that cycle the load in both compression and extension.

Chapter 6

Evaluation and Verification of

CASM and its Extensions

6.1 INTRODUCTION

An experimental investigation into the mechanical behaviour of Portaway sand has been undertaken in the previous chapters. In this chapter, the capabilities of several recently developed plasticity models are evaluated. Despite much of the success in modelling of soils, the following problems of CASM still remain:

- The hardening law used in CASM is of a volumetric strain hardening type. Therefore, CASM assumes that the hardening stops once the *CSL* or phase transformation line has been reached. This assumption, however, contradicts with the observed behaviour on loose sand under undrained conditions (e.g. test ICUC-7).
- As with other elastic-plastic models, CASM does not allow any plastic deformation to be developed within the yield surface. Therefore, it is

unable to predict the transition of stiffness smoothly from elastic region to elastic-plastic region.

- The model has not been able to predict the behaviour of soils under cyclic loading conditions, which is essential for solving many practical geotechnical problems.

The above shortcomings of CASM were investigated theoretically by Yu et al. (2004) and Khong (2004). As a result, three extended versions of CASM have been developed and they are:

- A combined volumetric-deviatoric hardening model CASM-d;
- A monotonic bounding surface model CASM-b;
- A cyclic bounding surface model CASM-c.

This chapter is arranged in the following order: firstly, the finite element method used in the numerical analysis is briefly introduced. The theoretical background of the three plasticity models is then described. Following in this, the capabilities of the models are evaluated by carrying out a parametric study. Finally, the comparisons between the numerical predictions and the experimental data are presented on Portaway sand over a wide range of confining pressures and initial densities under both drained and undrained loading conditions.

6.2 FINITE ELEMENT METHOD

6.2.1 Finite Element Programme – CRISP

The finite element program used in the following numerical simulations is known as SAGE CRISP (CRITICAL State Program), which was developed at Cambridge University (Britto and Gunn, 1987). CRISP is a geotechnical finite element

program incorporating the critical state soil mechanics theory and is frequently used as a test bed for new constitutive models. The program is used mainly in academic communities until 1990, when a PC based version (CRISP90) operating under MS DOS was released. The latest version, so-called SAGE CRISP, has been developed by SAGE Engineering Ltd by adding a Microsoft Windows graphical user interface and technical enhancement. SAGE CRISP operates in two dimensional plane strain, or axisymmetry. The finite element program is also capable of analysing three dimensional problems. The simulations of fully saturated drained and undrained soils can be carried out in the current program.

6.2.2 Implementation and Analysis

Figure 6-1 shows the mesh used in the finite element analysis for all the tests simulated by CASM and its extensions. Only a quarter of the soil specimen was modelled due to symmetry. The mesh consists of four fifteen-noded cubic strain triangle elements. For all the simulation, the loading is divided into 2000 increments that are found to be satisfactory for the simple element problem concerned.

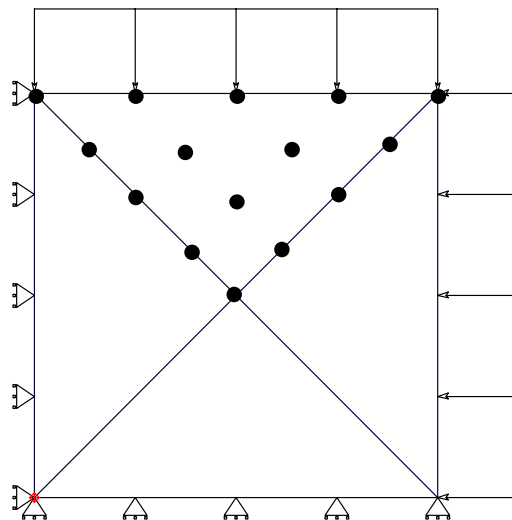


Figure 6-1. Finite element mesh used in the numerical analysis (Khong, 2004).

6.3 THEORETICAL BACKGROUND OF EXTENDED PLASTICITY MODELS FOR CASM

In the next three sub-sections, the backgrounds and main theoretical considerations of the extended models are presented. A graphical relationship between CASM and its extensions is shown in Appendix E. The detailed mathematical derivations of the models can be found in Khong (2004) and will not be repeated here. Some important concepts and modifications introduced into the new models, however, are presented in order to facilitate rational understanding of the numerical results obtained.

6.3.1 CASM-d: A Combined Hardening Model

6.3.1.1 Background

Figure 4-14 and Figure 4-15 show the quasi-steady behaviour of loose Portaway sand specimen (CIUC-7) under undrained loading condition. The characteristic of Portaway sand in this type of test is the reappearance of hardening after the material has experienced a peak shear stress followed by a softening response.

It has also been shown experimentally by many other researchers (e.g. Bishop and Henkel, 1957; Ishihara et al., 1975; Been and Jefferies, 1985; Coop, 1990) that the hardening function is assumed to depend on the previous history not only through the plastic volumetric strain but also through the plastic deviatoric strain for sands. Theoretically, the use of combined volumetric-deviatoric hardening models was first introduced by Nova (1977) assuming that the work done by the deviatoric stresses gave an additional contribution to the hardening.

During the construction of the CASM model by Yu (1995, 1998), the primary aim is to present a simple unified critical state model for soils, the volumetric strain

hardening of the standard Cam-clay models was then preserved. Therefore, CASM implies that the hardening stops and unlimited plastic deformation can take place once the critical state of zero incremental dilation has been reached. As can be seen in the experimental results, this assumption obviously contradicts the facts (see test CIUC-7). This section briefly describes how CASM can be further extended in order to model quasi-steady behaviour exhibited in undrained tests on loose sand. The new model is named as CASM-d.

6.3.1.2 A newly proposed combined hardening rule in CASM-d

In order to incorporate the contribution made by deviatoric stress on the hardening, the following assumption is used in the new model:

$$\delta p'_o = \frac{\nu p'_o}{(\lambda - \kappa)} (\delta \varepsilon_p^p + \alpha \delta \varepsilon_q^p) \quad (6-1)$$

where $\delta \varepsilon_p^p$ and $\delta \varepsilon_q^p$ are the plastic volumetric and deviatoric strain increments, respectively, and α is a new model parameter, which is used to control the relative contribution of the incremental plastic deviatoric strain to the rate of change of the hardening parameter p'_o . When α is equal to zero, the original model CASM will be recovered. Apart from the new combined hardening function, all other assumptions used in CASM-d are the same as those in CASM, which were described in section 2.5.2.

It is noted that, if the model parameter α is large, then the critical state is not reached even at a very high strain. This is because the size of the yield surface p'_o keeps increasing as the soil reaches its failure state. In this model, $\delta p'_o$ is also dependent upon the incremental plastic deviatoric strain $\delta \varepsilon_q^p$ and this quantity may not be zero at the critical state. Of course if predicted ultimate state is desired to be exactly the same as the critical state, a variable α value could be used rather than as a constant. If plastic hardening law uses an expression such as $\alpha = \alpha(\eta)$ so that it becomes zero when $\eta = M$, then the ultimate state will be the same as the

critical state. In other words, the plastic hardening law may take the following form (Yu et al. 2004):

$$\delta p'_o = \frac{\nu p'_o}{(\lambda - \kappa)} [\delta \varepsilon_p^p + \alpha(\eta) \delta \varepsilon_q^p] \quad (6-2)$$

6.3.1.3 Comparison between CASM and CASM-d

Figure 6-2 compares the predictions of an undrained test on loose sand by CASM and CASM-d. The model constants used in the calculations were $\mu = 0.16$, $\kappa = 0.005$, $\lambda = 0.025$, $\Gamma = 1.796$, $M = 1.19$, $n = 3.5$ and $r = 1.5$ ($\xi_R = \xi_0 = 0.008$). The new model parameter α was chosen as 0.02. It can be seen from Figure 6-2 (a) that nearly identical effective stress paths were produced by CASM and CASM-d before the *CSL* was reached. As expected, after effective stress paths reached the *CSL* ($\eta = M$), the stress-strain curve predicted by CASM-d shows a change from a compressive to dilatant pattern. The line for which this occurs has been defined as the phase transformation line (Ishihara et al., 1975). Figure 6-2 (b) gives predicted responses of the excess pore pressures by two models.

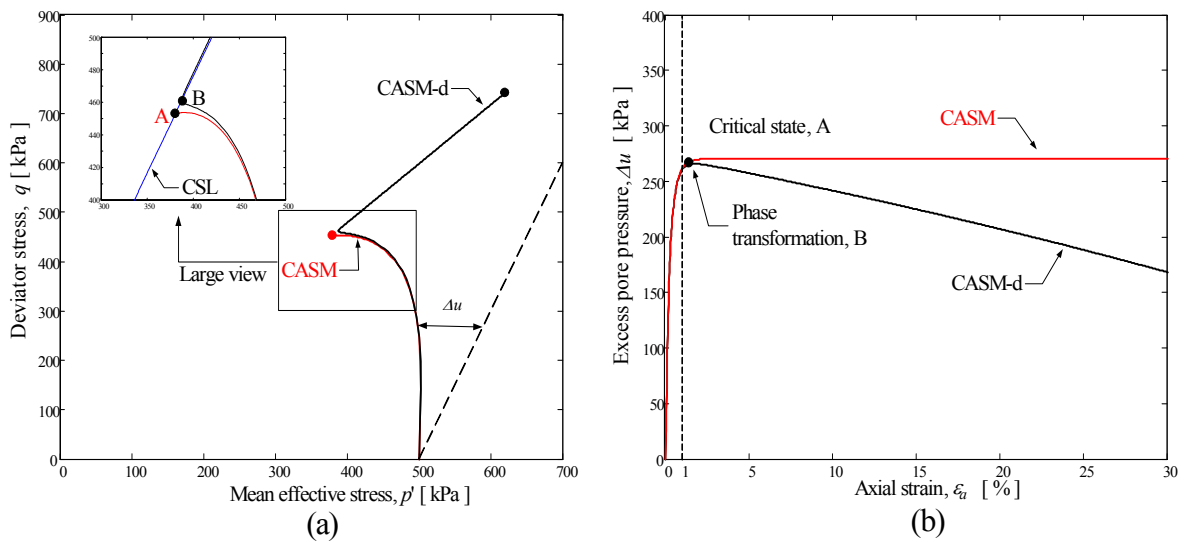


Figure 6-2. Undrained test on medium loose Portaway sand predicted by CASM and CASM-d.

6.3.2 CASM-b: A Monotonic Bounding Surface Model

6.3.2.1 Background

The bounding surface model was first introduced by Dafalias (1975) in order to allow a progressive accumulation of plastic strains during loading within the bounding surface that corresponding to the yield surface in conventional plasticity theory. The main advantage of this type of models is that abrupt change from elastic to elastic-plastic behaviour can be removed. This section briefly describes how CASM can be further extended in order to incorporate the bounding surface concept into CASM. The new model is named as CASM-b.

6.3.2.2 Bounding surface, mapping rule and hardening modulus

The principal modifications to the CASM are summarised as follows:

- *Bounding surface*: the shape of the bounding surface is the same as CASM and CASM-d, and takes the following form in terms of the mean effective and deviatoric stresses:

$$f(p', q, p'_{oj}) = \left(\frac{q}{Mp'} \right)^n + \frac{\ln(p'/p'_{oj})}{\ln r} = 0 \quad (6-3)$$

where p'_{oj} is the size of the bounding surface in the p' - q space.

- *Mapping rule*: the radial mapping rule is used in CASM-b as shown in Figure 6-3. The hardening modulus at the current stress point is assumed to depend on both hardening modulus at its corresponding image point H_j and the ratio of distance from these two stress points to the origin.
- *Hardening modulus*: in the new model CASM-b, the plastic strain is allowed to occur within the yield surface. By introducing two new model

parameters h and m , the hardening modulus H at the current stress point can be calculated as:

$$H = H_j + \frac{h}{p'} \frac{(1 - \gamma)^m}{\gamma} \quad (6-4)$$

where H_j is hardening modulus at the image stress point and γ is the ratio between the current stress and image stress (see Figure 6-3).

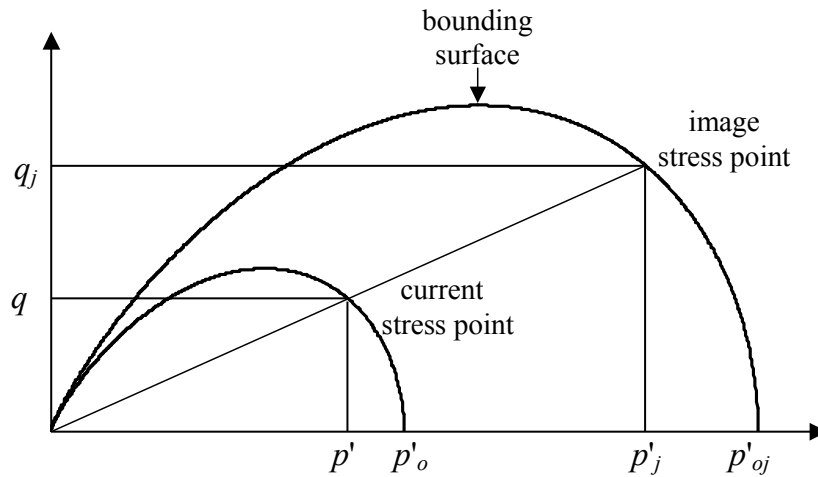


Figure 6-3. The mapping rule adopted in CASM-b (Khong, 2004).

Yu and Khong (2003) carried out a sensitivity study on these two new model parameters and found that m has much more impact than h on calculating H . When γ is between 0.6 and 1, both h and m have insignificant effects on H . Here, again, the elastic properties and plastic potential adopted in CASM-b are the same as those assumed in CASM.

6.3.2.3 Comparison between CASM and CASM-b

Figure 6-4 compares the predictions of a drained test (CIDC-3) on loose Portaway sand by CASM and CASM-b. The parameters used in the calculations were $\mu = 0.16$, $\kappa = 0.005$, $\lambda = 0.025$, $\Gamma = 1.796$, $M = 1.19$, $n = 3.5$ and $r = 19.2$. The new parameters h and m were chosen as 5 and 1, respectively.

It can be seen in Figure 6-4 (a) that a smooth transition of stiffness was reproduced in the simulation by CASM-b. Figure 6-4 (b) shows measured and predicted relationships between the volumetric strains and the axial strains. It is evident that CASM-b matches the measured data a little better than CASM.

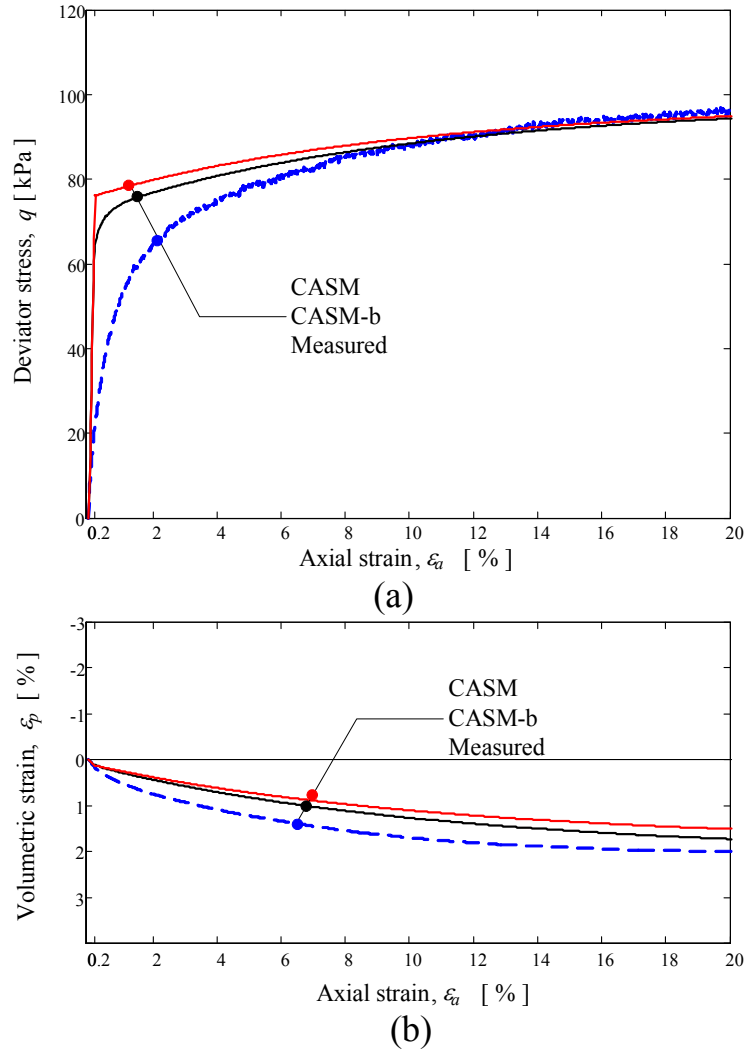


Figure 6-4. Drained test on loose Portaway sand (CIDC-3) predicted by CASM and CASM-b.

6.3.3 CASM-c: A Cyclic Bounding Surface Model

6.3.3.1 Background

CASM, CASM-d and CASM-b can only give the predictions of the behaviour of soils under monotonic loading conditions. The need for modelling cyclic behaviour becomes a necessity. A large number of constitutive models have been, and continue to be developed for simulation of cyclic behaviour. Most studies, however, dealt primarily with overall soil behaviour under specifically chosen cyclic conditions. Inevitably, the models developed based on such empirical approach provide little confidence on predicting mechanical behaviour of different materials and/or under different conditions. Other approaches such as models formulated in terms of the bounding surface concept (Dafalias, 1975) and kinematic hardening concept (Stallebrass, 1990) have shown some degree of success in modelling soil behaviour under cyclic loading conditions. Rational modelling of accumulated plastic deformation, hysteretic loops and excess pore pressure developments of sands, however, still remains a major challenge. In this regard, CASM is extended in order to simulate typical cyclic behaviours described in Chapter 5. The new model is called CASM-c, which is a further extension of the monotonic bounding surface model CASM-b.

6.3.3.2 Model description

The bounding surface, mapping rule, elastic parameters and plastic potential of CASM-c are the same as those assumed in CASM-b. Therefore, they will not be repeated here.

In the context of the bounding surface theory and the shakedown concept, the unloading and reloading behaviours of soils are assumed to be governed by three additional parameters in CASM-c with respect to CASM-b. This feature is described below.

6.3.3.3 Calculation of the hardening modulus

Three distinct stages are divided within CASM-c under cyclic loading, in which the assumptions for the calculation of hardening modulus are treated differently and summarised as follows:

- Virgin loading: the loading behaviour in this stage is equivalent to the specimen subject to monotonic loading. All the model assumptions made in CASM-c are the same as CASM-b.
- Unloading: a new parameter H_U is introduced and the hardening modulus H at the current stress point is assumed to be:

$$H = H_U \times \frac{1}{(1 - \gamma)} \quad (6-5)$$

where γ has been defined in section 6.3.2.2.

- Reloading: another two parameters H_R and k are adopted to control the reloading behaviour and H is expressed as:

$$H = H_j + H_R \times \left(\frac{1 - \gamma}{\gamma} \right) \times (1 + \varepsilon_q^p)^k \quad (6-6)$$

The physical meanings underlying the equations (6-5) and (6-6) are illustrated in the experimental results from two-way drained test TWD-3. Figure 6-5 shows two stress-strain loops for 1st and 8th cycle, respectively. After 1st cycle, the unloading was started from point 'A'. It is evident that the stiffness was very high at this 'turning point' and gradually decreasing until point 'B'. Such observed behaviour is well reflected in the Equation (6-5) so that:

$$\left\{ \begin{array}{lll} H = \infty & \gamma = 1 & \text{at } A \\ H_U < H < \infty & 0 < \gamma < 1 & A \sim B \\ H \rightarrow H_U & \gamma \rightarrow 0 & \text{at } B \end{array} \right. \quad (6-7)$$

The stress-strain loop of test TWD-3 at 8th cycle shows a typical plastic shakedown behaviour (Johnson, 1986). This type of behaviour can be achieved in CASM-c by choosing a positive value of k as shown in equation (6-6). When $k < 0$, the calculated H decreases with straining so that the plastic deformation increases with the number of cycles until ultimate collapse. When $k = 0$, the calculated H is independent on strain level and the plastic deformation increases with number of cycles.

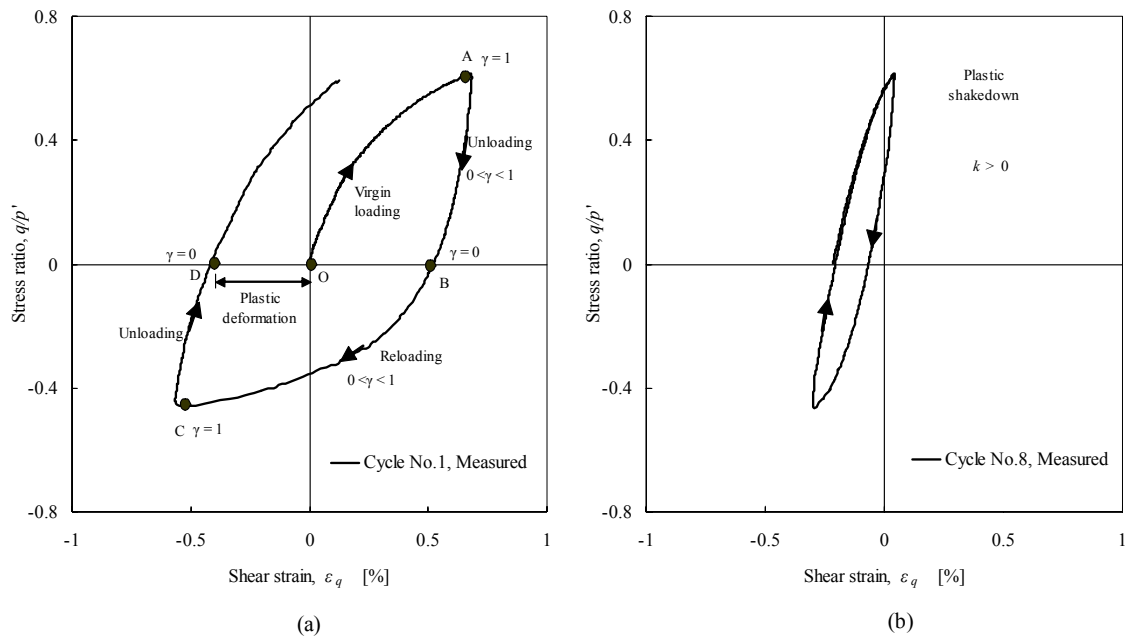


Figure 6-5. Calculation of the hardening modulus H in CASM-c and shakedown behaviour (TWD-3).

Based on the above assumptions, the new parameters H_U and H_R are directly related to the slope of the stress-strain curve or resilient modulus M_r , which is defined in section 2.2.6.1. So both of them control the stiffness of the stress-strain curve. The parameter k controls the rate of the occurrence of the shakedown behaviour after certain cycles.

6.4 PARAMETRIC STUDY

The main objective of the parametric study is to investigate the influences of the initial state parameter ξ_0 and some of the model constants introduced into CASM and its extensions on the computed stress-strain relations. The model constants used in the simulations have been calibrated in Chapter 4. Seven model constants obtained in Chapter 4 are used in first series of simulations with the different initial conditions on both drained and undrained tests. This is followed by an investigation of model constants r , n , κ and μ on drained tests. The critical state constants are unchanged during these simulations. They are $\lambda = 0.025$, $\Gamma = 1.796$ and $M = 1.19$. The parametric study on parameters ξ_0 , r , n , κ and μ are only carried out for CASM because the similar trend would be expected for its extensions. The influence of parameter α introduced in CASM-d is also investigated. The effects of other new parameters h , m , H_R , H_U and k introduced in CASM-b and CASM-c have been examined by Khong (2004), which will not be repeated in this thesis.

6.4.1 The Effect of Initial State Parameter ξ_0

The conventional drained and undrained triaxial tests (CIDC and CIUC) under monotonic loading in compression are simulated. The model constants used in the CASM predictions are as follows:

$$\mu = 0.16, \kappa = 0.005, \lambda = 0.025, \Gamma = 1.796, M = 1.19, n = 3.5, r = 19.2$$

6.4.1.1 Drained behaviour

Figure 6-6 shows the computed stress-strain curves for four specimens with different values of initial state parameter ξ_0 . It can be seen from Figure 6-6 that the typical behaviours of loose sands ($\xi_0 = 0.06$ and $\xi_0 = 0.025$) and dense sands

($\xi_0 = -0.06$ and $\xi_0 = -0.16$) can be reproduced by CASM. The simulations are in good agreement with the trend observed in Figure 4-8.

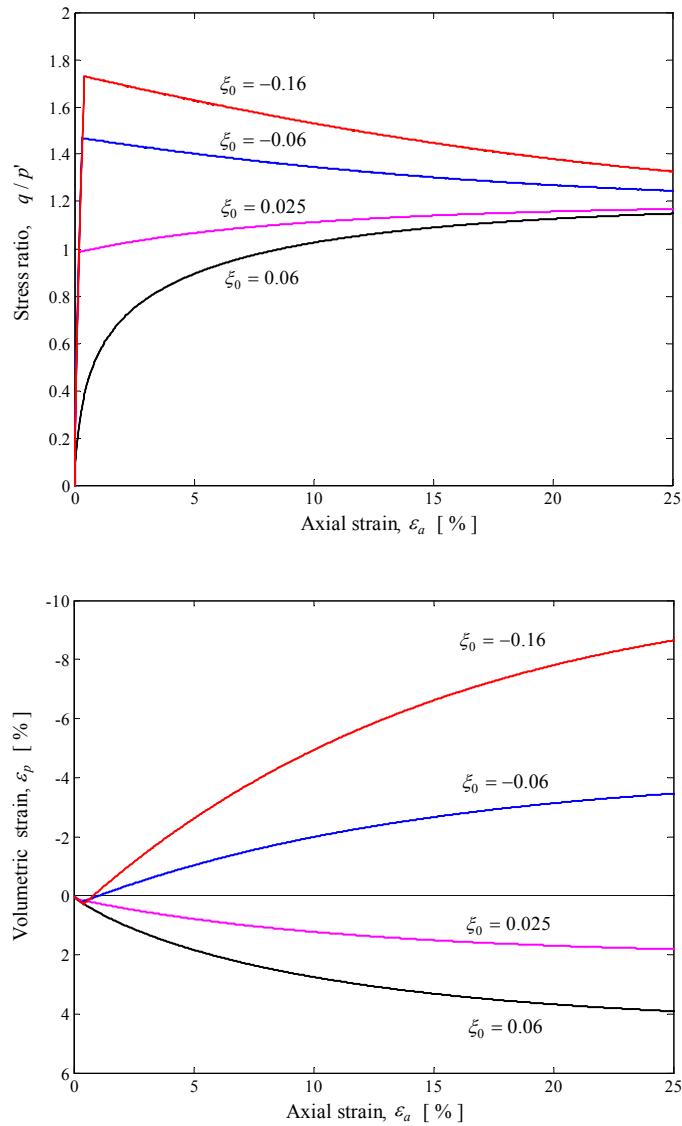


Figure 6-6. Effect of initial condition on drained behaviour of Portaway sand.

6.4.1.2 Undrained behaviour

Four tests were simulated in this series of tests with three specimens at a state looser than critical state ($\xi_0 = 0.06$, $\xi_0 = 0.025$ and $\xi_0 = 0.005$) and another one was denser than critical state ($\xi_0 = -0.005$). As recommended by Yu (1998), for sand at a state looser than critical, the initial state parameter of specimen was taken as reference state parameter ($\xi_R = \xi_0$). The computed stress-strain curves

and stress paths in Figure 6-7 clearly show how the initial condition influences the computed stress-strain behaviour of sands in undrained triaxial tests.

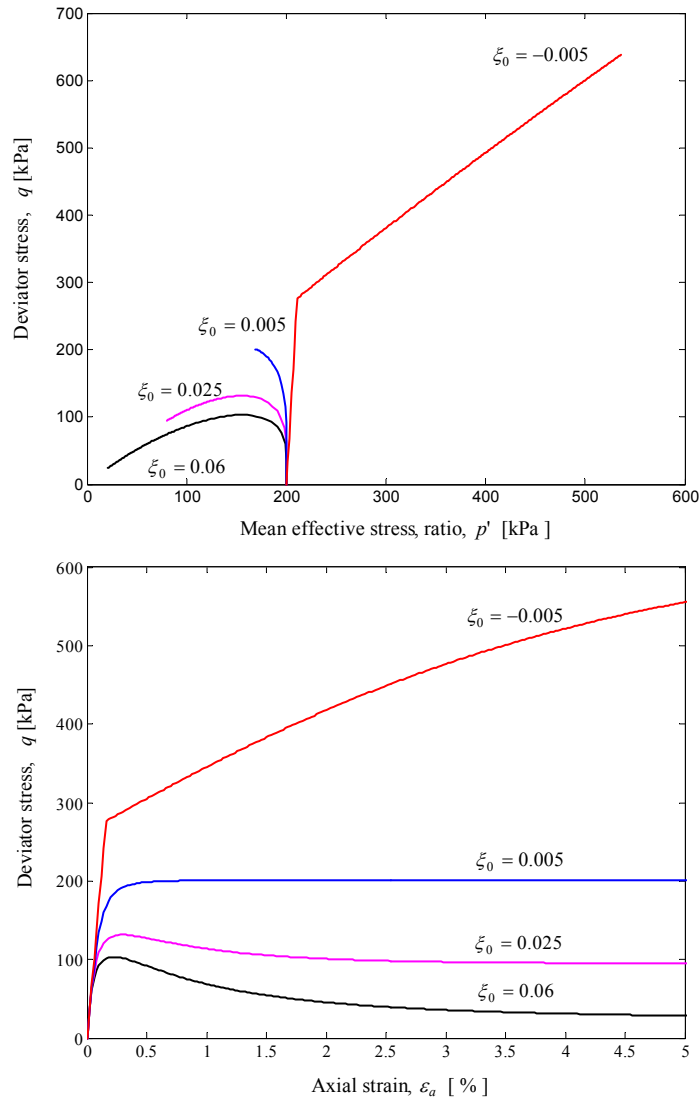


Figure 6-7. Effect of initial condition on undrained behaviour of Portaway sand.

6.4.2 The Effect of Spacing Ratio r

The spacing ratio r was determined previously as 19.2 for Portaway sand that corresponds to the loosest state ($\xi_0 = 0.06$). In the original and modified Cam-clay models, r is fixed at 2.72 and 2.0, respectively. However, for CASM, r is allowed to vary from 1 to ∞ depending on the type of soils. The influences of the spacing ratio r on the responses of both dense and loose sands were investigated in drained

compression tests with constant cell pressures. The initial conditions of sands are the same as tests CIDC-1 and CIDC-5 ($\xi_0 = 0.06$ and $\xi_0 = -0.159$, respectively). The model constants are given as:

$$\mu = 0.16, \kappa = 0.005, \lambda = 0.025, \Gamma = 1.796, M = 1.19, n = 3.5$$

Four simulations were performed with the spacing ratio r varying from 19.2 to 1000. Two opposite effects are found from Figure 6-8 and Figure 6-9 for dense sands and loose sands, respectively. It can be seen from the former that the computed behaviour shows strong dilation as the value of r decreases. The peak stress ratios are ranging from 1.5–1.7. In contrast, the behaviour shown in the latter exhibits the strong contraction as the value of r decreases.

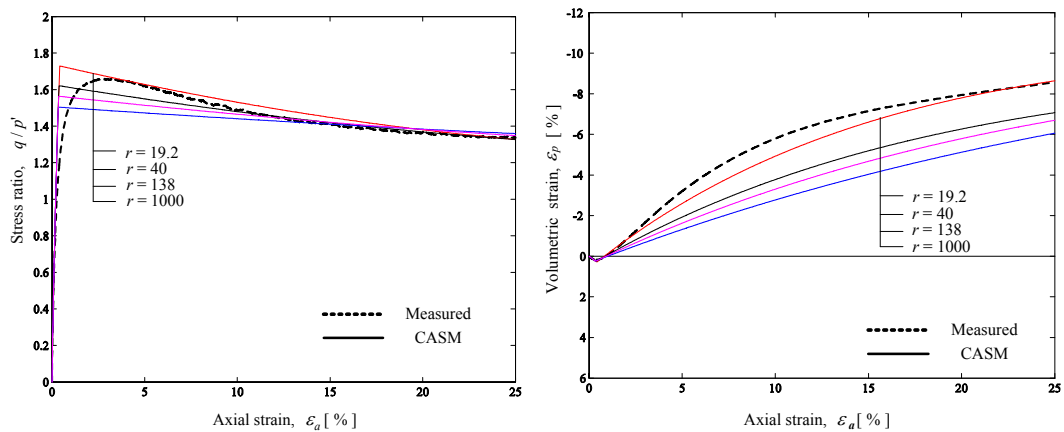


Figure 6-8. Effect of spacing ratio r on dense Portaway sand (CIDC-5).

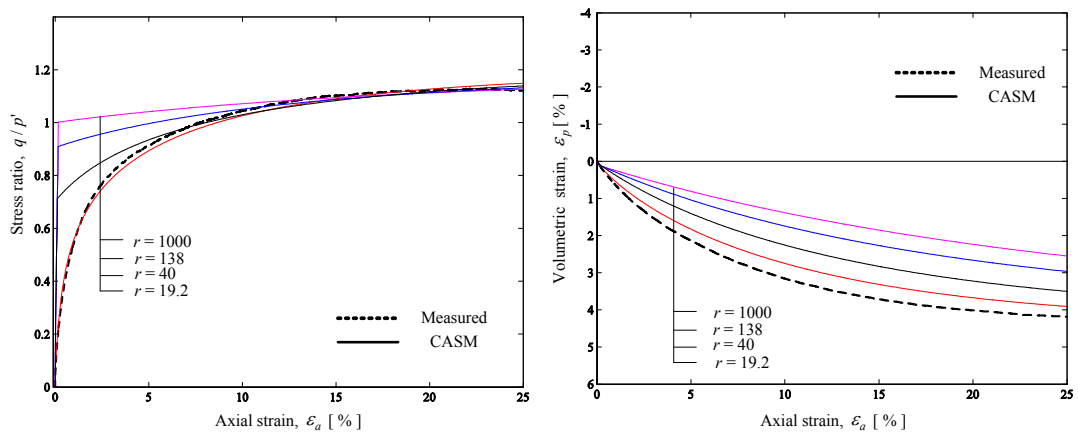


Figure 6-9. Effect of spacing ratio r on very loose Portaway sand (CIDC-1).

6.4.3 The Effect of Stress-State Coefficient n

The value of the stress-state coefficient n was determined previously as 3.5 for Portaway sand (see Figure 4-35). The model constants used in this set of simulations are as follows:

$$\mu = 0.16, \kappa = 0.005, \lambda = 0.025, \Gamma = 1.796, M = 1.19, r = 19.2$$

As with in section 6.4.2, tests CIDC-1 and CIDC-5 were simulated with varying values of n from 2 to 5. It can be seen from Figure 6-10 and Figure 6-11 that the similar effect obtained for the spacing ratio r is equally applied to the stress-state coefficient n .

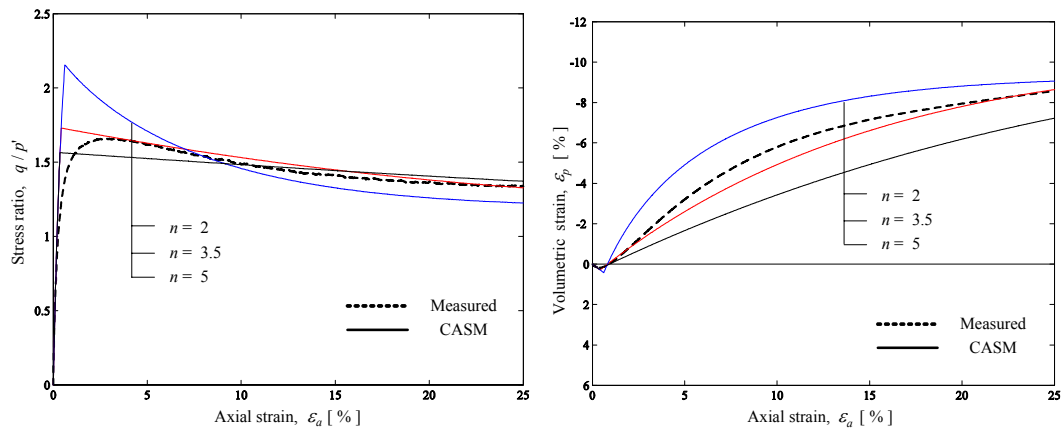


Figure 6-10. Effect of stress-state coefficient n on dense Portaway sand (CIDC-5).

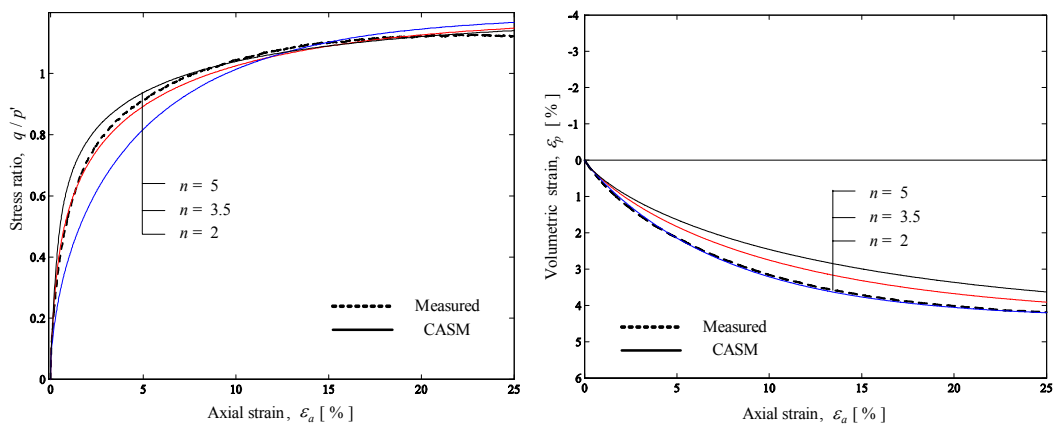


Figure 6-11. Effect of stress-state coefficient n on loose Portaway sand (CIDC-1).

6.4.4 The Effect of Elastic Constant μ

The value of Poisson's ratio μ was determined previously as 0.16 for Portaway sand (see Figure 4-33). It is well recognised that Poisson's ratio μ is typically in the range of 0.15-0.35 for both clay and sand. The model constants used in the CASM are as follows:

$$\kappa = 0.005, \lambda = 0.025, \Gamma = 1.796, M = 1.19, n = 3.5, r = 19.2$$

The drained test on dense sand (CIDC-5) was simulated with varying values of μ from 0.05 to 0.35. It is noted from Figure 6-12 that the computed initial stiffness increases as the value of μ decreases.

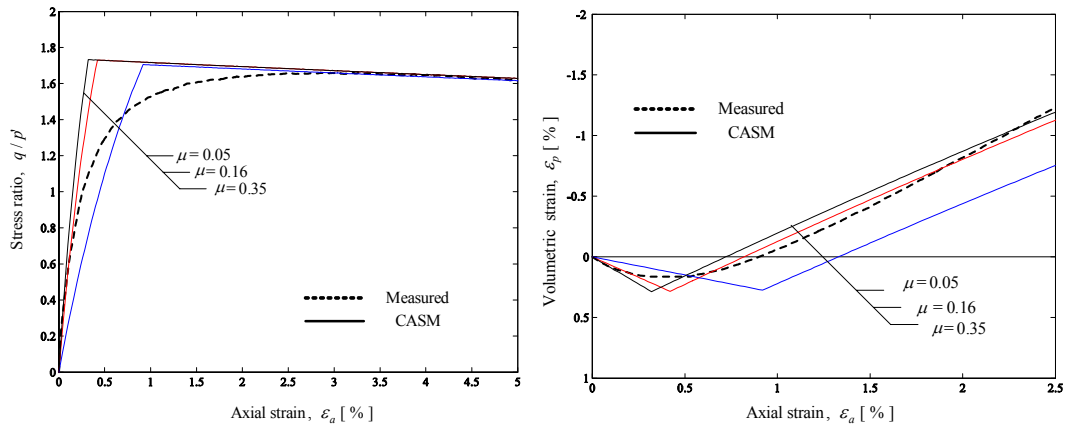


Figure 6-12. Effect of μ on dense Portaway sand (CIDC-5).

6.4.5 The Effect of Elastic Constant κ

It has been observed in the isotropic loading and unloading tests that the higher value of κ exists in dense specimen than in loose specimen within the range of 0.003-0.01. A constant value of κ is assumed in the following simulations by CASM as well as other three extended models. The model constants used are given as:

$$\mu = 0.16, \lambda = 0.025, \Gamma = 1.796, M = 1.19, n = 3.5, r = 19.2$$

The drained test on dense sand (CIDC-5) was simulated with varying values of κ from 0.003 to 0.008. Same as Poisson's ratio, Figure 6-13 shows that the computed initial stiffness increases as the value of κ decreases.

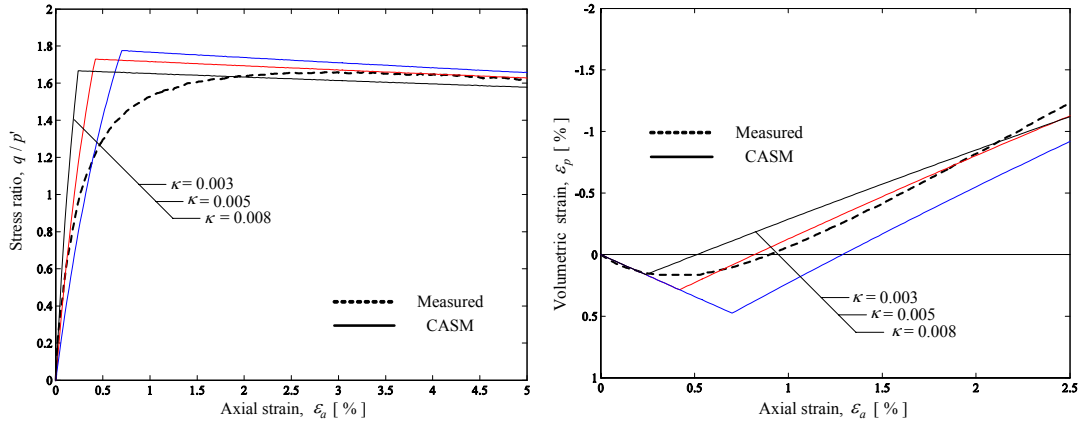


Figure 6-13. Effect of κ on dense Portaway sand (CIDC-5).

6.4.6 The Effect of Parameter α

α is a newly introduced model parameter in CASM-d in order to control the contribution of the deviatoric stress to the hardening of the soils. The undrained test CIUC-7 was simulated by CASM-d. The model constants used in CASM-d are as follows:

$$\mu = 0.16, \kappa = 0.005, \lambda = 0.025, \Gamma = 1.796, M = 1.19$$

$$n = 3.5, \xi_R = \xi_0 = 0.031$$

Model parameter α was varied from 0 to 0.05.

Figure 6-14 shows the computed stress paths and stress-strain curves. It can be seen that α has little impact on the prediction before the specimen reaches the peak strengths. As expected, the stress path with $\alpha = 0$ stops at the *CSL* while other two stress paths with a positive α still increase their deviatoric stresses.

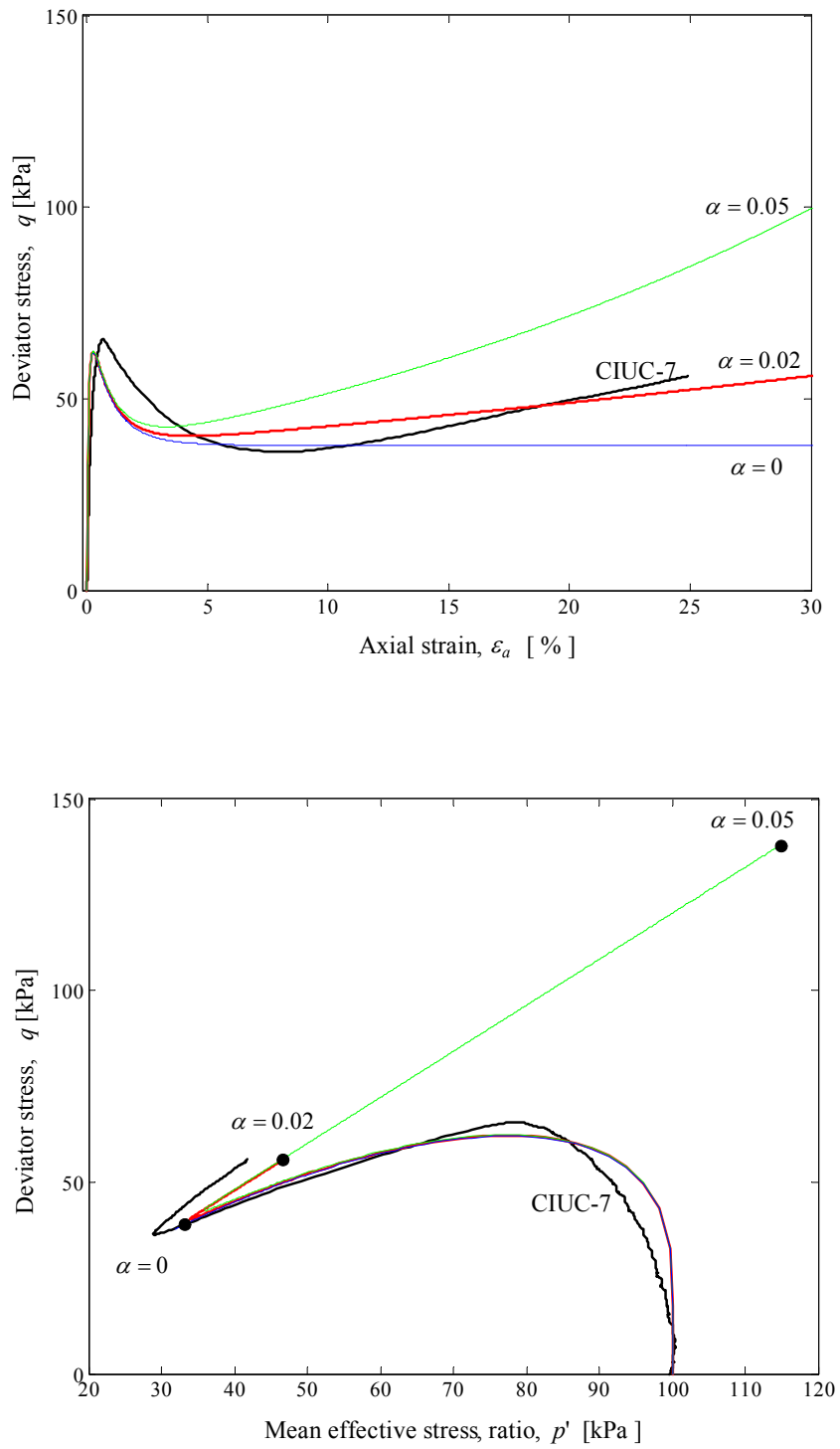


Figure 6-14. Effect of the parameter α on very loose Portaway sand (CIUC-7).

6.5 MODEL PERFORMANCE – CASM

To evaluate the model performance, seven typical conventional drained and undrained triaxial tests were simulated over a wide range of confining pressures, $50 \text{ kPa} \leq \sigma'_3 \leq 800 \text{ kPa}$, and void ratios, $0.537 \leq e_0 \leq 0.722$. Table 6-1 and Table 6-2 show the material constants used for CASM and the initial conditions of the tests simulated, respectively.

Table 6-1. CASM constants for Portaway sand.

μ	κ	λ	Γ	M	n	r
0.16	0.005	0.025	1.796	1.19	3.5	19.2

Table 6-2. The triaxial tests used for CASM predictions.

Test	e_0	σ'_3	ξ_0	Behaviour	Experiments
CIDC-1	0.699	500	0.060	Contraction	Figure 4-8
CIDC-3	0.715	50	0.018	Contraction	Figure 4-8
CIDC-4	0.537	300	-0.115	Contraction and dilation	Figure 4-8
CIDC-5	0.538	50	-0.159	Contraction and dilation	Figure 4-8
CIUC-1	0.712	300	0.060	Flow	Figure 4-17
CIUC-3	0.687	800	0.060	Flow	Figure 4-14
CIUE-1	0.722	200	0.060	Flow	Figure 4-17

Notes:

CIDC = Isotropically Consolidated Drained Compression

CIUC = Isotropically Consolidated Undrained Compression

CIUE = Isotropically Consolidated Undrained Extension

6.5.1 Drained Tests (CIDC-1, 3, 4 and 5)

Figure 6-15 compares the predicted and measured drained stress-strain behaviour of dense and loose specimens. The predictions are in relatively good agreement with the measured behaviours of strain-hardening (CIDC-1, 3) and strain-softening after the peak strength region (CIDC-4, 5). It is noted that CIDC-1 is a normally consolidated specimen whose plastic strain was initiated from the beginning of shearing so the curve has a smooth shape. As described previously, CASM is an elastic-plastic hardening/softening model, which introduces a yield surface that expands according to the corresponding preconsolidation stress p'_o . It automatically divides stress space, at any instant, into a high stiffness elastic region and an elastic-plastic region with suddenly decreased stiffness. This type of models inevitably causes a sudden transition of stiffness for over-consolidated specimens as shown in the stress-strain curves of CIDC-3, CIDC-4 and CIDC-5, which are not typical stress-strain behaviours of soils. However, as pointed out by Wood (2004), this does not mean that elastic-plastic models will be inappropriate, but merely that one can expect there to be some level of detail of response which they are unable to reproduce.

6.5.2 Undrained Tests (CIUC-1 and CIUC-3)

Figure 6-16 shows the results of two undrained compression tests on very loose specimens (CIUC-1, 3) and their model simulations with the same initial state parameters. The model predicts peak shear stress conditions within axial strain of $\varepsilon_a = 0.5\%$ followed by softening to the critical state at large strains. The predicted stresses remain constant during this stage and the well-known phenomenon of static liquefaction for fully saturated loose sands was reproduced. The curves of these two undrained stress paths support the similarity principal suggested by Roscoe and Poorooshasb (1963).

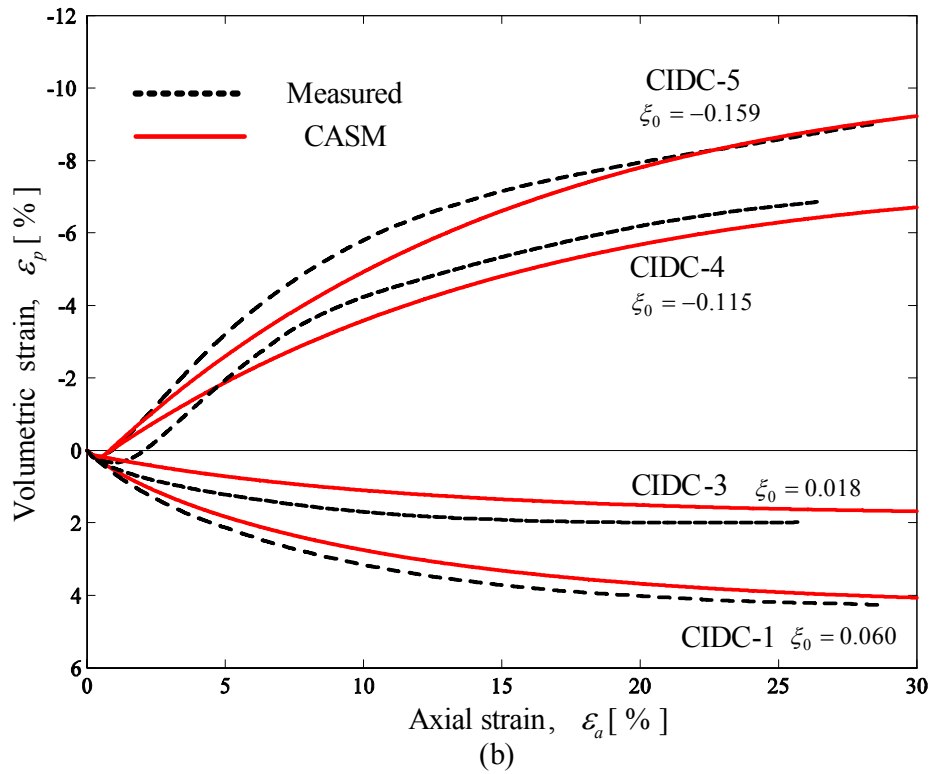
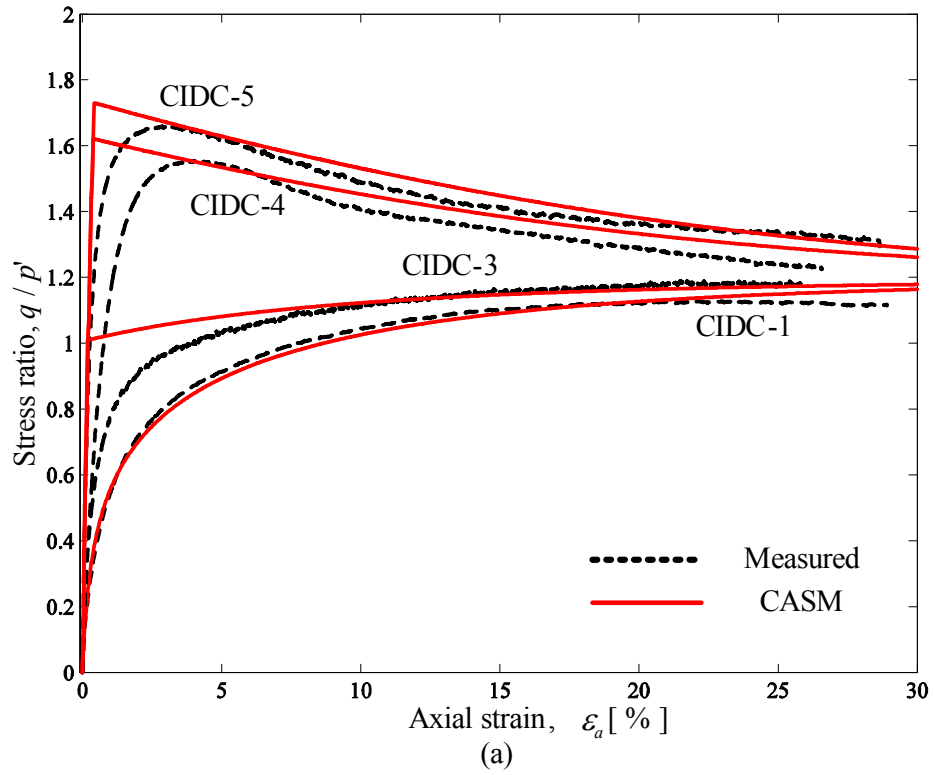


Figure 6-15. Comparison of CASM with measured behaviour for CIDC tests on dense and loose Portaway sand (CIDC-1, 3, 4 and 5).

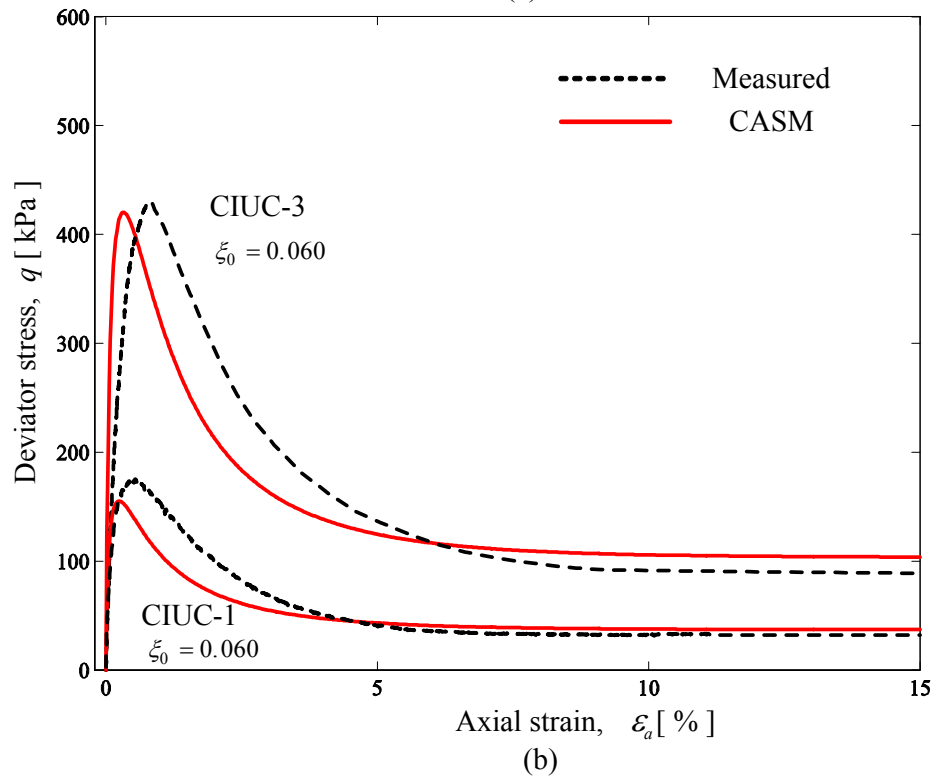
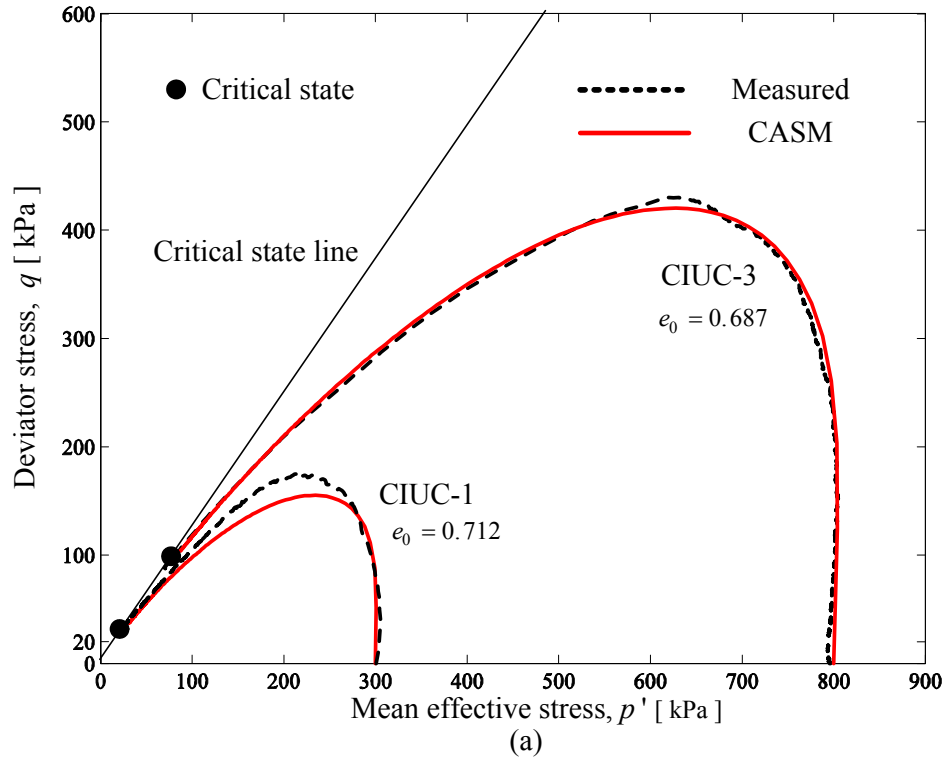


Figure 6-16. Comparison of CASM with measured behaviour for CIUC tests on very loose Portaway sand (CIUC-1 and 3).

6.5.3 Undrained Test in Extension (CIUE-1)

Most works on verifying constitutive models are based on triaxial compression tests. For the current study, the critical state stress ratio used in CASM has been made to be a function of Lode angle, θ , according to the expression proposed by Sheng et al. (2000):

$$M = M_{\max} \left[\frac{2\alpha^4}{1 + \alpha^4 - (1 - \alpha^4) \sin 3\theta} \right]^{1/4} \quad (6-8)$$

$$\alpha = \frac{M_e}{M_c} = \frac{3 - \sin \phi_c}{3 + \sin \phi_c} \quad (6-9)$$

M_{\max} is the slope of the *CSL* under triaxial compression ($\theta = 30^\circ$) in the p' - q plane.

Figure 6-17 shows the comparison between measured data and prediction of the extension test CIUE-1. The model captured the overall behaviour before occurrence of excessive influence of necking at axial strain $\varepsilon_a = 6\%$. CASM assumes an ideal isotropic elasticity and implies a vertical stress path ($\delta p' = 0$) during the initial shearing in undrained condition. However, the observations from experimental data indicate an apparent inclination of stress path for extension tests. There is sufficient experimental evidence (e.g. Vaid et al., 1990; De Gennaro et al., 2004) to suggest that by adopting different specimen preparation methods, the stress-strain curves may show markedly differences regardless of shape of particles. However, the absence of a practical method to quantify the packing arrangement of particles has led to a large number of conflicting conclusions on testing of sands. The difference in the observed compression versus extension response of Portaway sand is a reflection of its inherent anisotropy using the moist tamping technique. The similar result has been clearly reported by another independent experimental work (De Gennaro et al. 2004). More recently, a study using DEM (Jiang et al. 2003) to simulate this specimen preparation method has revealed that non-homogeneity

cannot be avoided in triaxial specimen and may offer an alternative explanation for the different behaviours shown in compression and extension.

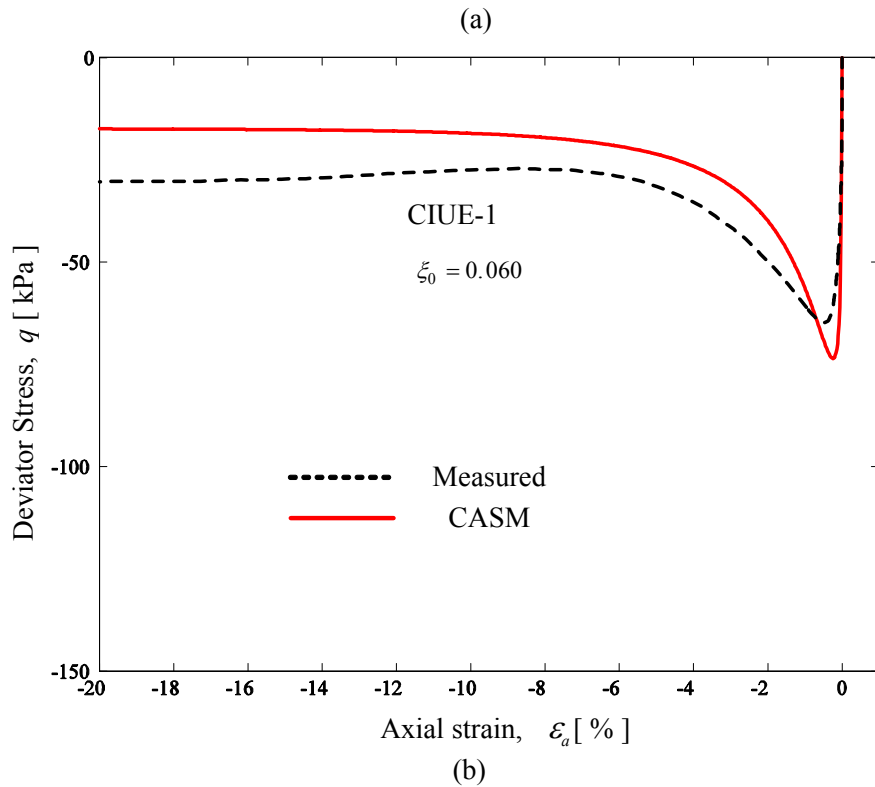
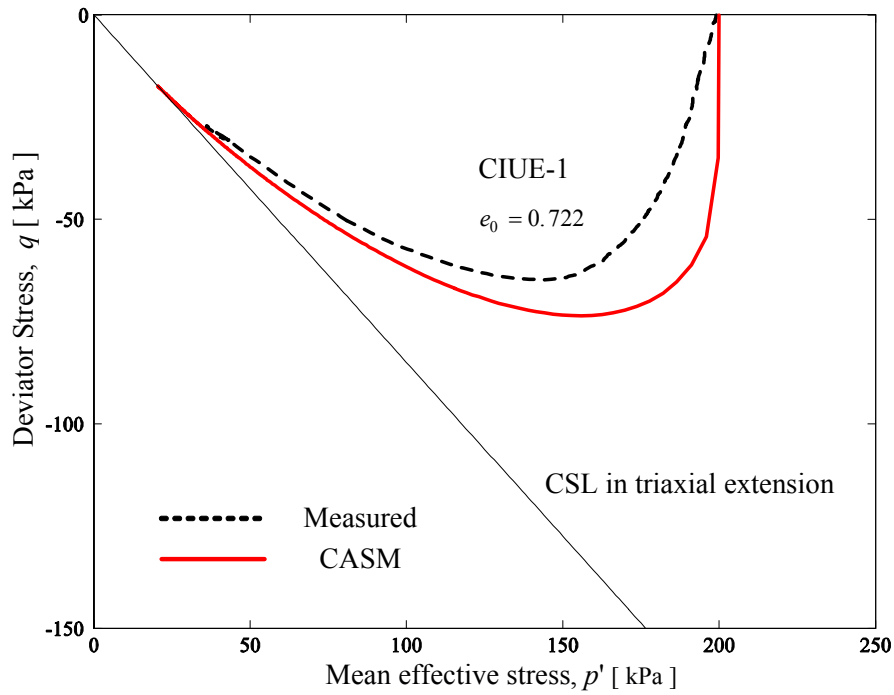


Figure 6-17. Comparison of CASM with measured behaviour for CIUE tests on very loose Portaway sand (CIUE-1).

6.6 MODEL PERFORMANCE – CASM-D

Table 6-3 and Table 6-4 show the material constants used for CASM-d and the initial conditions of tests, respectively.

Table 6-3. CASM-d constants for Portaway sand.

μ	κ	λ	Γ	M	n	r	α
0.16	0.005	0.025	1.796	1.19	3.5	19.2	0.02

Table 6-4. The triaxial tests used for CASM-d predictions.

Test	e_0	σ'_3	ξ_0	Behaviour	Experiments
CIUC-7	0.710	100	0.031	Flow with limited deformation	Figure 4-15
CIUC-9	0.648	100	-0.032	Non-flow	Figure 4-15
CIUC-12	0.739	100	0.060	Flow	Figure 4-15
CIDC-1	0.699	500	0.060	Contraction	Figure 4-8
CIDC-3	0.715	50	0.018	Contraction	Figure 4-8
CIDC-4	0.537	300	-0.115	Contraction and dilation	Figure 4-8
CIDC-5	0.538	50	-0.159	Contraction and dilation	Figure 4-8

Notes:

CIUC = Isotropically Consolidated Undrained Compression

CIDC = Isotropically Consolidated Drained Compression

6.6.1 Undrained Tests (CIUC-7, 9 and 12)

Figure 6-18 and Figure 6-19 present the results of another series of CIUC tests under the same initial effective confining pressure of 100 kPa. The specimens exhibited liquefaction (CIUC-12), limited liquefaction (CIUC-7) and dilative behaviour (CIUC-9). The experimental data clearly indicates a phase transformation state (see Figure 6-19 (b), labelled ‘B’) at which the behaviour of sand as a solid was lost and transformed into a liquefied state (Ishihara et al. 1975).

CASM-d was used here in order to simulate this reappearance of hardening behaviour once the material has softened. As expected, the numerical result shows the tendency of decrease in excess pore pressure and increase in deviatoric stress of this kind of limited liquefaction behaviour. Although the model under-predicted the axial strain at the quasi-steady state (labelled 'B'), overall agreement between the predicted and measured results is obtained. It should be mentioned here that the phase transformation state and the quasi-steady state coincide for this type of behaviour although their physical meanings are somewhat different.

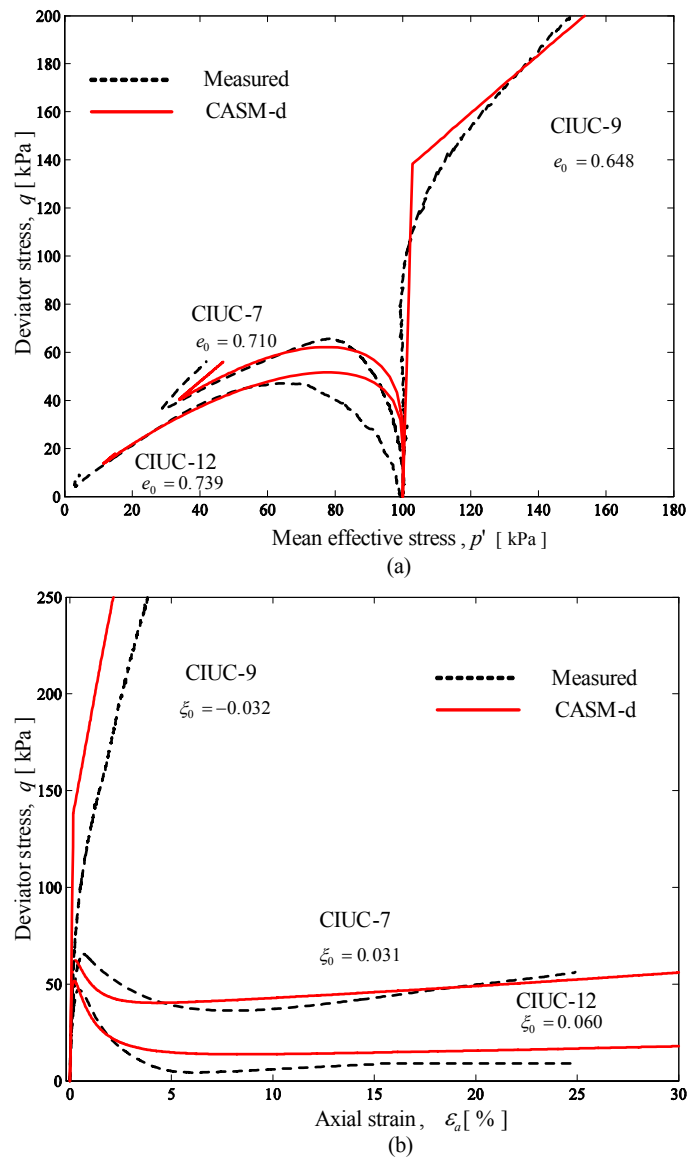


Figure 6-18. Comparison of CASM-d with measured behaviour for CIUC tests (CIUC-7, 9 and 12).

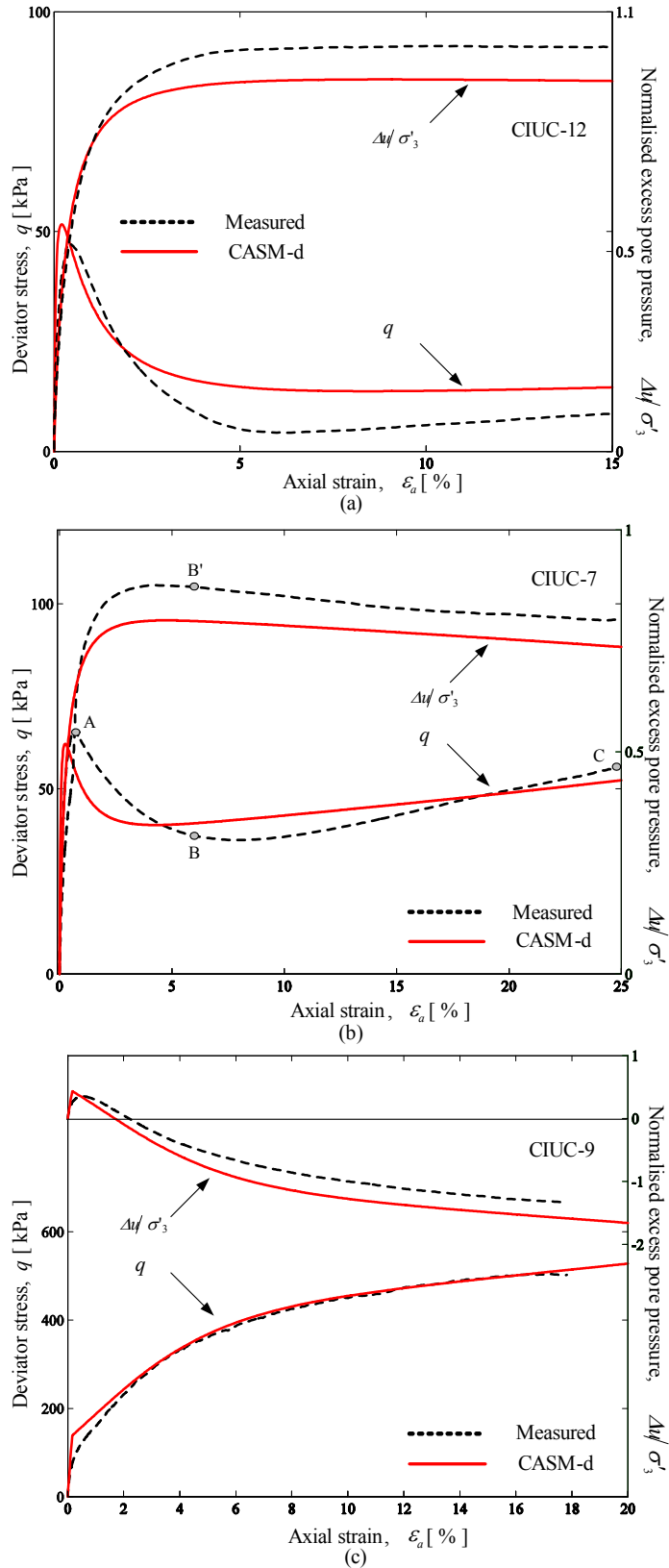


Figure 6-19. Comparison of CASM-d with measured behaviour for CIUC tests on excess pore pressure changes (CIUC-7, 9 and 12).

Ishihara (1996) has demonstrated that a boundary line (called the initial dividing line) exists in the $\nu - \ln p'$ space to separate the initial conditions with or without the occurrence of the phase transformation state. For Portaway sand, this line should lie between the *RCL* and *CSL* (see Figure 4-32).

Plotted in Figure 6-20 and Figure 6-21 are the results of a parametric study on Portaway sand with various initial conditions ($\xi_0 = 0.06 \sim -0.005$) with the value of $\alpha = 0.02$. For comparison purposes, the predictions from CASM-d with the value of $\alpha = 0$ have been presented. It is clear that the ultimate states of the specimens lie essentially on the *CSL* at very large deformations (40% axial strains). This is because that the value of α used is rather small. As shown in Figure 6-20 and Figure 6-21, the control parameter is the initial state parameter ξ_0 for liquefaction behaviour when the model is purely volumetric hardening (i.e. $\alpha = 0$). For a given set of soil parameters, then liquefaction would occur as long as the initial state parameter ξ_0 is large enough (i.e. the initial state is sufficiently looser than the critical state). The behaviour of phase transformation can be predicted only if the model makes use of a combined volumetric and shear plastic strain hardening (i.e. $\alpha > 0$). Both the initial state parameter and the α value will control when and at what level of deformation does this phase transition occur as shown in the figures.

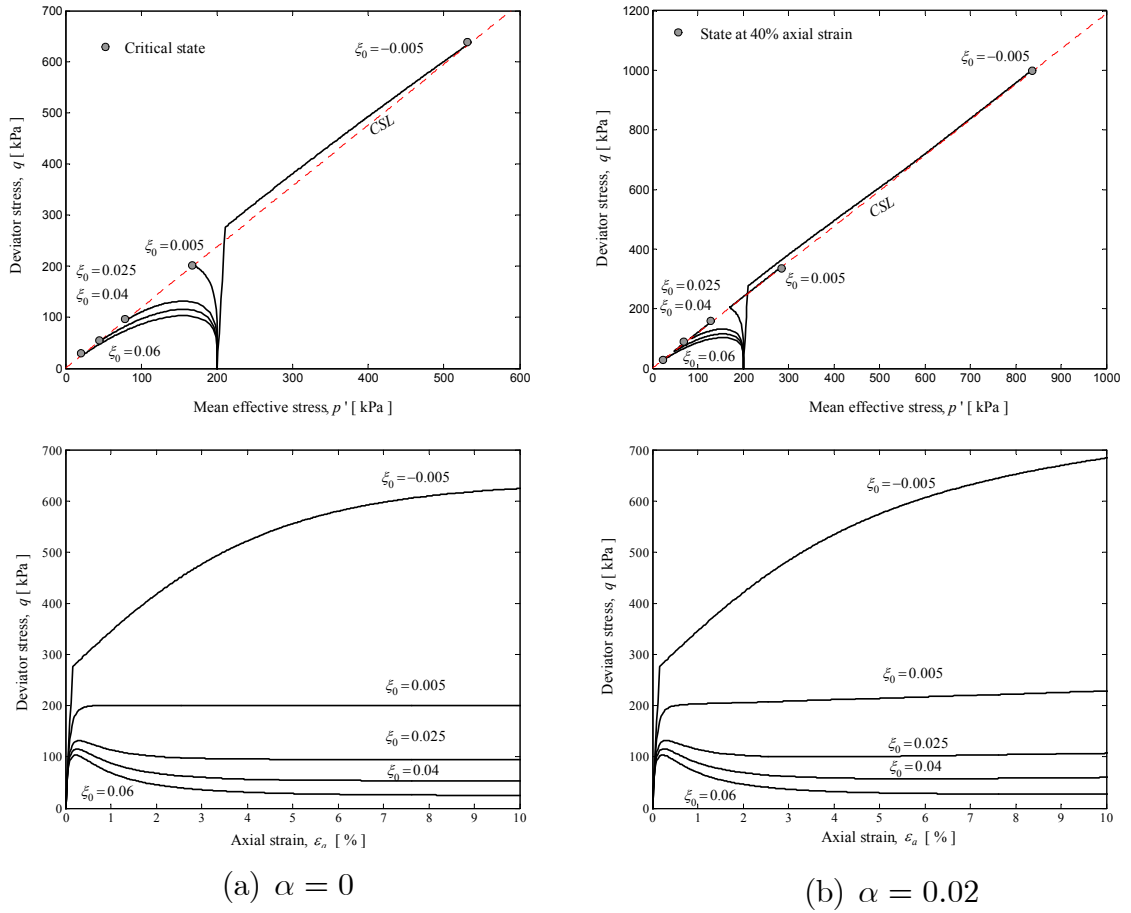


Figure 6-20. Effect of the initial state parameter on the occurrence of liquefaction and phase transformation.

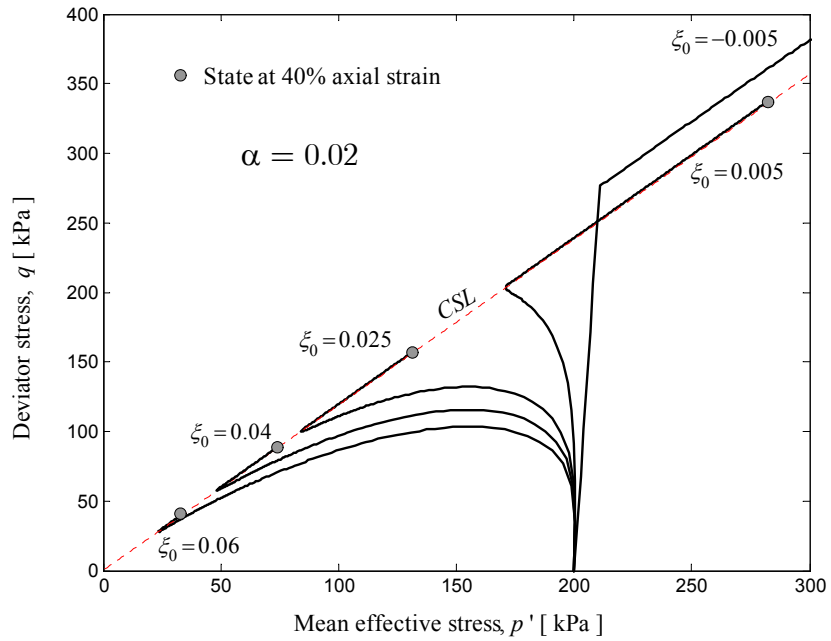


Figure 6-21. Enlarged view of the stress paths shown in Figure 6-20 (b).

6.6.2 Drained Tests (CIDC-1, 3, 4 and 5)

The same set of drained tests predicted by CASM are modelled herein by CASM-d. For comparison purposes, the predictions with $\alpha = 0$ (equivalent to CASM) have also been presented. It can be seen from Figure 6-22 that parameter α has less impact on drained tests.

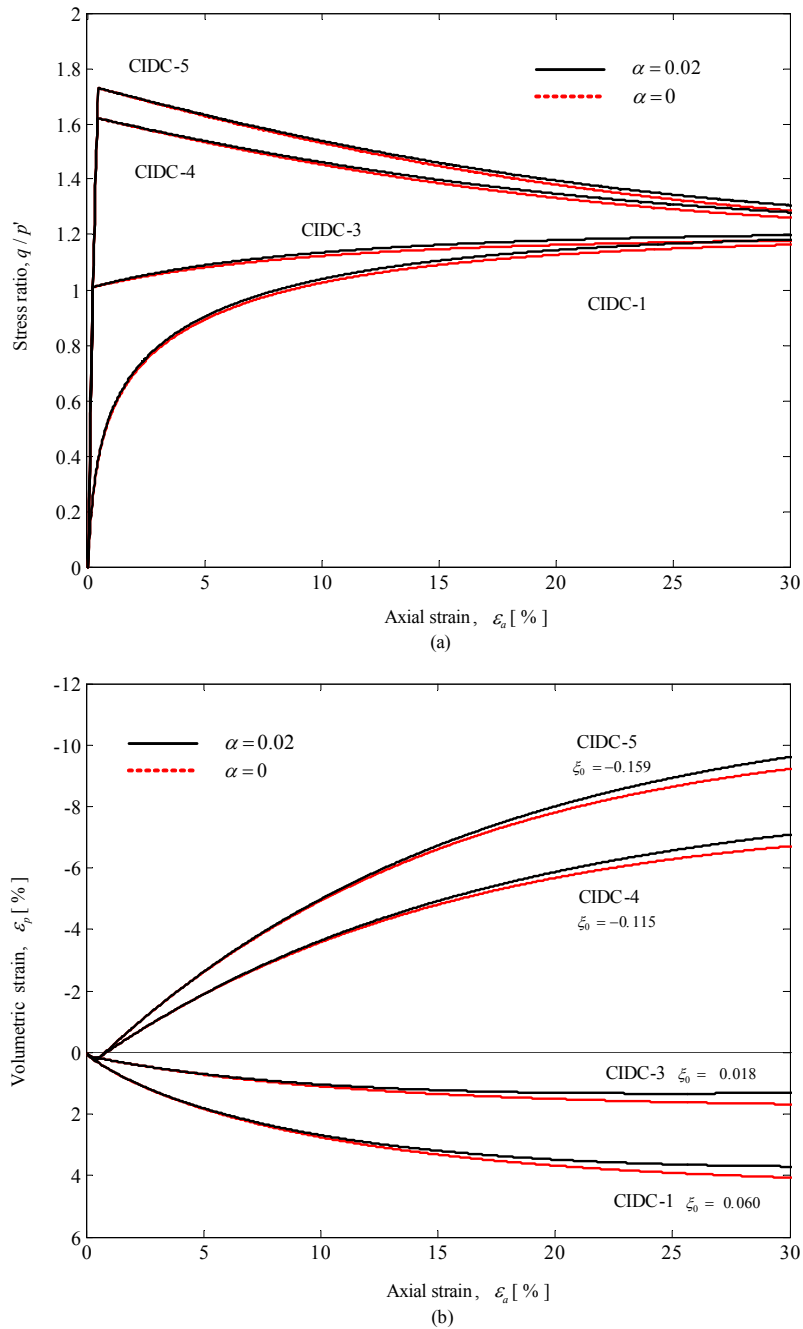


Figure 6-22. Effect of new parameter α on the drained tests (CIDC-1, 3, 4 and 5).

6.7 MODEL PERFORMANCE – CASM-B

It has been described in section 6.3.2.2 that CASM-b allows the occurrence of plastic deformations for stress states within the yield surface. When the initial state of the specimens lies on the *RCL*, CASM and CASM-b will produce the same results with smooth curves. Therefore, the normally consolidated specimens ($\xi_0 = 0.06$) CIDC-1, CIDE-1, CIUC-1-3 and CIUE-1 will not be simulated herein by CASM-b.

Table 6-5 and Table 6-6 show the material constants used for CASM-b and the initial conditions of tests simulated, respectively.

Table 6-5. CASM-b constants for Portaway sand

μ	κ	λ	Γ	M	n	r	h	m
0.16	0.005	0.025	1.796	1.19	3.5	19.2	5	1

Table 6-6. The triaxial tests used for CASM-b predictions.

Test	e_0	σ'_3	ξ_0	Behaviour	Experiments
CIDC-2	0.706	300	0.054	Contraction	Figure 4-8
CIDC-3	0.715	50	0.018	Contraction	Figure 4-8
CIUC-4	0.664	500	0.025	Flow	Figure 4-13
CIUC-6	0.705	300	0.053	Flow	Figure 4-13

Notes:

CIDC = Isotropically Consolidated Drained Compression

CIUC = Isotropically Consolidated Undrained Compression

6.7.1 Drained Tests (CIDC-2 and CIDC-3)

Figure 6-23 compares the predicted and measured drained stress-strain behaviour of two loose specimens. The predictions are in relatively good agreement with the measured behaviours of strain-hardening and volumetric contraction. It is evident that CASM-b predicts more realistic behaviour before the specimens approach the

yield surfaces. A sudden change from elastic to plastic behaviour produced by elastic-plastic model CASM (see Figure 6-15) has been removed by a smooth transition of the stiffness in CASM-b.

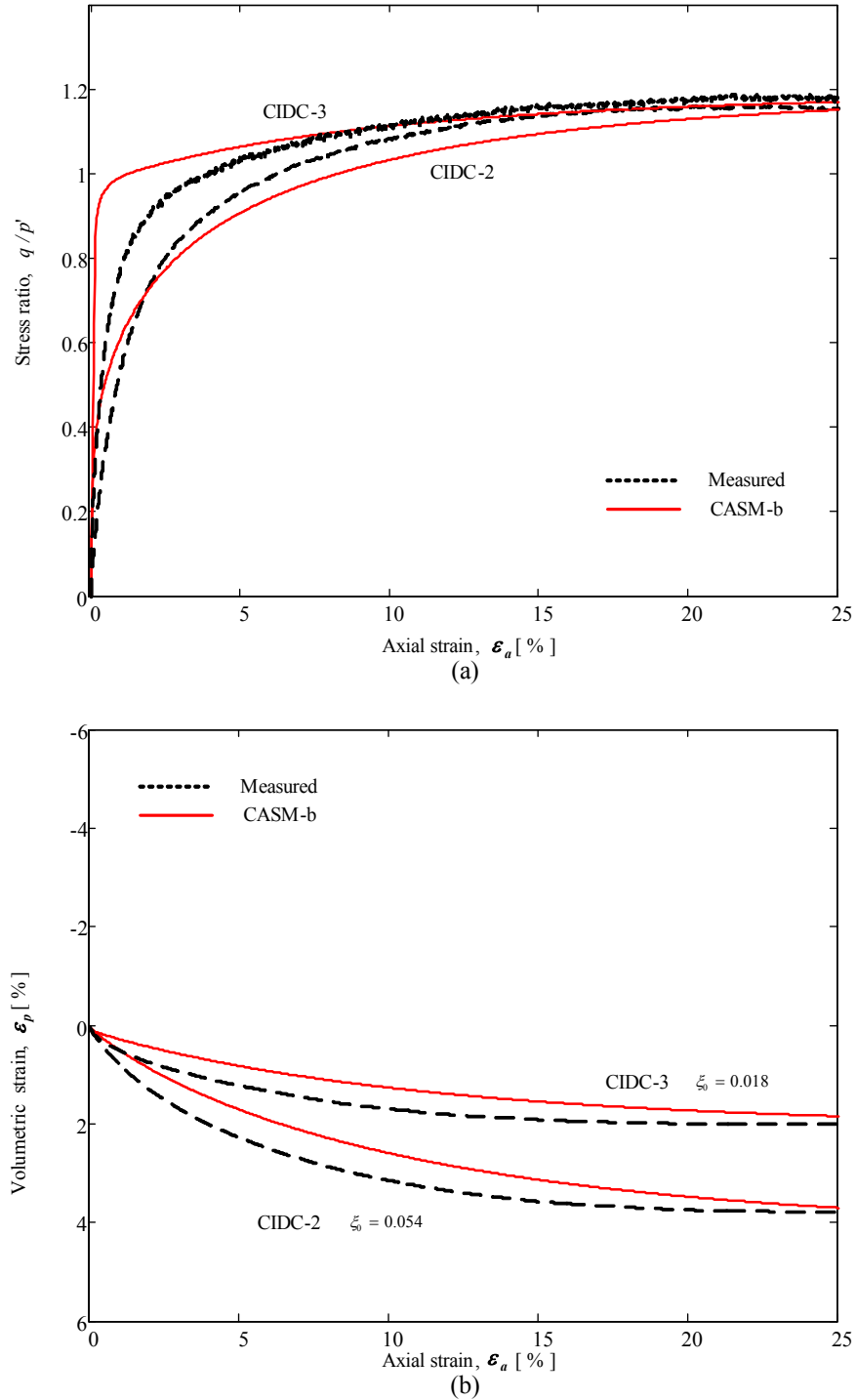


Figure 6-23. Comparison of CASM-b with measured behaviour for CIDC tests (CIDC-2 and 3).

6.7.2 Undrained Tests (CIUC-4 and CIUC-6)

Effective stress paths of two loose specimens CIUC-4 and CIUC-6 are shown in Figure 6-24. The flow liquefaction lines defined in section 4.4.3 are also indicated. It can be seen that the slope of the flow liquefaction line has a higher value with lower initial state parameter. The simulated results by CASM-b reflect the instability of Portaway sand well. Although the model somewhat over-predicted the peak strength, overall agreement is achieved.

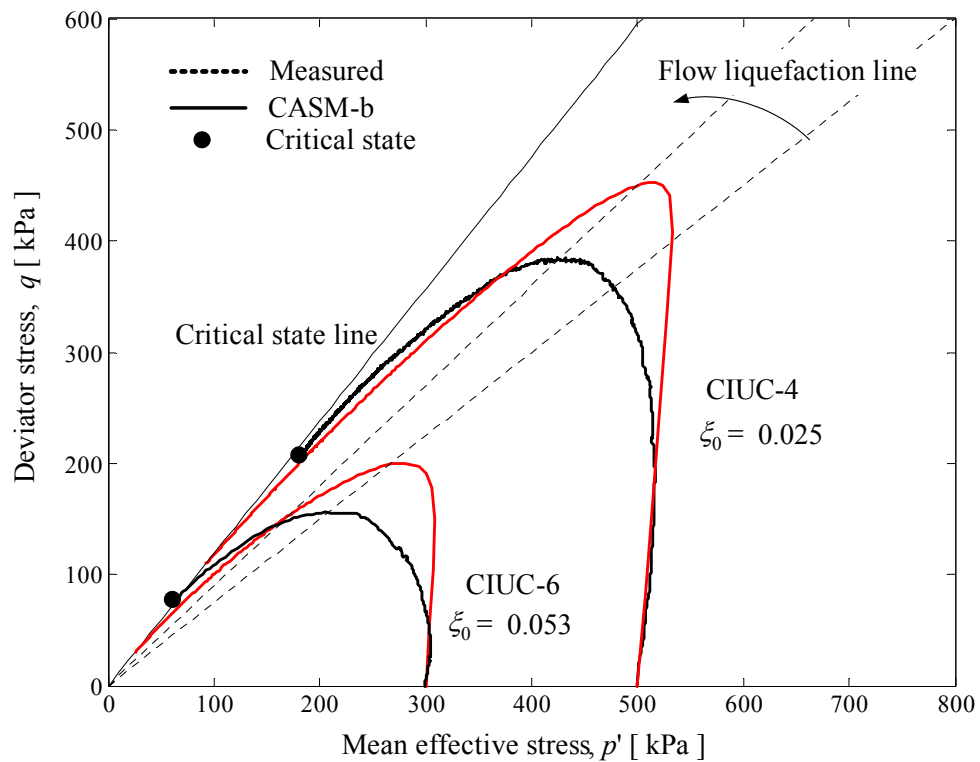


Figure 6-24. Comparison of CASM-b with measured behaviour for CIUC tests (CIUC-4 and 6).

6.8 MODEL PERFORMANCE – CASM-C

To evaluate the performances of CASM-c, four drained and undrained triaxial tests were simulated on very loose Portaway sand with the same initial consolidation stress of 300 kPa. Table 6-7 and Table 6-8 show the material constants used in CASM-c and the initial conditions of specimens, respectively.

Table 6-7. CASM-c constants for Portaway sand.

μ	κ	λ	Γ	M	n	r
0.16	0.005	0.025	1.796	1.19	3.5	19.2

h	m	H_U	H_R	k
5	1	0.1-0.4	3-10	100-200

Table 6-8. The triaxial tests used for CASM-c predictions.

Test	e_0	ξ_0	q_{cyc} (kPa)	Behaviour
OWDC-1	0.678	0.026	+ 200	Contraction at virgin loading, then undergoing dilation
OWUC-5	0.712	0.060	+115	Building up excess pore pressure and liquefied at 44 th cycle
OWUE-6	0.711	0.059	-85	Building up excess pore pressure and liquefied at 24 th cycle
TWD-3	0.712	0.060	+190–145	Continuing densification and achieving the state of shakedown after 8 th cycle

Notes:

OWDC = One-way drained loading in compression

OWUC = One-way undrained loading in compression

OWUE = One-way undrained loading in extension

TWD = Two-way drained loading with constant mean effective stress

6.8.1 One-Way Drained Cyclic Loading Tests (OWDC-1)

Figure 6-25 compares the predicted and measured stress-strain behaviour of medium loose sand (OWDC-1) under one-way drained cyclic loading in compression. Although the simulated virgin loading is stiffer than measured behaviour, the general agreement is achieved between the computed and measured data. CASM-c successfully reproduces the accumulated plastic deformation and resilient behaviour except the observed hysteretic loops. It is noted that smooth virgin loading curve is predicted by CASM-c and this cannot be achieved by any traditional elastic-plastic hardening/softening models.

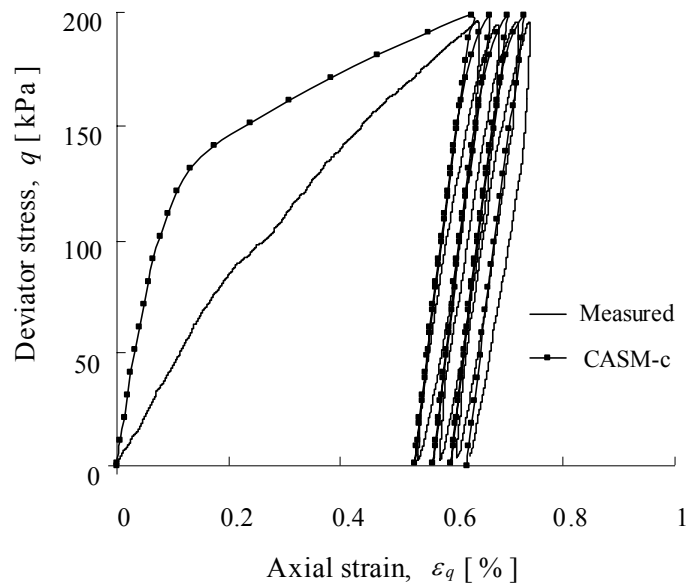


Figure 6-25. Comparison of CASM-c with measured behaviour for test OWDC-1.

$$(H_U = 0.1, H_R = 5.0, k = 200)$$

6.8.2 One-Way Undrained Cyclic Loading Tests (OWUC-5 and OWUE-6)

Figure 6-26 and Figure 6-27 show the results of one-way undrained cyclic loading in compression and extension, respectively on very loose specimens and their model simulations. Here, again, the simulated stress paths, stress-strain relationships and excess pore pressure developments are in general agreement with the experimental

results. Three distinct stages are discussed and only first two stages are modelled by CASM-c:

- Virgin loading: CASM-c captures two important features for test OWUC -5 during this stage, which are the occurrences of significant effective stress reduction and excess pore pressure increase at first cycle. The tendency of increase of excess pore pressure is not obvious in extension (OWUE-6), which is also predicted by the model.
- Before liquefaction: 20 cycles are simulated by CASM-c. A striking feature of the effective stress path at this stage is that significant reduction of mean effective stress occurs in the unloading segment, which is in agreement with many other independent experimental observations (e.g. De Gennaro et al., 2004; Ishihara et al., 1975). A slight increase of mean effective stress is observed in reloading segment. It can be seen that simulations of CASM-c follow the trends of the experimental stress paths very well, but observed hysteretic loops are not captured in the simulations on excess pore pressure and deviatoric stress versus axial strain.
- After liquefaction: This stage is characterised by rapid changes in plastic deformation, shear strength and excess pore pressure. The measured excess pore pressure is considered unreliable due to dynamic effect. Therefore, no attempts are made by CASM-c to match this kind of unstable behaviour.

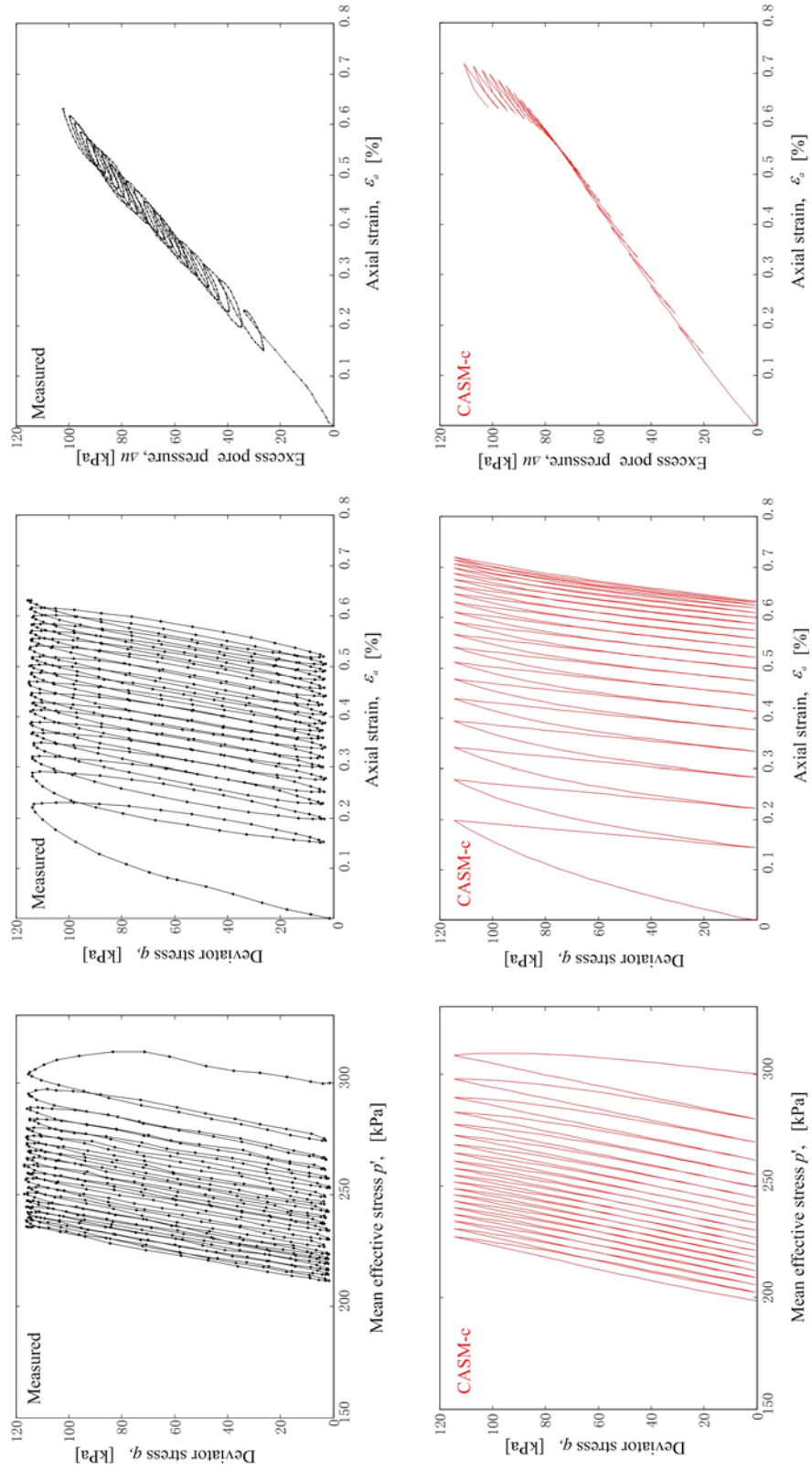


Figure 6-26. Comparison of CASM-c with measured behaviour for test OWUC-5.

$$(H_U = 0.1, H_R = 3.0, k = 200)$$

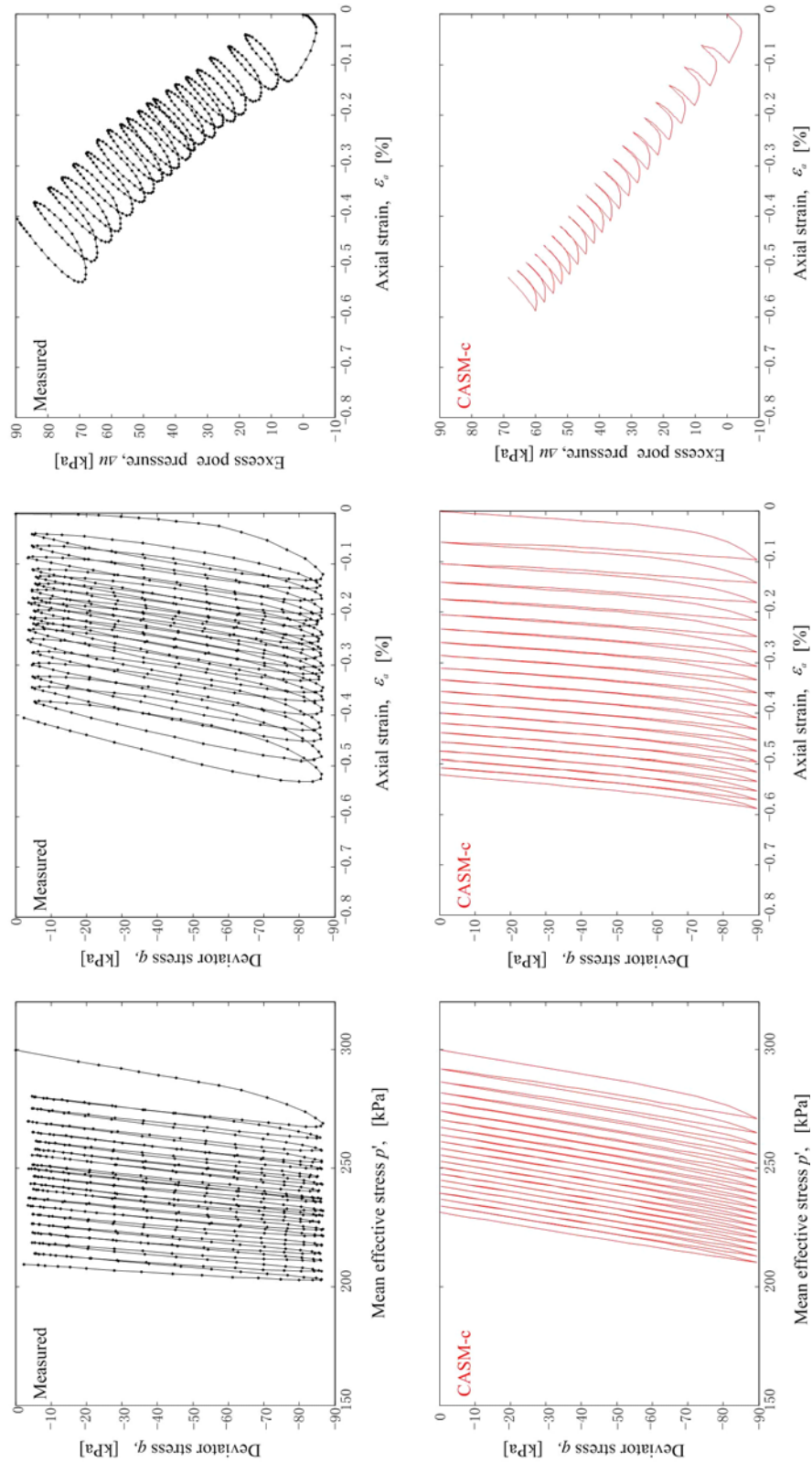


Figure 6-27. Comparison of CASM-c with measured behaviour for test OWUE-6.

$$(H_U = 0.4, H_R = 10.0, k = 100)$$

6.8.3 Two-Way Drained Cyclic Loading Tests (TWD-3)

The prediction of a two-way drained cyclic loading test on very loose Portaway sand is shown in Figure 6-28. A constant mean effective stress is maintained throughout the cyclic shearing. It can be seen that the size of stress-strain hysteretic loops is decreasing and the specimen is undergoing densification continuously with cycles. It is evident that the specimen has reached a ‘plastic shakedown’ state after 8 cycles, at which the elastic behaviour is dominant. The simulation of the model broadly matches the experimental results, although the agreement between the simulated and experimental volumetric strains is less precise than that of stress-strain relationship. It has also been illustrated in the simulation that the observed hysteretic loops can be reasonably well captured in this test by CASM-c.

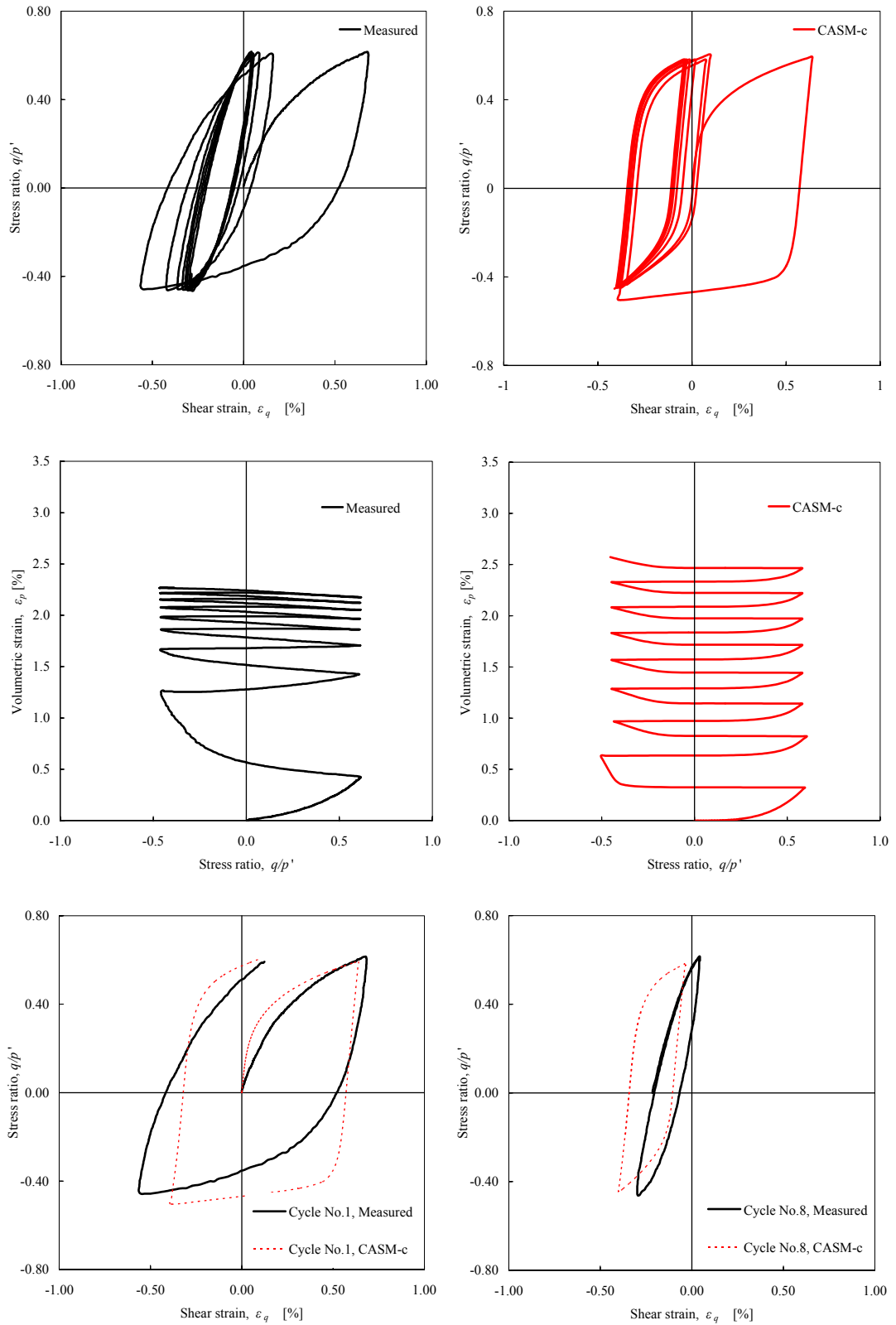


Figure 6-28. Comparison of CASM-c with measured behaviour for test TWD-3.

$$(H_U = 0.2, H_R = 5.0, k = 100)$$

6.9 SUMMARY

This chapter has presented an experimental evaluation of several plasticity models for sand. In general, the overall stress-strain behaviour of Portaway sand observed in both triaxial compression and extension tests can be well captured by these models. Some drawbacks of the original model CASM were identified experimentally and then tackled theoretically, which led to the developments of the following modified CASM models:

- CASM-d: The concept of combined hardening was assumed in CASM-d, in which the hardening is controlled not only by volumetric plastic strain rate but also by deviatoric plastic strain rate. In this extended model, only one additional model parameter α was introduced. By setting $\alpha = 0$, the new model CASM-d reduces to the original model CASM. In particular, the new model is able to simulate the undrained experimental behaviour of loose sands showing further hardening after exhibiting a softening behaviour.
- CASM-b: The bounding surface theory was introduced in CASM-b in order to allow the occurrence of the plastic deformation within the yield surface. A smooth transition of stiffness from the elastic region to elastic-plastic region is achieved using two additional model parameters h and m .
- CASM-c: The monotonic bounding surface model CASM-b was further extended to enable the cyclic behaviour to be modelled. The results of simulations show that CASM-c can predict hysteretic loops, accumulated plastic deformations and pore pressure developments of Portaway sand with a reasonable degree of accuracy. In addition, by introducing three new model parameters, H_U , H_R and k , the unloading behaviour, the reloading behaviour and shakedown behaviour can be modelled in a very flexible way.

Chapter 7

Concluding Remarks

7.1 SUMMARY AND CONCLUSIONS

A combined experimental and numerical investigation has been undertaken in order to gain some insight into the stress-strain and strength characteristics of sand under monotonic and cyclic loading conditions. The motivations behind this study were as follows:

- (a) To evaluate and extend the capabilities of the triaxial systems at the University of Nottingham to include the testing of sands;
- (b) To gain a better understanding of the stress-strain and strength characteristics of Portaway sand;
- (c) To present a simple procedure for determining all the model parameters from the triaxial test results;
- (d) To evaluate and verify the unified critical state model CASM and its extensions through comparison of experimental and numerical studies.

Objective (a) was met by first carrying out a full appraisal of the existing triaxial testing techniques and subsequently completing preliminary tests on dry sand using the NDTTS with necessary modifications and calibrations of the system. A complete testing procedure was then established for the ADVTTTS to test saturated sand. Objectives (b) and (c) were achieved through an extensive triaxial testing program under both monotonic and cyclic loading conditions. Objective (d) was met by first performing parametric studies on four plasticity models and then comparing the numerical results with the experimental data presented in Chapter 4 and Chapter 5.

In the following sections, these four aspects of the work are summarised, conclusions drawn, and recommendations for future work presented.

7.1.2 Experimental Techniques

The existing NDTTS was updated by commissioning an improved control system, a new triaxial cell and several additional transducers. A novel ‘on-specimen’ device was developed to measure the volumetric strain during testing of dry sand. The ADVTTTS supplied from GDS Ltd is capable of testing both sands and clays under drained or undrained conditions. Procedures were established for performing specimen preparation, saturation, consolidation and data correction.

Evaluations and Modifications (NDTTS)

- *Loading system:* the current system can provide a reasonable response for a loading frequency below 2 Hz.
- *Triaxial cell:* the existing triaxial cell was replaced by a new cell (see Figure 3-5), which has a maximum safe working pressure of 1000 kPa.
- *Calibration of transducers:* the load cell and LVDTs have been calibrated before each test as a matter of course. All the transducers are of AC type, which are compatible with the conditioning unit.

- *Control system and data acquisition:* the existing Dartec system was replaced by an Automated Testing System. The facility performed well throughout the test work. Five channels were available with the current configuration, although the system can be extended up to 16 channels.
- *'On-specimen' device:* a miniature LVDT transducer was employed to monitor the radial strain at the mid-height of the specimen.

Testing Method

- *Specimen preparation:* the methods of moist tamping and pluviation were developed to obtain a uniform sand specimen with any desired void ratio. The specimen preparation method was found to have a profound effect on the stress-strain behaviour of sands, but no influence on their strength at the critical state.
- *Stress path application:* only conventional drained tests were carried out using the NDTTS, while the full range of stress paths for triaxial tests were performed with the ADVTTS.
- *Saturation:* the saturation technique employed herein provided satisfactory results for most specimens tested. The process, however, lasted for 12 hours; this may be shortened by feeding carbon dioxide under low pressure through the specimens before flushing with water.
- *Determination of initial void ratio:* the volume change in the stage of saturation was taken into account during calculation of initial void ratio before shearing. Isotropic deformations were assumed in saturation.

7.1.3 Main Experimental Results

A large number of triaxial tests were performed on both dry and saturated Portaway sand (with four additional tests on Leighton Buzzard sand). Various stress paths and loading patterns have been applied to the specimens. From the

experimental results, some important conclusions have emerged and are summarised as follows:

Basic properties of Portaway sand

- *Composition of the sand:* the mineralogy of Portaway sand is mainly quartz. The fines content (percentage by weight smaller than 75 μm sieve size) is less than 2%. The red and brown colours are due to the existent of oxide of iron.
- *Index properties:* the maximum and minimum void ratios are 0.46 and 0.79, respectively. The particle size distribution indicates that Portaway sand is a well-graded, medium sand. The shapes of grains range from subrounded to subangular.
- *Critical state and elastic constants:* the critical state and elastic constants determined in Chapter 4 are summarised in Table 7-1.

Table 7-1. Critical state and elastic constants for Portaway sand.

μ	κ	λ	Γ	M_c	M_e
0.16	0.005	0.025	1.796	1.19	0.7

- *Experimental state boundary surface:* the general ‘stress ratio-state parameter’ relation can be used to describe the state boundary surface of Portaway sand very well. This supports the fundamental assumption made in CASM and its extensions. The stress-state coefficient n was found to equal 3.5 for Portaway sand.
- *Spacing ratio:* the spacing ratio r is fixed at 2.72 and 2.0 in original and modified Cam-clay models, respectively, while it was found that 19.2 is a suitable value for Portaway sand. The corresponding reference state parameter ξ_R is equal to 0.06.

Behaviour under monotonic loading

- *Critical state friction angle:* the critical state friction angles are about 29.8° and 24.5° in compression and extension, respectively. The specimen when packed in dense state, is not suitable for determining the critical state using conventional drained tests. This is due to the fact that excessive non-uniformity occurs inside the specimen.
- *Critical state line:* a unique *CSL* was obtained ($p' < 1000$ kPa), which is independent of the initial conditions, drainage conditions and specimen preparation method.
- *Stress-dilatancy relation:* Rowe's relation represents the observed behaviour of Portaway sand very well in the loose state. After passing the critical state stress ratio, Rowe's relation seems to overestimate the stress ratios for specimens packed in dense states.
- *State parameter concept:* the stress-strain and strength characteristics are controlled by the state parameter prior to reaching the critical state.
- *Flow liquefaction line:* the flow liquefaction line is not unique, but varies with the state parameters in undrained conditions. The correlation between the flow liquefaction line and the state parameter has been defined (see Figure 4-41).
- *Small strain behaviour:* a threshold yield strain of 0.001-0.0015% has been determined for Portaway sand. This is appropriate for various uncemented sands.

Behaviour under cyclic loading

- *Strength:* the strength at the critical state is not affected by pre-cyclic loading in drained conditions. Undrained cyclic shear strength is dependent on the initial condition, the cyclic stress ratio and the type of loading.

- *Stress path effects*: the specimens undergoing various stress paths as shown in section 5.5 show different characteristics. The conventional method (path CD) commonly used in pavement engineering may lead to an unsafe design.
- *Experimental state boundary surface*: the state boundary surface defined under monotonic loading is also applicable to cyclic loading.

7.1.4 Experimental Evaluation of CASM and Its Extensions

With respect to the evaluation and verification of the four plasticity models, the following conclusions have been drawn:

- *CASM*: all the material constants used in CASM have been determined and are discussed in Chapter 4. The parametric study shows that CASM can be used satisfactorily to model sands with different hardening and softening responses by varying the model constants. A total of seven typical monotonic tests were simulated using CASM. The predicted stress-strain curves and excess pore pressure changes match the experimental data very well. It was found, however, that CASM consistently under-estimates the axial or shear strain at the peak strength. Another shortcoming of CASM is that the predicted curve has an abrupt stiffness transition.
- *CASM-d*: the original CASM model assumes that hardening depends solely on plastic volumetric strain. Loose sand under undrained monotonic loading (e.g. ICUC-7), however, showed that plastic shear strain might also contribute to hardening. In order to simulate this particular behaviour of sands (quasi-steady state as defined in section 2.2.3), a new model parameter α was introduced in CASM-d. The parameter α was calibrated as 0.02 for Portaway sand.

- *CASM-b*: one of the disadvantages mentioned above for the original CASM model has been successfully tackled by incorporating bounding surface plasticity theory into CASM. The penalty, however, is that two more model parameters h and m are needed. These were found to be 5 and 1, respectively, by fitting the numerical results to the experimental data.
- *CASM-c*: Three more parameters, H_U , H_R and k were introduced into the cyclic model CASM-c with respect to monotonic bounding surface model CASM-b. The four cyclic tests presented in Chapter 5 were predicted with CASM-c. The results of the model simulations show encouraging agreement with the data obtained from triaxial tests subjected to one-way and two-way cyclic loading conditions.

7.2 ORIGINAL CONTRIBUTIONS

The research work presented in this thesis has made the following contributions:

- Modifications and improvements have been made to existing equipment, technique. The developments of an ‘on-specimen’ measuring instrument and tamping device have allowed testing of granular materials with fine grains (Chapter 3).
- The interpretation of results obtained from an extensive triaxial test should lead to a better understanding of the stress-strain and strength characteristics of Portaway sand within the critical state soil mechanics framework (Chapter 4 and Chapter 5).
- For the first time, CASM and its extensions have been thoroughly assessed and validated with experimental data from sand. (Chapter 6).

This research work has provided further evidence supporting the application of the critical state theory and state parameter concept to sands. The investigation into the state boundary surface of Portaway sand using monotonic and cyclic loading triaxial tests confirm that the ‘general stress ratio-state parameter’ relation assumed in CASM offers a suitable framework for modelling sand behaviour.

7.3 RECOMMENDATIONS FOR FUTURE RESEARCH

It is clear that the current research has provided some understanding of the fundamental behaviour of uncemented sands. However, there are a number of unanswered questions and the need for further research to be carried out on both the experimental aspect as well as the theoretical aspect. The following points outline the areas in which future research could be carried out.

7.3.1 Experimental Testing

The modifications made to the NDTTS in this research program were not complete. Only dry sand was tested with a constant cell pressure. For the development and verification of new constitutive models, it is necessary to apply various stress paths to the specimens. Therefore, further efforts should be placed on developing a complete stress path controlled triaxial system based on the current work.

Research is also needed to study the aspects of the stress-strain and strength characteristics that were not covered in this thesis. These include:

- Unsaturated behaviour;
- Anisotropic consolidated behaviour;
- Creep and aging behaviours.

7.3.2 Theoretical Modelling

The state parameter models CASM and its extensions presented in this thesis appear to offer a simple theoretical framework for modelling sand behaviour under both monotonic and cyclic loading. The models have been validated using experimental data from reconstituted Portaway sand. More laboratory tests on cemented sands are required in order to further extend those models by taking the ‘structure’ into consideration.

With respect to the phase transition and liquefaction exhibited by Portaway sand, there is a need for further research in order to clarify what is the main cause of the two different behaviours observed in the tests. It is believed that a boundary line exists in the $\ln p' - \nu$ space to separate the initial conditions with or without the occurrence of the phase transformation state, which should lie between the *RCL* and *CSL*. More triaxial tests could be conducted to define this threshold condition to enable the combined hardening model CASM-d to be used in a rational way.

The new model parameters H_U , H_R and k introduced in CASM-c have been chosen arbitrarily in Chapter 6 in order to match the experimental data. It is believed that these parameters are dependent on several factors such as intrinsic properties of soils, stress history and state parameters. A systematic testing program needs to be designed to clarify the influencing factors on these parameters.

References

- Alarcon-Guzman, A., Leonards., G.A. & Chameau, J.L. (1988). Undrained monotonic and cyclic strength of sands. *Journal of Geotechnical Engineering, ASCE* **114**, No. 10, 1089-1108.
- Arthur, J.R.F. (1971). New techniques to measure new parameters. *Stress-strain behaviour of soils, Roscoe Memorial Symposium*, G.T. Foulis & Co. LTD, 340-346.
- ASTM, D4523. (1996). American Society for Testing and Materials. *Standard Test Methods for Maximum Index Density and Unit Weight of Soils Using a Vibratory Table*.
- ASTM, D4524. (1996). American Society for Testing and Materials. *Standard Test Methods for Minimum Index Density and Unit Weight of Soils and Calculation of Relative Density*.
- Austin, G. (1979). The behaviour of Keuper Marl under undrained creep and repeated loading. *PhD Thesis*, University of Nottingham.
- Baldi, G., Hight, D.W. & Thomas, G.E. (1988). A reevaluation of conventional triaxial test methods. *ASTM STP* **977**, 219-263.
- Baldi, G. & Nova, R. (1984). Membrane penetration effects in triaxial testing. *Journal of Geotechnical Engineering, ASCE* **110**, 403-420.
- Bardet, J.F. (1986). Bounding surface plasticity model for sands, *Journal of Engineering Mechanics, ASCE* **112**, No.11, 1198-1217.
- Barksdale, R.D. (1972). Laboratory of rutting in base course materials. Proceedings of *3rd International Conference on Structural Design of Asphalt Pavements*, London, 161-174.
- Been, K. & Jefferies, M.G. (1985). A state parameter for sands. *Géotechnique* **35**, No. 2, 99-112.
- Been, K., Jefferies, M.G. & Hachey, J. (1991). The critical state of sands. *Géotechnique* **41**, No. 3, 365-381.

-
- Been, K., Jefferies, M.G. & Hachy, J. (1992). Discussion on: The critical state of sands. *Géotechnique* **42**, No. 4, 655-663.
- Bishop, A. W. & Henkel, D. J. (1957). *The Measurement of Soil Properties in the Triaxial Test*. Edward Arnold Ltd.
- Bishop, A.W. & Wesley, L.D. (1975). A hydraulic triaxial apparatus for controlled stress path testing. *Géotechnique* **25**, No. 4, 657-670.
- Bolton, M.D. (1986). The strength and dilatancy of sands. *Géotechnique* **36**, No. 1, 65-78.
- Boyce, J.R. (1980). A non-linear model for the elastic behaviour of granular materials under repeated loading. *Proceedings of International Symposium of Soils under Cyclic Transient Loading*, Swansea, 285-294.
- Boyce, J.R. & Brown, S.F. (1976). Measurement of elastic strain in granular material, technical note, *Géotechnique* **26**, No. 4, 637-640.
- British Standards. (1990). *BS 1377: British Standard methods of test for soils for civil engineering purposes*. B.S.I, London.
- British Standards. (1990). *BS 1377-2: Classification Tests, Determination of Particle Size Distribution*. B.S.I, London.
- British Standards. (1990). *BS 1377-4: Compaction-related Tests. Determination of Maximum and Minimum Dry Densities for Granular Material*. B.S.I, London.
- British Standards. (1990). *BS 1377-8: Shear Strength Tests (effective stress), Consolidated Drained and Undrained Triaxial Compression Tests*. B.S.I, London.
- Britto, A.M. & Gunn, M.J. (1987). *Critical State Soil Mechanics via Finite Elements*. John Wiley & Sons.
- Brown, S.F. (1967). Stresses and deformations in flexible layered pavement systems subjected to dynamic loads. *PhD Thesis*, University of Nottingham.
- Brown, S.F. (1996). Soil mechanics in pavement engineering. *Géotechnique* **46**, No. 3, 383-426.

-
- Brown, S.F., Austin, G. & Overy, R.F. (1980). An instrumented triaxial cell for cyclic loading of clays. *Geotechnical Testing Journal* **3**, No. 4, 145-152.
- Brown, S.F. & Hyde, A.F.L. (1975). The significance of cyclic confining stress in repeated load triaxial testing of granular materials. *Transportation Research Record*, No. 537, 49-58.
- Brown, S.F., O'Reilly, M.P. & Pappin, J.W. (1989). A repeated load triaxial apparatus for granular materials, in *Unbound Aggregates in Road*, London, 143-158.
- Brown, S.F. & Snaith, M.S. (1974). The Measurement of recoverable and irrecoverable deformations in the repeated load triaxial test, *Géotechnique* **24**, No. 2, 255-259.
- Castro, G. (1969). Liquefaction of sands. *PhD Thesis*, Harvard University.
- Castro, G. (1975). Liquefaction and cyclic mobility of saturated sands. *Journal of Geotechnical Engineering, ASCE* **101**, No. 6, 551-569.
- Chan, F.W.K. (1990). Permanent deformation resistance of granular layers in pavements. *PhD Thesis*, University of Nottingham.
- Chan, F.W.K. & Brown, S.F. (1994). Significance of principal stress rotation in pavements. *Proceeding of 13th International Conference on Soil Mechanics and Foundation Engineering* **4**, Delhi, 1823-1826.
- Chandler, H.W. (1985). A plasticity theory without Drucker's postulate for granular materials. *Journal of the mechanics and physics of solids* **33**, 215-226.
- Cheung, L.W. (1994). Laboratory assessment of pavement foundation materials. *PhD Thesis*, University of Nottingham.
- Chu, J. (1995). An experimental examination of the critical state and other similar concepts for granular soils. *Canadian Geotechnical Journal* **32**, 1065-1075.
- Chu, J. & Leong, W.K. (2001). Pre-failure strain softening and pre-failure instability of sand: a comparative study. *Géotechnique* **51**, No. 4, 311-321.
- Chu, J., Lo, S-C.R. & Lee, I.K. (1992). Strain-softening behaviour of granular soil in strain-path testing. *Journal of Geotechnical Engineering, ASCE* **118**, No. 2, 191-208.

-
- Clayton, C. R. I, Khattrust, S. A., Bica, A. V. D. & Siddique, A. (1989). The use of hall effect semiconductors in geotechnical instrumentation. *Geotechnical Testing Journal* **12**, No. 1, 69-76.
- Collins, I.F. & Houlsby, G.T. (1997). Application of thermomechanical principles to the modelling of geotechnical materials. *Proceedings of Royal Society Series A* **453**, 1975-2001.
- Collins, I.F., Pender, M.J. & Wan, Y. (1992). Cavity expansion in sands under drained loading conditions. *Journal of Numerical and Analytical Methods in Geomechanics* **16**, 3-23.
- Coop, M.R. (1990). The mechanics of uncemented carbonate sands. *Géotechnique* **40**, No. 4, 607-626.
- Coop, M.R. & Lee, I.K. (1993). The behaviour of granular soils at elevated stresses. *Predictive Soil Mechanics, Wroth Memorial Symposium*, Thomas Telford, London, 1993, 186-198.
- Crouch, R.S., Wolf, J.P. & Dafalias, Y.F. (1994). Unified critical state bounding surface plasticity model for soil, *Journal of Engineering mechanics, ASCE* **120**, No.11, 2251-2270.
- Cuccovillo, T. & Coop, M.R. (1997). Yielding and pre-failure deformation of structured sands. *Géotechnique* **47**, No. 3, 491-508.
- Cuccovillo, T. & Coop, M.R. (1999). On the mechanics of structured sands. *Géotechnique* **49**, No. 6, 741-760.
- Dafalias, Y. F. (1975). On cyclic and anisotropy plasticity. *PhD Thesis*, University of California at Berkeley.
- Dawson, A., Thom, N.H. & Paute, J.L. (1996). Mechanical characteristics of unbound granular materials as a function of condition. *Flexible Pavements, Proceedings of Europe Symposium, Euroflex 1993*, Rotterdam, The Netherland, 35-44.

- De Gennaro, V., Canou, J., Dupla, J.C. & Benahmed, N. (2004). Influence of loading path on the undrained behaviour of a medium loose sand. *Canadian Geotechnical Journal* **41**, 166-180.
- GDS Instruments Limited. (2002). *GDS Laboratory manual*.
- Germaine, J.T. & Ladd, C.C. (1988). Triaxial testing of saturated cohesive soils. *Advanced Triaxial Testing of Soil and Rock, ASTM STP 977*, 421-459.
- Ghaboussi, J. & Momen, H. (1982). Modelling and analysis of cyclic behaviour of sands, *Soil Mechanics – Transient and Cyclic Loads, edited by Pande, G.N. and Zienkiewicz, O.C*, 313 - 342.
- Hardin, B.O. & Richard, F.E. (1963). Elastic wave velocities in granular materials. *Journal of Geotechnical Engineering, ASCE* **89**, No. SM1, 33-65.
- Hau, K.W. (2003). Application of a three-surface kinematic hardening model to the repeated loading of thinly surfaced pavements. *PhD Thesis*, University of Nottingham.
- Hicks, R.G. & Monismith, C.L. (1971). Factors influencing the resilient response of granular materials, *Highway Research Record*, No. 345, Highway Research Board, 15-31.
- Hird, C.C. & Hassona, F.A.K. (1990). Some factors affecting the liquefaction and flow of saturated sands in laboratory tests. *Engineering Geology* **28**, 149-170.
- Ishihara, K., Tatsuoka, F. & Yasuda, S. (1975). Undrained deformation and liquefaction of sand under cyclic stresses. *Soils and Foundations* **15**, 29-44.
- Ishihara, K. (1993). Liquefaction and flow failure during earthquakes. *Géotechnique* **43**, No. 3, 351-415.
- Ishihara, K. (1996). *Soil Behaviour in Earthquake Geotechnics*, Oxford.
- Jamiolkowski, M., Ladd, C.C., Germaine, J.T. & Lancellotta, F. (1985). New developments in field and laboratory testing of soils. *Proceedings of the 11th SMAFE* **1**, 57-155.
- Jamiolkowski, M., Lancellotta, R., Lo Presti, D.C.F. & Pallara, O. (1994). Stiffness of Toyoura sand at small and intermediate strain. *Proceedings of the 13th*

-
- International Conference on Soil Mechanics and Foundation Engineering*, New Delhi, 169-172.
- Jefferies, M.G. (1993). Nor-sand: a simple critical state model for sand. *Géotechnique* **43**, No.1, 91-103.
- Jefferies, M.G. & Been, K. (2000). Implications for critical state theory from isotropic compression of sand. *Géotechnique* **50**, No.4, 419-429.
- Jefferies, M.G. & Been, K. (2004). Discussion on: Non-uniqueness of flow liquefaction line for loose sand. *Géotechnique* **54**, No.1, 66-68.
- Jiang, M.J., Konrad, J.M. & Leroueil, S. (2003). An efficient technique for generating homogeneous specimens for DEM studies. *Computers and Geotechnics* **30**, 579-597.
- Johnson, K. L. (1986). Plastic flow, residual stresses and shakedown in rolling contacts. *Proceeding of the 2nd International Conference on Contact Mechanics and Wear of Rail/Wheel Systems*, University of Rhode Island, Waterloo Ontario.
- Karasahin. M. (1993). Resilient behaviour of granular materials for analysis of highway pavements. *PhD Thesis*, University of Nottingham.
- Khong, C.D. (2004). Development and numerical evaluation of unified critical state models. *PhD Thesis*, University of Nottingham.
- Klotz, E.U. & Coop, M.R. (2002). On the identification of critical state lines for sands. *Geotechnical Testing Journal* **25**, No. 3, 1-14.
- Koerner, R.M. (1970). Behaviour of single mineral soils in triaxial shear. *Journal of Geotechnical Engineering, ASCE* **96**, No. SM4, 1373-1390.
- Kolymbas, D. & Wu. W. (1990). Recent results of triaxial tests with granular materials. *Powder Technology* **60**, 99-119.
- Kolymbas, D. (1977). A rate-dependent constitutive equation for soils. *Mechanics Research Communications* **4**, 367-372.
- Konard, J.M. (1990). Minimum undrained strength versus steady-state strength of sands. *Journal of Geotechnical Engineering, ASCE* **116**, No. 6, 932-947.

-
- La Rochelle, P., Leroueil, S., Trak, B., Blais-Leroux, L. & Tavenas, F. (1988). Observational approach to membrane and area corrections in triaxial tests. *Advanced Triaxial Testing of Soil and Rock, ASTM STP 977*, 715-731.
- Lade, P.V. (1977). Elasto-plastic stress-strain theory for cohesionless soil with curved yield surfaces. *International Journal of Solids and Structures* **13**, 1019-1035.
- Lade, P.V. & Duncan, J.M. (1975). Elastoplastic stress-strain theory for cohesionless soil. *Journal of Geotechnical Engineering, ASCE* **101**, 1037-1053.
- Lade, P.V. & Duncan, J.M. (1976). Stress-path dependent behavior of cohesionless soil. *Journal of Geotechnical Engineering, ASCE* **102**, No. GT1, 51-68.
- Lade, P.V., Jerry, A. & Skyers, B.D. (1996). Effects of shear band formation in triaxial extension tests. *Geotechnical Testing Journal* **19**, No. 4, 398-410.
- Lade, P.V., Nelson, R.B. & Ito, Y. M. (1988). Instability of granular materials with nonassociated flow. *Journal of Engineering Mechanics, ASCE* **114**, No. 12, 2173-2191.
- Ladd, R.S. (1978). Preparing specimens using undercompaction. *Geotechnical Testing Journal* **1**, No. 1, 16-23.
- Lambe, T.W. (1967). Stress path method. *Journal of Geotechnical Engineering, ASCE* **93**, No. SM6, 309-331.
- Lam, W.K. & Tatsuoka, F. (1988). Effects of initial anisotropic fabric and σ_2 on strength and deformation characteristics of sand. *Soils and Foundations* **28**, No. 2, 89-106.
- Lee, I.K. (1966). Stress-dilatancy performance of feldspar. *Journal of Geotechnical Engineering, ASCE* **92**, No. SM2, 79-103.
- Lee, K.L. & Seed, H.B. (1967). Drained strength characteristics of sands. *Journal of Geotechnical Engineering, ASCE* **93**, No. SM6, 117-141.
- Lekarp, F., Isacsson, U. & Dawson, A. (2000). State of the art I: Resilient response of unbound aggregates. *Journal of Transportation Engineering, ASCE* **126**, No. 1, 66-75.

-
- Li, X.S., Dafalias, Y.F. & Wang, Z.L. (1999). State-dependent dilatancy in critical-state constitutive modeling of sand. *Canadian Geotechnical Journal* **36**, 599-611
- Lo Presti, D.C.F. (1995). General Report: Measurement of shear deformation of geomaterials in the laboratory. *International Symposium of Pre-Failure Deformation Characteristics on Geomaterials*, IS-Hokkaido **1**, 1067-1088.
- Luong, M.P. (1980). Stress-strain aspects of cohesionless soils under cyclic and transient loading. *International symposium on soil under cyclic and transient loading*, Swansea **1**, 7-11.
- McDowell, G.R., Nakata, Y. & Hyodo, M. (2002). On the plastic hardening of sand. *Géotechnique* **52**, No. 5, 349-358.
- McVay, M. & Taesiri, Y. (1985). Cyclic behavior of pavement base materials. *Journal of Geotechnical Engineering, ASCE* **111**, No. 1, 1-17.
- Menzies, B.K. (1988). A computer controlled hydraulic triaxial testing system. *Advanced Triaxial Testing of Soil and Rock, ASTM STP 977*, 82-94.
- Mitchell, J.K. (1976). *Fundamentals of Soil Behaviour*, New York, Wiley.
- Mitchell, J.K. (1993). *Fundamentals of Soil Behaviour*, New York, Wiley.
- Newland, P.L. & Allely, R.H. (1959). Volume changes during undrained triaxial tests on saturated dilatant granular materials. *Géotechnique* **9**, No. 10, 174-182.
- Nova, R. (1977). On the hardening of the soils. *Archiwum Mechaniki Stosowanej* **29**, 445-458.
- Oda, M. (1972). Initial fabrics and their relations to mechanical properties of granular material, *Soils and Foundations* **12**, No. 1, 17-37.
- O'Reilly, M.P. (1985). Mechanical properties of granular materials for use in thermal energy stores. *PhD Thesis*, University of Nottingham.
- O'Reilly, M.P. & Brown, S.F. (1991). *Cyclic Loading of Soils: from Theory to Design*, Blackie and Son LTD, Glasgow and London.
- Pappin, J.W. (1979). Characteristics of a granular material for pavement design. *PhD Thesis*, University of Nottingham.

-
- Polous, S.J. (1981). The steady state of deformation. *Journal of Geotechnical Engineering, ASCE* **107**, 553-562.
- Pradhan, T.B.S. & Tatsuoka, F. (1989). On stress-dilatancy equations of sand subjected to cyclic loading. *Soils and Foundations* **29**, No. 1, 65-81.
- Pradhan, T.B.S., Tatsuoka, F. & Sato, Y. (1989). Experimental stress-dilatancy relations of sand subjected to cyclic loading. *Soils and Foundations* **29**, No. 1, 45-64.
- Preseta, J.M. & Whittle, A.J. (1999). Formulation of a unified constitutive model for clays and sands. *Journal of Numerical and Analytical Methods in Geomechanics* **23**, 1215-1243.
- Prévost, J.H. (1978) Plasticity theory for soil stress-strain behaviour. *Journal of the Engineering Mechanics, ASCE*, **104**, No. 5, 1177-1194.
- Raybould, M.J. (1992). The Response of silt-clay mixtures to cyclic loading. *PhD Thesis*, University of Nottingham.
- Richardson, I.R. (1999). The stress-strain behaviour of dry granular material subjected to repeated loading in a hollow cylinder apparatus. *PhD Thesis*, University of Nottingham.
- Riemer, M.F. & Seed, R.B. (1997). Factors affecting apparent position of steady-state line. *Journal of Geotechnical Engineering, ASCE* **123**, No. 3, 281-288.
- Roscoe, K.H. & Burland, J.B. (1968). On the Generalised Stress-Strain Behaviour of Wet Clay, *Engineering Plasticity*, Cambridge University Press, 535-609.
- Roscoe, K.H. & Poorooshasb, H.B. (1963). A fundamental principal of similarity in model tests earth pressure problems. *Proceedings, 2nd Asian Conference on Soil Mechanics* **1**, 134-140.
- Roscoe, K.H. & Schofield, A.N. (1963). Mechanical behaviour of an idealised wet clay. *Proceedings of the European Conference on Soil Mechanics and Foundation Engineering* **1**, 47-54.
- Roscoe, K.H., Schofield, A.N. & Wroth, C.P. (1958). On the yielding of soils. *Géotechnique* **8**, No.1, 22-53.

-
- Rowe, P.W. (1962). The Stress-dilatancy relation for static equilibrium of an assembly of particles in contact. *Proceeding of Royal Society* **A269**, 500-527.
- Sasitharan, S., Robertson, P. K. & Morgenstern, N.R. (1993). Collapse behaviour of sand. *Canadian Geotechnical Journal* **30**, 569-577.
- Schofield, A.N. & Wroth, C. P. (1968). *Critical State Soil Mechanics*, McGraw-Hill, London.
- Seed, H.B., Chan, C.K. & Lee, C.E. (1962). Resilience characteristics of subgrade soils and their relation to fatigue failure. *Proceeding of International Conference of Structural Design of Asphalt Pavements*, Ann Arbor, Michigan, 611-636.
- Shaw, P. (1980). Stress-strain relationships for granular materials under repeated loading. *PhD Thesis*, University of Nottingham.
- Shaw, P. & Brown, S.F. (1986). Cyclic simple shear testing of granular materials. *Geotechnical Testing Journal* **9**, No. 4, 213-220.
- Sheng, D., Sloan, S.W. & Yu, H.S. (2000) Aspects of finite element implementation of critical state models. *Computational Mechanics* **26**, 185-196.
- Silver, M., Chan, C., Ladd, R., Lee, K., Tiedmann, D., Townsend, F., Valera, J. & Wilson, J. (1976). Cyclic strength of standard test sand. *Journal of Geotechnical Engineering, ASCE* **102**, No. 5, 511-523.
- Sladen, J.A., D'Hollander, R. D. & Krahn, J. (1985). The liquefaction of sands, a collapse surface approach. *Canadian Geotechnical Journal* **22**, 564-578.
- Sladen, J.A. & Oswell, J.M. (1989). The behaviour of very loose sand in the triaxial compression test. *Canadian Geotechnical Journal* **26**, 103-113.
- Sladen, J.A. & Handford, G. (1987). A potential systematic error in laboratory testing of very loose sands. *Canadian Geotechnical Journal* **24**, 462-466.
- Stallebrass, S.E. (1990) The effect of recent stress history on the deformation of overconsolidated soils, *PhD Thesis*, City University, UK.
- Stroud, M.A. (1971). The behaviour of sand at low level in the simple shear apparatus. *PhD Thesis*, University of Cambridge.

-
- Sousa, J.B. & Chan, C. K. (1991). Computer applications in the geotechnical laboratories of the University of California at Berkeley, *Proceedings of Geotechnical Engineering Conference, ASCE*, Boulder, Colorado.
- Sweere, G.T.H. (1990). Unbound granular bases for roads. *PhD Thesis*, University of Delft, The Netherlands.
- Tatsuoka, F. (1972). Shear tests in a triaxial apparatus – A fundamental study of the deformation of sand. *PhD Thesis*, Tokyo University.
- Tatsuoka, F. (1988). Some recent developments in triaxial testing systems for cohesionless soils. *Advanced Triaxial Testing of Soil and Rock, ASTM STP 977*, 7-67.
- Tatsuoka, F. & Ishihara, K. (1973) Stress path and dilatancy performance of a sand. *Proceedings of the 8th International Conference on Soil Mechanics and Foundation Engineering* **1**, No. 2, 419-424.
- Tatsuoka, F. & Ishihara, K. (1974a). Yielding of sand in triaxial compression. *Soils and Foundations* **14**, No. 2, 63-76.
- Tatsuoka, F. & Ishihara, K. (1974b). Drained deformation of sand under cyclic stresses reversing direction. *Soils and Foundations* **14**, No. 3, 51-65.
- Tatsuoka, F., Sakamoto, M., Kawamura, T. & Fukushima, S. (1986). Strength and deformation characteristics of sand in plane strain compression at extremely low pressures. *Soils and Foundations* **26**, 65-84.
- Thurairajah, A. (1973). Shear behaviour of sand under stress reversal. *Proceedings, 8th International Conference on Soil Mechanics and Foundation Engineering*, 439-445.
- Vaid, Y.P., Chung, E.K.F. & Kuerbis, R.H. (1990). Stress path and steady state. *Canadian Geotechnical Journal* **27**, 1-7.
- Vaid, Y.P., Eliadorani, A., Sivathayalan, S. & Uthayakumar. M. (2001). Laboratory characterization of stress-strain behavior of soils by stress and/or strain path loading. *Geotechnical Testing Journal* **24**, No. 2, 200-208.
- Vaid, Y.P. & Sasitharan, S. (1992). The strength and dilatancy of sand. *Canadian Geotechnical Journal* **29**, 522-526.

-
- Vaid, Y.P., Sivathayalan, S. & Stedman, D. (1999). Influence of specimen-reconstituting method on the undrained response of sand. *Geotechnical Testing Journal* **22**, No. 3, 187-195.
- Vasquez, A. & Dobry, R. (1988). The behaviour of undrained contractive sand and its effect on the seismic liquefaction flow failure of earth structures. *Report of Rensselaer Polytechnic Institute*.
- Verdugo, R. (1992). Discussion on: The critical state of sands by Been, K., Jefferies, M.G. & Hachey, J. *Géotechnique* **42**, No. 4, 655-663.
- Verdugo, R. & Ishihara, K. (1991). Characterization of the undrained behaviour of sandy soils. *Int. Symp. Natural Disaster Reduction & Civ. Engng. Osaka, Japan* Society of Civil Engineers.
- Verdugo, R. & Ishihara, K. (1996). The steady state of sandy soils. *Soils and Foundations* **36**, No. 2, 81-91.
- Verdugo, R., Ishihara, K., Daud, A. & Towhata, I. (1989). Effects of aging and fine content on the undrained behaviour of sand. *Proceeding of the 44th Annual Conference of Japan Society for Civil Engineers* **3**, 484-485.
- Wood, D.M. (1982). Laboratory investigation of the behaviour of soils under cyclic loading: A review, *Soil Mechanics - Transient and Cyclic Loads*, edited by Pande, G.N. and Zienkiewicz, O.C, 513 - 582.
- Wood, D.M. (1990). *Critical State Soil Mechanics*, McGraw-Hill, London.
- Wood, D.M. (2004). Experimental inspiration for kinematic hardening soil models. *Journal of Engineering Mechanics, ASCE* **130**, No. 6, 656 – 664.
- Wroth, C.P. & Bassett, N. (1965). A stress-strain relationship for the shearing behaviour of sand. *Géotechnique* **15**, No. 1, 32-56.
- Wroth, C.P. & Houlsby, G.T. (1985). Soil mechanics - property characterization and analysis procedures. *Proceeding of the 11th International Conference on Soil Mechanics and Foundation Engineering* **1**, 1-57.
- Wu, W. (1998). Rational approach to anisotropy of sand. *Journal of Numerical and Analytical Methods in Geomechanics* **22**, 921-940.

-
- Wu, W. (2000). Non-linear analysis of shear band formation in sand. *Journal of Numerical and Analytical Methods in Geomechanics* **24**, 245-263.
- Wu, W. & Kolymbas, D. (1991). On some issues in triaxial extension tests. *Geotechnical Testing Journal* **14**, No. 3, 276-287.
- Wu, W. & Niemunis, A. (1997). Beyond failure in granular materials. *Journal of Numerical and Analytical Methods in Geomechanics* **21**, 153-174.
- Yamamuro, J.A. & Lade, P.V. (1997). Static liquefaction of very loose sands. *Canadian Geotechnical Journal* **34**, 905-917.
- Yang, J. (2002). Non-uniqueness of flow liquefaction line for loose sand. *Géotechnique* **52**, No. 10, 757-760.
- Yu, H.S. (1994). State parameter from self-boring pressuremeter tests in sand. *Journal of Geotechnical Engineering, ASCE* **120**, No. 12, 2118-2135.
- Yu, H.S. (1995). A unified critical state model for clay and sand. *Civil Engineering Research Report No 112.08.1995*. University of Newcastle, NSW 2308, Australia.
- Yu, H.S. (1996). Interpretation of pressuremeter unloading tests in sands. *Géotechnique* **46**, No. 1, 17-31.
- Yu, H.S. (1998). CASM: A unified state parameter model for clay and sand. *Journal of Numerical and Analytical Methods in Geomechanics* **22**, 621-653.
- Yu, H.S. (2000). *Cavity Expansion Methods in Geomechanics*, Kluwer Academic Publishers, The Netherlands.
- Yu, H.S. (2004). In situ testing: from mechanics to interpretation. *First James K. Mitchell Lecture, Proceedings of 2nd international conference on site characterization ISC-2*, Porto, Portugal, 1-38.
- Yu, H.S. & Khong, C.D. (2003). Bounding surface formulation of a unified critical state model for clay and sand *Proceeding of the 3rd International Symposium on Deformation Characteristics of Geomaterials*, Lyon, 1111-1118.
- Yu, H.S., Khong, C.D., Wang, J. & Zhang, G. (2004) Experimental evaluation and extension of a simple critical state model for sand models, Submitted to *Granular Matter*.

Zhang, G. (2002). Laboratory characterization of a highly weathered old alluvium in San Juan, Puerto Rico. *PhD Thesis*, Massachusetts Institute of Technology.

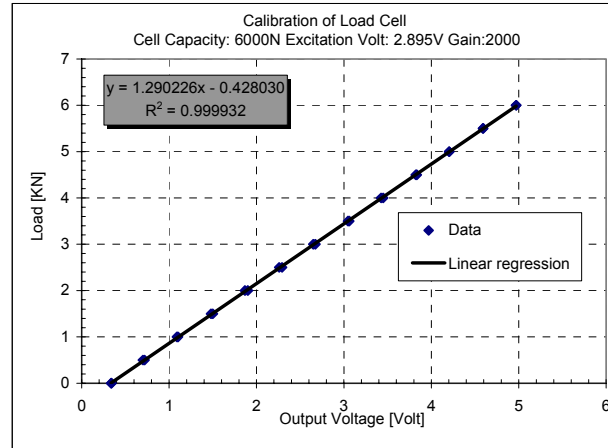
Appendix A - Updated Nottingham Dynamic Triaxial Testing System

A-1. Specifications

Purpose		The strength and deformation characteristics of soils under various stress paths when subjected to cyclic undrained / drained triaxial loading
Soil type		Mainly granular materials
Apparatus & tools	Triaxial cell	Stress path cell Internal tie bar
	Strain measurement	Two measurements of the axial deformation ε_a are taken: External deformation ε_a using a long stroke ACT2000A LVDT. Range, resolution are 100 mm and 24 μm , respectively. Internal deformation ε_a using miniature LVDT. Range, resolution are 10 mm and 1.2 μm , respectively. Radial deformation ε_r using miniature LVDT. Range, resolution are 10 mm and 1.2 μm , respectively.
	Confining pressure	< 1000 kPa
	Frequency and wave forms	0.1-10 Hz Triangle, square, and sinusoid
	Data sampling	A computer with a data acquisition board (C10-AD12) is used
	Loading system	Hydraulic loading system by E/P converter (Axial load and cell Pressure)
	Volume change	IC volume gauge
Specimen	Diameter	50 / 75 mm
	Height	100 / 150 mm
	Specimen preparation	Air pluvation and compaction method
Standards	ASTM D3999-91	Standard test method for the determination of the modulus and damping properties of soils using the cyclic triaxial apparatus
	ASTM D5311-92	Load controlled cyclic triaxial strength of soil
	BS1377	Soil for civil engineering purposes

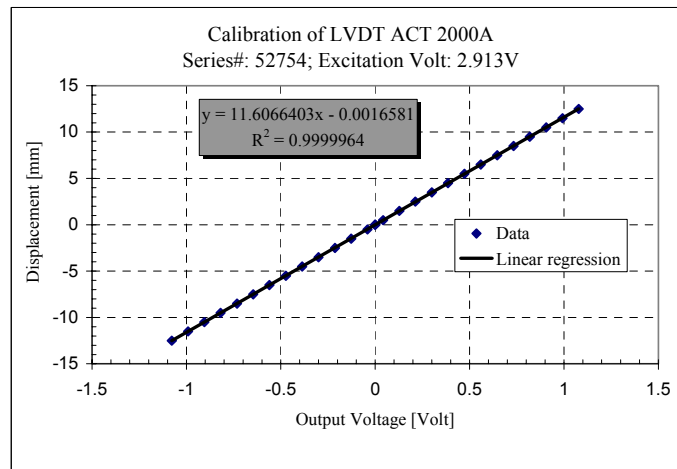
A-2. Calibration of the transducers

Rising		Falling	
Ref. Load (kN)	Output (v)	Ref. Load (kN)	Output (v)
0	0.338	0	0.34
0.5	0.701	0.5	0.719
1	1.089	1	1.102
1.5	1.479	1.5	1.5
2	1.868	2	1.901
2.5	2.259	2.5	2.293
3	2.65	3	2.674
3.5	3.046	3.5	3.061
4	3.425	4	3.448
4.5	3.822	4.5	3.833
5	4.203	5	4.205
5.5	4.594	5.5	4.59
6	4.97	6	4.97



(a)

Dis (mm)	Output (v)
0	0
0.5	0.042
1.5	0.128
2.5	0.213
3.5	0.3
4.5	0.386
5.5	0.473
6.5	0.559
7.5	0.646
8.5	0.733
9.5	0.819
10.5	0.906
11.5	0.992
12.5	1.078
0	0
-0.5	-0.041
-1.5	-0.127
-2.5	-0.213
-3.5	-0.3
-4.5	-0.387
-5.5	-0.473
-6.5	-0.56
-7.5	-0.646
-8.5	-0.732
-9.5	-0.819
-10.5	-0.905
-11.5	-0.991
-12.5	-1.077



(b)

A-3. Private communication (E-mail) with Dr. Matthew Coop



07/04/2003

A-4. Development of specimen preparation method for dry sand

In order to improve the specimen uniformity and obtain desired density of sands, a specimen preparation method using a newly developed compaction device was designed. The development of this tamping technique was inspired by the undercompaction method proposed by Ladd (1976).

Figure A-1. shows the schematic view of the tamping system. The specimens were prepared by attaching the split mould to the bottom platen of the triaxial cell.

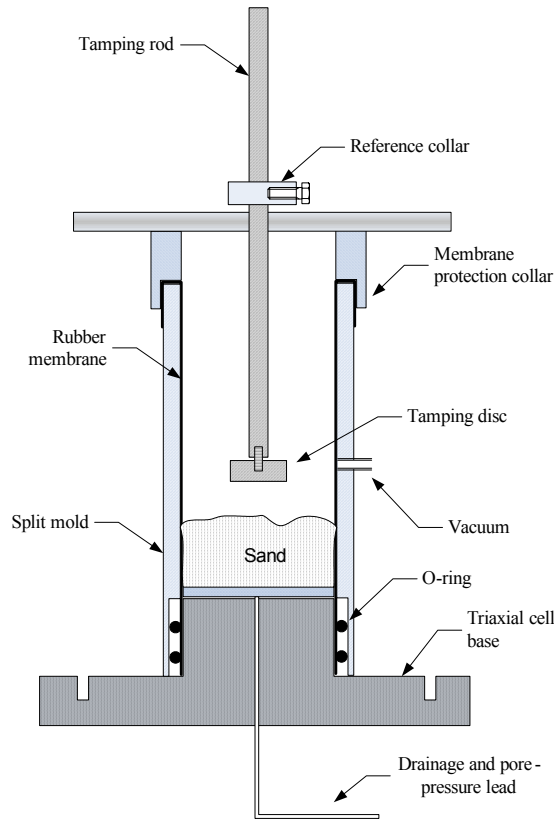


Figure A-1. Schematic view of a newly developed tamping device for Portaway sand.

The reason of using this kind of ‘internal’ split mould is that it eliminates many of the problems associated with the extrusion of the compacted specimens from a non-split mould (Ladd, 1976). Many researchers have questioned the validity and the efficiency of Ladd’s undercompaction technique for forming uniform sand specimens. For example, Vaid et al. (1999) argued that direct evidence showing the void ratio over the specimen height had rarely been presented using such method. More recently, Jiang et al. (2003) have theoretically demonstrated that Ladd’s method may not yield homogenous specimen. Hence, for practical purpose, six equal layers of sands with the same weight were compacted to predetermined heights for achieving any desired void ratio. The reference collar on the tamping rod as shown in Figure A-2 was used to obtain correct height of each layer. Following the procedure used by Ladd (1976), the surface of the sands was compacted in a circular pattern starting at the periphery of the mould and gradually tamping toward the centre of the mould (see Figure A-3).

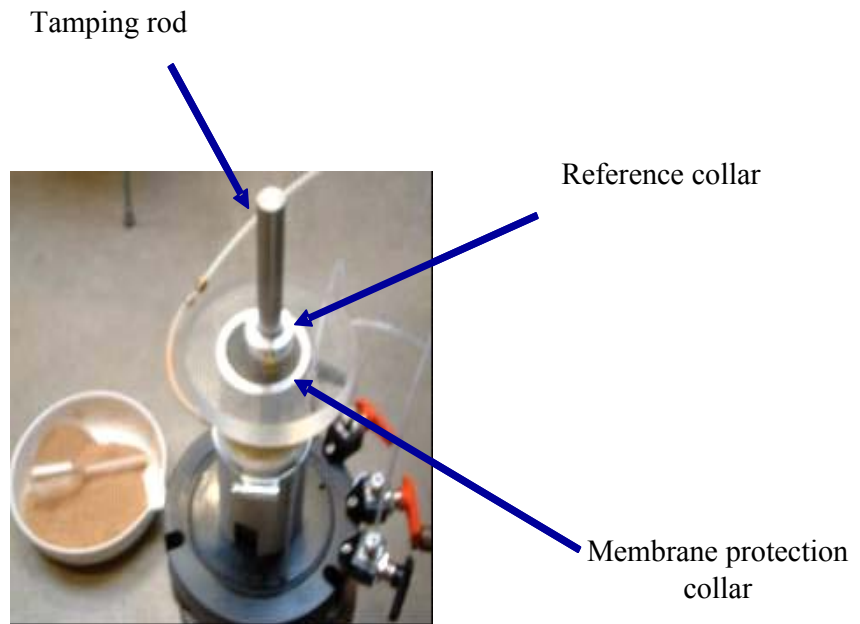


Figure A-2. Preparation of dry specimen using new tamping device.

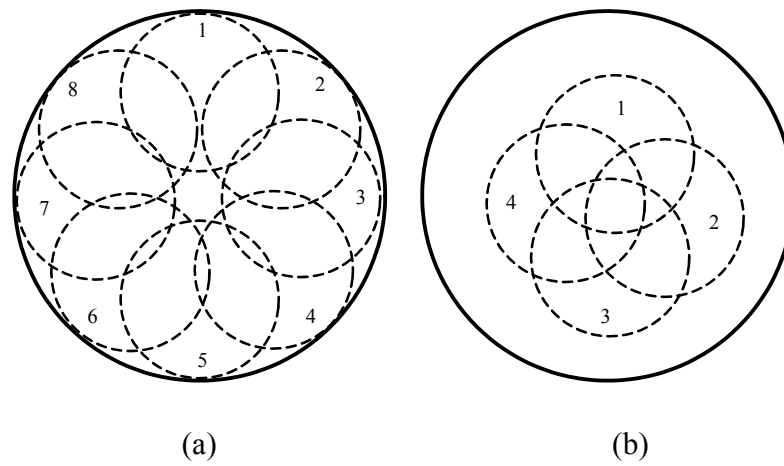


Figure A-3. Tamping pattern during the compaction of sands.

Appendix B - Advanced Stress Path Triaxial Testing System

B-1. Development of the specimen preparation methods for saturated sand

Following Been et al. (1991), the techniques used for reconstitution by wet pluviation (PV) and moist tamping (MT) have been employed in this study. Figure B-1. shows the schematic view of the devices used.

The very loose specimens were created by compaction of the sands in an unsaturated condition at 5% water content using the method proposed by Been et al. (1991).

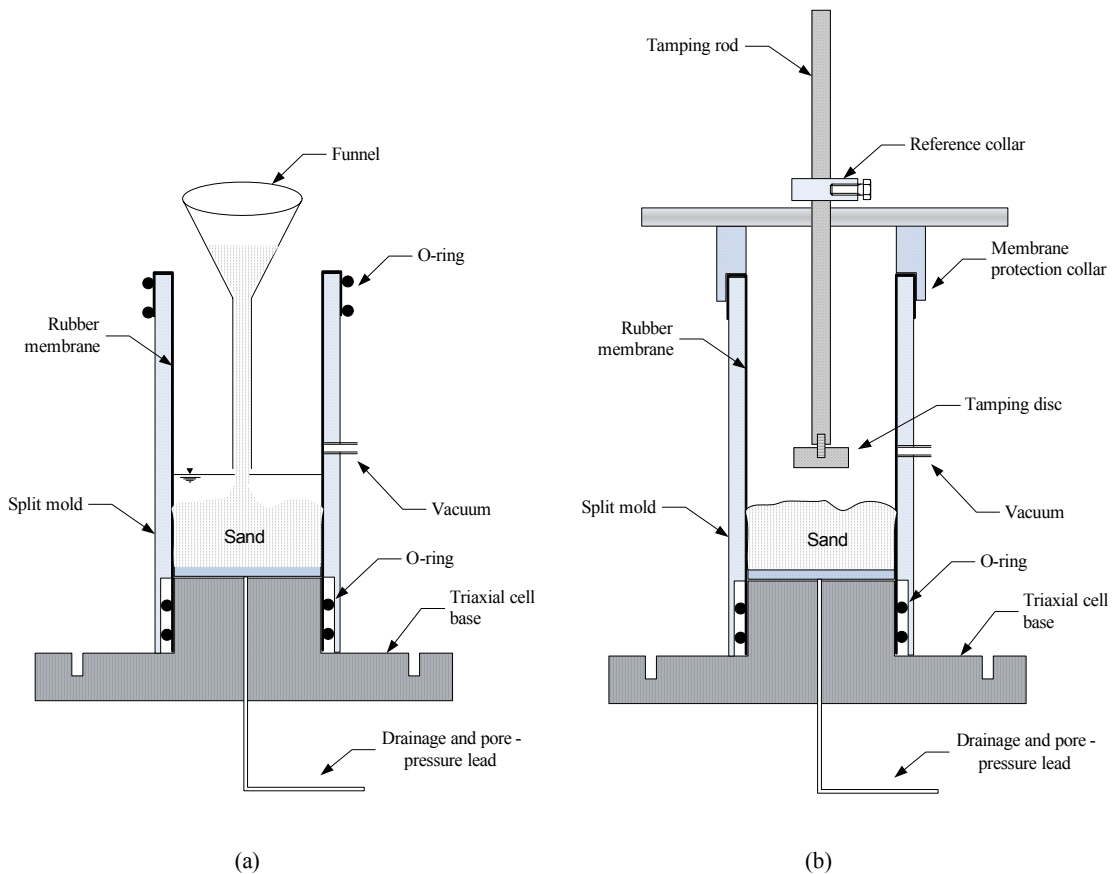


Figure B-1. Schematic view of the devices used for saturated sand specimens: (a) wet pluviation, (b) moist tamping.

The tamping device and procedure used are the same as those developed for dry sand. The wet pluviated specimens were created using a funnel placed within the mould, which was initially filled with water. The saturated sand was poured out just above the surface of the water. After filling the sands, the mould was gently tapped in order to achieve any desired densities.

B-2. Accuracy and range of measurements (GDS Instruments Ltd, 2002)

Item	Sensitivity	Accuracy	Range	Function
Load cell (STAL-23014)	0.10899 kN/mV	2N (1.76 kPa)	2000 N	Axial load measurement
External LVDT	-	0.1 mm	40 mm	External axial strain measurement
Pore pressure transducer	-	2 kPa	2000 kPa	Pore pressure measurement
STDDPC	-	2 kPa	2000 kPa	Cell and lower chamber pressure measurement
STDDPC	-	0.5 cm ³	200 cm ³	Cell and lower chamber volume measurement
ADVDP	-	2 kPa	2000 kPa	Back pressure measurement
ADVDP	-	0.2 cm ³	200 cm ³	Specimen volume measurement
Hall effect (38-415)	2.3345315 μm/mV	0.05 mm	6 mm	Local axial strain measurement (1)
Hall effect (38-517)	2.2962844 μm/mV	0.05 mm	6 mm	Local axial strain measurement (2)
Hall effect (38-515)	2.472020 μm/mV	0.05 mm	6 mm	Local radial strain measurement

Appendix C - Results from Monotonic Loading Tests

C-1. Designation of tests used in section 4.3

Preliminary tests on dry sand

P: Portaway sand

L: Leighton Buzzard sand

Constant Cell Pressure (CCP)

- Isotropically Consolidated Drained Triaxial Tests in Compression (**CIDC**);
- Isotropically Consolidated Drained Triaxial Tests in Extension (**CIDE**);
- Isotropically Consolidated Undrained Triaxial Tests in Compression (**CIUC**);
- Isotropically Consolidated Undrained Triaxial Tests in Extension (**CIUE**);
- Isotropically Consolidated Pre-sheared Undrained Triaxial Tests (**CIPU**).

Variable Cell Pressure (VCP)

- Isotropically Consolidated Drained Triaxial Tests in Compression with Constant Mean Effective Stress (**CIDCP**);
- Isotropically Consolidated Drained Triaxial Tests in Compression with Constant Axial Stress (**CIDCA**);
- Isotropically Consolidated Drained Triaxial Tests in Extension with Constant Axial Stress (**CIDEA**);
- Isotropically Consolidated Drained Triaxial Tests in Compression with Combined Stress Paths (**CIDCC**).

C-2. Testing program on dry Portaway sand

Series	Test	e_0	D_r %	σ'_0 (kPa)	ξ_0	p'_o (kPa)
A	P-01	0.589	61	207	-0.072	138584
	P-02	0.587	62	138	-0.084	168995
	P-03	0.590	61	69	-0.099	172917
	P-04	0.489	91	138	-0.182	21108966
	P-05	0.586	62	138	-0.085	177528
	P-06	0.669	37	138	-0.002	2976
	P-07	0.485	92	300	-0.167	21231352
	P-08	0.489	91	150	-0.180	20679866
	P-09	0.490	91	50	-0.207	25803074
	P-10	0.667	37	300	0.015	2712
	P-11	0.669	37	150	0.000	2915
	P-12	0.668	37	50	-0.029	4014
B	P-13	0.641	46	300	-0.011	9762
	P-14	0.460	100	300	-0.192	72748339
	P-15	0.492	90	100	-0.187	19712354
	P-16	0.600	58	50	-0.097	114380
	P-17	0.502	87	50	-0.195	14287151
	P-18	0.564	68	30	-0.146	764138
	P-19	0.636	47	100	-0.043	16369
	P-20	0.533	78	400	-0.111	1859094
	P-21	0.526	80	200	-0.136	3113174
	P-22	0.592	60	450	-0.049	98734
	P-23	0.460	100	450	-0.181	65834092
	P-24	0.560	70	200	-0.102	583195

C-3. Testing program on dry Leighton Buzzard sand

Series	Test	e_0	D_r %	σ'_0 (kPa)	ξ_0	p'_o (kPa)
	L-01	0.740	93	300	-	-
	L-02	0.740	93	50	-	-
	L-03	0.930	27	300	-	-

The stress-strain and strength characteristics of Portaway sand

L-04 0.900 37 150 - -

C-4. Testing program on saturated sand (Series A–G)

Series	Test	e_0	σ'_0 (kPa)	ξ_0	p'_o (kPa)	p_c (kPa)	q_c (kPa)	e_c
A	CIDC-1	0.699	500	0.060	500	795	890	0.627
	CIDC-2	0.706	300	0.054	397	485	558	0.641
	CIDC-3	0.715	50	0.018	396	84	99	0.677
	CIDC-4	0.537	300	-0.115	1638699	509	626	0.642
	CIDC-5	0.538	50	-0.159	2425315	91	108	0.677
B	CIDE-1	0.701	200	0.039	561	-	-	-
	CIDE-2	0.547	200	-0.115	1106453	-	-	-
C	CIUC-1	0.712	300	0.060	300	21	26	0.712
	CIUC-2	0.699	500	0.060	500	33	39	0.699
	CIUC-3	0.687	800	0.060	800	71	89	0.687
	CIUC-4	0.664	500	0.025	2772	187	213	0.664
	CIUC-5	0.740	300	0.071	-	-	-	-
	CIUC-6	0.705	300	0.053	791	66	80	0.705
	CIUC-7	0.710	100	0.031	427	30	37	0.710
	CIUC-8	0.655	100	-0.024	6420	140	160	0.655
	CIUC-9	0.648	100	-0.031	9063	420	503	0.648
	CIUC-10	0.638	300	-0.014	11316	416	461	0.638
	CIUC-11	0.620	500	-0.019	24220	-	-	-
	CIUC-12	0.739	100	0.060	100	-	-	-
D	CIUE-1	0.722	200	0.060	200	-	-	-
	CIUE-2	0.714	500	0.075	-	-	-	-
	CIUE-3	0.664	800	0.037	2469	-	-	-
	CIUE-4	0.672	1200	0.055	1506	-	-	-
E	CIDCP-1	0.520	500	-0.119	3338501	456	542	0.650
	CIDCP-2	0.702	200	0.040	534	195	218	0.666
	CIDCA-3	0.512	900	-0.112	4283778	415	507	0.643
	CIDEA-4	0.704	200	0.042	484	-	-	-
	CIDCC-5	0.690	100	0.011	1145	807	928	0.630
	CIDCC-6	0.665	400	0.039	561	813	951	0.638
F	CIPU-1	0.687	300	0.035	1012	165	190	0.670

The stress-strain and strength characteristics of Portaway sand

	CIPU-2	0.683	300	0.041	753	269	301	0.659
G	S-1	0.540	300	-0.112	1413571	-	-	-
	S-2	0.580	100	-0.099	258275	-	-	-
	S-3	0.538	50	-0.159	2425315	-	-	-
	S-4	0.699	500	0.060	494	-	-	-
	S-5	0.678	300	0.026	1578	-	-	-
	S-6	0.715	50	0.018	396	-	-	-
	S-7	0.710	100	0.031	427	-	-	-
	S-8	0.610	50	-0.087	69890	-	-	-

Appendix D - Results from Cyclic Loading Tests

D-1. Designation of tests used in cyclic loading

- One-Way Drained Tests in Compression (**OWDC**);
- One-Way Undrained Tests in Compression (**OWUC**);
- One-Way Undrained Tests in Extension (**OWUE**);
- Two-Way Drained and Undrained Tests (**TWD, TWU**);
- Two-Way Drained Tests with Small Cyclic Loading (**TWDS**);
- Moving Wheel Loading (**MV**);

D-2. Testing program

Series	Test	e_0	σ'_0 (kPa)	ξ_0	p'_o (kPa)
H	OWDC-1	0.678	300	0.026	1578
	OWDC-2	0.560	50	-0.137	820549
	OWDC-3	0.512	300	-0.140	5614933
	OWDC-4	0.518	100	-0.161	5476452
	OWUC-5	0.711	300	0.060	300
	OWUE-6	0.712	300	0.060	300
I	TWD-1	0.540	300	-0.112	1413571
	TWD-2	0.581	100	-0.098	245861
	TWD-3	0.711	300	0.060	300
	TWD-4	0.570	100	-0.109	422689
	TWU-5	0.712	300	0.060	300
	TWU-6	0.711	300	0.060	300
	TWDS-7	0.500	300	-0.152	10140758
	TWDS-8	0.530	100	-0.149	3032309
J	MW-1	0.520	100	-0.159	4962627
	MW-2	0.519	100	-0.160	5213213

The stress-strain and strength characteristics of Portaway sand

Appendix E - Numerical Modelling

E-1. Mathematical relations between CASM, CASM-b, CASM-c and CASM-d

